HYDROGEOLOGICAL APPLICATION OF ELECTRICAL RESISTIVITY TOMOGRAPHY: IMPLEMENTING A FIXED-ELECTRODE STRATEGY

by

PARSA PEZESHKPOUR

A thesis

presented to the University of Waterloo

in fulfillment of the

thesis requirement for the degree of

Doctor of Philosophy

in

Earth Sciences

Waterloo, Ontario, Canada, 1999

©Parsa Pezeshkpour 1999

National Library of Canada
Acquisitions and Bibliographic Services
395 Wellington Street
Ottawa ON K1A 0N4
Canada

Bibliothèque nationale du Canada
Acquisitions et services bibliographiques
395, rue Wellington
Ottawa ON K1A 0N4
Canada

Your file Votre référence

Our file Notre référence

The author has granted a non-exclusive licence allowing the National Library of Canada to reproduce, loan, distribute or sell copies of this thesis in microform, paper or electronic formats.

L'auteur a accordé une licence non exclusive permettant à la Bibliothèque nationale du Canada de reproduire, prêter, distribuer ou vendre des copies de cette thèse sous la forme de microfiche/film, de reproduction sur papier ou sur format électronique.

The author retains ownership of the copyright in this thesis. Neither the thesis nor substantial extracts from it may be printed or otherwise reproduced without the author's permission.

L'auteur conserve la propriété du droit d'auteur qui protège cette thèse. Ni la thèse ni des extraits substantiels de celle-ci ne doivent être imprimés ou autrement reproduits sans son autorisation.

0-612-38291-5

Canada

The University of Waterloo requires the signatures of all persons using or photocopying this thesis. Please sign below, and give address and date.

ABSTRACT

Abstract- The requirements of environmental assessments and of understanding and monitoring in-situ mass and heat processes in porous media have led to the development of geophysical methods for remote mapping and monitoring of contaminant plumes and fluid migration. With the possible exception of seismic approaches, electrical methods known as Electrical Resistivity Tomography (ERT) have become the most widely studied and used for these purposes. Wherever a sufficient contrast in ground resistivity is generated by human or natural processes, monitoring the resistivity structure over time may give insight into these processes. ERT has monitoring applications in processes such as Enhanced Oil Recovery (EOR), Slurry Fracture Injection (SFI), and monitoring transport processes in hydrogeology. A permanent electrode arrangement for long term monitoring removes the effects of Earth's heterogeneity and anisotropy when a process is analyzed as a function of time.

As a starting point on the work described in this thesis, ERT data were collected from a Cambridge, Ontario, sand pit before, immediately after and one week following a 11000 liters slurry injection. These measurements verified that ERT could detect changes caused by the injection and later movement of this conductive mixture in the ground. The commercial equipment used for these measurements was not well suited to the tasks, mainly because it was extremely slow. Further, there was a lack of robust and user-friendly three-dimensional modeling software to use as a means of predicting response and - eventually - as the engine of an inversion routine. Finally, it was difficult to analyze the injection situation in terms of how best to place a limited number of surface and borehole electrodes to most effectively monitor the injection fluids. The remainder of the thesis addresses these problems.

The first objective was to design and construct a more suitable ERT measurement system.

The image resolution of the basic ERT technique is usually poor. Given the normal limitations of excitation current and geology, there are three approaches to improving the resolution of these images:

- Increasing the accuracy and precision of the measuring instruments.
- Using optimal electrode arrangement with respect to the resistivity anomaly in question.

- Processing data with methods that eliminate noise and improve the resolution of the resistivity (conductivity) distribution map.

With an appropriate measuring system, it should be possible to increase the speed, repeatability, and accuracy of ERT data collection considerably. The system described here consists of the following:

i. Expandable network switches for signal input and output;
ii. Low-pass filter (10 Hz) for noise reduction ;
iii. Programmable gain for efficient data collection;
iii. A 16-channel, 16-bit A/D board having software for range control; and,
iv. A proper field computer system (i.e., minimum of 80486 PC).

Since the stabilized portion of each of positive and negative induced current pulses in each cycle is about 0.4 second in a 0.5 Hz current, it is possible to collect the voltage differences of an electrode array in a matter of minutes.

The second objective was to adapt SALTFLOW as a platform for both the resistivity and hydrogeological modeling of the saline groundwater flow resulting from waste injection.

Because steady-state groundwater and direct electrical current flow obey the same governing equations, it has been possible to make use of the modeling expertise and one of the software programs available through the Waterloo Groundwater Simulation Group (SALTFLOW and FRAC3DVS) to experiment with three-dimensional ERT monitoring scenarios.

Further improvement of the forward model have been achieved by comparing a combination of different iterative sparse solver methods (such as: Conjugate Gradient (CG), Bi-Conjugate Gradient (BICG), Conjugate Gradient Stabilized (CGStab), Generalized Minimum Residual (GMRES)) and four ordering methods (natural, RCM, Min Degree, Nested dissection). Considering the same resolution and tolerance, it has been determined that the combination of nested dissection ordering with preconditioned conjugate gradient method shows faster convergence. Implementing line elements for current electrode in the forward model, which has been used for groundwater modeling (as a highly conductive line element to represent wells), reduces the oscillation of the model results on the grids around the current electrodes.

The third objective was to develop methods of sensitivity analysis that will allow a more efficient examination of the electrode arrays that could be effectively used in a given situation.

The sensitivity analysis is based on the state sensitivity and adjoint sensitivity techniques. These have been implemented in the forward model.

The electrode setup is one of the most important issues in an ERT survey. The closer the electrodes are to the anomaly, the better will be the quality of the ERT images; however, the optimal electrode arrangement depends not just on the target, but also on the field conditions, the availability of boreholes, project budget and the client's expectations. We are using sensitivity analysis and an improved forward model to estimate the optimal electrode placement for a given target under given circumstances.

The fourth objective was to demonstrate the ERT method and the improvements undertaken by the author on the data collected at the Cambridge injection site.

The thesis has not, in fact, met all these objectives, but has made substantial progress towards them. The complete design of the measurement system and the construction of its potential measurement components were achieved. A lack of capacity in the science shops, however, resulted in the power (current) supply not being constructed in time for field evaluation of the injection or its aftermath.

ACKNOWLEDGEMENTS

I would like to thank my supervisors Maurice B. Dusseault and John P. Greenhouse for their encouragement, patience, enthusiasm and guidance during the course of my Ph.D. program. Additional thanks to the members of my advisory committee and examining board, Dr. Peter Annan, Dr. Richard C. Bailey, Dr. Giovanni Cascante, and Dr. Jon Sykes, for their suggestions.

The models used the program SALTFLOW developed by Dr. Emil Frind and John Molson, and FRAC3DVS developed by Dr. E.A. Sudicky, Dr. R. Therrien and R.G. McLaren of the Groundwater simulation group at the University of Waterloo. Particular appreciation is given to John Molson and Rob McLaren for their assistance in implementing these unusual applications. Help from Andre Rogozhinski (Androtex) in the use of his equipment for collecting ERT data is also appreciated. I thank my friend Dr. Ardeshir Namdar-Mehdiabadi for improving my electronic knowledge and his suggestions to finish the electronic part of this thesis. In addition, acknowledgment is extended to Elizabeth Dusseault, Douglas Hirst, Scott Piggott, David Redman, and the late Elizabeth Edwards, for their technical and editorial assistance in this research. Also I would like to convey my gratitude to Dr. J.E.E. Kingman for passing valuable information on staking to me.

Thanks to all my friends (Jos Bakers, Uli Mayer, Rob McLaren, John Molson, Mario Schirmer, and those that I forgot to name) for those moments of short talks, discussions and suggestions. I also like to thank, my friend, Mansour Ataollahi Eshkoor who has done many things for me beyond friendship.

I also thank Dr. Greenhouse's family members (especially Jane) for the hospitality and friendship they have shown toward my family and me during the last few years.

Finally, I would like to thank my wife Afsaneh Amirabadi, for her patience, encouragement, and support during the last few years.

I appreciate funding provided for this research by a scholarship from the Iranian Ministry of Culture and Higher Education; and Dr. M. B. Dusseault's funding from the Geomechanics Group at University of Waterloo.

DEDICATION

To my brother and my best friend:

Parviz Pezeshkpour,

who without whose support and encouragement I could not fulfill this destiny,

To my family (parents, brothers and sisters):

whose love and concern made life easier for me,

To my wife:

Afsaneh Amirabadi,

who has gone through a lot while this seed has evolved ,

And to my children:

Paymun and Parneyan,

who brought laughter and joy to my life.

TABLE OF CONTENTS

SUBJECT	PAGE
Abstract	iv
Acknowledgement	vii
Table of contents	ix
List of Tables	xii
List of Figures	xiv
Chapter1: Introduction	1
1. Introduction	1
1.2 Monitoring	3
1.3 The problem	4
General	4
Challenges specific to the waste injection application	5
1.4 Objectives of this thesis	5
1.5 The history of the project	7
1.6 Explanation of each chapters	9
Chapter 2: Background	10
2. Background	10
2.1 Theory	10
Basic theory	10
Boundary condition	13
2.2 Modeling	13
Forward model description	13
2.3 Equipment	16
Commercial	16
Requirements of an ERT system	16
Other systems in developing process	17
2.4 Uncertainty and error analysis	18
The uncertainty concept	18
Sensitivity analysis for evaluation of uncertainty	19
Adjoint sensitivity analysis	21
Measurement errors	25
Uncertainty of measurement	26
2.5 Slurry injection	27
2.6 Field site	28
Description	28
Chapter 3: Modification to the forward model	32
3. Modification to the forward model	32
3.1 Comparison of iterative and direct methods	34
3.2 Ordering methods	36
Nested dissection ordering method	36
Minimum degree ordering method	36
Reverse Cuthill-McKee (RCM) ordering method	37

SUBJECT	PAGE
3.3 Preconditioning	37
Preconditioned incomplete Cholesky decomposition	37
3.4 Acceleration methods	38
3.5 Non-stationary Iterative methods	39
3.6 Modification to the forward model	39
Results of forward model modification	40
Chapter 4: An electrical resistivity tomography measuring system	44
4: An electrical resistivity tomography measuring system	44
4.1 Data Acquisition and control system (switch network and computer interface)	44
The computer system and interface	44
Electronic switch network	53
Software	61
4.1 Cabling	65
4.2 Assembling the system	68
4.3 Power Supply	71
4.4 Cost evaluation	72
4.5 ERT time requirement	72
Chapter 5: Field testing	73
5. Field testing	73
5.1 Preliminary experiment (description)	73
Chapter 6: Results	82
6.1 Cambridge Resistivity Measurements, January 1996	82
6.2 Simulation of groundwater regime following the injection	90
6.3 Simulation of the ERT response to the injection	96
6.4 Adjoint sensitivity analysis	106
6.5 Evaluation New ERT measuring system	111
Precision	111
System noise	112
Accuracy	114
Environmental influence	114
Chapter 7: Conclusion	117
Chapter 8: Recommendations for future work	121
8.1 Modeling	121
Forward	121
Inversion	122
8.2 Equipment	122

SUBJECT	PAGE
Data acquisition	122
Power supply	122
References	123
APPENICES	
Appendix A: Literature review	140
Appendix B: An example of a solved forward problem	152
B.1 Application	159
Appendix C: Equipment evaluation	161
C.1 Field tests	161
C.2 Laboratory tests	163
C.3 Equipment evaluation results	170
Appendix D: The specifications of the devices, components and softwares used in the ERT system	171
D.1 Switch network and computer interfacing	171
D.2 Components	178
D.3 Software	184
Appendix E: Cambridge preliminary experiment results	185
Appendix F: New ERT system evaluation and calibration results	188
Appendix G: Input data file to FRAC3DSV and SLATFLOW models	191
G.1 FRAC3DVS inputs	191
G.2 SALTFLOW inputs	200
Appendix H: Glossary	202
Appendix I: Logs of wells at Cambridge site	227
Appendix J: ERT Model Calibration	230

LIST OF TABLE

SUBJECT	PAGE
Table 3.1a Results of iteration based on level of fill of ILL^t(0,0.0)	41
Table 3.1b Results of iteration based on level of fill of ILL^t(1,0.0)	41
Table 3.1c Results of iteration based on level of fill of ILL^t(2,0.0)	41
Table 3.2a Results of iteration based on drop tolerance of ILL^t(∞,0.1)	43
Table 3.2b Results of iteration based on drop tolerance of ILL^t(∞,0.01)	43
Table 3.2.c Results of iteration based on drop tolerance of ILL^t(∞,0.001)	43
Table 4.1 Cost evaluation of ERT system for 64 to 256 electrodes single-ended inputs	72
Table 6.1 Simulated and measured potential values for downhole electrodes at Cambridge site	98
Table 6.2 Statistical evaluations of simulated and measured potential values for the Cambridge site	101
Table 6.3 Environmental operating ranges of different components used in the new ERT measuring system	115
Table 6.4 Measurement uncertainty of new ERT system	116
Table A.1 Engineering and industrial applications of ERT	142
Table A-2 Core and soil sample analysis	142
Table A-3 Steam injection monitoring	143
Table A-4 Monitoring groundwater processes	144
Table A-5 Monitoring leaks from storage ponds and liners under waste	145
Table A-6 ERT Case studies	146
Table A-7 Three-dimensional resistivity and ERT evaluations	147
Table A-8 Inversion	148
Table A-9 Resistivity instrumentation, power supply and waveform analysis for ERT	150
Table A-10 Study of physical properties by resistivity methods	151
Table C-1 Commercial resistivity meters specifications	162
Table E.1 The data sets of Figure 6.1 to 6.3 for Cambridge preliminary experiment electric potential measurements (in TECPLOT format)	185
Table F.1 Calculated precision data of the new ERT measuring system (graphically presented in Figure 6.18)	188

Table F.2 Laboratory evaluation of the new ERT measuring system results for different voltage ranges (graphically presented in Figure 6.19 and 6.20) 189

Table F.3 Laboratory evaluation of the new ERT measuring system results for different voltage ranges (graphically presented in Figure 6.20) 190

Table J.1 Statistical results of two scenarios solved analytically and by the SALTFLOW model 232

LIST OF FIGURES

SUBJECT	PAGE
Figure 2.1 Groundwater and electrical field equivalent relationships	15
Figure 2.2 Shallow waste injection	28
Figure 2.3 Site location map	30
Figure 2.4 Schematic plan view of installed wells in the Cambridge site	30
Figure 2.5 Stratigraphy of drilled layers at Cambridge site	31
Figure 3.1 The timing-iterations required to complete a 95 by 77 by 28 grid model calculation with the most effective combinations for the levels of fill and orderings	42
Figure 3.2 The timing-iterations required to complete a 95 by 77 by 28 grid model calculation with the most effective combinations for the drop tolerance and orderings	42
Figure 4.1 Schematic diagram of an analog-to-digital converter	46
Figure 4.2 Schematic diagram of a comparator	47
Figure 4.3 Schematic diagram of a successive approximation A/D converter	48
Figure 4.4 A/D used in ERT system (AT-MIO-16XE -50 from National Instruments)	50
Figure 4.5 Multiplexer used in ERT system (AMUX64T from National Instruments)	51
Figure 4.6 Standard TTL and LS series logic levels	52
Figure 4.7 Illustration of current during input to a parallel port	52
Figure 4.8 Digital output used to assemble ERT system (DO 192H from ComputerBoards Inc.)	53
Figure 4.9 Digital input used to assemble ERT system (DI 192 from ComputerBoards Inc.)	53
Figure 4.10 Prototype switching board and its components on a bread board	54
Figure 4.11 Schematic diagram of switching board components and the connections for one electrode	55
Figure 4.12 Simplified field-new measuring system circuit sketch	56
Figure 4.13 Shielding interference is prevented by placing a metal partition around the receptor to prevent noise infiltration	58
Figure 4.14 Common types of filters	59
Figure 4.15a The front panel of the virtual instrument (VI) program handling the quality control of data of the ERT system	66

Figure 4.15b The front panel of the virtual instrument (VI) program handling the switching part of the ERT system though digital I/O devices 66

Figure 4.15c The front panel of the virtual instrument (VI) program handling the data input for the ERT system 67

Figure 4.15d Diagram of the virtual instrument (VI) program of the new ERT measuring system 67

Figure 4.16 The view of the wiring at the back of switching boards 68

Figure 4.17a Side view of two switching boards and one plexiglas sheet (for multiplexer and required input banana plugs as receivers to the switching boards) mounted on a rack inside the stain-less steel shielded box 69

Figure 4.17b Top view of switching boards and one plexiglas sheet (for multiplexer and required input banana plugs as receivers to the switching boards) mounted on a rack inside the stain-less steel shielded box 69

Figure 4.18a Side view of home-made switching box with external connectors to be connected to electrodes and computer 70

Figure 4.18b Side view of home-made connector board at the back on a modified computer box for interface connectors 70

Figure 4.19. Schematic diagrams of the shapes of the power supply pulses 71

Figure 4.20 Primary test results of the power supply generated pulse passing through a 100 Ω resistor detected with HP545 oscilloscope 71

Figure 5.1 X-Y plane view of electrical potential simulation at the Cambridge scenario: (a) background, (b) for the same scenario including a conductive anomaly, (c) after introducing 1% change to the conductivities of the anomaly, and (d) the difference between the background and scenario with a conductive anomaly. Units are in V/A 75

Figure 5.2 X-Z plane view of electrical field simulation at the Cambridge scenario: (a) background, (b) for the same scenario including a conductive anomaly, (c) after introducing 1% change to the conductivities of the anomaly, and (d) the difference between the background and scenario with a conductive anomaly. Units are in V/A 76

Figure 5.3 Schematic diagram of electrode placement with respect to anomaly and the potential distribution; a) both current electrodes at the sides on the surface; b) one current electrode at the surface and the other one inside the anomaly; c) both current electrodes at the sides of the anomaly close to it; and d) both current electrodes inside the anomaly 77

Figure 5.4 Plan view of installed monitoring elements for the Cambridge experiment 78

Figure 5.5 Schematic cross-section of well and electrode configuration 80

Figure 6.1 Background potential field at surface electrodes with respect to a reference point (14, 0, 0), current electrodes at the bottom of the SW monitoring well (10.5, 17.25, 16.75) and at surface 80m west of the SW monitoring well (-70, 17.25, 0). Collected on January 19, 1996. Units are mV/A 84

Figure 6.2 The potential field (mV/A) at surface electrodes with respect to a reference point (14, 0, 0) collected on January 20, 1996, one day following the slurry injection using the same electrode configuration as Figure 6.1. Units are mV/A 85

Figure 6.3 The potential field (mV/A) at surface electrodes with respect to a reference point (14,0,0) collected on January 26, 1996, 6 days following the slurry injection using the same electrode configuration as Figure 6.1. Units are mV/A 86

Figure 6.4 The potential differences between background and one day following injection. Units are mV/A 87

Figure 6.5 The potential differences between background and 6 days following injection. Units are mV/A 88

Figure 6.6 The potential differences between one day and 6 days following the injection. Units are mV/A 89

Figure 6.7 Simulated pressure head variations in the X-Z plane at Cambridge site: (a) background, (b) following slurry injection, (c) one day after slurry injection, (d) 6 days after slurry injection 92

Figure 6.8 Simulated total head (pressure head plus elevation head) variations in the X-Z plane at Cambridge site: (a) background, (b) following slurry injection, (c) one day after slurry injection, (d) 6 days after slurry injection. Units are m 93

Figure 6.9 Simulated saturation variations in X-Z plane at Cambridge site: (a) background, (b) following slurry injection, (c) one day after slurry injection, (d) 6 days after slurry injection. The change in the pattern saturation of clay layer compare to sand layer is because of difference in soil-water characteristic curves of these two materials 94

Figure 6.10 Simulated salt concentration in the X-Z plane at Cambridge site: (a) background, (b) following slurry injection, (c) one day after slurry injection, (d) 6 days after slurry injection 95

Figure 6.11 Simulated potentials with respect to a reference point the X-Z plane for Cambridge scenario: (a) background, (b) one day after slurry injection, (c) 6 days after slurry injection, (d) the potential difference between one day and 6 days after slurry injection. Units are V/A 99

Figure 6.12 Simulated potentials with respect to a reference point in the X-Y plane for the Cambridge scenario: (a) background, (b) one day following the slurry injection, (c) 6 days following the slurry injection, (d) the potential difference between one day and 6 days following the slurry injection. Units are V/A 100

Figure 6.13 Scatter and residual plots of background measured and predicted potentials at Cambridge site: (a) scatter plot of potential at surface, (b) residual plot of potential at surface, (c) scatter plot of potential at downhole electrodes, (d) residual plot of potential downhole electrodes 102

Figure 6.14 Scatter and residual plots of measured and predicted potentials one day following the injection at Cambridge site: (a) scatter plot of potential at surface, (b) residual plot of potential at surface, (c) scatter plot of potential at downhole electrodes, (d) residual plot of potential downhole electrodes 103

Figure 6.15 Scatter and residual plots of measured and predicted potentials one week following the injection at Cambridge site: (a) scatter plot of potential at surface, (b) residual plot of potential at surface, (c) scatter plot of potential at downhole electrodes, (d) residual plot of potential downhole electrodes 104

Figure 6.16 Simulated and measured changes in potential (V/A) between 1 day and 6 days following the injection in the Cambridge site at X-Z plan: (a) simulation, (b) measured 105

Figure 6.17 Potential (V/A) and state sensitivity distribution in the X-Z plane for a dipole set at surface and downhole: (a) background, (b) including conductive anomaly in the scenario, (c) the potential differences between background and after the existence of conductive anomaly, (d) state sensitivity distribution 107

Figure 6.18 Potential (V/A) and state sensitivity distribution In the X-Y plane for a dipole set at surface and downhole: (a) background, (b) including anomaly in the scenario, (c) the potential differences between background and after the existence of conductive anomaly, (d) state sensitivity distribution 108

Figure 6.19 Potential and state sensitivity distribution in the X-Z plane for a dipole set at surface (AB/2 = 15 m): (a) background, (b) including anomaly in the scenario, (c) the potential differences between background and after the existence of conductive anomaly, (d) state sensitivity distribution 109

Figure 6.20 Potential and state sensitivity distribution in the X-Y plane for a dipole set at surface (AB/2 = 15 m): (a) background, (b) including anomaly in the scenario, (c) the potential differences between background and after the existence of conductive anomaly, (d) state sensitivity distribution 110

Figure 6.21 Precision achieved at each input voltage range of the ERT measurement system. The percentage error is given with respect to the minimum in each range, except for the lowest range where it is with respect to the maximum 112

Figure 6.22 The new ERT measuring system laboratory setup 113

Figure 6.23 Noise level of new ERT measuring system 113

Figure 6.24 Standard deviations of data collected at different voltage levels 115

Figure B-1 Schematic projection of a cylindrical object 152

Figure C-1 Resistivity meter response in repeated measurements in the field for different gage positions 161

Figure C-2 Plot of two set of repeated measurements in the field for the same electrode arrangements 163

Figure C-3 Schematic diagram of laboratory setup 164

Figure C-4 Syscal Junior resistivity meter readings for 1.0 kΩ resistor at different gage positions 165

Figure C-5 Syscal Junior resistivity meter readings for 1.0 kΩ resistor at different gage positions 166

Figure C-6 Syscal Junior resistivity meter readings for 120 kΩ resistor at different gage positions 166

Figure C-7 Syscal Junior resistivity meter readings for 220 kΩ resistor at different gage positions 167

Figure C-8 Syscal Junior resistivity meter readings for 2.2 kΩ resistor at different gage positions 167

Figure C-9 Schematic diagram of two resistance networks: (a) first resistor network, (b) second resistor network 168

Figure C-10 Repeated lab measurements of the first resistor network for different gage positions 169

Figure C-11 Repeated lab measurements of the second resistor network for different gage positions 169

Figure D-1 Electromechanical Reed Relays: (a)DS4E-M-12V from Aromat Canada, Inc. (for elements K1 and K2 of Figure 4.11), (b) DS2E-M-12V from Aromat Canada, Inc. (for element K3 of Figure 4.11) 178

Figure I-1 Stratigraphic units in Injection well of Cambridge site 227

Figure I-2 Stratigraphic units in NE-monitoring well of Cambridge site 227

Figure I-3 Stratigraphic units in NW-monitoring well of Cambridge site 228

Figure I-4 Stratigraphic units in SE-monitoring well of Cambridge site 228

Figure I-5 Stratigraphic units in SW-monitoring well of Cambridge site 229

Figure J-1 Schematic diagram of one layer model 230

Figure J-2 Scatter and residual plots of a one-layer case solved analytically and by SALTFLOW: a) scatter plot, and b) residual plot 230

Figure J-3 Schematic diagram of three-layer model with a high resistive vertical column in the middle 231

Figure J-4 Scatter and residual plots of a three-layer case three-layer model with a high resistive vertical column in the middle solved analytically and by SALTFLOW: a) scatter plot, and b) residual plot 231

Chapter 1

INTRODUCTION

1. Introduction

The requirements of environmental assessments, understanding and monitoring in-situ mass and heat transfer processes in porous media have led to the development of geophysical methods for remote mapping and monitoring of contaminant plumes and fluid migration. With the possible exception of seismic approaches, electrical methods have become the most widely studied and used for these purposes, especially for hydrogeological investigations. For example, resistivity surveys have been used to: detect the location of the water table and fresh-saline water interfaces (*Van Overmean,* 1989; *El-Waheidi et al.,* 1992); survey groundwater pollution in coastal environment (*Frohlich et al.,* 1994); assess aquifer hydraulic conductivity and transmissivity (*Kelly,* 1976; *Mazac et al.,* 1987 & 1990a); evaluate electric-hydraulic conductivity correlation in fractured crystalline bedrock (*Frohilch et al.,* 1996); estimate travel times through unsaturated groundwater protective layers (*Kalinski et al.,* 1993); determine the extent of oil contamination in groundwater (*Mazac et al.,* 1990b); and delineate highly contaminated zones (*Pfannkuch and Labno,* 1977; *Pfannkuch,* 1982; *Urish,* 1983; *Tamburi et al.,* 1988; *de Lima et al.,* 1995). To increase the resolution of a resistivity distribution map, authors have used various mathematical approaches (*Dey and Morrison,* 1979; *Das and de Hoop,* 1995; *Spitzer,* 1995; *Straub,* 1995a & b; *Zhang et al.,* 1995; *Mogilatov and Balashov,* 1996; *Santos et al.,* 1997). They have also experimented

with the placement of electrodes beneath the ground surface to improve the resolution of subsurface anomalies (*Daniels*, 1977 & 1983; *Yang and Ward*, 1985; *Beasley and Ward*, 1986; *Bevc and Morrison*, 1991; *Wang et al.*, 1991).

A problem that is encountered with all surface configurations of electrodes is that near-surface variations in conductivities can have a strong effect on the apparent resistivities, thereby masking the effects of resistivity structure at depth. In general, resistivity mapping using subsurface electrodes permits greater accuracy and resolution than can be obtained with surface arrays only (*Asch and Morrison*, 1989), as it becomes possible to penetrate below the surface effects. The theory and field applications of subsurface electrode procedures have been developed (e.g., *Alfano*, 1962; *Merkel*, 1971; *Snuder and Merkel*, 1973; *Daniels*, 1977 & 1983;*Dey and Morrison*, 1979; *Narayan*, 1994).

Many authors, among them *Dey* (1976) and *Dey and Morrison* (1979) have initially developed 2-D and 3-D electrical resistivity numerical programs. These have been modified (*Asch and Morrison*, 1989) to permit analysis of the responses of hole-to-surface and cross-hole electrode arrays to analyze arbitrarily shaped resistivity inhomogeneities. To improve resistivity resolution, recent research projects have concentrated on so called "Electrical Impedance Tomography (EIT)" or " Electrical Resistivity Tomography (ERT)".

The problem of computerized tomography, in mathematical terms, is the reconstruction of a 3-D function from integration of data collected over straight lines or planes, or collected at points in a 3-D volume. Although the mathematical reconstruction is only a rough model of the actual ground structure, which is the "real" problem, the goal is to achieve a "good enough" picture of the real structure to meet engineering and scientific goals. An adequate understanding of reconstruction approaches is a prerequisite for any approach to the field of computerized tomography.

Many of the first practical applications of tomographic imaging were developed for medical uses in the early 1960's, but the mathematics behind the technique was first addressed by *Radon* (1917). Modern computerized tomography began in 1971 when *Hounsfield* (1972) developed the first scanner capable of producing clear images of planar slices of the brain. He used gamma rays, scanning the brain from a number of angles, and imaged the density structure of the brain. This invention marked the beginning of the application of tomography in medicine. Other applications of

tomography are found in many branches of science and engineering, including geotechnique and geophysics. *Bios and et al.* (1972), who used seismic wave-travel time to detect major structural boundary between boreholes, published the pioneering work in geophysical tomography, or geotomography. The boundaries they sought to identify were characterized by different seismic velocities, and the reconstruction wave of the velocity structure of the 2-D rock slice between the boreholes. Since then, this seismic technique has been successfully used in a wide range of geophysical imaging situations. Variations of it are called 3-D cross-hole seismic tomography and vertical seismic profiling.

The increasing interest in environmental and exploration problems has prompted many studies on resistivity tomography, where the resistivity structure of the ground is the object of the reconstruction exercise. ERT is the 2- or 3-D reconstruction of an internal resistivity distribution from a set of electrical potential distribution measurements in and/or around the volume of interest. In spite of the fact that the resistivity of the earth cannot be related to the observed data by a line integral, the term "resistivity tomography" seems to have been accepted, as numerous model studies (*Yorkey,* 1986; *Shima and Sakayama,* 1987; *Daily and Owen,* 1991; *LaBrecque et al.,* 1996; *Ramirez et al.,* 1996) have shown that the accuracy and resolution of the resistivity method can be improved substantially by including the data for cross-hole geometries. A review of the ERT literature is presented in Appendix A.

1.2 Monitoring

Tomographic monitoring of regions within the earth where natural or anthropogenic change may take place is gaining increasing importance. Whereas spatial detection of an anomalous zone may require searching through large volumes of the subsurface, an exercise for which tomography is not well suited, monitoring usually begins with a prescribed region on which the measurements are to be made. The objective is to detect changes in the physical properties of that region, measured against a background of their normal values. ERT (or EIT) is increasingly being used for monitoring anomalous conditions. Some noteworthy examples published in the past decade are: *Tamburi et al.* (1987); *Daily et al.* (1992); *Daily and Ramirez* (1995); *Daily et al.* (1995); *Lundegard and LaBrecque* (1995); *Osiensky and Donaldson* (1995); *Spies and Ellis* (1995); *Binley et al.* (1996); *LaBrecque et al.* (1996); *Ramirez et al.* (1996a & b); *Schima et al.* (1996); *Slater et al.* (1996a & b); *Binley et al.* (1997); *Ramirez et al.* (1997); *Daily and Ramirez* (1998).

ERT involves repeated current injections through many electrode pairs and into the region of interest (i.e., ground) and the recording of the potential distribution at all other electrodes for each current electrode pair. This procedure generates several electric potential images of the region of interest from different geometries of current injection. Analysis of these images is processed through a forward and an inverse algorithm, which combines all the data to yield 3-D resistivity distribution inside the studied region.

1.3 The problem

ERT is in its infancy as a monitoring tool, requiring both improvements in its technology and a wider variety of applications to reach its eventual potential. This thesis has resulted from a very specific potential application, the injection under high pressure of wastes, in the form of liquids or slurries, into the deep subsurface. In the test phases of this technology a saline solution is often used as a surrogate for the waste, and indeed the wastes eventually contemplated for this type of disposal are likely to be highly saline as well. The problem is to determine what will happen to this waste once injected, and ERT seemed one of the likely technologies for this purpose.

The basic ERT technology has been well developed but there remain a number of areas where improvements are needed, both for the methodology in general and for our problem in particular. These areas are described below.

1.3.1. General

ERT monitoring attempts to image those regions within the monitored volume where resistivity contrasts develop with respect to the background. The resolution obtained with this image depends on:

i. the size of the anomaly;
ii. the location of the anomaly with respect to the electrodes;
iii. the electrode arrangement;
iv. the sensitivity of the equipment, including the available power, achievable signal to noise, and so on; and,
v. the processing and inversion of the data.

At the same time, the practicality of the method depends on the speed with which the survey can be undertaken and interpreted (real time being the goal), the availability of suitable equipment, and the ability to make reasonable simulations of the situation prior

to the measurements so that the electrode arrays can be optimized for those measurements.

Areas of ERT to be addressed therefore include:

i. the accuracy and precision of the measuring instruments;
ii. the speed with which measurements can be made;
iii. data processing; and
iv. fast, accurate forward models for simulation of the situation and inversion of the data.

1.3.2 Challenges specific to the waste injection application

The waste injection technology involves, at least initially, a very restricted volume of the subsurface centred around the injection well. The sensitivity of a monitoring technique falls off very quickly as the monitoring electrodes are removed from the anomaly source, and it is clearly advantageous to have as many electrodes as possible in the vicinity of the injection. For example, the slurry injection well itself can also be used for passing electric current into the bulk of the waste, and nearby hydrogeological monitoring wells can be used for subsurface current and potential measurements. The number of these subsurface "windows" is limited by their cost and by their availability if there are pumps or piezometer bundles installed. The optimal ERT monitoring arrangement will therefore of necessity involve surface electrodes, and it is the number and positioning of these for efficient and practical monitoring that needs to be established.

The salinity of the surrogate (and probably the actual) waste results in rather specific hydrogeological conditions. The movement of the resulting plume is to some extent density driven and will tend to sink, other conditions being equal. It is clearly to our advantage to use the known salinity of the waste to help in predicting its likely movement. By the same token, the results of a resistivity monitoring inversion, showing the distribution of the injected saline materials, will need to be interpreted in light of the dynamics of this particular contaminant. Easy interaction between the hydrogeological and resistivity modeling procedures will be an asset.

1.4 Objectives of this thesis

In examining the problem of ERT monitoring of waste injections it became clear that a number of issues should be addressed. First, the injection process is very fast and

significant changes in the subsurface will occur over periods of minutes and hours, as well as over days and months. The data collection instruments available at the University of Waterloo, or from rental agencies (catering mainly to the exploration market), were not fast enough. They could handle multiple electrodes, but made potential measurements on only one electrode pair at a time. Faster equipment may exist within research groups elsewhere, but not accessible to public.

The first objective, then, was to design and construct a more suitable ERT measurement system.

Secondly, the forward – and eventually inverse – modeling of the electrical potentials in a three dimensional context requires good software and a good "front end" to allow the many thousands of parameters to be changed quickly. While three-dimensional resistivity models are available for sale, and as freeware from certain research groups, the cost of the former and the unknown quantities and generally poor front ends of the latter did not make them attractive. Following the lead of some other practioners, notably Janson (1995), we decided to adapt 3-D groundwater models written at the University of Waterloo for this purpose. These models solve the same equations as required for electrical current flow, and a fairly straightforward substitution of parameters (electrical conductivity for hydraulic, for example) is possible. Whereas Janson used a version of the industry standard MODFLOW, we had access to what is probably the next standard WATFLOW, a finite element as opposed to a finite difference program. Further, we decided to adapt a version of WATFLOW called SALTFLOW (*Frind and Molson,* 1993) written specifically for modeling dense, saline groundwater. Bundling the resistivity and hydrogeological models within the one code has logistical benefits, although they could certainly be run on separate software platforms and combined later. SALTFLOW, however, is not optimized for the steady state conditions of resistivity, and it was decided that this aspect of the code could be improved. This version is denoted henceforth as SALTFLOW*.

The second objective was to adapt SALTFLOW as a platform for both the resistivity and hydrogeological modeling of the saline groundwater flow resulting from waste injection.

Thirdly, an element of the problem that needed addressing was the question of sensitivity of a given electrode or electrode array to a specific scenario. This can be done by running a large number of forward SALTFLOW* models (general state sensitivity), but it

is more efficient to undertake sensitivity analyses of a base model to small perturbations anywhere in the volume of earth under observation. For this the thesis examines an adjoint sensitivity technique. The adjoint technique is more cost efficient and rapid than general state sensitivity because it requires solving only two sets of problems: the response function and sensitivity of parameters. For any individual scenario, these problems require to be solved only once. It is also a step along the path toward an inversion procedure- although that path has not been taken in this thesis.

The third objective is to develop methods of sensitivity analysis that will allow a more efficient examination of the electrode arrays that could be effectively used in a given situation.

Lastly, an experimental injection at a site in Cambridge, Ontario, was chosen as the location to test the ERT method and the various improvements. The site was instrumented with available equipment before the injection and then twice after the injection.

The fourth objective is to demonstrate the ERT method and the improvements undertaken by the author at the Cambridge injection site.

The thesis has not, in fact, met all these objectives but has made substantial progress towards them. SALTFLOW has been adapted and modified as planned. The complete design of the measurement system and the construction of its potential measurement components were achieved. A lack of capacity in the science shops, however, resulted in the power (current) supply not being constructed in time for field evaluation of the injection or its aftermath. Measurements were made at the Cambridge site before and following the injection using commercially available equipment.

1.5 The history of the project

This project started as a joint part of a shallow fracture injection experiment in a sandpit site in Cambridge, Ontario in spring 1995. The purpose of this experiment from an ERT viewpoint was first to check if ERT is capable of detecting and monitoring the injection process, and second to evaluate the commercially available equipment for monitoring. Also, it was important to check the combined ERT-hydrogeological model comparison to field measurements. At the first stage, two monitoring wells and one injection well with PVC casing were installed in the site. The injection well casing did not have sufficient

strength, and exploded during the first injection attempt. There was another injection attempt where an accident happened to the injection equipment and pipes. The last attempt was set for January 19,1996. 6000 liters of fresh water (EC of 950 mS/cm) followed by 5000 liters of artificial slurry (fine sand, gel, salt, water) were injected into the ground in less than one hour.

The fine-grained sand that was the simulated waste in this injection clogged the injection casing perforations and slurry injection was stopped. Since the fluid part of the slurry had high electrical conductivity, it provided on opportunity to watch the plume creation through the ERT technique. The ERT data were collected before the injection and at one week following the injection for different current electrode combinations with two commercial resistivity meters.

The first instrument was an Androtex resistivity meter. This resistivity meter could not detect potential voltages below 20 mVolts. After a survey of available resistivity meters, a Syscal Junior II was rented and the last injection episode was monitored using this resistivity meter.

Since this measurement was fully manual it was a very slow procedure to obtain data. In addition, the performance of the Syscal Junior II resistivity meter was checked in a set of both field and laboratory measurements. The test results showed a zero-base drift in the measurement and also some unexplained behavior that could not be corrected. The requirement for a new measuring system became obvious.

The receiver of new ERT measuring system was designed. The transmitter for the ERT system (with desired specifications) was requested from the Science Faculty electronic shop of the University of Waterloo. Because of some problems (high voltage and current, safety, current regulator problems...), the first version of the transmitter was only finished in May 1998. Because of a voltage offset, no current regulation, 30% noise involvement in high voltages, and automation deficiency, the transmitter was returned to the electronic shop for modification and is not yet completed (May 1999).

The designed receiver was built. The capability of the new receiver for current setup is for 256 single-ended measurements, but the switching board used is built only for 64 signal inputs. The receiver was lab tested for internal noise and 64-single-ended-electrode measurements.

The last issue looked at was the electrode configuration. The adjoint sensitivity analysis approach was implemented in SALTFLOW and partially in FRAC3DVS groundwater models.

1.6 Explanation of each chapter

This thesis has eight chapters. Chapter 1 introduces the problem and presents the contribution of this work to the problem. Chapter 2 discusses the theory of 3-D resistivity, describes the forward model, discusses commercially available equipment, and explains the theory of sensitivity and error analysis. At the end it presents the description of test site. The modification of the forward model is presented in Chapter 3. Chapter 4 is devoted to the new ERT measuring system. The field experiment, made with one of the commercial resistivity meters, is described in Chapter 5. The results of the field experiment, sensitivity and error analysis, and laboratory testing of the new ERT system are presented in Chapter 6. In Chapter 7, the accomplishment of this research is compared with the objectives of the project. Finally, Chapter 8 gives recommendations for future work.

The Appendices found after the main text present:

- A review of the literature on ERT;
- An analytical solution for a cylindrical case of Laplace's Equation;
- An equipment evaluation and the specifications of the devices, components and softwares used in the ERT system;
- The Cambridge experiment preliminary results;
- Results of new ERT system evaluation and calibration;
- Input data file listings to FRAC3DVS and SALTFLOW models to simulate the Cambridge experiment;
- A glossary of terms used in this document;
- Logs of wells at Cambridge site; and,
- ERT Model Calibration.

Chapter 2
BACKGROUND

2. Background

This chapter has six major sections, which are:

i. Theory;
ii. Modeling;
iii. Equipment;
iv. Uncertainty and error analysis;
v. Slurry injection; and
vi. Field site.

These sections present the background of the thesis research.

2.1 Theory

The theory of the three-dimensional electrical resistivity method has been presented in several publications (*Dey and Morrison,* 1979a & b; *Scriba,* 1981; *Wurmstich and Morgan,* 1994; *Zhang et al.,* 1995; *Spitzer,* 1995). The following section presents a brief description of the theory behind the ERT method.

2.1.1 Basic theory

The distribution of electrical potential V within an inhomogeneous anisotropic conducting medium through which a steady current passes is given by Poisson's equation:

$$\nabla.(\sigma \nabla V) = 0 \qquad (2\text{-}1)$$

where σ is the electrical conductivity of the medium and $\rho = (1/\sigma)$. According to the continuity equation:

$$\nabla . \mathbf{J} + \frac{\partial \rho}{\partial t} = 0 \qquad (2\text{-}2)$$

For a steady state condition:

$$\frac{\partial \rho}{\partial t} = 0 \qquad (2\text{-}3)$$

therefore:

$$\nabla . \mathbf{J} = 0 \qquad (2\text{-}4)$$

The current density, J and the electric field E are related through Ohm's law:

$$\mathbf{J} = \sigma \mathbf{E} \qquad (2\text{-}5)$$

where E is in volts/meter and σ is the conductivity of the (assumed isotropic) medium. The formation electrical conductivity also may be approximated through Archie's Law, which is written as:

$$\sigma_t = a \sigma_w \Phi^n S_w^n \qquad (2\text{-}6)$$

where σ_t and σ_w are effective formation and pore water electrical conductivity respectively;

Φ^n is porosity;

S_w^n is pore water saturation; and,

a, m and n are empirically determined constants taken as $0.5 < a < 2.5$, $1.3 < m < 2.5$ and $n \sim 2$.

The ratio of σ_w/σ_t is called the formation factor (*Reynolds*, 1998).

The electric field is the gradient of a scalar potential (a voltage field):

$$\mathbf{E} = -\nabla V \qquad (2\text{-}7)$$

Then:

$$\mathbf{J} = -\sigma \nabla V \tag{2-7}$$

and:

$$\nabla . \mathbf{J} = \nabla . (\sigma \nabla V) = 0 \tag{2-8}$$

By expanding the divergence for inhomogeneous isotropic conductivity, we get:

$$\nabla \sigma . \nabla V + \sigma \nabla^2 V = 0 \tag{2-9}$$

If the conductivity is uniform and isotropic, then equation (2-9) reduces to Laplace's equation:

$$\nabla^2 V = 0 \tag{2-10}$$

There are two basic approaches to solving these equations in electrical impedance tomography: numerical methods and analytical methods. Among the numerical methods used are the popular finite-element (FEM) and finite-difference (FDM) methods. In principle, boundary element methods could also be used. Analytic methods attempt to find general solutions of these equations (2-1 and 2-3) and then extract a particular solution that satisfies specified boundary conditions (Appendix B). For a laboratory setup with a uniform geometry (or in cases of extreme geometrical symmetry and constant electrical properties), it is possible to solve the governing equation analytically (*Wait*, 1982).

The solution in the Appendices is included to show that for any analytical solution of the governing equations (Equation 2-10), it is necessary to make some assumptions. Furthermore, these assumptions may be far removed from any real case encountered in the field. Ideally, for an analytical solution, a coordinate system is chosen in which the boundary conditions can be expressed simply. Often, this means that only a two-dimensional problem or axi-symmetric problem with homogeneous resistivity can be solved, and often a simple solution cannot be found.

Ideally, a coordinate system is chosen in which the boundary conditions can be expressed simply. Often, this means that only a two-dimensional problem or axi-symmetric problem with homogeneous resistivity can be solved, and often a simple solution cannot be found.

Finding analytic solutions for Poisson's equation is generally much more difficult. Solutions are sometimes possible if the region being investigated can be divided into a small number of regions within which conductivity is uniform and therefore within which Laplace's equation holds. Then the effect of these regions can be summed.

2.1.2 Boundary conditions

The determination of appropriate boundary conditions to obtain a unique and physically reasonable solution for Poisson's (or Laplace's) equation may exist inside the bounded region. Physical experience leads us to believe that specification of the potentials on a closed surface (e.g., a system of conductors held at different potentials) defines a unique potential field within the surface for a given resistivity distribution. This is called a Dirichlet problem, or a Dirichlet boundary condition. Similarly, it is plausible that specification of the electric field (normal derivative or flux of the potential) on the entire surface (corresponding to a given surface-charge density) also defines a unique potential field within the surface for a given resistivity distribution. Specification of the normal derivative (flux) is known as the Neumann boundary condition.

2.2 Modeling

Because steady-state groundwater and direct electrical current flow obey the same governing equations (Figure 2.1), it has been possible to make use of the modeling expertise and software in the groundwater modeling group at the University of Waterloo to experiment with three-dimensional ERT monitoring scenarios.

2.2.1 Forward model description

The SALTFLOW computer program (*Frind and Molson*, 1993) is a finite element model based on the solution to the 3-D saturated density-dependent groundwater flow equation and on the 3-D advection-dispersion equation. These equations are:

$$\frac{\partial}{\partial x_i}\left[K_{ij}\left(\frac{\partial \psi}{\partial x_i}+\rho_r \bar{n}_j\right)\right]-\sum_{k=1}^{N} Q_k(t)\,\delta(x_k,y_k,z_k)=S_s\frac{\partial \psi}{\partial t} \qquad (2\text{-}11)$$

where x_i are the 3-D spatial co-ordinates, K_{ij} (T) is the hydraulic conductivity, Ψ is the equivalent freshwater head, ρ_r (T) is the concentration-dependent relative density of water, Q_k is the fluid volume flux for a source or sink located at (x_k, y_k, z_k), S_S is specific storage, and:

$$\frac{\partial}{\partial x_i}\left[\left(\frac{D_{ij}}{R}\right)\frac{\partial c}{\partial x_i}\right]-\frac{\partial}{\partial x_i}\left(\frac{v_i}{R}c\right)-\lambda c+\sum_{k=1}^{N}\frac{Q_k(t)c_k(t)}{R\theta}\delta\left(x_k', y_k', z_k'\right)=\frac{\partial c}{\partial t} \tag{2-12}$$

where D_{ij} is the hydrodynamic dispersion tensor; v_i is the average linear groundwater velocity; c_k is the source concentration for an injection well; c is the unknown aquifer concentration; λ is the first-order decay term given as ln(2)/half-life time; R is the retardation factor defined as $1 + \rho_b K_d/\theta$, where ρ_b is bulk density of saturated porous medium; K_d is the distribution coefficient that governs the partitioning of solute into dissolved and absorbed phases (*Freeze and Cherry* 1979), and θ is the porosity. An adaptation of the symmetric matrix time-integration scheme of *Leismann and Frind* (1989) has been employed in conjunction with a standard Galerkin finite element method.

The *Leismann/Frind* scheme has been tested in generating a symmetric coefficient matrix for the transport problem (*Frind and Molson*, 1993). The coefficient matrix is solved using a preconditioned conjugate gradient (PCG) solution for symmetric matrices (*Schmid and Braoss*, 1988).

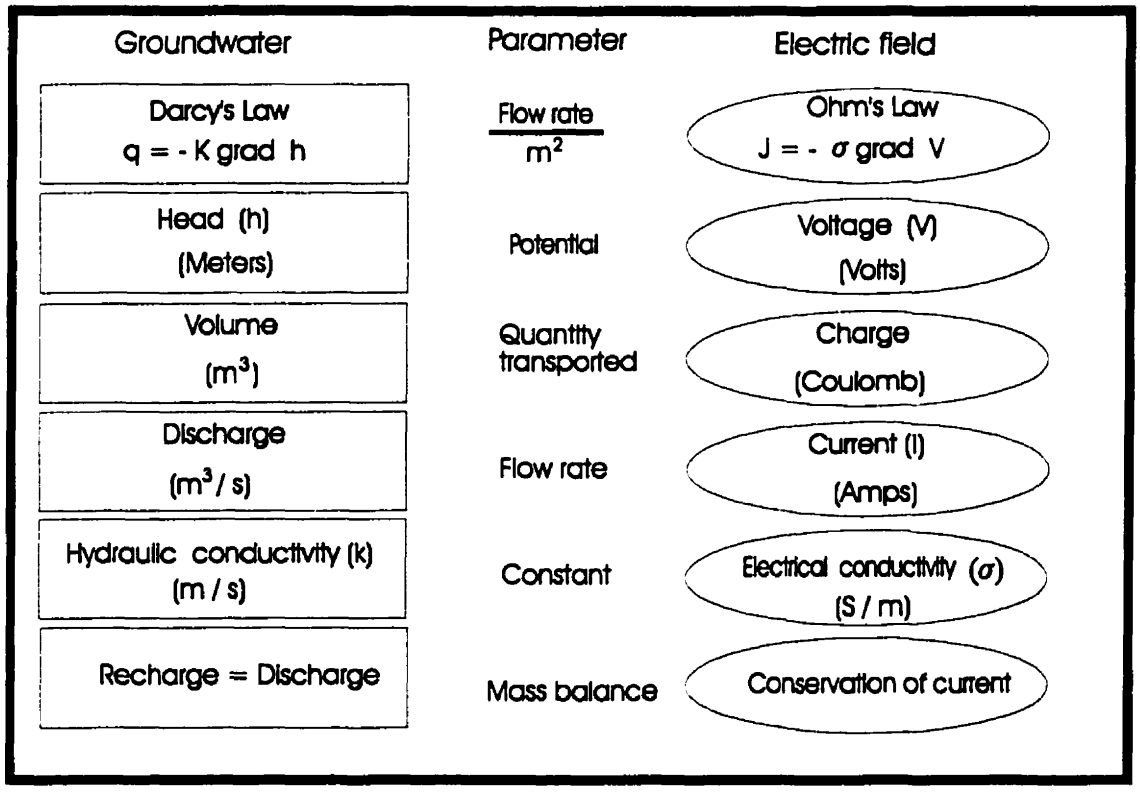


Figure 2.1 Groundwater and electrical field equivalent relationships

The SALTFOW software (*Frind and Molson*, 1993) is a 3-D finite element program that has been used to experiment with three-dimensional ERT monitoring scenarios as a forward model. This software initially was validated, verified, and used for the Camp Borden Site (*Frind and Molson*, 1989), and it has been verified in several case studies (*Molson et al.*, 1992; *Engesgaard et. al.*, 1996; *Molson et al.*, 1997; *Engesgaard and Molson*, 1998; *Ghassemi et al.*, 1998a & b).

The model verification for ERT scenarios was performed in several comparisons of the model results with analytical solutions available in the literature. An Appendix (Appendix J) is provided containing comparisons of the model with the following analytical solutions:

1. A one-layer case analytical solution, and
2. A three-layer case analytical solution with a vertical barrier in the center of two current electrodes (*Telford et al.*, 1993).

2.3 Equipment

2.3.1 Commercial

Commercial resistivity systems are designed mostly for a four-electrode measurement that is for a measurement cycle involving two current electrodes and two potential electrodes. Commercial systems which were evaluated before the Cambridge preliminary experiment in June 1995 are listed in Appendix C. The updated version of this evaluation has been presented in Table C-1 of Appendix C.

Two commercial resistivity meters were tested for the Cambridge slurry injection experiment. The results of lab tests (Appendix C) indicated that the two commercial receivers tested did not operate to their own specifications. The average error detected was 5% compared to a 0.1% claimed error. The manufacturers were informed but no explanation was given for the performance detected.

In addition, an increasing zero-base drift was detected for a set of repeated measurements (Figure C.1). These difficulties, along with lack of repeatability, the need for a higher accuracy, and particularly a need for higher sampling speed (the devices had only manual switching), made usage of conventional resistivity meters impractical in the long term injection monitoring. However, as this area is of substantial interest and the instrumentation field is rapidly growing, manufacturers will overcome these instrument deficiencies in the next few years.

2.3.2 Requirements for an ERT system

The requirements of ERT measurement depend on the type of project. If the volume to be imaged is small, and the duration of the monitor is short, then the (generally light weight and portable) commercial instruments will do the job. But in the case of a long term monitoring project, portability is not a big issue but automation and speed are.

The requirements of a superior ERT monitoring systems can be divided into three major categories: transmitter (power supply), receiver (acquisition), and cables.

In general, the major issues in the design of a transmitter are flexibility of the system in programming, achieving a large dynamic range of input/output, capability for real time measurements, user friendly interfaces, repeatability, and accuracy. The requirements

can be summarized as: a large dynamic range of voltage and current; a high current delivery; no safety earth pole in the circuit connected to the ground; and an output range of low frequency square wave (not greater than 100 Hz).

The specifications of the receiver can be listed as follow:

i. Repeatability and accuracy;
ii. Large dynamic input range;
iii. Flexibility in modifications (such as programming, filtering, electrode arrangement, increasing the number of system inputs);
iv. Detection of anomalous readings (for example, as a result of problem with connections);
v. Ability to measure the contact resistance at all the electrodes;
vi. Correction for the SP dc offset due to natural and/or electrode contact potentials;
vii. Ability to perform quality control on the data and the system itself during the measurements (i.e., visual presentation of results in each steps);
viii. Ability to monitor processes in real time (by mean of rapid sampling);
ix. Ability to handle a large number of electrodes in a single measurement;
x. Synchronization of data collection;
xi. Ability to carry out statistical measurements (e.g. to evaluate the signal to noise ratio); and,
xii. Ability to measure background potentials and to stack the data the same way as the time the current is passing through for evaluation of environmental noise level.

There is always noise and cross-talk in wide spread. Shielded cables to the electrodes are very helpful in reducing the signal/noise ratio.

The monitoring process often needs a real time set of data collection. This is only feasible by having a computerized ERT system so that both the power supply and the data acquisition are controlled by software. The computerized ERT system is described in Chapter 4.

2.3.3 Other systems under development

There are a few research groups working on the design and improvement of resistivity systems for ERT measurement. At least one, the geophysics group at the Lawrence

Livermore Laboratory, has achieved a practical system. Some of the publications introducing these resistivity systems are listed in Table A-9 in Appendix A.

2.4 Uncertainty and error analysis

In experimental measurements the accuracy of the results is always a concern. In any experiment designed to measure the physical parameters of a system, there is interference between the experimental device and the system. Even with careful scientific methodology, these measurements are always subject to some degree of uncertainty. Uncertainty and error analysis involve the study, evaluation, and prediction of these uncertainties, based on observation of the scattering in the raw data used in calculating the results, and the selection of proper procedures to reduce the errors in these results. In fact, one of the essential ingredients in the planning, controlling, and reporting of experiments is uncertainty and error analysis (*Kline*, 1985b). The following sections are descriptions of the theory applied to our data. The data itself will be presented in Chapter 6.

2.4.1 The uncertainty concept

Since there is no perfectly accurate measurement, it is necessary to define inaccuracies or uncertainties. The description of inaccuracy is made by following a procedure called uncertainty or error analysis. This analysis is a vital part of any scientific experiment.

An uncertainty is slightly different from an error. The difference between the true value and the recorded or measured value is a fixed number, termed error. It cannot be a statistical variable as well. An uncertainty is a possible value that the error might take in a given measurement (*Kline*, 1985a). Since this value can vary over a range, it is inherently a statistical variable. In fact, uncertainty is frequently linked to the statistical treatment of the data.

Uncertainty analysis is the heart of quality control in experimental work. Uncertainty analysis is not a replacement for calibration, cross-checking, closures using governing equations, nor for careful technique. Nor is it a substitution for understanding the problem. In fact, uncertainty analysis could be defined in two statements:

i. It is a procedure that provides a framework inside which the checks just mentioned as well as other information can be used much more effectively; and,

ii. It is a powerful cross-checking procedure for ensuring that requisite accuracy is actually obtained with minimum cost and time (*Kline*, 1985a).

The major sources of uncertainty derive from the fact that all the input parameters that determine the response have themselves different degrees of uncertainty. A second source of uncertainty is the fact that it is not possible to consider all the parameters involved in the system. A third source is our incomplete knowledge of the phenomenon and the system. One can add a fourth source of uncertainty, namely the mathematical simplification necessary in order to obtain a solution (*Renon*, 1988).

The introduction of computers with large memories and fast computation time allows the use of accurate models for many cases. As a result, the uncertainty involved in the computation is due mainly to the uncertainties of the inputs of the computational model. The uncertainties of the input parameters are usually the measured (experimental) uncertainties. Uncertainty analysis in this area is defined as the analysis of the effect of the uncertainties involved in all stages of calculations of the model responses.

Several methods are available to deal with uncertainty calculations. The most popular methods are based on surface methodology, perturbation theory, or sensitivity analysis. The most effective way to treat the problem of calculating the uncertainties in the responses due to uncertainties of the input parameters is to use a quantitative uncertainty analysis based on sensitivity analysis.

2.4.2 Sensitivity analysis for evaluation of uncertainty

Sensitivity is a measure of the effect of a given input parameter on a required response. The sensitivity is also defined as the first order derivative of the response change with respect to an input parameter change. For a given response $R(\alpha_1, \ldots, \alpha_n)$ and an input parameter α_k (k=1, ..., n), where n is the number of parameters, the sensitivity S_k is defined as:

$$S_k = \frac{dR}{d\alpha_k} \tag{2-13}$$

or non-dimensionally (normalized) as:

$$S_k = \frac{dR/R}{d\alpha_k/\alpha_k} \tag{2-14}$$

These expressions are for linear systems and are known as linear sensitivities. For non-linear problems higher order sensitivities are required (*Renon*, 1988).

It is usual to define the sensitivity in relative terms that present the importance of the input parameter in a normalized form. The higher the sensitivity, the more important the parameter. Therefore, one of the major aspects of sensitivity analysis is to determine the most important input parameter. Identification of the most important parameter is also used for uncertainty analysis. The sensitivities and variance-covariance matrices are the main ingredients of the uncertainty analysis based on sensitivity analysis.

In general, there are three major advantages to sensitivity methods:

i. The identification of the important input parameters;
ii. The simplicity or complexity of the method used to evaluate the response uncertainty; and,
iii. The ease of calculation of the sensitivity for any changes in the uncertainty of the input parameter after the first calculation.

There are also several potential disadvantages or limitations to sensitivity analysis approaches:

i. It is difficult to obtain sensitivities in cases of small values for input parameters; and,
ii. Non-linearity of the problem causes difficulties in the local derivative analysis i.e. change in α_k may result in change in S_k.

The following are the major methods of uncertainty analysis:

i. Adjoint sensitivity analysis;
ii. Latin hypercube;
iii. Moment method;
iv. Monte Carlo method;
v. Perturbation theory; and,
vi. Taylor's Series expansion.

The adjoint sensitivity analysis approach is the most effective method for our purposes where there are a large number of input parameters.

2.4.3 Adjoint sensitivity analysis

Adjoint sensitivity analysis has been applied to evaluate uncertainty in nuclear waste repository analysis (*Renon et al.*, 1980; *Thomas*, 1982), electrical engineering (*Direct and Rohrar*, 1969), nuclear reactor assessments (*Lewins* 1964; *Oblow*, 1978), history matching of petroleum reservoirs (*Chavent et al.*, 1975; *Dogru* and *Seifield*, 1981), and parameter estimation for groundwater flow (*Vemeiri and Karplus*, 1969; *McElwee et al.*, 1978; *Neuman*, 1980 a & b; *McElwee*, 1982). *Sykes et al.* (1985) applied adjoint sensitivity analysis to a 2-D steady-state groundwater flow system. They developed adjoint sensitivity theory for both continuous and discrete (numerical) equations of 2-D steady-state flow regimes in a confined aquifer. They used the Galerkin finite element method to implement the adjoint solution. This solution has been developed for performance measures of piezometric head and velocity.

Since steady-state groundwater and direct electric current flow obey the same governing equations, it has been possible to extend Sykes and his colleagues' procedure to evaluate the uncertainty involved in the ERT problem. The following equation is based largely on the methodology described by *Sykes et al.* (1985).

Governing equations

The governing equations for a 3-D electric field are:

$$\nabla.\mathbf{J} = \nabla.(\sigma\nabla\mathbf{V}) = 0 \qquad (2\text{-}15)$$

or :

$$\nabla.\mathbf{J} = \frac{\partial}{\partial x_i}\left[b\sigma_{i,j}\frac{\partial V}{\partial x_j}\right] + I = 0 \qquad i,j=1,2,3 \qquad (2\text{-}16)$$

which has been presented in Section 2.1 of this document. The boundary conditions have been defined as:

$$V(\Gamma_1) = \hat{V} \qquad \text{on } \Gamma_1 \quad \text{at } \infty \quad \hat{V} = 0 \qquad (2\text{-}17)$$

$$J_i(\Gamma_2)\, n_i = \hat{J} \qquad \text{on } \Gamma_2 \qquad (2\text{-}18)$$

where $\Gamma_1 + \Gamma_2 = \Gamma$ is the boundary of the domain governed by Equation (2-16), and components n_i are the unit inward normal .

For sensitivity analysis, it is necessary to define a response function (R), which in this case can be written as:

$$R = \int_{v} f(\{\alpha\}, V)\, dv \tag{2-19}$$

$f(\{\alpha\}, V)$	is a unspecified function of the system state;
$\{\alpha\}$	is system parameters;
V	is electric potentials; and,
v	is the spatial domain volume v.

The system parameters $\{\alpha\}$ are electric conductivity (σ_{ij}), formation thickness (b), induced electric current (I), voltage on boundary ($\hat{V}$), and current density normal to the boundary ($\hat{J}$). For the ERT case $f(\{\alpha\}, V)$ has the following form:

$$f(\{\alpha\}, V) = g(\mathbf{x})\, V(\mathbf{x}) \tag{2-20}$$

where $\mathbf{x} = \{x_1, x_3, x_3\}$ and $g(\mathbf{x})$ is an arbitrary weighting function for identification of the region of importance.

The marginal sensitivity of the performance measure R was defined as changes in any of system parameters as $dR/d\alpha_k$. Considering the definition of R, equation (2-19), marginal sensitivity becomes:

$$\frac{dR}{d\alpha_k} = \int_{v} \left[\frac{\partial f(\{\alpha\}, V)}{\partial \alpha_k} + \frac{\partial f(\{\alpha\}, V)}{\partial V} \psi \right] dv \tag{2-21}$$

ψ is $dV/d\alpha_k$, the sensitivity of electric potential (V) to the system parameter α_k and has been defined as the "state sensitivity". The first term of the integral in equation (2-21) represents a so-called "direct effect", indicating the explicit dependence of R on α_k; and the second term is called an "indirect effect" due to the implicit dependence of R on α_k.

Several methods are available to perform this calculation but the most efficient and cost effective method is the adjoint sensitivity analysis method, which is less time consuming and easier to implement.

In the adjoint sensitivity analysis approach, an arbitrary function (ψ^*), which is called an adjoint state or importance function, is chosen to replace the unknown "state sensitivity" (ψ). The new function (ψ^*) has to be calculated only once for any given response function (R) and $f(\{\alpha\},V)$. This procedure reduces the multiple solutions that are required for calculating the "state sensitivity" (ψ).

The ERT system becomes a linear system of equations when a discrete numerical technique is used to solve the governing equation (2-16, 2-17, and 2-18):

$$[A]\{V\} = \{b\} \tag{2-22}$$

where [A] is the coefficient matrix;

$\{V\}$ is the unknown electric potentials or solution vector; and,

$\{b\}$ is the right hand side (RHS) or forcing vector, usually a vector of measurements.

Following the same procedure as Sykes and his colleagues (1985), the adjoint equation for ERT is:

$$[A\{\alpha\}]^T\{\psi^*\} = \frac{\partial R(\{\alpha\},\{V\})}{\partial\{V\}} \tag{2-23}$$

where $\{\psi^*\}$ represents the nodal values of the adjoint state.

After a few mathematical operations, the marginal sensitivity becomes:

$$\frac{dR}{d\alpha_k} = \frac{\partial R(\{\alpha\},\{V\})}{\partial\alpha_k} + \{\psi^*\}^T\left(\frac{\partial\{b(\{\alpha\})\}}{\partial\alpha_k} - \frac{\partial[A\{\alpha\}]}{\partial\alpha_k}\{V\}\right) \tag{2-24}$$

The procedure to obtain $dR/d\alpha_k$ (the marginal sensitivity) can be summarized in the following steps:

i. Use the forward model to obtain {V};

ii. Solve the adjoint equation to obtain $\{\psi^*\}$;

iii. Determine $\partial\{b\}/\partial\alpha_k$ and $\partial[A]/\partial\alpha_k$; and ,

iv. Calculate $\partial R/\partial\alpha_k$ based on the obtained results in steps 1 to 3 for each α_k.

Since the ERT system has been solved by the discretized numerical technique (Galerkin finite element method), the voltage must be calculated for specific nodal points p, within the domain, and the arbitrary weighting function $g(\mathbf{x})$ is defined as:

$$g(\mathbf{x}) = \delta(\mathbf{x} - \mathbf{x}_p) \tag{2-25}$$

then:

$$f(\{\alpha\},\{\mathrm{V}\}) = \sum_p \left[V(\mathbf{x}_p)\delta(\mathbf{x} - \mathbf{x}_p)\right] \tag{2-26}$$

Therefore, the response function R becomes:

$$R = \{\mathrm{g}\}^{\mathrm{T}}\{\mathrm{V}\} \tag{2-27}$$

where,

g_i=1 at node points p; and,

g_i=0 at all other points.

Then:

$$\frac{\partial R}{\partial\{V\}} = \{\mathrm{g}\} \tag{2-28}$$

and:

$$\frac{\partial R}{\partial\alpha_k} = \frac{\partial\{\mathrm{g}\}^{\mathrm{T}}}{\partial\alpha_k}\{V\} = 0 \tag{2-29}$$

Since $\partial g_i/\partial\alpha_k = 0$, the adjoint equation therefore becomes:

$$[\mathrm{A}]^{\mathrm{T}}\{\psi^*\} = \{g\} \tag{2-30}$$

Solving this equation will yield the values of $\{\psi^*\}$, with the unit of T/L^2. By introducing 1% perturbation on one of the system parameters (α_k), the values for $\partial\{b\}/\partial\alpha_k$ and $\partial[A]/\partial\alpha_k$ will be available. After all the results are calculated, the marginal sensitivity can be determined. Using SALTFLOW as the forward model, this procedure has been implemented in the computer code to calculate the sensitivity automatically.

2.4.4 Measurement errors

Since there is an experimental section in this research, an error evaluation will contribute to a better understanding of the results. The following section explains the theory behind the error evaluation of the experimental part of this research. The results of this error evaluation are presented in Chapter 6.

All measurements have errors, which represent the differences between the measurements and the true values. The total error (δ_k) can be divided into two components:

i. Precision error ε_k (random); and,
ii. Bias error β (fixed)

where;

$$\delta_k = \beta + \varepsilon_k \tag{2-31}$$

The main sources of measurement errors are calibration errors, data acquisition errors, and data reduction errors (*Benedict et al.*, 1986).

Precision error

Random errors always occur in repeated measurements, and may arise from various sources. These types of errors are called precision errors and the standard deviation (σ) is a measure of the distribution of the precision errors. The precision index, which is the statistical estimate of the standard deviation (σ_n), is defined as:

$$\sigma_n = \left[\frac{\sum_{k=1}^{N} \left(X_k - \overline{X}\right)^2}{N-1} \right]^{1/2} = \left[\frac{\sum_{k=1}^{N} X_k^2 - \frac{\left(\sum_{k=1}^{N} X_k\right)^2}{N}}{N-1} \right]^{1/2} \quad (2\text{-}32)$$

where N is the number of measurements made and $\overline{X}$ is the average value of the measurements X_k given by (*Benedict et al.*, 1986):

$$\overline{X} = \frac{1}{N} \sum_{k=1}^{N} X_k \quad (2\text{-}33)$$

Bias Error

Bias error is another term for systematic errors that are constant over the duration of an experiment. Bias errors include those which are:

i. Known and can be calibrated out;
ii. Negligible and are ignored; and,
iii. Estimated and are included in uncertainty analysis (*Benedict et al.*, 1986).

Combining errors

Precision and bias errors have calibration, data acquisition, and data reduction error components. Some combination of these components can also be considered as another parameter for error analysis (*Benedict et al.*, 1986).

2.4.5 Uncertainty of measurements

The first step in the process of uncertainty analysis of a measurement is to identify and qualify all the elemental sources of errors such as bias and precision errors. The second step is the combination of these errors to obtain the bias limit (an upper limit of the bias error) and the precision index. The final step is the estimation of the degree of freedom of the precision index of the measurement (*Benedict et al.*, 1986).

For simplicity of presentation, a single number (U), which is the combination of bias and precision error, is often evaluated to express a reasonable limit of error in the measurement. This interval can be expressed as:

$$\overline{X} \pm U \tag{2-34}$$

which represents the expected band width within which the true value may lie (*Benedict et al.* 1986).

2.5 Slurry injection

Conventionally, low and intermediate toxicity wastes that cannot be reused or recycled are placed in landfills. Problems of landfill siting and maintenance have made alternate methods attractive. One of these methods is deep Slurry Fracture Injection (SFI), where wastes are slurried and injected at very high pressures into horizontally stratified sediments of high porosity and permeability that are bounded by low permeability formations. Typically, a slurry will contain 65-85% liquid by volume and 35-15% granular solid wastes. As injection takes place, excess fluid flows into the surrounding pore space. When injection stops, the weight of the overburden will reduce the granular solid waste porosity to perhaps 35%; as a result further water is expelled. Figure 2.2 depicts the phenomena.

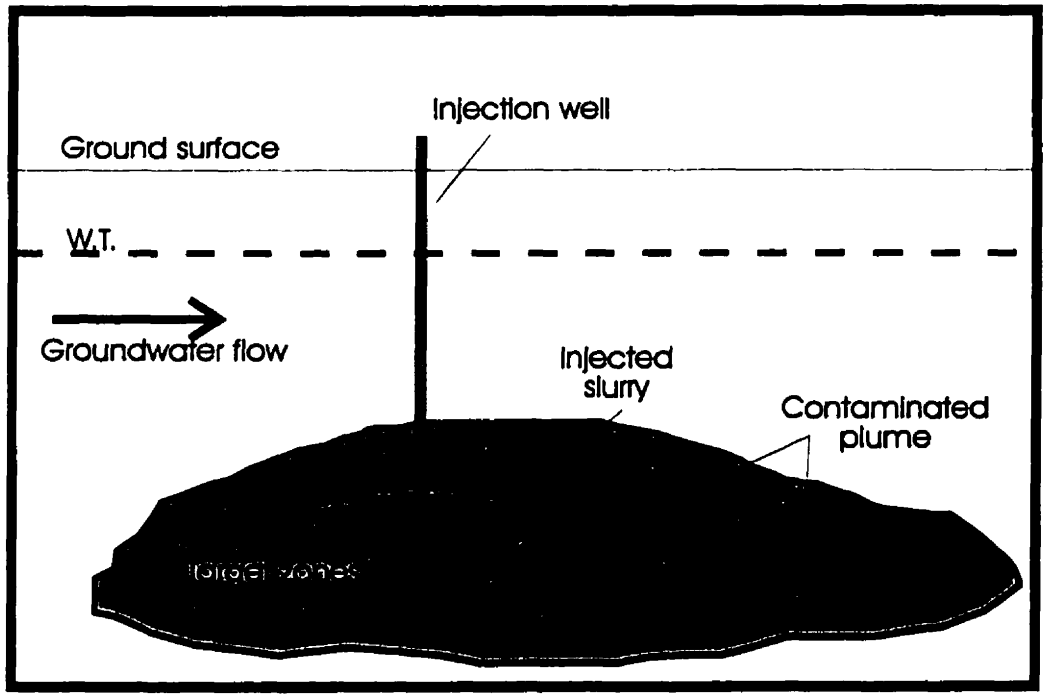


Figure 2.2 Shallow waste injection

The injected solids remain near the wellbore as the excess fluid bleeds off, creating a plume of higher resistivity if the conductivity of the injected fluid is less than the conductivity of the original fluid in the host rock. For environmental security and for regulatory reasons, SFI processes must be monitored, and it is here that geophysical techniques such as ERT may be useful. Current electrodes placed in or near the injected mass will create the possibility for generation of electrical potentials that will be modified through time by changes in the slurry or plume configuration.

2.6 Field site

2.6.1 Description

The sandpit site is at Lot 24, Concession 10, Road 47 in the Township of North Dumfries, approximately 40 km south of Kitchener-Waterloo and 10 km west of Cambridge, Ontario (Figure 2.3). This site is an active sand and gravel quarry located in the Paris Till Moraine, a 6-km wide moraine stretching 120 km from the Forks of the Credit in the north-east to Delhi in the south-west (*Chapman and Putnam*, 1984). Lenses of loose loam inside the coarse grain outwash outcrop in the excavated quarry.

Four 16.75 m monitoring wells with 2.5 inch diameter PVC casing and one 13.2 m injection well with 2 inch steel casing were drilled near the bottom of a gently sloping field (Figure 2.4). The samples collected during the well drillings have been used to depict the stratigraphy of Figure 2.5 (logs of injection and monitoring wells are presented in Appendix I). The monitoring wells were back-filled with native sand below a depth of about 9 meters, and the rest was filled with cement grout. A Grade 3 sand filter was used to back fill around the perforated part of the injection well casing below 11 meters (to ease off the flow of injected solution to the aquifer), and a 1m-bentonite filling was placed between the filter and the sealing cement which has been injected from 10m depth to the surface. The purpose of using bentonite and cement grouting was to prevent the possibility of flow of injected material to the surface. The monitoring wells were also used for our geophysical measurements.

The aquifer in this site is a thick, non-uniform clean sandy-gravel glacial outwash that is covered by a 1.7m silty-clay soil layer. The water table is at 16.0m depth and groundwater movement is toward the west. The groundwater electrical conductivity of the site is about 600 μS/cm.

The induction well log indicated that the conductivities of unsaturated and saturated zones were about 4 and 9 mS/m respectively. The neutron log of the south-eastern well showed that the cement grouting was not complete (*Gilson*, 1996).

The hydraulic conductivity of the injection level was measured in the lab (5.2×10^{-4} m/s) using disturbed samples and also in the field (9.4×10^{-4} to 10.4×10^{-4} m/s) using the Hvorslev technique (*Reed*, 1996).

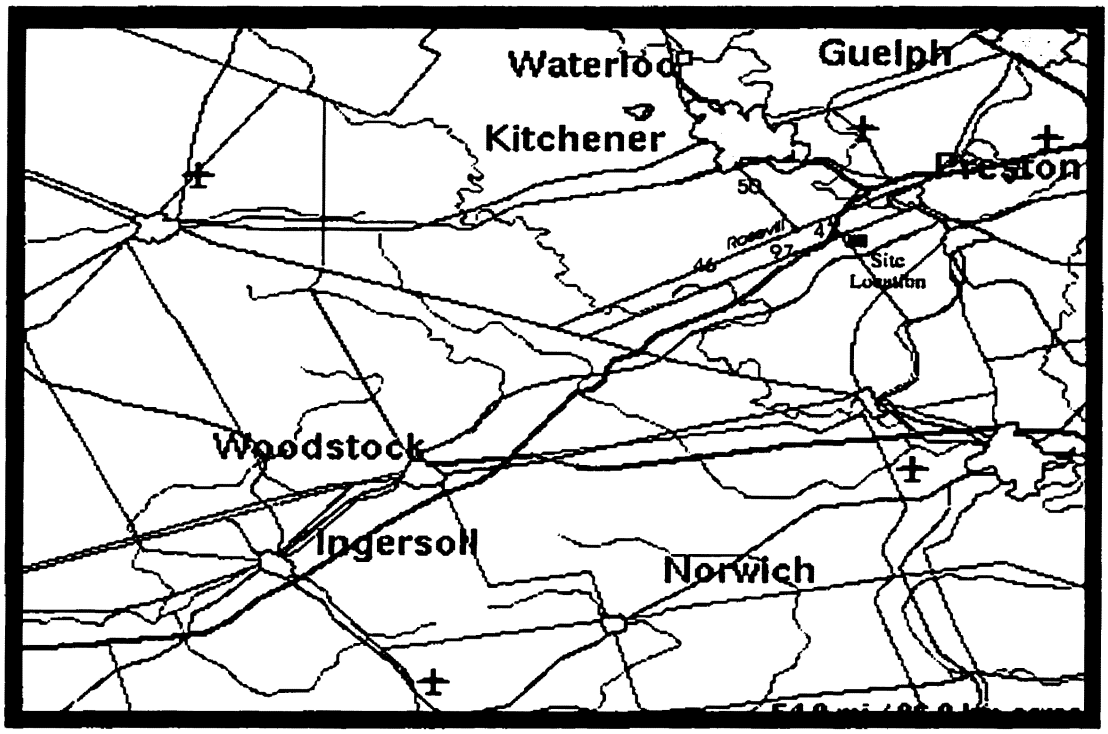


Figure 2.3 Site location map

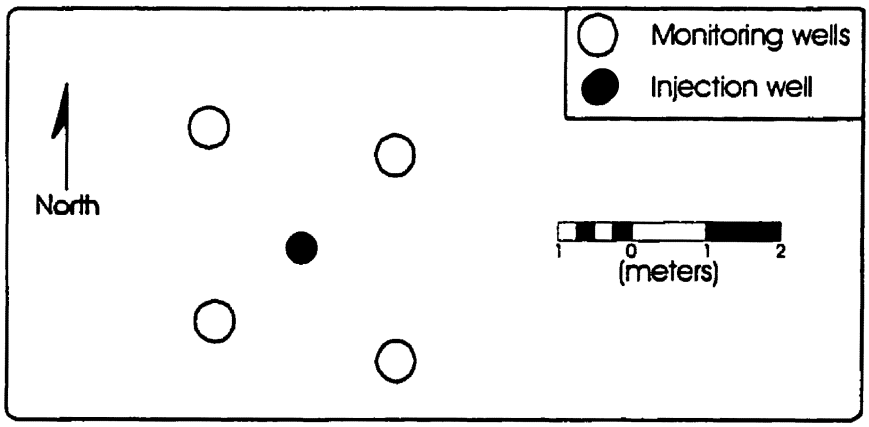


Figure 2.4 Schematic plan view of installed wells in the Cambridge site

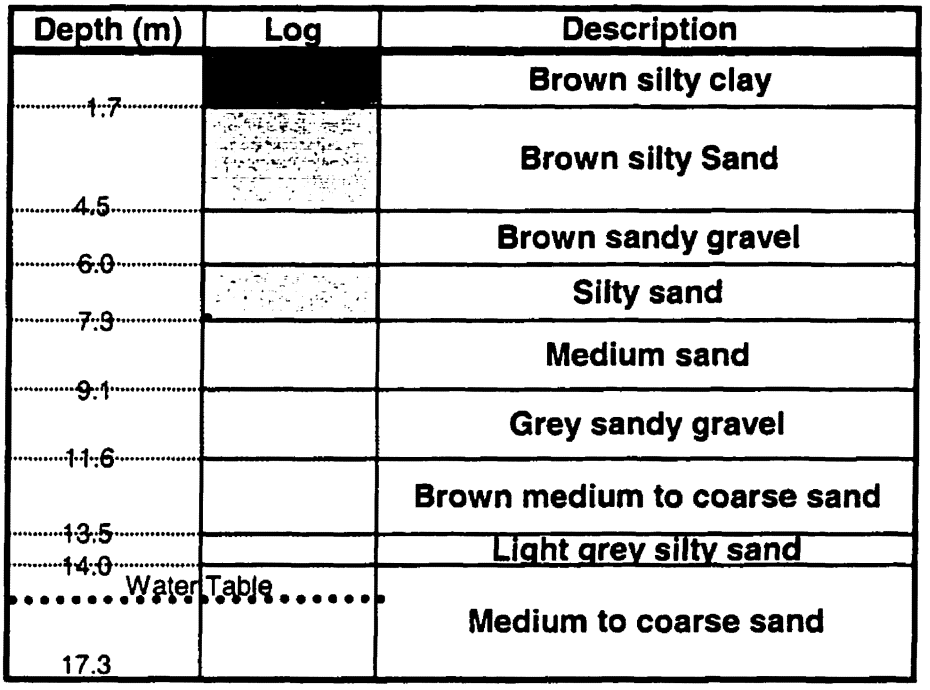


Figure 2.5 Stratigraphy of drilled layers at Cambridge site

Chapter 3

MODIFICATIONS TO THE FORWARD MODEL

3. Modification to the forward model

The resistivity image reconstruction in ERT involves a forward and an inverse problem. The forward problem is solving for the electric potential distribution based on a known resistivity distribution. The inverse part tries to find out the resistivity distribution based on measured electric potentials in or around for the region of interest. Solution of the inverse problem involves a numerical approach, using iterative solutions of the forward model. Therefore, any increase in the speed of convergence in the forward model will exponentially reduce the time required for inverse solution. The fast ERT model (inverse and forward) is required especially for monitoring the progress of real-time phenomena.

SALTFLOW and FRAC3DVS (Therrien et al., 1998) are the computer programs that were used as the forward models in this research. The solver of SALTFLOW is based on conjugate gradient method with natural ordering, and FRAC3DVS uses WATSOLV (VanderKwaak et al., 1998) as the matrix solver, which is set for a combination of Bi-conjugate gradient stabilized and reverse Cuthill-McKee ordering. These two programs are set for transient flow condition and their solvers work well for that condition. A comparison of different combinations of iterative methods and ordering techniques is required to determine the optimized combination steady-state flow condition, which is equivalent to electric potential. Therefore, the FORTRAN codes for

some of the iterative methods and ordering techniques were added to the WATSOLV computer code to improve the ability of this solver to perform the required combinational comparisons. The following sections present a brief description of the matrix solver techniques, different approaches for increasing the convergence speed of the forward model, and the results of the implementation of these techniques in the solver computer program.

Discretization of Equation (2-12) under steady-state conditions leads to a system of linear algebraic equations of the form:

$$\mathbf{A}\,\mathbf{x} = \mathbf{b} \tag{3-1}$$

where $\mathbf{A}$ is the coefficient matrix;
$\mathbf{x}$ is the unknown (solution) vector; and,
$\mathbf{b}$ is the forcing vector or the right hand side (RHS).

The coefficient matrix $\mathbf{A}$ is usually sparse. This means that most of its entries are zeros, i.e., for a given N by N matrix (N is the number of unknowns), which has α non-zero entries per row, the sparsity (S) can be defined as:

$$S = \frac{\alpha}{N} \tag{3-2}$$

ERT problems usually are faced with a coefficient matrix size bigger than 10^4. Depending on the discretization method used, the number α varies. For example, in a 3-D finite element model with rectangles, $\alpha = 27$, and in the case of triangles, $\alpha = 7$.

All numerical approaches to solving the 3-D governing equations of the electric field must eventually deal with the solution of a coefficient matrix A. In general, this matrix has the following properties:

i. $A_{jj} > 0$ for j=1,2,3, ..., LMN;
ii. Diagonally dominant,

$$\mathbf{A}j,j \geq \sum_{\substack{j=1 \\ k \neq j}}^{LMN} |\mathbf{A}j,k| \qquad \text{for} \quad j = 1,2,3, \quad , LMN \tag{3-3}$$

iii. Symmetric, positive definite (most of the time), sparse banded matrix.

This type of matrix is called an M-matrix. Generally, there are two classes of numerical methods for solving sparse matrices:

i. Direct methods (such as Gaussian-elimination, LU decomposition, Gauss-Jordan elimination, Cholesky); and,
ii. Iterative methods.

Some solutions may combine the two methods to get a better result. In the direct methods, a sequence of operations is performed only once, providing a solution that is exact except for machine round-off error. Iterative methods attempt a solution by a process of successive approximation. They involve making an initial guess at the matrix solution, then improving this guess by some iterative process until an error criterion is attained. Therefore, in iterative methods, the convergence and its rate are the main points of concern.

3.1 Comparison of iterative and direct methods

A typical iterative method involves the initial selection of an approximate value $x^{(1)}$ to x and specifying a sequence $x^{(2)}$, $x^{(3)}$, ... such that;

$$\lim_{i \to \infty} x^{(i)} = x \tag{3-4}$$

Usually the calculation of $x^{(i+1)}$ involves only **A** and **b**, and one or two of the previous iteration values. Assuming infinite precision arithmetic, the solution only approximates the exact solution within a given tolerance in a finite number of iterations. On the other hand, the direct methods reach an exact solution, which is obtained in a finite number of iterations.

Direct methods have two disadvantages:

i. Dealing with storage requirements and computation time for large systems of equation is much more complex than for iterative methods; and,

ii. Dealing with round-off errors is more time consuming than the one for iterative methods. Because many arithmetic operations are performed, round-off errors can be accumulated for certain types of matrices.

The advantages of direct methods are:

i. The sequence of operations is performed only once;
ii. No initial estimates are required;
iii. No iteration parameters are required; and...
iv. No error tolerance is needed as an input parameter.

The direct methods are usually applied to dense matrices (few zero entries) and intermediate-size sparse matrices (less than 10^4).

The main weakness of iterative methods is their poor robustness and often narrow range of applicability. Often, a particular iterative solver may be found to be very efficient for a specific class of problems, but when used for other cases it becomes excessively slow or breaks down. Preconditioned iterative methods, which are based on an approximate factorization, can be considered as a compromise between direct and iterative solvers. In general, advantages and disadvantages of iterative methods can be classified as:

Advantages:

i. Efficiency in term of storage and computation time for large problems;

Disadvantages:

i. Required iteration parameters;
ii. Required tolerance; and,
iii. Required well-conditioned matrix.

In many cases exact solutions are not necessary or even achievable for either method; also, there are uncertainties involved in the input parameters. Iterative methods achieve almost the same results as direct methods, but with the exception of less requirements of storage and operation time. In addition, with proper preconditioning and acceleration approaches, iterative methods can be faster. Ordering methods and termination criteria of iterative techniques play important roles in speed and accuracy of obtained results (*Duff et al.*, 1986; *Saad*, 1996).

3.2 Ordering methods

Rearranging the rows or columns or both the rows and columns of a sparse matrix is called ordering (or reordering). The permutation matrix resulting from reordering can be represented compactly as an ordering vector.

Often, ordering is beneficial for approximation factorization. Ordering methods have two major purposes:

i. Mesh generation leads to scattered entries in the coefficient matrix. In general, a better preconditioner can be obtained using reordering of initial entries (i.e., keeping the important fill).
ii. Higher quality preconditioning is provided.

The following are the most popular ordering methods:

i. Natural (consecutive numbering by rows and columns);
ii. Nested-dissection;
iii. Minimum degree; and,
iv. RCM (Reverse Cuthill-McKee).

3.2.1 Nested-dissection ordering method

The nested-dissection ordering method attempts to minimize the numbers of fill-in during elimination and to reduce the amount of storage required. The procedure is to divide the elements into four groups with a "+" shaped cut, then divide each group into four parts again with a "+" shaped cut and so on. George (1973) has shown that a two-dimensional problem consisting of a regular n x n grid of square elements could be solved in $O(n^3)$ operations and $O(n^2 \log n)$ storage locations instead of $O(n^4)$ and $O(n^3)$, respectively. The main advantages of this method are the increase in convergence speed due to fewer operations and smaller memory requirements (*George et al.*, in press).

3.2.2 Minimum degree ordering method

The minimum degree ordering algorithm was introduced for symmetric and positive definite matrices (*Tinney* and *Walker*, 1967). This simplifies two things. It is not necessary to carry numerical values to check for stability (since the matrix is stable) and the search for the pivot is simplified to finding i such that;

$$r_i^{(k)} = \min_t r_t^{(k)} \qquad (3\text{-}5)$$

and using $a_{ii}^{(k)}$ as pivot (*Duff et al.*, 1986).

3.2.3 Reverse Cuthill-McKee (RCM) ordering method

The most widely used reduction ordering is a variant of the Cuthill-McKee technique. The *Cuthill and McKee* (1969) technique was designed primarily to reduce the bandwidth of a sparse symmetric matrix. The scheme is presented as: let y be a labeled node, and z an unlabeled neighbor of y. To minimize the bandwidth of the row associated with z, it is apparent that the node z should be ordered as soon as possible after y. This scheme therefore reduces the bandwidth via localized minimization.

George (1970) discovered that the ordering obtained by reversing the Cuthill-McKee technique often turns out to be much superior to the original ordering in terms of profile reduction, although the bandwidth remains unchanged. He called this Reverse Cuthill-McKee ordering (RCM). It has since been proven that the reverse scheme is never inferior as far as envelope storage and operation counts are concerned (*Liu and Sherman*, 1976).

3.3 Preconditioning

Although iterative methods are theoretically well developed, they are sometimes slow in convergence. This lack of robustness has been widely recognized as a weakness of iterative methods. It is possible to improve the efficiency of iterative methods by applying preconditioning. *Saad* (1996) defines preconditioning as:

> " *... simply a means of transforming the original linear system into one which has the same solution, but which is likely to be easier to solve with an iterative solver*".

3.3.1 Preconditioned incomplete Cholesky decomposition

In this method the coefficient matrix **A** is only approximated by the preconditioner matrix **LU**. Note that each elimination step results in additional fill in, which has to be eliminated in upcoming elimination steps. Therefore, a small number of additional entries will be retained. There are two popular methods in determination of the entries that should be retained, and these are:

i. Drop tolerance based incomplete factorization method; and
ii. Level based incomplete factorization method.

3.4 Acceleration methods

The idea in acceleration methods is to speed up the convergence of the simple iterative methods:

$$LU(\mathbf{x}^{(k+1)}-\mathbf{x}^{k})=r^{k} \tag{3-6}$$

A value for $\mathbf{x}^{(k+1)}$ is obtained so that:

$$(r^{k+1},r^{k+1})=\sum_{i} i(r_i^{k+1})^2 \tag{3-7}$$

is small where,

$$r^{k+1}=\mathbf{b}-\mathbf{A}\mathbf{x}^{(k+1)} \tag{3-8}$$

Therefore, the original problem has been considered as a minimization problem $\mathbf{Ax=b}$. Now Equation (3-6) can be rewritten as:

$$\mathbf{x}^{k+1}=\mathbf{x}^{k}-(LU)^{-1}r^{k} \tag{3-9}$$

In case of optimization problems, it becomes:

$$\mathbf{x}^{k+1}=\mathbf{x}^{k}-w^{k}q^{k} \tag{3-10}$$

The new solution is updated by a factor of w^k in the search direction q^k.

The new solution is a linear combination of the initial guess and all previous search directions. It should be noted that the acceleration method for a symmetric coefficient matrix is the conjugate gradient method (CG). This method uses information obtained in previous iteration steps to minimize the residual. These methods are also called "non-stationary" methods. On the other hand, iteration methods such as Gauss-Seidel do not have this property and because of that they are relatively slow (stationary methods). The

CG method forces orthogonality of previous-to-new search vectors during each iteration, and the new search direction can be obtained by short recurrences (*Forsyth*, 1994).

3.5 Non-stationary iterative methods

The term "iterative method" refers to a wide range of techniques that use successive approximations to obtain more accurate solutions to a linear system at each step. There are two types of iterative methods. Stationary methods are older, simpler to understand and implement, but usually not as effective. Non-stationary methods are a relatively recent development; their analysis is usually harder to understand, but they can be highly effective. The non-stationary methods are based on the idea of sequences of orthogonal vectors. (An exception is the Chebyshev iteration method, which is based on orthogonal polynomials.)

The stationary iterative method performs the same operations on the current iteration vectors. In contrast, the non-stationary iterative method is an approach that has iteration-dependent coefficients. Detailed descriptions of these methods are given in most textbooks (i.e., *Axelsson*, 1994, *Duff et al.*, 1986, *Saad*, 1996, *Barrett et al.*, 1994).

The rate at which an iterative method converges depends greatly on the spectrum of the coefficient matrix. Hence, iterative methods usually involve a second matrix that transforms the coefficient matrix into one with a more favorable spectrum. The transformation matrix is called a preconditioner. A good preconditioner improves the convergence of the iterative method sufficiently to overcome the extra cost of constructing and applying the preconditioner. Indeed, without a preconditioner the iterative method may even fail to converge.

Since the ERT coefficient matrix is symmetric, non-stationary methods will give better results. Combinations of a few of these iterative methods with some of the reordering techniques are implemented in the computer program to explore the best combination of these techniques for ERT forward modeling.

3.6 Modification to the forward Model

The coefficient matrix in the ERT problem is an M-matrix (symmetric positive definite). If a preconditioned incomplete Cholesky decomposition matrix solver (ILU) is used, the running time will be reduced. In addition, using nested-dissection ordering will decrease the running time of this program and increase model efficiency. The speed of

convergence also depends on different levels of fill in. An optimal combination of preconditioning, iterative method, and reordering algorithms is necessary and is evaluated here through different combinations of:

i. Preconditioning (such as level of fill and drop tolerance);
ii. Iterative methods (such as ILU, CG, CGSTAB, GMRES); and,
iii. Ordering methods (such as natural, nested-dissection, RCM, minimum degree).

This has been implemented in the matrix solver code and results are presented in the next section.

3.6.1 Results of forward model modification

Type of preconditioning has a strong effect on the convergence of the iterative method applied in the solution of a sparse matrix. For preconditioning, an approximate (incomplete LL^t) factorization (ILL^t) may be either level based (based on the graph matrix or levels of fill) of drop tolerance based. The notation ILL^t (*level*, ε) denotes an incomplete factorization, with level *level*, and drop tolerance ε. The sequence of ordering the unknowns can also change the convergence rate. The convergence tolerance for all combinations was:

$$\frac{\|r^0\|}{\|r^k\|} < 10^{-8} \qquad (3\text{-}11)$$

where $\|r^0\|$ is the initial l_2 norm of the residual and $\|r^k\|$ is the l_2 norm residual after k^{th} iterations.

A mesh of 95 by 77 by 28 has been used for a scenario including an anomaly in the center of X-Y grids close to surface. The FRAC3DVS program was run on a Pentium II-300 with 128Mb RAM. The applied preconditions and the results are presented in Tables 3.1a to 3.1c. Computation time range from $ILL^t(0,0.0)$ to $ILL^t(2,0.0)$ decreases between $ILL^t(0,0.0)$ and $ILL^t(1,0.0)$. The use of $ILL^t(2,0.0)$ caused a reduction in the number of iterations but an increase in required time for convergence over $ILL^t(1,0.0)$. The iterations and timing for the most effective combinations are compared in Figure 3.1.

For drop tolerance preconditioning the results are presented up to $ILL^t(\infty,0.001)$ in Tables 3.2a to 3.2c. There was a shortage of memory in the computer for checking more than

that. The results show that the maximum efficiency of the model is achieved in ILL^t(∞,0.01). The timing iterations of the most effective combinations are compared in Figure 3.2.

Tables 3.1 and 3.2 show that Incomplete Cholesky-Conjugate Gradient (ICCG) method is the most efficient of the models for both level-based and drop-tolerance based preconditioning. The most efficient results were obtained by ILL^t(1,0.0) and ILL^t(∞,0.01) using the ICCG algorithm with nested dissection ordering.

Table 3.1a Results of iteration based on level of fill of ILL^t(0,0.0)

Iterative method	Ordering methods (time required in sec)			
	Natural	RCM	Min-degree	Nested-Dissection
ICCG	4506.44	4662.42	8002.41	3968.99
Bi-CGSTAB	17427.93	16383.80	17645.86	19118.69
GMRES	9893.57	9209.28	9726.86	8469.98

Table 3.1b Results of iteration based on level of fill of ILL^t(1,0.0)

Iterative method	Ordering methods (time required in sec)			
	Natural	RCM	Min-degree	Nested-Dissection
ICCG	4069.02	3865.57	6781.70	3390.85
Bi-CGSTAB	15736.28	13583.66	14954.12	16333.78
GMRES	8933.25	7635.33	8243.10	7236.21

Table 3.1c Results of iteration based on level of fill of ILL^t(2,0.0)

Iterative method	Ordering methods (time required in sec)			
	Natural	RCM	Min-degree	Nested-Dissection
ICCG	4998.11	4692.94	6629.11	4323.33
Bi-CGSTAB	19329.40	16491.04	14617.65	20825.57
GMRES	10973.01	9269.56	8057.63	9226.17

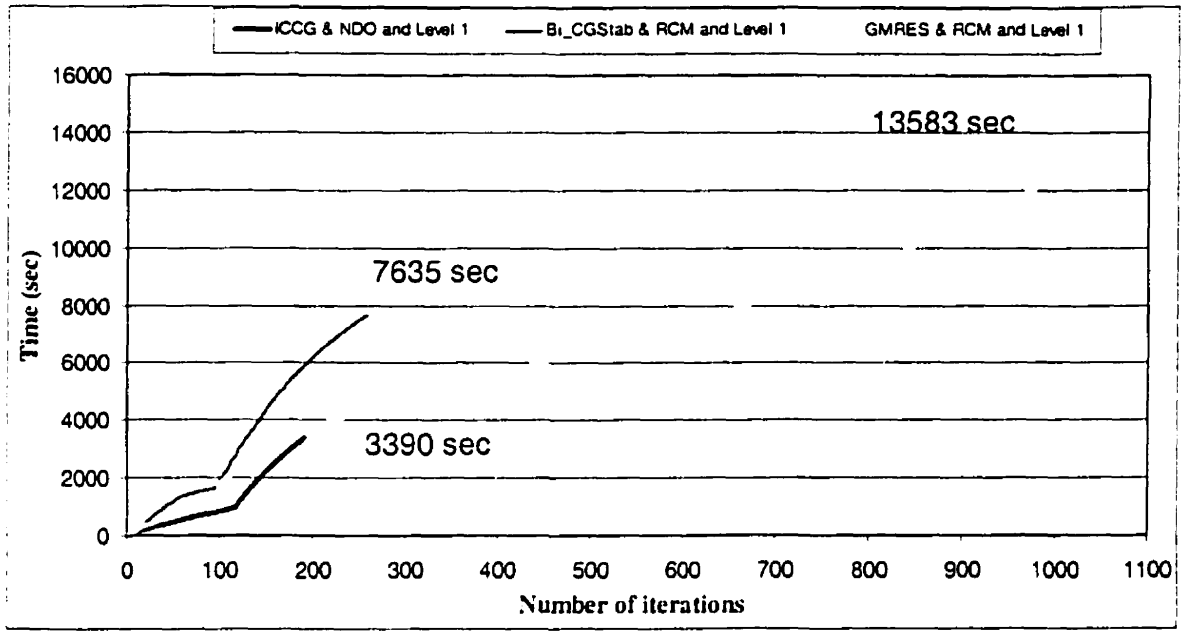


Figure 3.1 The timing-iterations required to complete a 95 by 77 by 28 grid model calculation with the most effective combinations for the levels of fill and orderings

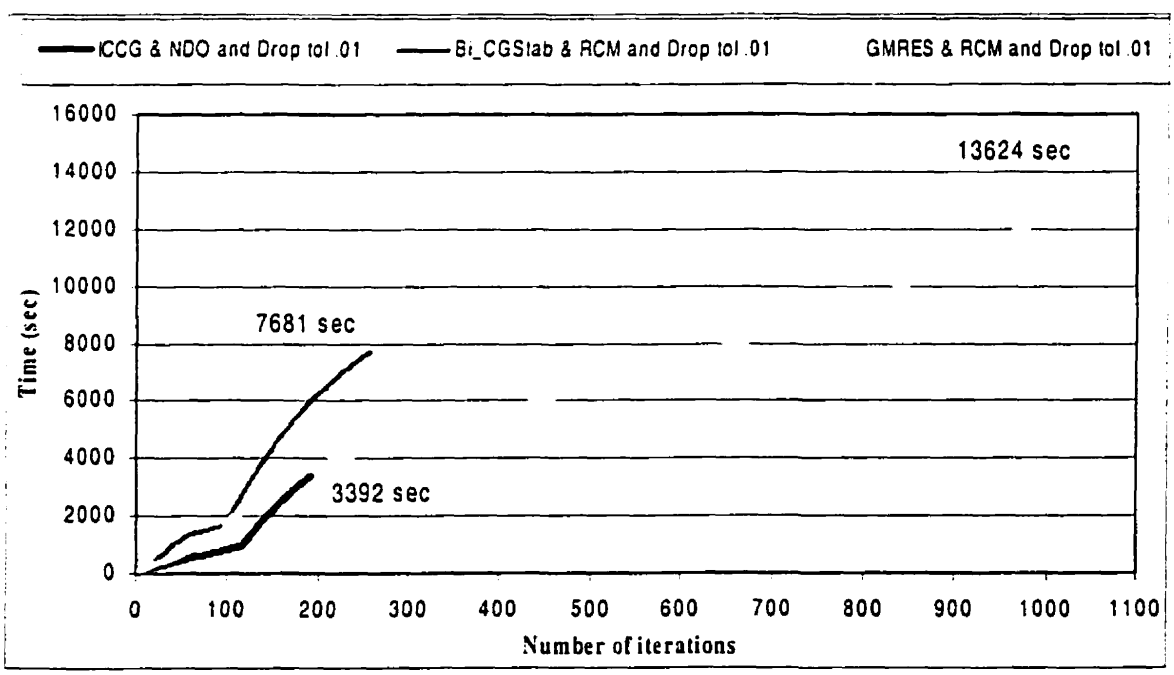


Figure 3.2 The timing-iterations required to complete a 95 by 77 by 28 grid model calculation with the most effective combinations for the drop tolerance and orderings

Table 3.2a Results of iteration based on drop tolerance of ILL^t(∞,0.1)

Iterative method	Ordering methods (time required in sec)			
	Natural	RCM	Min-degree	Nested-Dissection
ICCG	4519.96	4656.41	8011.41	3969.90
Bi-CGSTAB	17464.21	16419.95	17675.80	19158.05
GMRES	9912.26	9222.91	9743.04	8474.39

Table 3.2b Results of iteration based on drop tolerance of ILL^t(∞,0.01)

Iterative method	Ordering methods (time required in sec)			
	Natural	RCM	Min-degree	Nested-Dissection
ICCG	4086.92	3892.63	6798.65	3392.55
Bi-CGSTAB	15807.09	13624.41	15013.94	16358.28
GMRES	8977.92	7681.14	8309.04	7254.30

Table 3.2.c Results of iteration based on drop tolerance of ILL^t(∞,0.001)

Iterative method	Ordering methods (time required in sec)			
	Natural	RCM	Min-degree	Nested-Dissection
ICCG	5003.61	4696.69	6639.06	4327.66
Bi-CGSTAB	19346.79	16524.02	14635.19	20848.48
GMRES	10989.47	9292.73	8064.88	9239.08

Chapter 4

AN ELECTRICAL RESISTIVITY TOMOGRAPHY MEASURING SYSTEM

4. An electrical resistivity tomography measuring system

There are three main parts in the ERT system: data acquisition and control system (switch network and computer interface); cables; power supply; and electrodes. The author is a hydrogeologist by training and had to learn the required automation and electronics background for the data measuring system. Assuming that is also the case for most readers of this thesis, a brief discussion of the theory behind each component is presented in the early sections. The new ERT measuring system is presented in the last sections.

4.1 Data acquisition and control system (switch network and computer interface)

The data measuring system is discussed below under the headings: computer system and its interface to the measuring system, electronic switching, and the software required for these functions.

4.1.1 The computer system and interface

The computer and its interface to the geophysical data are the major parts of an automated system. The minimum requirement is not always the best choice. One should bear in mind future developments and probable requirements for extending the system.

Computer system

Data acquisition can be adequately undertaken with an 86486-50Hz processor with 16Mb RAM. The forward modeling, however, needs at least 128Mb RAM and, to allow both modeling and data acquisition to be undertaken with the same computer, the current system has been assembled with a Pentium II 300Hz PC. The specifications of the computer system are:

i. Pentium II-300Hz;
ii. 128Mb static RAM;
iii. 4Gb hard disk;
iv. 512kb cashe;
v. Windows95 operating system;
vi. Motherboard with four ISA and 3 PCI connections; and,
vii. Monitor, keyboard and mouse.

Computer interfacing

Interfacing to the computer requires the following devices:

i. A/D converter board (multifunction I/O 20 kS/s, 16-Bit, 16 analog single ended inputs);
ii. Expandable multiplexer board (multiplexing 64 single-ended/32 differential inputs);
iii. Digital output board; and,
iv. Digital input board.

The digital input and output have been modified to handle the system requirements.

A/D & multiplexer

Analog-to-digital conversion

The function of an analog-to-digital (A/D) converter is to change an analog voltage signal from a sensor to digital value so that a computer (central processing unit or CPU) can read and process it. There are three major connections to an A/D as shown in Figure 4.1.

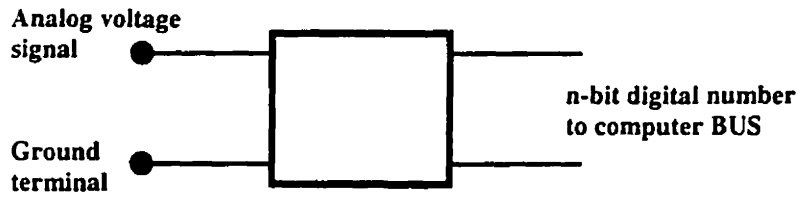


Figure 4.1 Schematic diagram of an analog-to-digital converter

This unit converts the voltage between signal and ground to an n-bit digital value. The digital value is transferred to the computer CPU. Based on the speed of the A/D and the pattern of the signal, it may measure either a single signal or, alternatively, read a series of signals to record a time-variant voltage.

The A/D converter usually has been set up to divide its input rage into discrete steps. The input voltage is measured by locating the step that contains that specific voltage. The resolution of the measured voltage is the size of the steps. The maximum number of steps can be determined by the number of output bits:

$$\text{Steps number} = 2^n \qquad (4\text{-}1)$$

where n is the number of output bits (i.e. a 16-bit A/D converter has $2^{16} = 65536$ possible states). The larger the number of output bits the finer the measurement resolution. A 16-bit a/d converter with a range of 0 to 10 volts measures with a resolution of 0.15 mV (10V/65536). Most common A/D converters used in computer interfacing have 8- and 12-bits resolution.

The size of the discrete steps is defined as one least-significant bit (LSB). The output of an A/D is delivered to the computer in the form of an integer number that is equal to the number of LSBs the input voltage is above the minimum voltage. The software converts the integer value to an octal value. The A/D converter can read very small values (i.e., voltage, current, and resistance) with a proper signal conditioning and interface-system setup.

The relationship between the input analog signal and the output digital value is called the "transfer function". The integer number delivered to the computer should be converted to a voltage using the transfer function. The transfer function is typically:

$$\text{Output number} = \frac{V_{in} - V_{min}}{V_{step}} \tag{4-2}$$

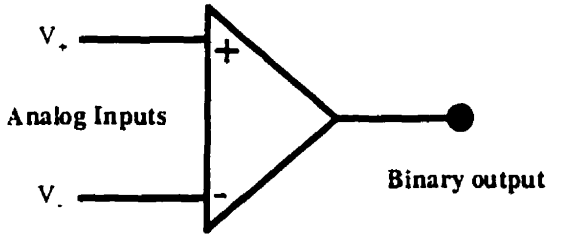
where

$$V_{step} = \frac{V_{max} - V_{min}}{2^n} \tag{4-3}$$

and V_{max} and V_{min} are the maximum and minimum input voltages respectively, and n is the number of bits.

A/D converter hardware

The main element of all A/D converters in computer interfacing is the comparator (Figure 4.2). The comparator is a simple circuit with two analog input terminals, which compares the voltage between its terminals. The single digital output goes to the high state (1) if the voltage is higher on the + terminal, and the output state is low (0) if the voltage on the – terminal is higher.



Inputs	Output
$V_+ > V_-$	1
$V_+ < V_-$	0

Figure 4.2 Schematic diagram of a comparator

There are three main types of A/D converters popular in computer interfacing applications: combinational, dual-slope and sequential. In a combinational A/D converter there is one comparator for every possible output state and it performs the conversion in a single step. Combinational A/D converters have low resolution (16 bits widely available) and high speed (in excess of 100 million samples/sec). The dual-slope A/D converters collect a very high-resolution sample by integrating the input over a short time window.

But integration reduces the speed of this type of A/D converters. A sequential A/D converter uses a single comparator in conjunction with a digital-to-analog converter (D/A) and a logic circuit and requires several steps to determine the input voltage. A popular sequential A/D converter is the successive approximation A/D converter (Figure 4.3), which has been selected for the new ERT measuring system.

The successive approximation register is a logic circuit that alters the output digital number and checks the response of the comparator output to determine if the converted output is above or below the input signal. The successive approximation method is the fastest of the sequential algorithms.

The successive approximation A/D converter divides the input range into two successive steps. The first step is to set the most significant bit of the output to one, then compare the input voltage to the D/A converter output. If the comparator shows that the input voltage is higher than the D/A converter output, the input is the upper half of the voltage range and the bit set must be changed to one. Otherwise, the input voltage is in the lower half of the input range and the bit has to be reset to zero. Then the procedure continues for the next steps until it reaches to the least-significant bit. Therefore, in n steps (where n is the number of bits of resolution) this algorithm converges to the correct digital value.

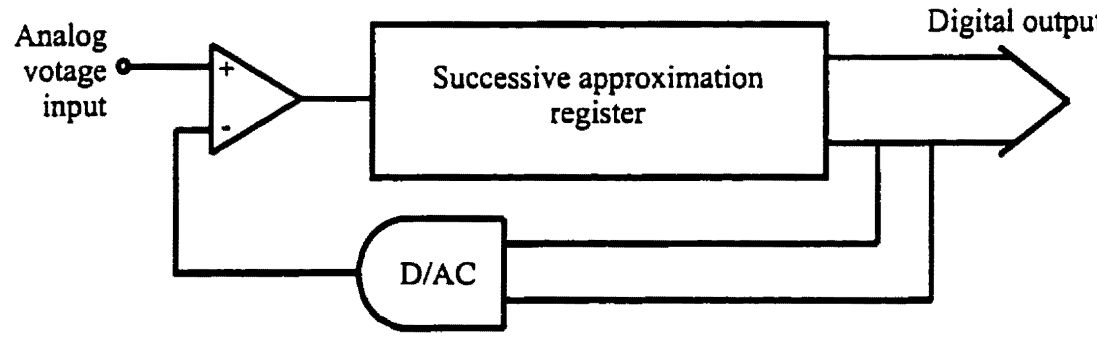


Figure 4.3 Schematic diagram of a successive approximation A/D converter

Auxiliary hardware is always required to use an A/D converter board with a computer system. This auxiliary hardware is called an analog multiplexer (AMUX) which is in fact, a computer control switch. Plug-in boards allow as many as 64 analog voltage input available for PCs. External AMUX allows a huge number of inputs to a signal A/D converter.

The analog multiplexer (AMUX) is a circuit primarily utilized to time-share a computer-input data conversion system among multiple input signals. This device selects one signal among all available signals, according to a digital code, to optimize the cost by sharing the conversion component at the multiplexer output. An AMUX consists of a switch array, usually provided in binary multiples, and connected in parallel at its output. These are bilateral devices that permit signal flow in either direction for multiplexing and demultiplexing applications. The switch-control logic is normally designed to open the switches faster than it closes them (break-before-make) to avoid shorting channels together, with only one switch closed at a time (*Garrett*, 1994). There should be a bus interface unit along with the control logic to obtain data and control words from the computer system bus. The bus interface includes an interrupt system and may also include the hardware to allow the A/D converter to transfer data via a direct memory access channel. In addition, the A/D converter needs a timing source to allow voltage measurements at precise time intervals (*Eaton & Eaton*, 1995).

The A/D converter also requires some additional hardware including:

i. One or more sample and hold amplifiers to freeze the input signal while the conversion is being done;
ii. A multiplexer to connect the A/D converter to multiple input channels;
iii. A variable gain preamplifier to allow the A/D converter to accurately measure low-level voltage signals; and,
iv. First-in-first-out (FIFO) buffer memory to temporarily store samples before they are transferred to the processor or memory (*Eaton & Eaton*, 1995).

Selection criteria

There are a large number of manufacturers building A/D converter interface boards with a wide variety of features and prices. The specifications required for a particular design should be carefully determined.

The main parameters to consider for an A/D converter selection are the following:

i. Range;
ii. Resolution;
iii. Conversion speed (sampling rate);
iv. DMA capability;

v. Number of channels;

vi. Type of input (differential or single ended);

vii. Software; and,

viii. Budget.

These parameters have been explained in most textbooks (*Cripps*, 1989; *Carr*, 1991; *Garrett*, 1994; *Eaton and Eaton*, 1995).

Considering the selection parameters and the requirement of ERT system for an A/D converter board, the AT-MIO-16XE-50x (Figure 4.4) board from National Instruments has been selected. This board is a multifunction I/O with 20 kilo-sample/s speed, 16-bit resolution and 16 analog inputs. The detailed specifications are presented in Appendix D. This board can be connected to four multiplexer boards to handle up to 256 single-ended/128 differential sensors.

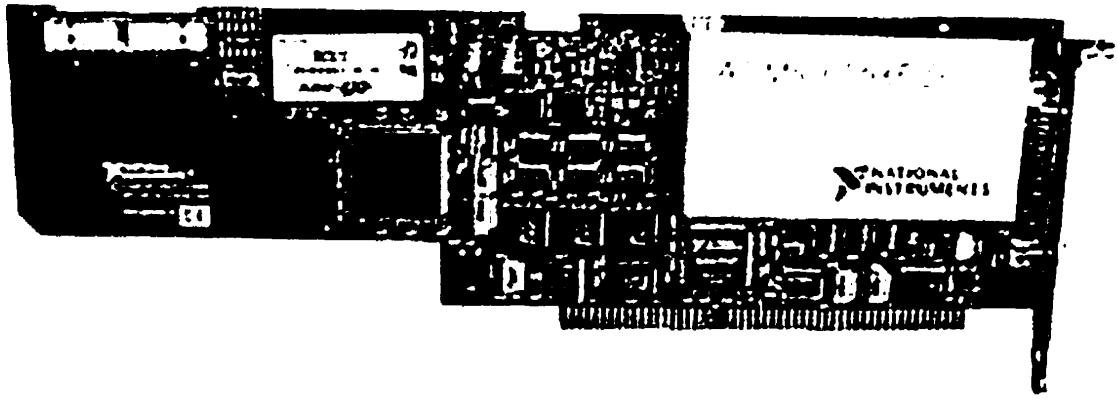


Figure 4.4 A/D used in ERT system (AT-MIO-16XE -50 from National Instruments)

The multiplexer board matched with the A/D board was an AMUX-64T (Figure 4.5) from National Instruments. This multiplexer board gives the opportunity of expanding the inputs up to 64 single-ended/32 differential inputs.

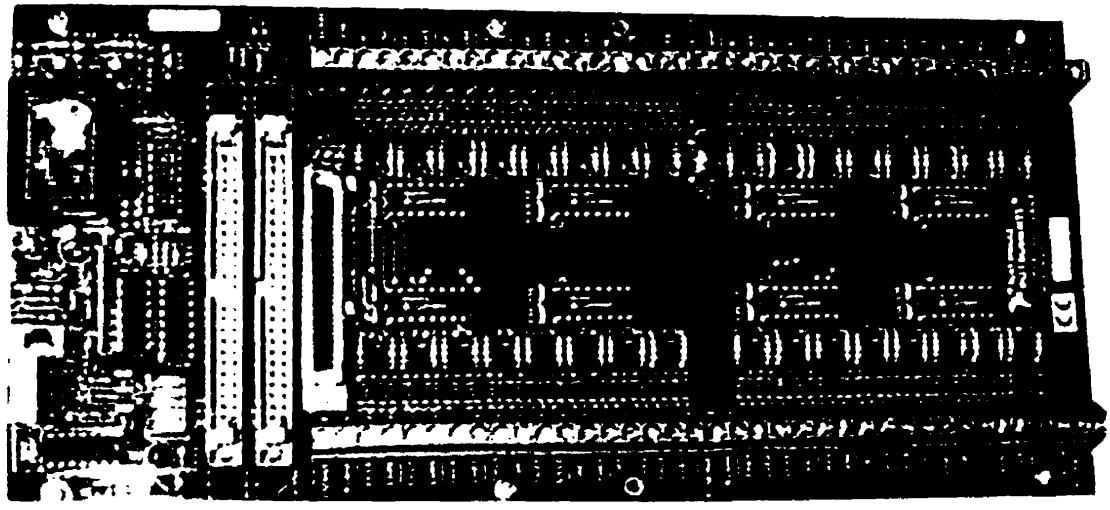


Figure 4.5 Multiplexer used in ERT system (AMUX64T from National Instruments)

Digital input/output (I/O)

Digital input/output (I/O), also called digital communication, is a signal conductor that can carry only a single bit of information at a time. The applied voltage is either low or high and is interpreted as either a 0 or a 1. An important property of digital communication links is their noise immunity. Analog links do not operate accurately in a noisy environment. On the other hand, the noise must be fairly high to affect a digital communication link where the receiver has only to differentiate between low and high voltage levels

The major digital interfacings are serial and parallel techniques. In serial interfacing, data bytes or words are disassembled into individual bits, which are sent one at a time over a single conductor (or optical) pathway. The receiving device must be able to reassemble the bits in the correct pattern in order to make sense of the data transmitted. In parallel interfacing, several bits (usually 8 or 16) are communicated simultaneously over multiple conductors. The special purpose of parallel interfacing is or high-speed communication between a device and a computer.

The parallel interface ports for computer interfacing applications use TTL (Transistor/Transistor Logic) levels for the input latches. Most digital transducers are set up to use TTL signal levels. The nominal signal levels are 0 volt for the low state and 5 volts for the high state. In a standard TTL the receiver interprets any voltage above 2.0

volts as high signal input and any voltage below 0.8 volts as low signal input (Figure 4.6). The mechanism of the TTL logic in parallel interfacing with the computer is presented in Figure 4.7.

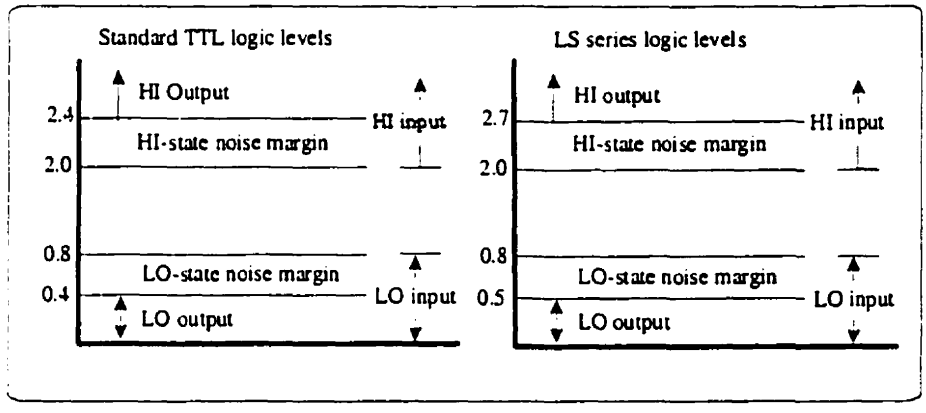


Figure 4.6 Standard TTL and LS series logic levels

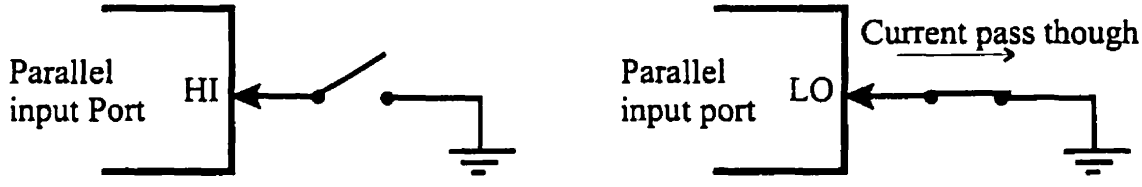


Figure 4.7 Illustration of current during input to a parallel port

The digital input and output for the ERT system have been selected from ComputerBoards Inc., based on the required output signals and the budget. The CIO-DI 192 board (Figure 4.8) is the selected digital input board and the CIO-DO 192H (Figure 4.9) is the selected digital output board. The detailed specifications of these boards are presented in Appendix D.

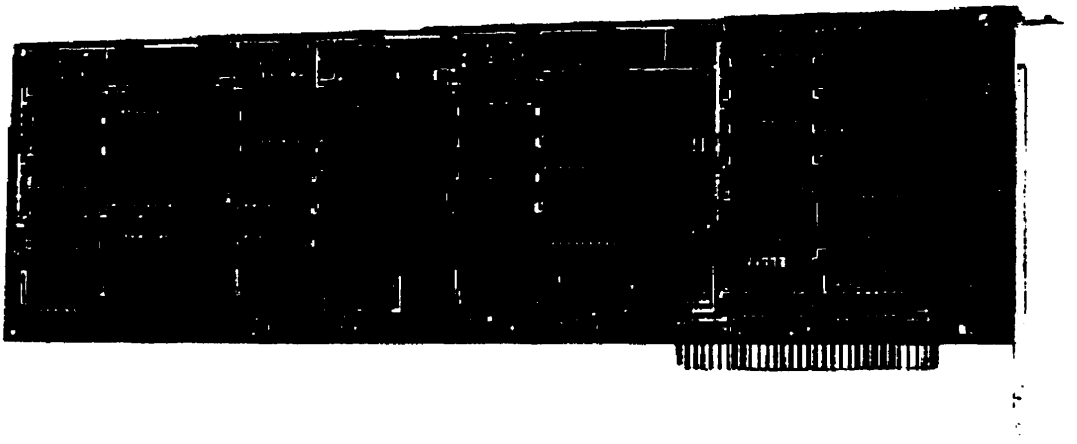


Figure 4.8 Digital output used to assemble ERT system (DO 192H from ComputerBoards Inc.)



Figure 4.9 Digital input used to assemble ERT system (DI 192 from ComputerBoards Inc.)

4.1.2 Electronic switching network

The switching network (Figure 4.10) consists of two sets of 32-input connections on two 30×30-centimeter boards. The pattern of connections is based on 16-input connections. Since the board was manually wired, two sets of 16-input were mounted on a single 30 by 30 cm bread board. The time required for switching is at most 20 msec. Most of the elements have been mounted on the board through a set of sockets, to facilitate repair and

to protect the sensitive elements from soldering heat. The schematic diagram of the switching board for one electrode is presented in Figure 4.11. This combination of elements is repeatable for as many electrodes as the computer addressing permits. The major divisions on this board are:

i. Input connectors (+5, +12, ±400 volts and ground);
ii. Output connectors (50 pine connectors to DI and DO, terminals to the AMUX, and terminals to the electrodes);
iii. Electromechanical reed relays (switching components)
iv. Protection circuit (resistive voltage divider and zener diodes); and,
v. Noise reduction technique (low pass filter).

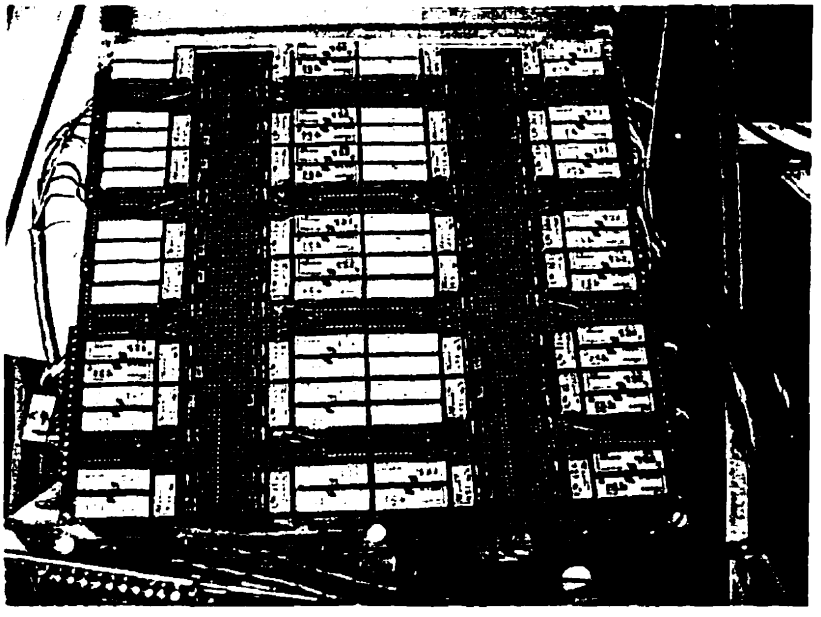


Figure 4.10 Prototype switching board and its components on a bread board

Electromechanical reed relays

A reed relay is a magnetically operated switch that is operated by a permanent magnet or a liquid-level touch electrode. The presence of strong magnetic fields, created by transformers, magnets, iron plates, etc., in close proximity to the reed relay, may cause a change of its characteristics and result in error in its operation.

Placing two or more reed relays in close proximity to one another may also cause magnetic interference between them. Adjacent relays should be spaced a minimum of 5mm from one another to eliminate such interference.

The switching components are the elements K1, K2, K3 and UA shown in Figure 4.11. The element K1 handles positive and negative currents passing to the proper electrodes. The K2 element controls the connection between the electrodes and power supply or AMUX board. The K3 component is implemented to control the requirement of resistive voltage divider whenever it is needed. Since the signals of the DO board are about 2.5 volts and the reed relays need +12 volts to switch, the UA element was implemented in the circuit to drive the transferred signals to a higher level acceptable for the reed relays. Detailed information about the switching components is presented in Appendix D. It is assumed that the signal always needs voltage protection for the safety of the interfacing boards and computer system. A set of IC sockets has been mounted on the circuit board to prevent damage from heat during soldering and also to facilitate replacement in case of malfunctioning.

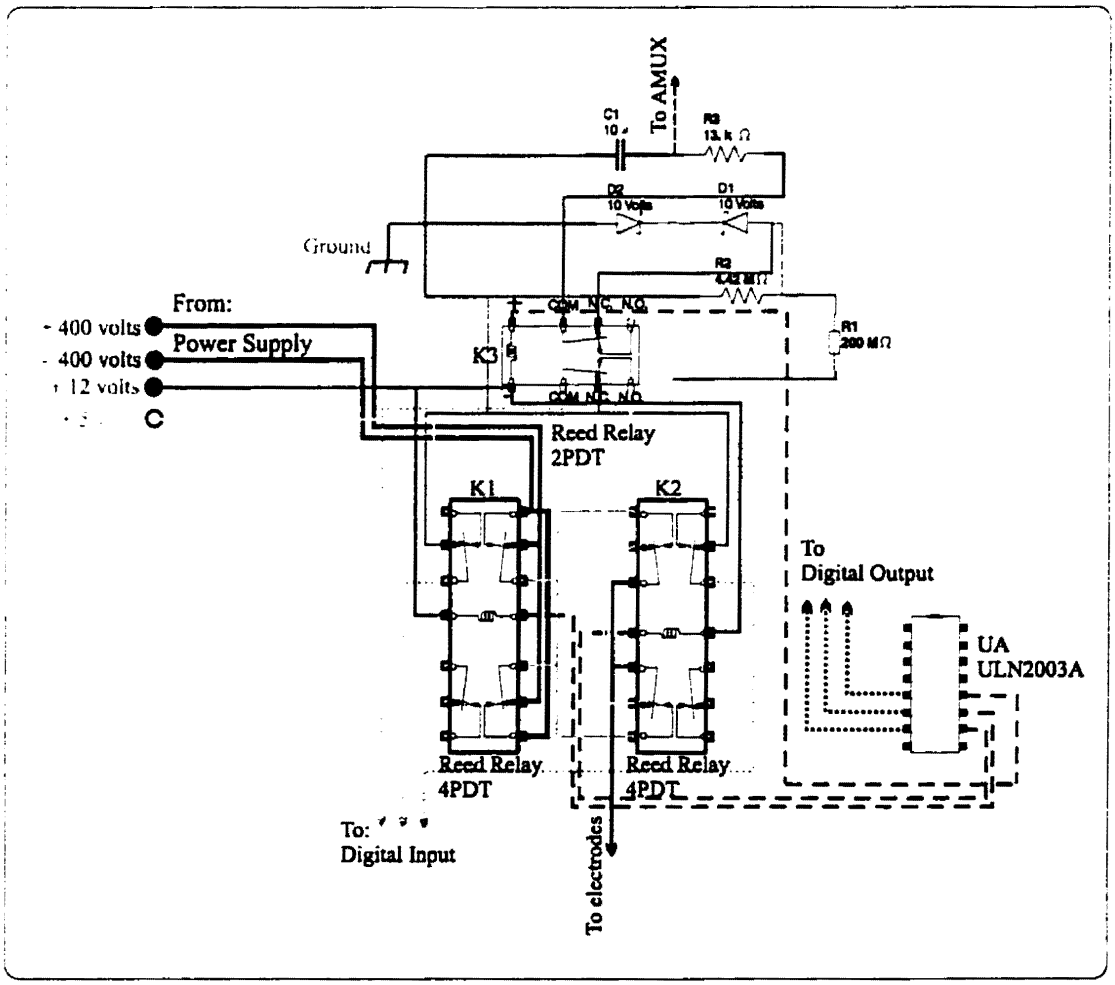


Figure 4.11 Schematic diagram of switching board components and the connections for one electrode

Assuming a 200kΩ resistor for the ground, the field-new measureing system setup can be simplified as in Figure 4.12. The internal resistor has been selected as a 200 mega-Ω resistor (±1%) so that the difference between the measured and the internal resistance is high, and the error involving in current passing through the internal resistor is negligiable. There always exists a contact resistance between the electrodes and the ground, which is usually high; in this case it is assume to be 100 kΩ.

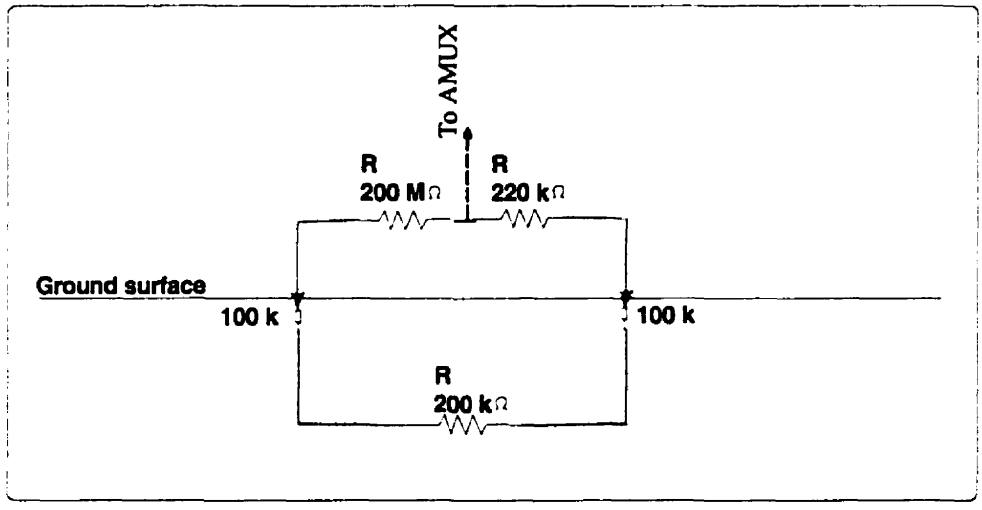


Figure 4.12 Simplified field-new measuring system circuit sketch

Protection circuit

A combination of resistor voltage divider for high level voltage (R1 and R2 elements in Figure 4.11) and zener diodes for voltage less than 10 volts (D1 and D2 elements in Figure 4.11) has been designed in the circuit board.

The zener diodes were used for the protection of A/D and AMUX boards for voltages over 10 volts. The diodes work in the reverse breakdown. Usually an individual diode works in forward bias and the reverse bias is huge. But zener diode real working region is reverse bias. A zener diode can be used as a regular diode provided the reverse bias in the circuit never reaches to the breakdown voltage. When voltage across the zener diode reaches the breakdown voltage, in theory the voltage across it would not change. However, in practice it would change a little as long as the current passing through is not larger than the power diode can dissipate. Therefore, the voltage will be constant. The circuit is used to limit the voltage so the A/D board will not be damaged. However, the design includes a resistor divider to limit the current of the zener diode with a resistive

divider so that the current is limited to the voltage across the resistor divided by the resistor. That will limit the current passing through the zener diode.

Noise reduction techniques in electronic systems

This section covers the aspects of noise suppression and control in designed system. Some of the most difficult and frustrating problems faced by design engineers concern elimination of noise from their circuits or systems. Solutions to noise problems are usually found by trial and error with little understanding of the mechanisms involved. They can be classified into two major divisions: hardware control and software control.

Hardware noise control techniques

The interference between electronic circuits can be eliminated or at least reduced by using the following primary methods:

i. Shielding;
ii. Grounding;
iii. Balancing;
iv. Filtering;
v. Isolation;
vi. Separating and orientation;
vii. Circuit impedance level control;
viii. Cable design; and,
ix. Cancellation techniques.

There is a more detailed checklist for the more commonly used noise reduction techniques in Appendix B (page 359 to 361) of *Ott* (1988) for further reference. Even with all these methods available, it should be remembered that noise usually cannot be eliminated; it can only be minimized to the point where it no longer causes interference.

Shielding

A shield is a metallic partition placed between two regions of space to control the propagation of electric and/or magnetic fields from one region to the other. The application is either for preventing the noise from interfering with measurement inside the shield or preventing a noisy source from distributing noise to the outside of the shield. There is always the possibility of interference of noise even with a shielding approach. Therefore, it is good practice to filter the noise even with a proper shielding (Figure 4.13).

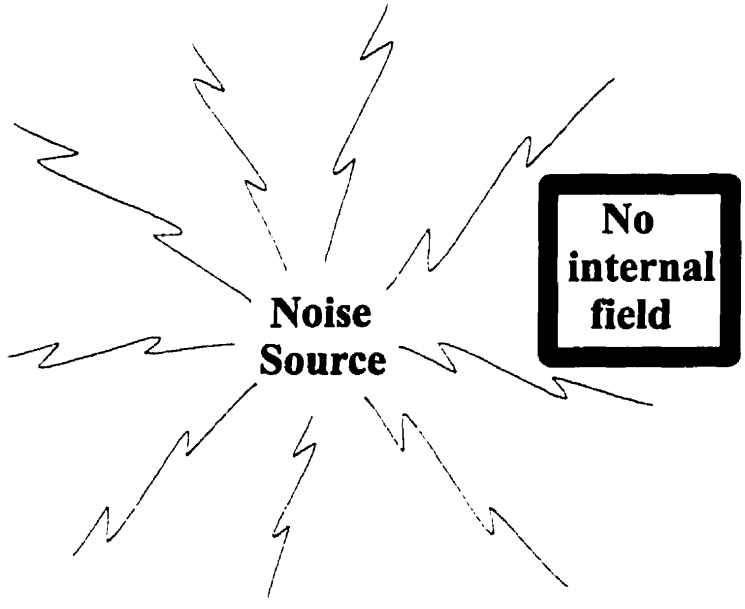


Figure 4.13 Shielding interference is prevented by placing a metal partition around the receptor to prevent noise infiltration

The switching boards have been mounted in a closed stainless steel box and all the external lines to the boards have been connected by the proper installed connectors on the outside of the box. This box is connected to the general grounding of the system to reduce the environmental noise effects.

Grounding

Grounding is one of the primary procedures to minimize the noise level. Proper use of grounding and cabling can eliminate a large percentage of the entire system noise. One of the advantages of a well-designed ground system is the protection against unwanted interference and emission.

The design of the ERT system is based on the consideration of proper grounding to reduce the intake noise as much as possible. This includes the connections, cabling, switching broads and their box, and the pulse generator.

Filters

Filters are an extremely important electronic concept and are essential in many electronic systems (such as radio, television, voice and data communications). A filter is defined as a frequency-selective network that favors certain frequencies of input signals at the expense of others. Although there are several possible types of filters, there are only three very common types of filter (Figure 4.14):

i. Low-pass filter
ii. Band-pass filter;
iii. High-pass filter.

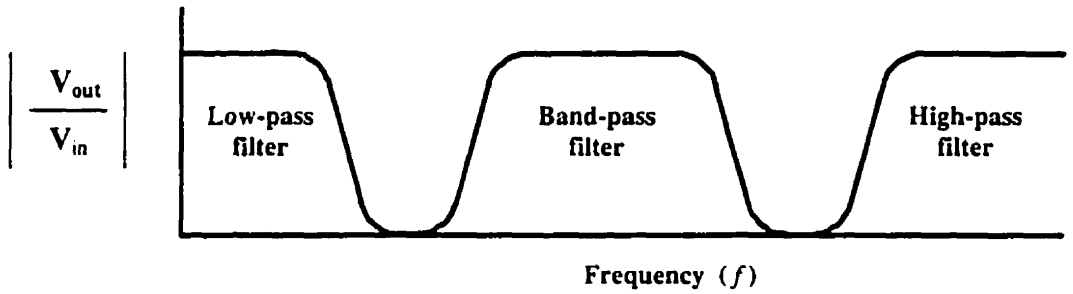


Figure 4.14 Common types of filters

A low-pass filter allows signals up to a certain maximum frequency to pass on; signals with frequencies above this cutoff frequency are rejected to a greater or lesser degree. A band-pass filter selects a range of median frequencies while attenuating or rejecting other frequencies above and below those desired. Similarly, a high-pass filter blocks frequencies below its cutoff frequency while favoring those above. The cutoff frequency is calculated from the following general equation:

$$f_c = \frac{1}{2\pi RC} \tag{4-4}$$

where f_c is the cutoff frequency, R is the resistance of the resistor applied, and C is the capacitance of the applied capacitor.

Capacitors and inductors are the main components of the filters because they are inherently frequency-dependent devices. Capacitors more easily pass high frequencies and inductors better handle lower frequencies. Filters with these types of components are

called passive filters. There is also another way to handle the filtering by using integrated circuitry. In particular, the IC op-amp combined with resistors and capacitors can perform an accurate filtering. These types of filters are called active filters because this approach usually has gain and needs some supply of power. More detailed information is available in most textbooks (*Lancaster*, 1975; *Meiksin*, 1990).

A low-pass filter was implemented in the ERT switching boards to filter the noise above the 10Hz not generated by the pulse generator. This filter is passive, and consists of a 13 kΩ (element R3 in Figure 4.11) resistor and a10 μf capacitor (element C1 in Figure 4.11).

Software noise control techniques

Signal filtering and stacking

Data sampling

A fundamental requirement of sampled-data systems is the transformation of continuous-time signals to a representative set of numbers which can be used by a digital computer. When the signal shape is known, and a relative value between the output signal and the response of the object is the one that is required, another option is to collect data synchronously and to stack that data for a period. This will reduce the noise effect and provide a value close to the real one.

Stacking procedure

A popular stacking procedure in the time-domain electrical method is obtained by subtracting the positive current results from the negative current results on a period by period basis. This approach cancels the DC offset in the measured data for steady state conditions and is called normal stacking. Let us assume a periodic waveform comprised only of odd harmonics (positive and negative portions are identical) such as a square wave (we also assume that in the received signal, steady state has been reached). Normal stacking averages the differences of plus and minus (first half and second half period) portions of a single period to produce an estimate over a single half period (note that the other half period must be the negative of that). The governing equation for stacking of one period can be shown as:

$$Y(n) = \frac{\left(x(n) - x\left(n + \frac{T_x f_s}{2} \right) \right)}{2} \qquad (4\text{-}5)$$

where

T_x is the waveform period;
f_s is the sample rate;
n is the sample number index;
$x(n)$ is the digital waveform; and,
$y(n)$ is the stacked (or filtered) waveform.

Since this method cannot eliminate linear drift, another method known as the Halverson stacking is used. Halverson stacking estimates a single half period based on a combination of 1.5 periods: for square waves this is the first 3 pulses (pos., neg., pos.). If we take the average of the start (first half) of two adjacent periods and subtract the second half-period in between, we have an estimate (twice the amplitude) of the single half-period that completely cancels the effects of linear drift. The governing equation for stacking of one period can be shown as (*Kingman*, personal communication):

$$Y(n) = \frac{(x(n) - x(n + T_x f_s))}{4} - \frac{\left(x(n) - x\left(n + \frac{T_x f_s}{2}\right)\right)}{2} \qquad (4\text{-}6)$$

4.1.3 Software

Software reliability vs hardware reliability

Modern microprocessor technology and powerful personal computers have had an enormous impact on the procedures of experimental work. In most laboratories computers control instrumentation systems. Experiment results are transferred directly to the computer for signal processing.

The experimentalist can work more conveniently with the aid of computers during testing. This removes human error in the reading and recording of data. When computers are used in data acquiring, sampling rates increase, and errors in data are reduced. The ability to process data during or immediately after collection is a great advantage because it offers the opportunity of checking the data before changing the experimental setup.

Years ago, in the dark ages of computer learning, the use of a computer was intimidating. Now the computer systems are relatively inexpensive and the software is more user friendly. Therefore, the experimentalist does not need a great deal of knowledge (electrical, hardware and software engineering) to conduct a computerized experiment. Considering the improvement in the computer interfacing programs and cheap computer

systems, it is possible for a person with general laboratory skills to set up a computerized system for experiments.

Software control systems are more dynamic and can easily be modified and adjusted to new procedures. Software development is essentially a design process. As the failure of software is always due to human errors in creating that software, it can in principle be made perfect. Good software should, theoretically, give correct output for all possible input data. For hardware systems, failures are caused by random phenomena (such as the physical aging of the product) and human design errors similar to those of software.

There are many substantial differences between software and hardware systems. Because software design is strongly influenced by its hardware counterpart, it is necessary to discuss their differences. The most significant differences between software and hardware systems that should be identified are the following.

Firstly, software has no aging property: that is, it does not age like hardware does in the sense that the failure occurrence rate changes due to unknown aging processes. Under constant testing intensity, software failure is also constant if it has not been subjected to any change. For hardware systems, failure probability usually increases, due to the wearing-out of mechanical elements. This, together with a burn-in period at the beginning for which the intensity of failure decreases, results in a bathtub-shape failure intensity function.

Secondly, once a software fault is removed from the software, it will never cause the same failure again. In fact, with enough testing effort and by a total testing of all input data that is theoretically finite due to truncation, all software faults can be detected and removed and the software is then perfect. But in practice this is impossible, since it will take millions of years even for software of moderate size. However, software reliability may be improved by increasing the testing effort and by removing detected faults. For a hardware system, reliability is usually increased by using better material, improved design, increase strength, etc.

Thirdly, copies from a software program are identical. Hence, executions of two copies will give exactly the same results. Commonly defined redundancy methodology has no meaning in studying software reliability problems and it is not an applicable tool to increase software reliability. However, software redundancy can be achieved by using

other modifications, e.g. a multi-version programming technique, but in that case the software would not be the same, and the dependency between different versions is another problem that should be considered. This may also affect the software maintenance.

Software faults have some deterministic properties. Software does not fail due to unknown reasons. In data-domain, however, an input data will either cause a failure or not, no matter when it is used because the output will not be changed. However, in the time-domain, it cannot be predicted when a software failure will occur in practice. The random nature is due to the unknown location of faults in the program and the random chosen input data.

The development of hardware reliability has a long history and there are many reliability handbooks, which can be used, both for the assessment of the reliability and for the planning of reliability tests. Methods such as fault tree analysis, failure modes and effects analysis, sneak-circuit analysis, etc., have also been developed for hardware reliability purposes.

ERT control software

Interfacing and writing the data acquisition control have been done by using LabVIEW 5.0 (National Instruments). LabVIEW is a graphical programming language for data acquisition and control, data analysis, and data presentation. With LabVIEW it is easy to control the system and present the results through interactive front panels. Using interactive front panel gives the opportunity to control the quality of collected data and remove any difficulties (such as loose connections, interruptions, and electrode contact) before and during the experiment. Since this system is mainly software control, it is very easy to modify for a new application.

The computer interface established the connection between the computer and the other parts of the instrument system as well as the connections between the computer and the user. Any computer programming language (e.g., Assembly, C, C++, Fortran, LabVIEW, Pascal, Visual Basic, etc.) would suffice for interfacing the receiver. The LabVIEW package was available in the Geomechanics Group of the University of Waterloo, and is designed for instrument-computer interfacing. The LabVIEW program is user-friendly and most of the interfacing boards have drivers ready to be used in the

interface program. The computer coding system of LabVIEW is a high-level programming language called G or Virtual Instrument (VI) and is defined as:

> *"... G is a general-purpose programming system, but it also includes libraries of functions and development tools designed specifically for data acquisition and instrument control. G programs are called virtual instruments (VIs) because their appearance and operation can imitate actual instruments. However, VIs are similar to the functions of conventional programming languages (National Instrument,* 1996*). "*

Development of virtual instruments (VI) has as objective to use a general-purpose computer to mimic real instruments with their dedicated control and displays, but with the added versatility that comes with software. Instead of buying an instrument, one may buy a high performance A/D converter and a computer running the LabVIEW program

The goal of interfacing was to give a dynamic opportunity to the user to allow easy modification of the program to suit the application. LabVIEW gives the opportunity to the programmer to explore a wide range of options for a particular use.

Figures 4.15a to 4.15d show the front panel and diagram of the virtual instrument program. There are several major selections on this panel that user should define before starting the program.

The following are the major parts:

i. Contact resistance control;
ii. Switching division; and
iii. Required input for each set of data collection.

The required input should be given to the software at first (Figure 4-15c). The ERT interface program requires the following inputs:

- Pulse shape and frequency;
- Number of electrodes and their spacing (from an input file);
- File name for output;
- Number of stacks in each half cycle;
- Maximum time for stacking in each current setup;
- Time and date of data collected;
- Automatic backup time for collected data; and,

- Comments on the data collected.

In different environments the noise level is different; therefore, it is best for the operator to decide how to configure the instrument to reduce the noise level. This can be easily achieved because the interface program was designed to be flexible. The default setup is as follows:

Current cycle: 0.5 Hz
Sampling time: 55% to 95% of each half pulse period
Stacking: 10 samples for 1 minute for each current electrode arrangement calculate through Halverson stacking method.

The software starts with checking the electrodes contact resistance and gives a report based on the results. Then, it asks for confirmation to continue collection of ERT data. The software saves the collected data in the file name that has been provided as part of the initial information. The induced electrical current and voltage (amount passing through current electrodes) are monitored during the data collection and recorded along with the collected potentials in the given file.

4.2 Cabling

The subjects of cabling and grounding are very closely related and should be evaluated at the same time. In fact, a cable shield is required to suppress electric fields by grounding and a proper grounding is necessary to locate the appropriate place for the ground connection.

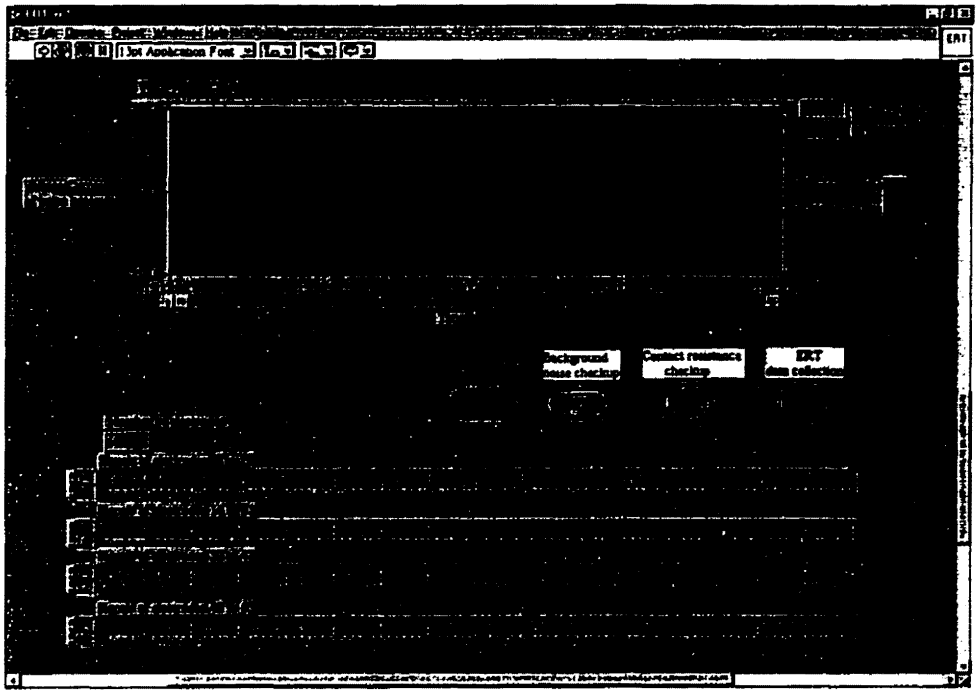


Figure 4.15a The front panel of the virtual instrument (VI) program handling the quality control of data of the ERT system

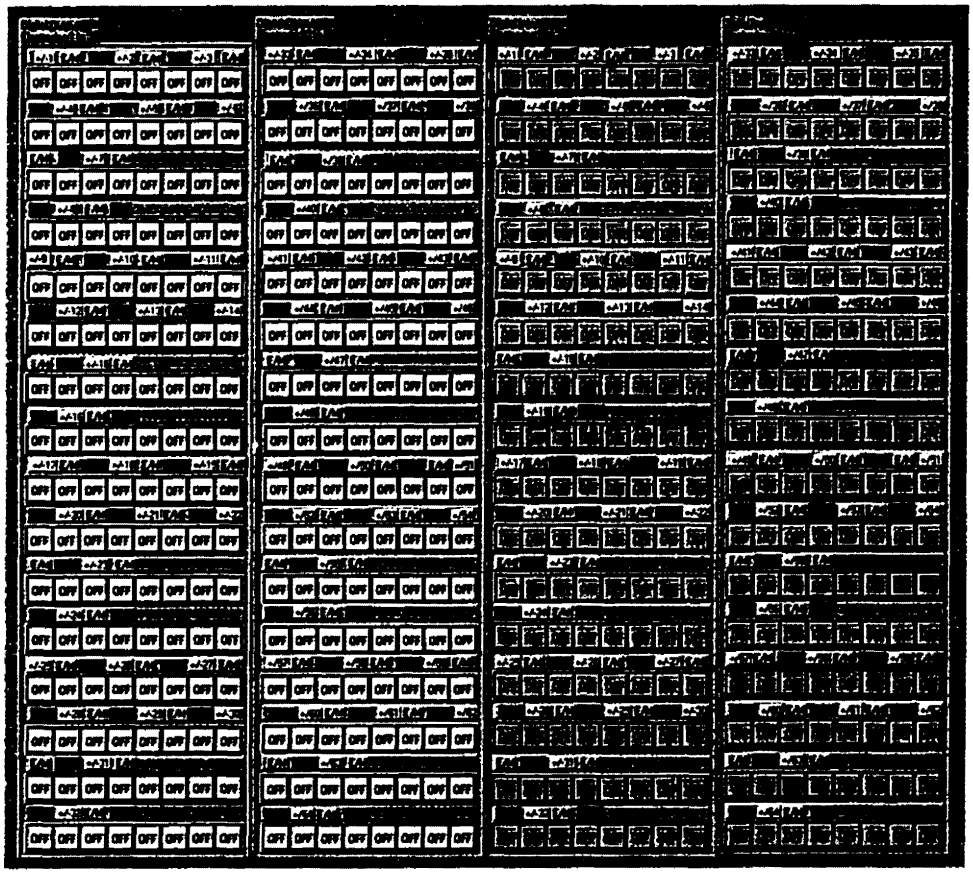


Figure 4.15b The front panel of the virtual instrument (VI) program handling the switching part of the ERT system though digital I/O devices

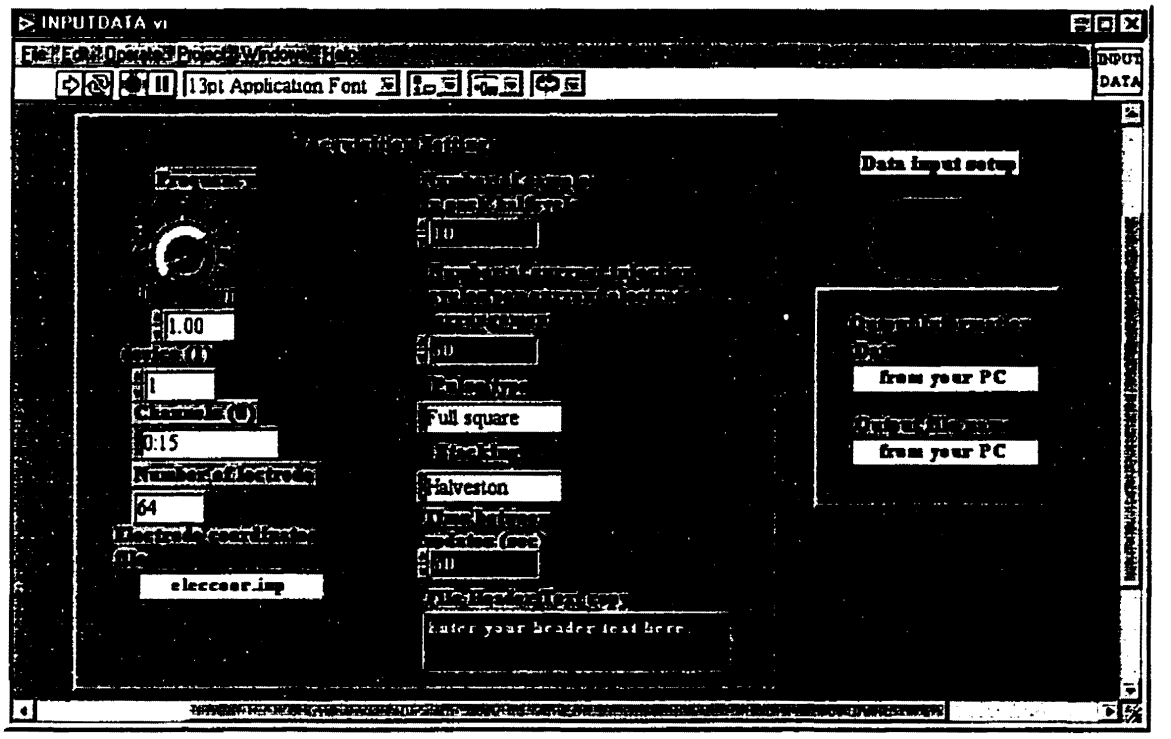


Figure 4.15c The front panel of the virtual instrument (VI) program handling the data input for the ERT system

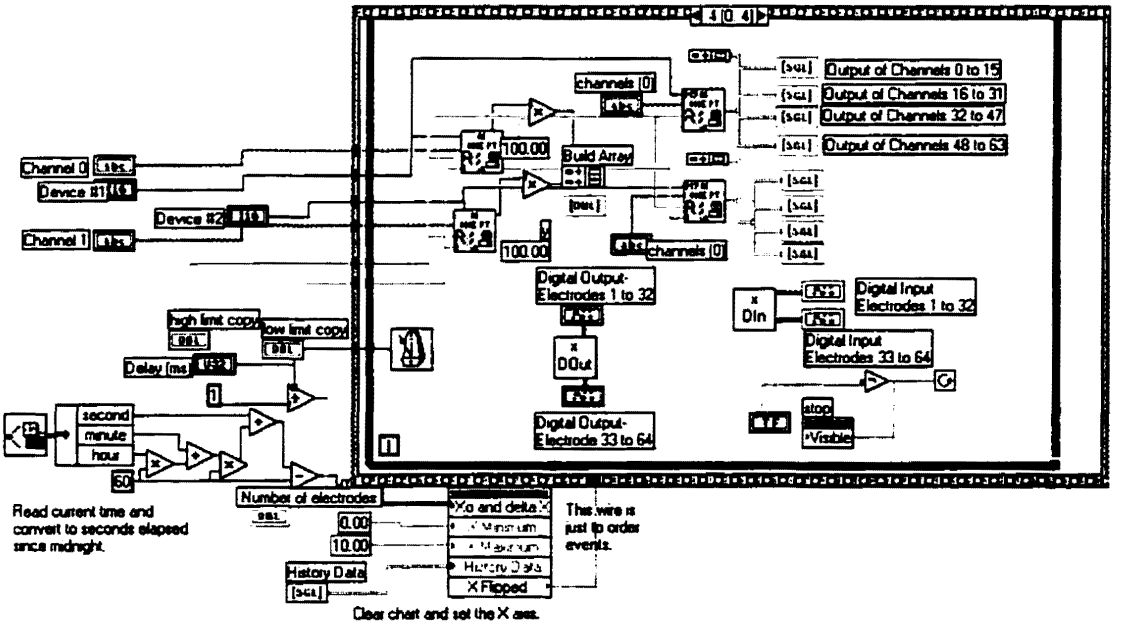


Figure 4.15d Diagram of the virtual instrument (VI) program of the new ERT measuring system

Cables are important because they are the longest parts of a system and therefore act as efficient antennas that pick up and/ or radiate noises by coupling mechanism between the fields and the cables and between cables (cross-talking). The shield cables are selected for the interfacing connections. It will improve the signal to noise ratio if a shielded cable is used to connect the electrodes too.

4.3 Assembling the system

The electronic elements of switching boards have been connected manually on two breadboards instead of using printed circuit boards. The main reason was to check the operation of designed circuit before requesting a printed circuit board. Therefore, a great amount of wiring was required to handle the connections (Figure 4.16). Because of that the noise level of the system might be a little higher than the noise in a printed circuit board.

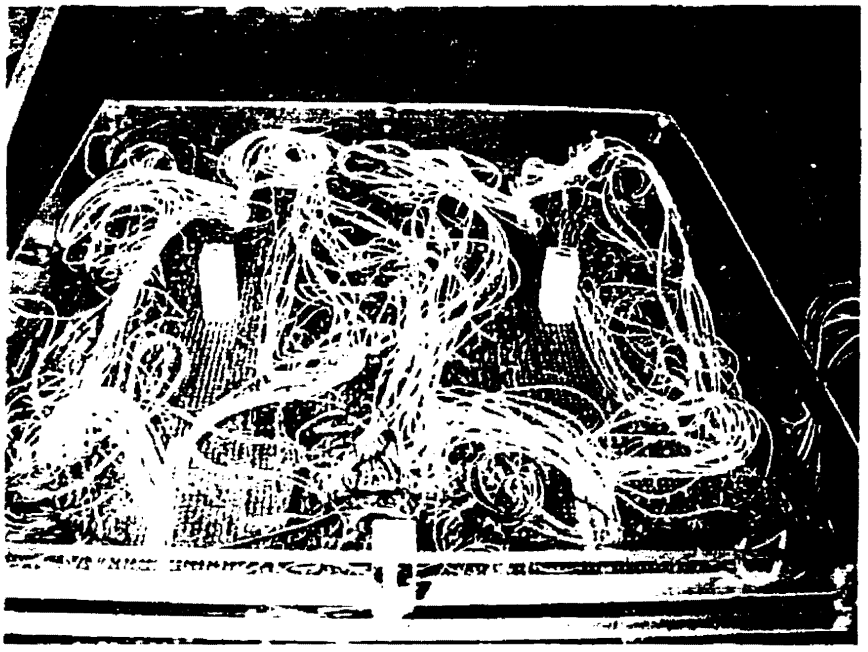


Figure 4.16 The view of the wiring at the back of switching boards

The A/D, DI, and DO boards were installed in the computer box and the multiplexer board was mounted in the switching box (Figures 4.17). Connections between the switching box and computer were by means of shielded cables (Figures 4.18).

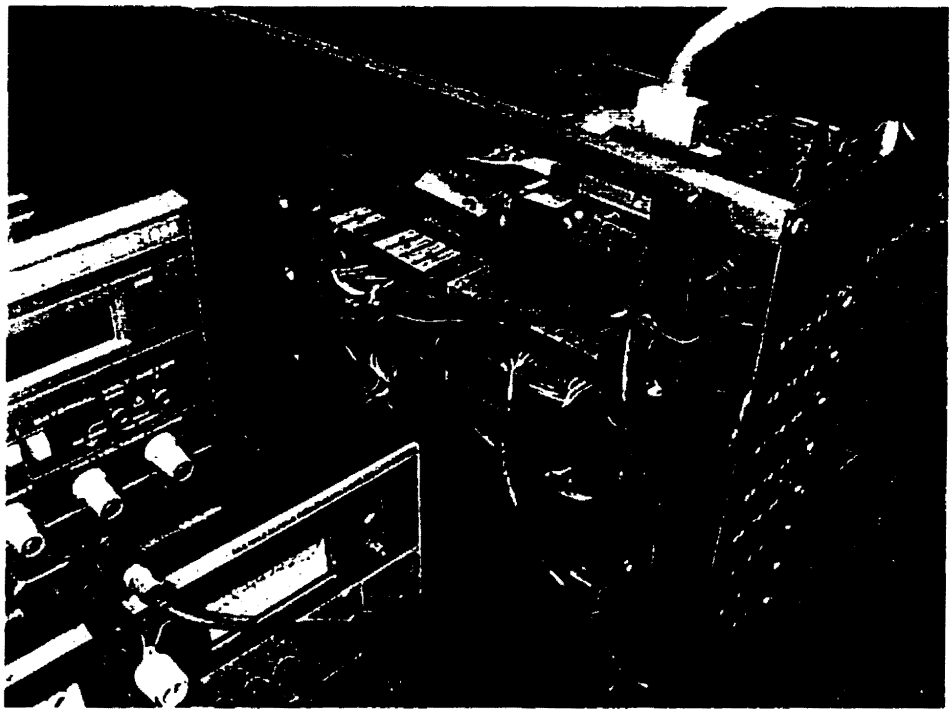


Figure 4.17a Side view of two switching boards and one plexiglas sheet (for multiplexer and required input banana plugs as receivers to the switching boards) mounted on a rack inside the stain-less steel shielded box

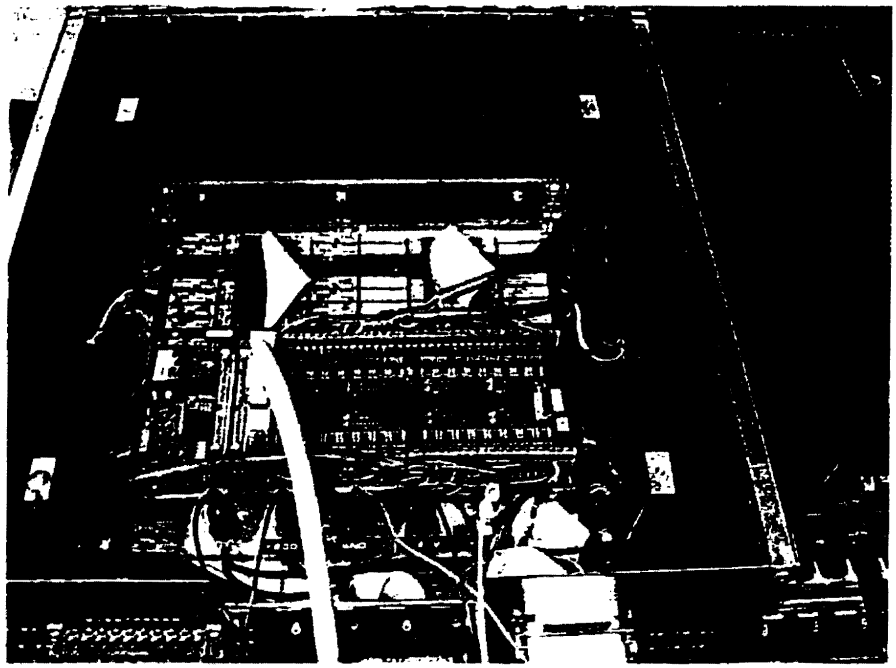


Figure 4.17b Top view of switching boards and one plexiglas sheet (for multiplexer and required input banana plugs as receivers to the switching boards) mounted on a rack inside the stain-less steel shielded box

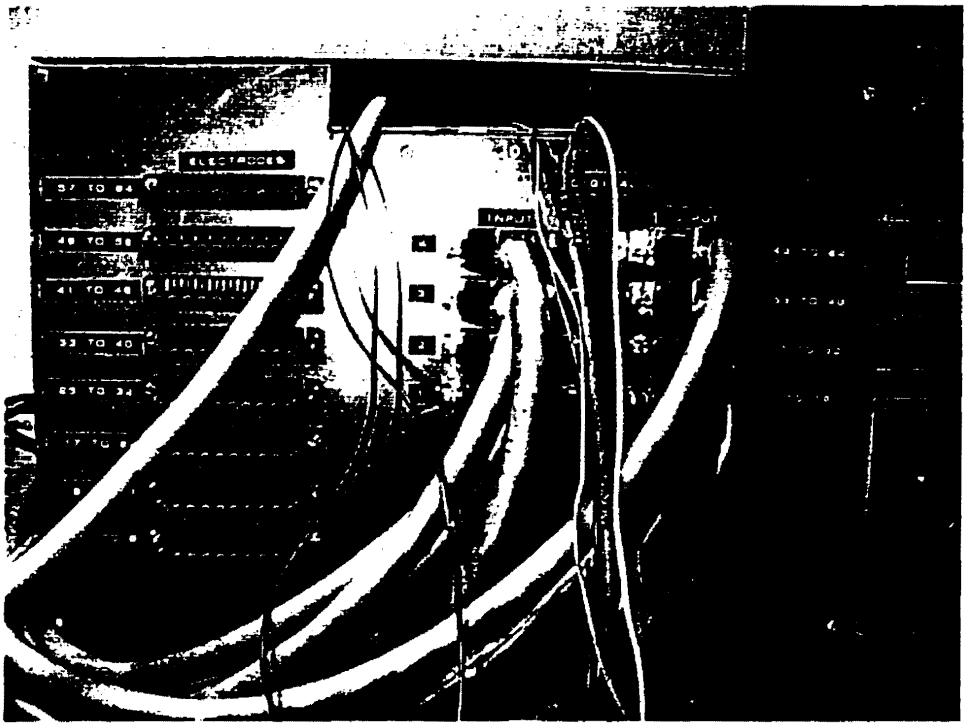


Figure 4.18a Side view of home-made switching box with external connectors to be connected to electrodes and computer

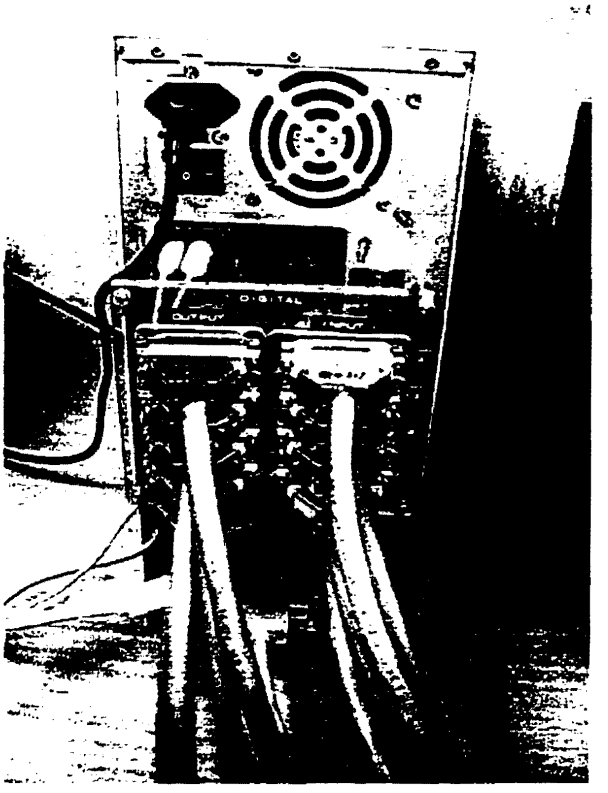


Figure 4.18b Side view of home-made connector board at the back on a modified computer box for interface connectors

4.4 Power supply

In general, this system has a programmable power supply that is controlled by the computer and the interface boards. The power supply can also be operated manually. The power supply can generate a variant voltage of 0 to ±200 Volts DC @4 Amps and a frequency range of 0.07 to 10 Hz. There are two types of Pulse shape available (Figure 4.19). The resolution output of the power supply is 8 bits.

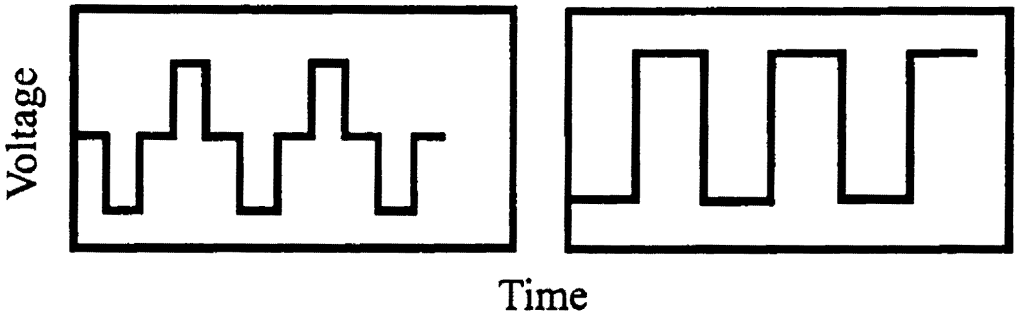


Figure 4.19. Schematic diagrams of the shapes of the power supply pulses

A set of preliminary tests of the power supply has been done in the VLSI (very large-scale integration) lab of the electrical engineering department of the University of Waterloo. Figure 4.20 shows the results of generated pulse passing through a 100 Ω resistor detected with a HP545 oscilloscope. The power supply has been returned to the supplier for modification to a high resolution, voltage regulation and implementing a proper control on the output frequency.

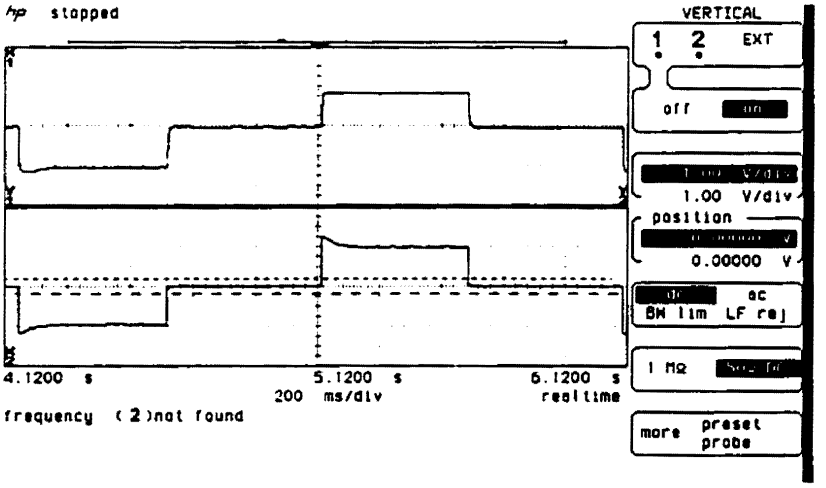


Figure 4.20 Primary test results of the power supply generated pulse passing through a 100 Ω resistor detected with HP545 oscilloscope

4.5 Cost evaluation

The cost of this system has been evaluated for four options of having 64 to 256 electrodes input (Table 4.1).

Table 4.1 Cost evaluation of ERT system for 64 to 256 electrodes single-ended inputs

Requirements	64 electrodes	Up to 128 electrodes	Up to 192 electrodes	Up to 256 electrodes
Analog to digital board	$1,500	$1,500	$1,500	$1,500
Multiplexer board	$1,500	$3,000	$4,500	$6,000
Digital output board	$250	$500	$750	$1,000
Digital input board	$200	$400	$600	$800
Electronic parts	$2,200	$4,400	$6,600	$8,800
Miscellaneous items	$1,000	$2,000	$3,000	$4,000
Labor	$500	$1,000	$1,500	$2,000
PC printed board	$2,000	$2,000	$2,000	$2,000
Programming	?	?	?	?
Total = CND$	$9,150	$14,800	$20,450	$26,100
Power supply	$10,000	$10,000	$10,000	$10,000

4.6 ERT time requirement

The ERT time requirement for a full data collection of 124 electrodes with the current system is 1 hr. This range is not sufficient for rapid flow systems that need real time monitoring, but it is fast enough for slow injection and usual ground water plume injection monitoring.

Chapter 5

FIELD TESTING

5. Field testing
5.1 Cambridge experiment

The Cambridge experiment was a joint project for monitoring slurry fracture injection at shallow depths with eight different methods: ERT, GPR, well logging, slurry flow rate, wellhead pressure, piezometer response, tiltmeters, and level survey. The slurry flow rate, wellhead pressure, piezometer and tiltmeter responses were measured throughout the injection. ERT, GPR, well logging, and level survey data were collected before and after slurry injection. The design, installation, and results of GPR and well logging techniques, and also slurry flow rate, wellhead pressure, piezometer response, tiltmeter readings, and level survey can be found in the M.Sc. theses by *Gilson* (1996) and *Reed* (1996). The design, installation, and the ERT response of the injection are presented in the following sections.

There were three attempts to inject slurry into the formation between July 1995 and January 1996. Because of technical difficulties, the January 1996 attempt was the only trial that in fact reached the stage of monitoring of the injection. *Reed* (1996) presents a detailed description of each trial.

The objectives of the electrical resistivity tomography technique in the preliminary experiment at the Cambridge site were to:

i. Evaluate commercial measuring systems for this task;

ii. Verify the ability of ERT to detect subsurface SI resistivity anomalies; and

iii. Determine the ability of ERT to monitor the movements of these anomalies.

Prior to the experiment the decision was made to add salt to the slurry to provide a resistivity contrast between the formation and the injected (recharge) cone. To decide where electrodes should be placed to monitor the injection, the ERT response to the injection was modelled as follows. It was assumed that the current electrodes were located at the bottom of slurry injection well (C_1) and at the surface 10 meters away from the slurry injection well (C_2). The first simulation was of the background potential field based on the well logging conductivity results (Figures 5.1a and 5.2a). Note that in this figure and hereafter a normalized potential in units of Volts per Amperes injected were used. The next step was to simulate the injection of the saline fluid plume, based on the proposed volume of the injection and assuming an effective porosity of the host matrix of 35%. The immediate post-injection model consists of four conductive zones. Three of these were arranged in concentric cubes {small one (6x6x6m) with formation electrical conductivity of 1×10^{-1} S/m, medium one (12x12x6m) with formation electrical conductivity of 5×10^{-2} S/m, large one (18x18x9m) with formation electrical conductivity of 1×10^{-2} S/m} around the injection point. Figure 5.2b shows these zones in X-Z cross-section. In addition, a cubic conductive zone (6x6x3m) with formation electrical conductivity of 1×10^{-1} S/m, has been placed immediately above the smaller zone of the three conductive zones to model the plume immediately following the injection (Figure 5.2b). The injection was to be 10000 litres of fresh water followed by 11,000 litres of the saline mixture. The fourth zone was necessary because the injection point was at 13 meters, 3 meters above the current electrode. The formation electrical conductivity of the background was assigned to the rest of the region. Based on this new scenario, another electrical field simulation was conducted (Figures 5.1b and 5.2b). Under the assumption that there would be a saturation change and plume movement during the first week, the simulation was repeated for a change in the shape of the injection (recharge) cone and incorporating some movement of the plume toward the west (groundwater flow direction). Figures 5.1c and 5.2c show this simulated result in plan view and XZ cross-section (the fourth zone was removed for this simulation).

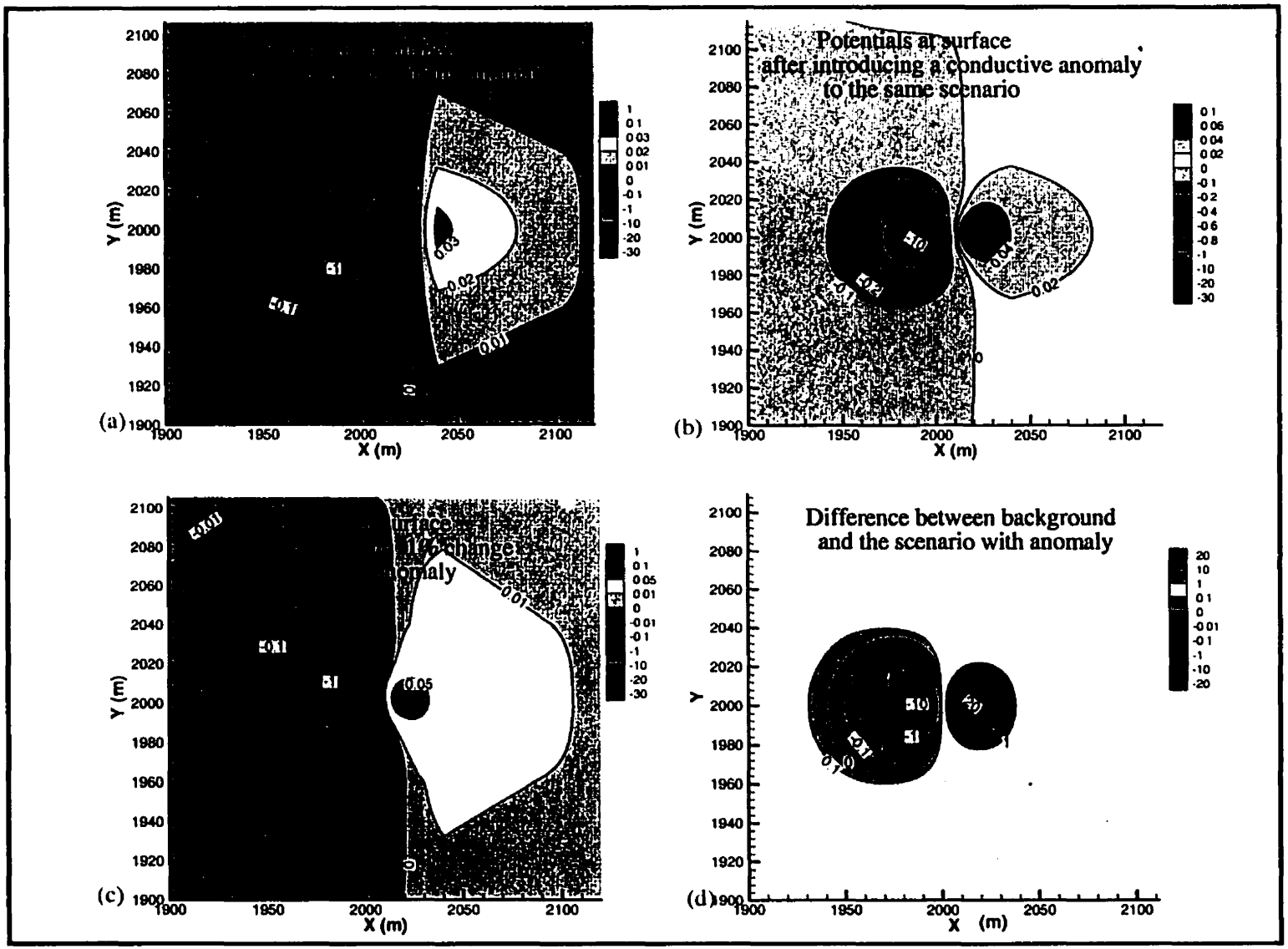


Figure 5.1 X-Y plane view of electrical field simulation at the Cambridge scenario: (a) background, (b) for the same scenario including a conductive anomaly, (c) after introducing 1% change to the conductivities of the anomaly, and (d) the difference between the background and scenario with a conductive anomaly. Units are in V/A

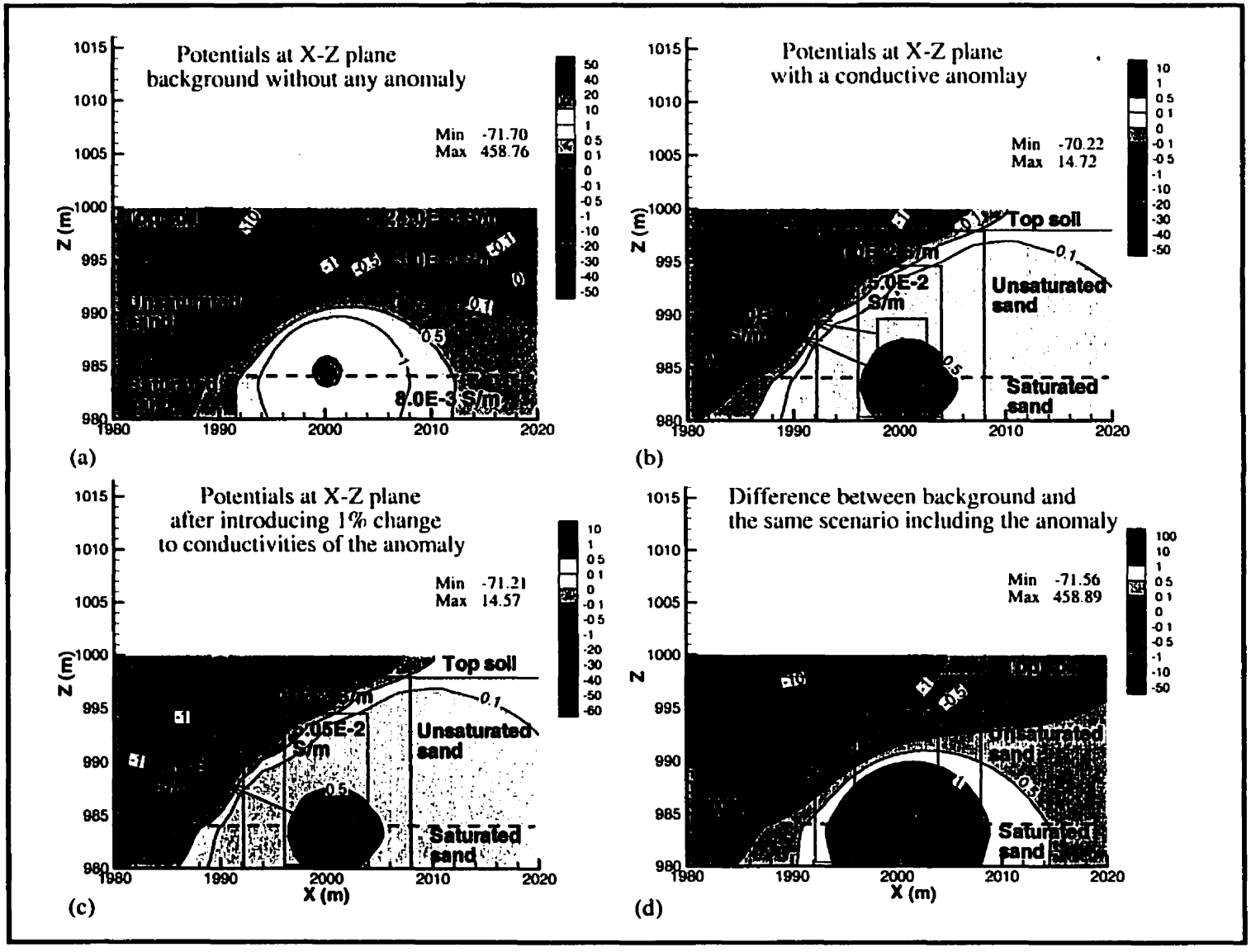


Figure 5.2 X-Z plane view of electrical field simulation at the Cambridge scenario: (a) background, (b) for the same scenario including a conductive anomaly, (c) after introducing 1% change to the conductivities of the anomaly, and (d) the difference between the background and scenario with a conductive anomaly. Units are in V/A

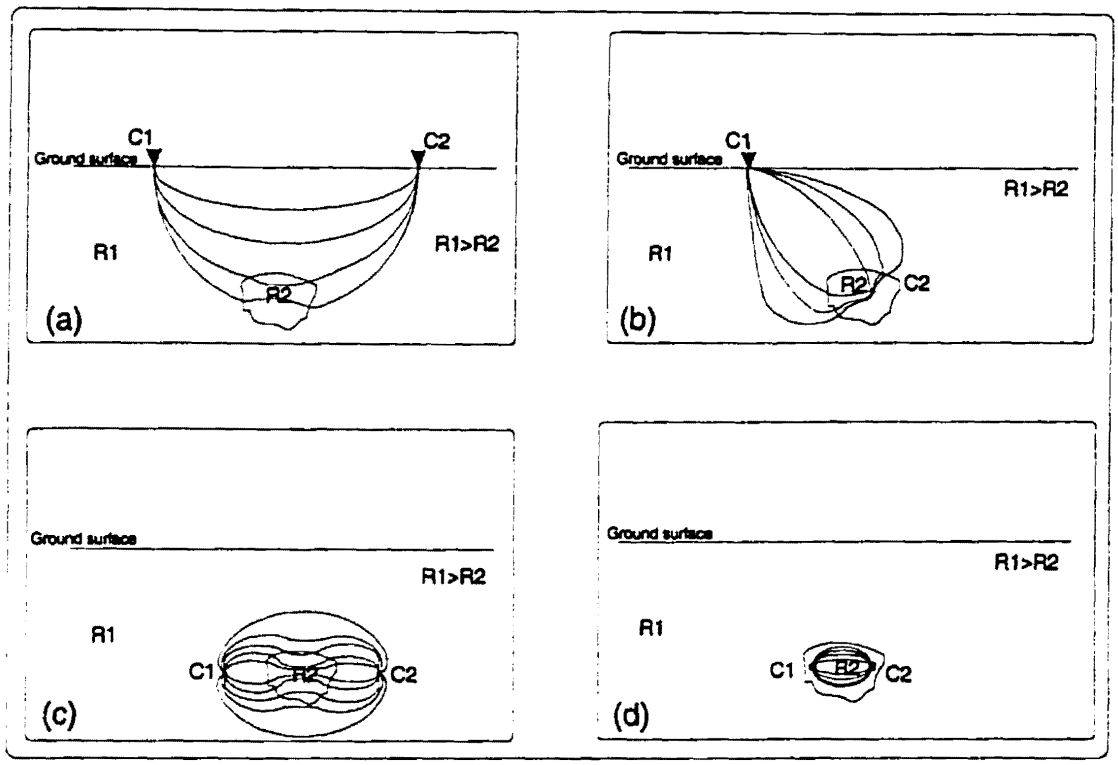


Figure 5.4 Schematic diagram of electrode placement with respect to anomaly and the potential distribution; a) both current electrodes at the sides on the surface; b) one current electrode at the surface and the other one inside the anomaly; c) both current electrodes at the sides of the anomaly close to it; and d) both current electrodes inside the anomaly.

The electrode placement is an important part of any resistivity measurement. Narayan (1994) gives a literature review and simulated evaluation of electrode positioning with respect to the anomaly. Figure 5.3 shows a schematic diagram of a few general combinations of current electrodes with respect to the position of a conductive anomaly. When electrodes are only at the surface and either the anomaly is small, or it is very deep, or the resistivity contrast between the anomaly and its host is very low, it is almost impossible to detect the anomaly form the surface electrode configuration (Figure 5.3a). It is possible to collect a fully 3-D resistivity data set but it is very expensive. Cross illumination is probably better, but the electrodes should not be too close (Figures 5.3b and 5.3c). If both current electrodes are placed inside the anomaly (Figure 5.3d), most of the energy would be transferred inside the more conductive zone (anomaly) and there would not be a considerable change of potentials because of the anomaly.

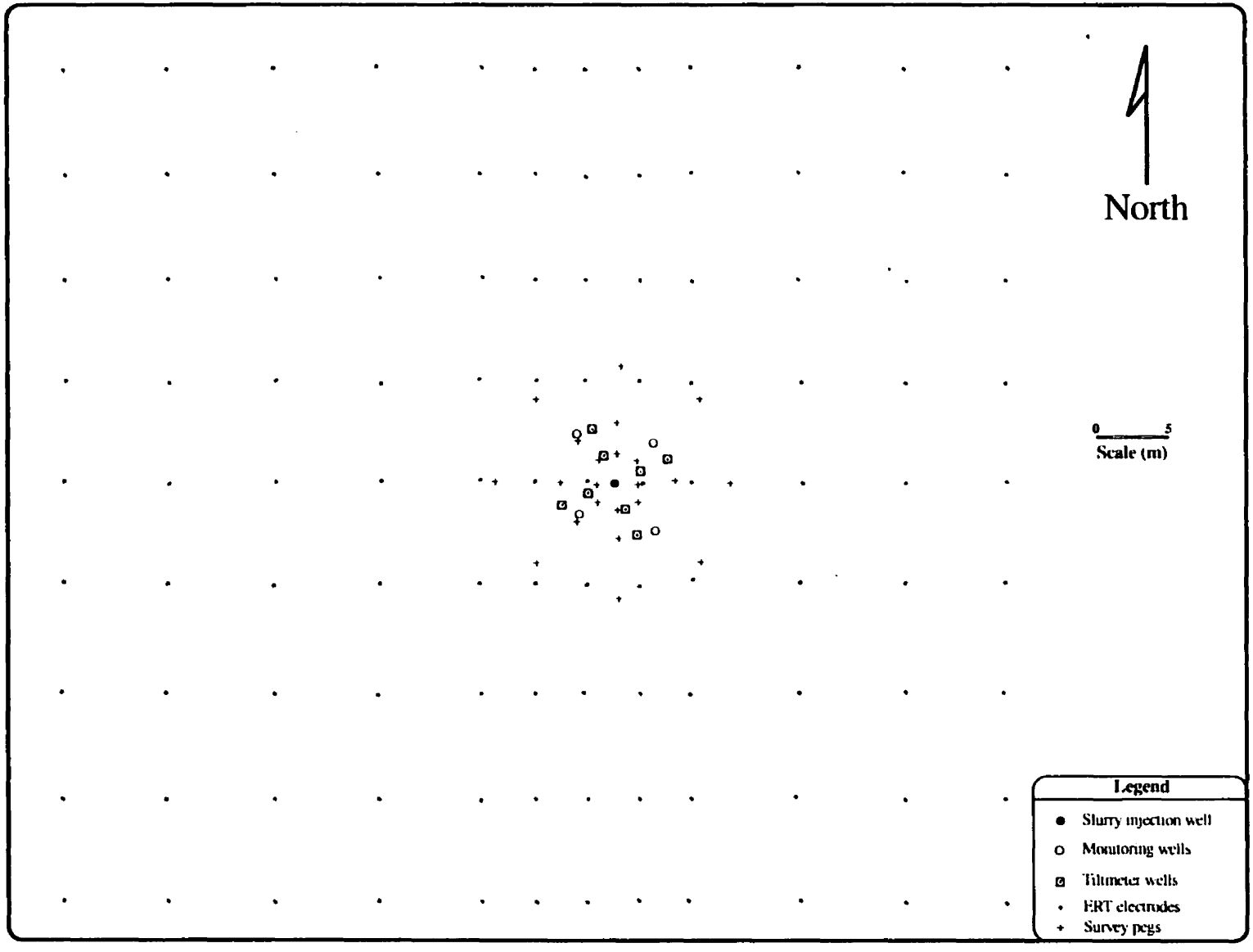


Figure 5.4 Plan view of installed monitoring elements for the Cambridge experiment

Differences between these three potential field distributions obtained were used to optimise the placement of electrodes for the actual field experiment (Figures 5.1d and 5.2d). Based on these results, and making compromises to overcome conflicts with the other methods, an array of electrodes (surface and downhole) and well arrangements were designed and installed (Figure 5.4 and 5.5). The Cambridge slurry injection was carried out in January 1996. Unfortunately, the adjoint sensitivity analysis was not available at that time. Therefore, the electrode setup was a best guess based on the simulation results. It is evident from Figure 5.2d that large changes in potential will occur in the vicinity of the injection and that any effective monitoring of this process will require electrodes in that region. At the surface, voltage changes of 500 mV/A is observed close to the epicentre of the injection, and we also needed to anticipate plume movement in the groundwater (assuming X-) direction. Accordingly, the designed field system consisted of:

i. A square grid of 12 by 9 of 45 cm stainless-steel 0.5-inch rods as surface electrodes (each electrode was hammered 30 cm into the ground);

ii. One electrode (45 cm stainless-steel 0.5-inch rods, of which about 30 cm were hammered down into the ground) at 80 meters away from the injection epicentre. 80m was used instead of 10 meter because further models showed that the influence of that electrode's position on the data was minimal at 75 meters or more;

iii. A set of downhole electrodes in the slurry injection well (2 inches diameter) at a depth of 13.2m at the centre of the surface electrode grid (Figure 5.4). At the bottom of the injection well casing, a 1.5 inch solid PVC rod was installed with six electrodes, each a plate of 5×16 cm 18 gage stainless steel wrapped around the PVC rod every 0.5 m from the bottom of injection well and wired to the surface (from 13.2m to 16.2m depth); and,

iv. Four monitoring wells at the corners of a 3 by 3m square, with the injection well at the centre of this square. Four 45-cm long stainless steel rods (1 inch diameter) were installed at the bottom of these wells (16.75m depth). Since these wells were also to be used for GPR and well logging measurements, passing a wire from the bottom electrode to the surface interfered with those measurements. Therefore, the contact with these electrodes was achieved through a plastic rope and a removable cable connected to a stainless steel electrode.

January 1996 slurry injection procedure

A few days before each injection background readings were taken to provide a base for comparison of the effects of slurry injection on the electrical field. The trial described here started in the morning of January 19, 1996. About 11000 litres of a mixture of water, salt, gel (hydroxypropylguar powder) and fine dyed sand was prepared. The dye was used to differentiate the injected sand from the formation sands after the injection. At the beginning of each test, clean fresh water with EC of 950 μS/cm was injected (at the rate of 200-400 litres/min) to test the flow rate of the formation and to clean up any possible blocked zone at the injection point. Six thousands litres of the mixture were injected into the aquifer in less than one hour. The electrical conductivity (EC) of this solution was 2500 μS/cm, about four times that of aquifer. At this point the sand particles clogged the perforations of the injection well casing and the test was stopped.

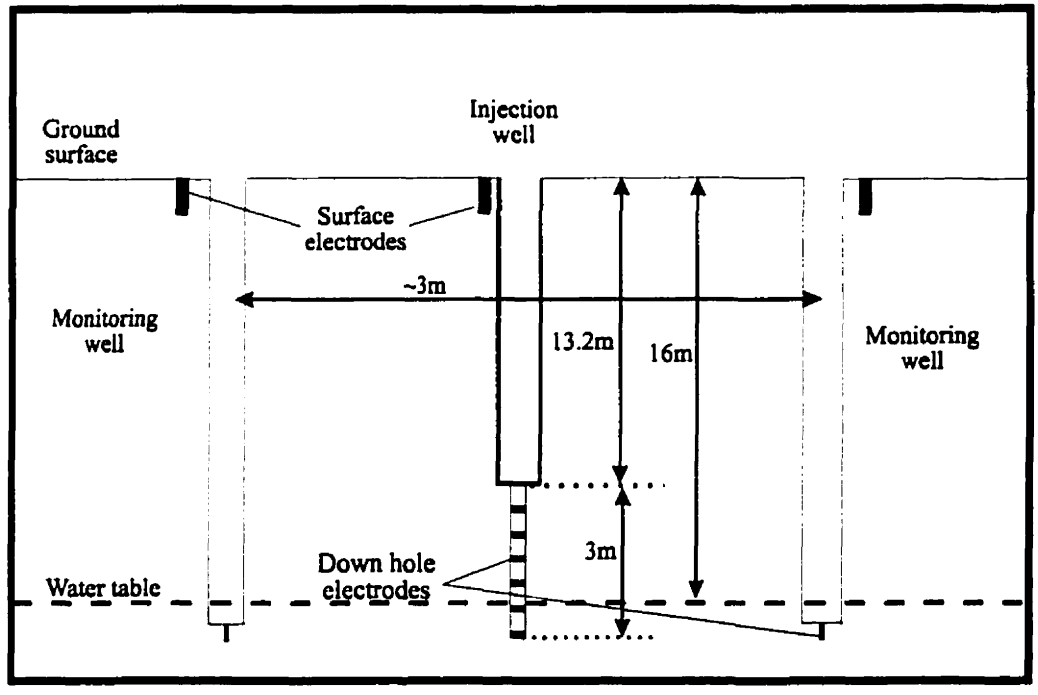


Figure 5.5 Schematic cross-section of well and electrode configuration

The brine density is not an issue in the Cambridge experiment because the salinity of the slurry was low. To prevent any environmental problem there was only 2kg of cooking salt in 5000 liters of slurry, which is about 2000 gr/5000000 gr = 400 ppm of added salt. Compared to sea water, which is 35000 ppm, this is negligible. The electrical conductivity of slurry was 2500 mS/cm, twice as much as drinking water on the

University of Waterloo campus. In fact, this modest salinity leads to a small conductivity contrast at depth, making detection even more challenging.

The ERT technique was performed repeatedly before and after the injection. The measurements are presented in Appendix E. The results of the measurements are described in Chapter 6.

Chapter 6

RESULTS

The main results of this thesis are presented in this chapter. First, the data obtained for the Cambridge field experiment are shown and described. This is followed (section 6.2) by a simulation of these data obtained by (a) modeling the contaminant flow about the injection and, on the basis of that hydrological model, (b) modeling the variation in electrical potential that would result. The goal of this exercise is to demonstrate the feasibility and usefulness of direct modeling using SALTFLOW for both the hydrological and ERT simulations. Section 6.3 discusses a sensitivity analysis of the ERT model derived from SALTFLOW. This is useful for estimating the optimal placing of electrodes in a field experiment, but it is also a step towards the ultimate goal (not fully achieved with this thesis) of using SALTFLOW as the engine of an inversion of the data.

Section 6.4 examines the performance of the ERT measuring system that has been designed and built, evaluating it against the requirements outlined in Chapter 2.

6.1 Cambridge resistivity measurements, January 1996

The background electrical potentials of the Cambridge sandpit were originally collected with an Androtex Instrument (November 13-20, 1995). As a result of reading difficulties using this system, the Syscal Junior System (manufactured by IRIS Instruments of France) was used instead, and the background electrical potential of the Cambridge

sandpit collected (November 29 to December 2, 1995) for all six current electrodes at the bottom of the monitoring wells with a surface return current electrode 80 meters away from the injection well. Current injection was at the SW monitoring well and the voltage reference electrode was placed at (10.5, 17.25, 0). A 6 by 4 subset of the surface electrodes was selected for potential measurement directly above the injection well. Post-injection ERT measurements were conducted for combinations of the selected surface electrodes and all downhole electrodes during the period January 19 to 26, 1996. Data for the following specific times are plotted in Figures 6.1 to 6.3; background, one day following injection, and 6 days following the injection. The differences in potential between background and post-injection measurements are plotted in Figures 6.4 to 6.5.

The data show that, as expected, the injection results in a significant difference in the potential field at the downhole and surface electrodes between pre-injection and post-injection measurements. The nature of the reaction reflects, in general terms, the facts that (i) a lower voltage is required to drive one ampere through the ground between the current electrodes and (ii) less of that voltage (energy) is used in moving current from the downhole electrode to the surface where it sweeps past the electrode array. Because of (i) the voltage drops initially drops at the downhole potential electrodes (typically by 0.5 volts) and because of (ii) it initially rises at the surface electrodes (by as much as 3 volts). With time, the downhole electrode voltages rise back towards their initial values, presumably reflecting the fact that the saline plume has moved away somewhat from their immediate vicinity, while the surface voltages fall as the energy loss from downhole electrode to surface increases (that is, the path is becoming more resistive).

Figure 6.6 shows the difference in potential between the first day and 6^{th} day of post-injection measurements. Note that voltages have dropped by 200 to 1000 mVolts in the area contoured, a very substantial difference, given measurement sensitivities that should be no more than a millivolt. The important point is that there is no shortage of ERT signal at the surface or downhole for the processes underway in the subsurface.

On the other hand, an intuitive interpretation of the difference map of Figure 6.6 is complicated. Asymmetry in the contour pattern, perhaps linked to lateral movement of the plume, is also brought about by the electrode and injection geometries. To make any sense of Figure 6.6 we need to be able to model the process in three dimensions.

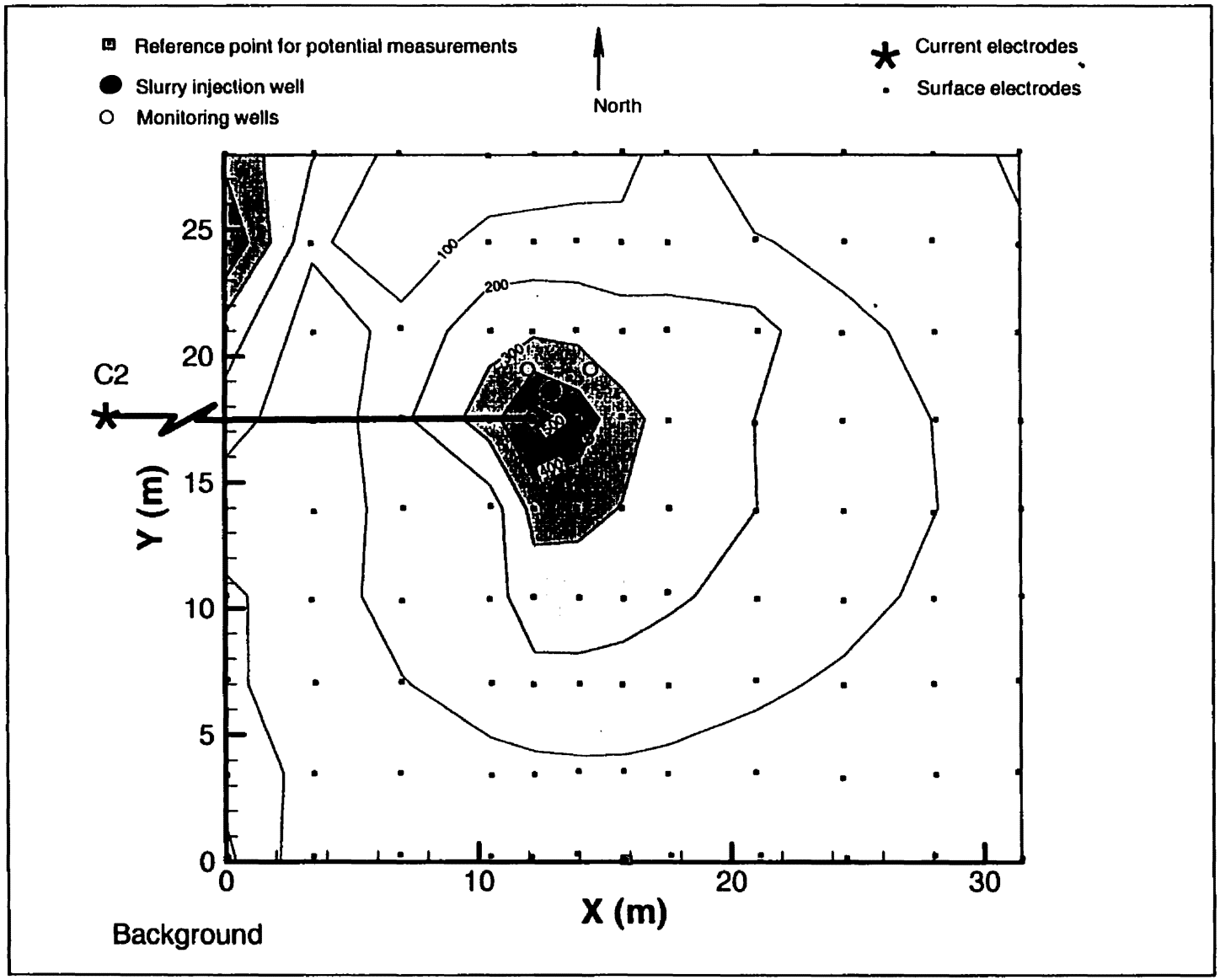


Figure 6.1 Background potential field at surface electrodes with respect to a reference point (14,0,0), current electrodes at the bottom of the SW monitoring well (10.5, 17.25, 16.75) and at surface 80m west of the SW monitoring well (-70, 17.25, 0). Collected on January 19, 1996. Units are mV/A

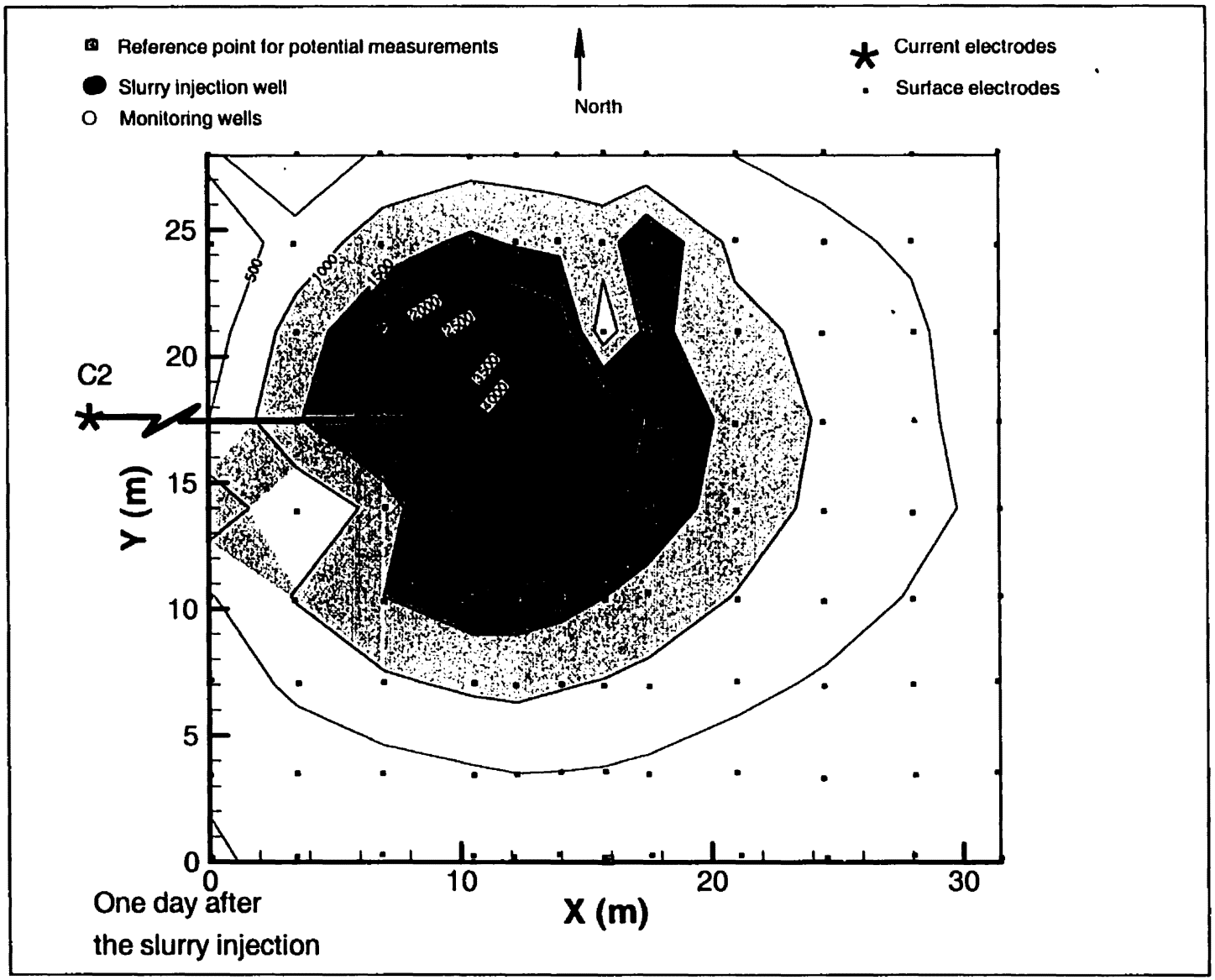


Figure 6.2 The potential field (mV/A) at surface electrodes with respect to a reference point (14, 0, 0) collected on January 20, 1996, one day following the slurry injection using the same electrode configuration as Figure 6.1. Units are mV/A

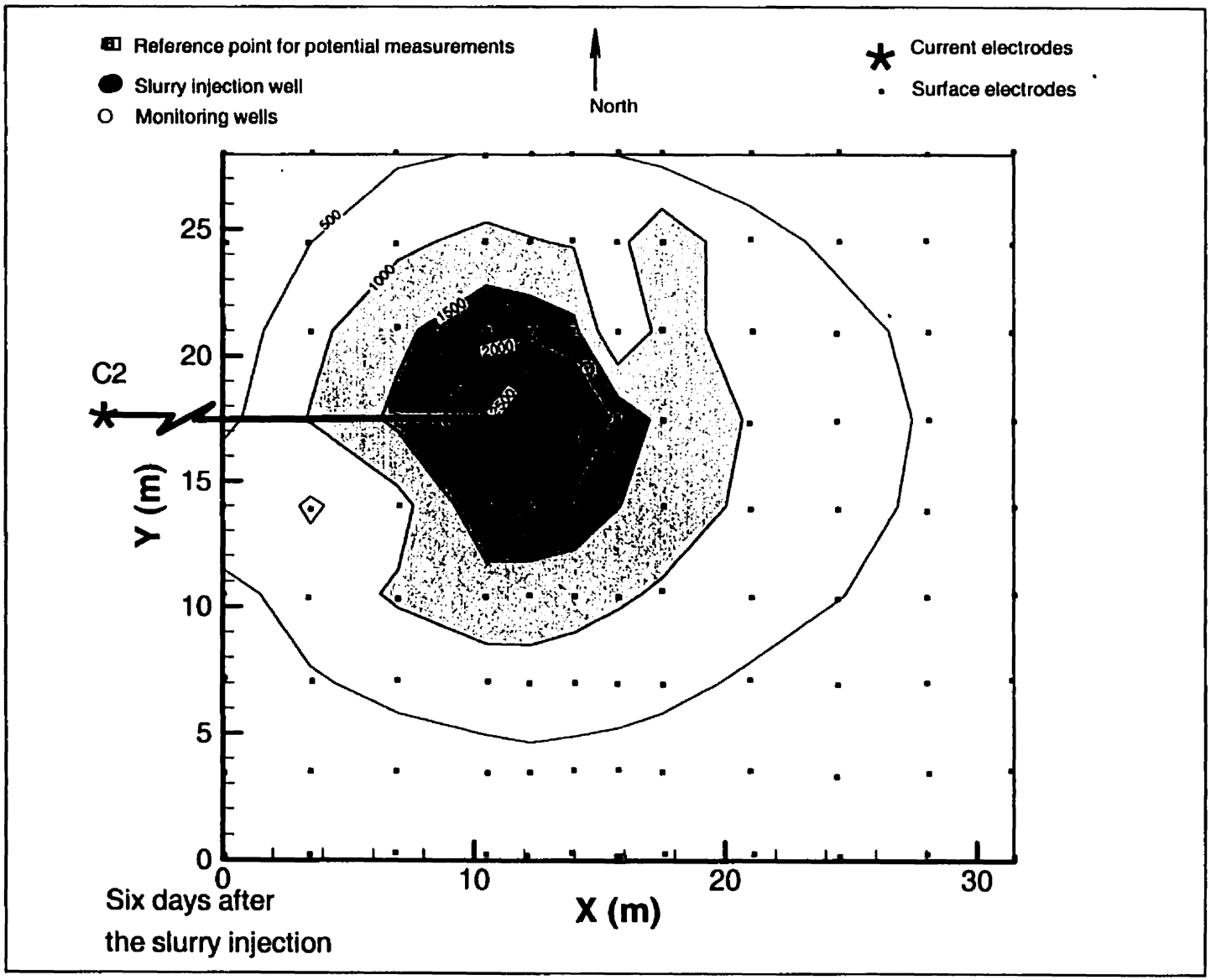


Figure 6.3 The potential field (mV/A) at surface electrodes with respect to a reference point (14, 0, 0) collected on January 26, 1996, 6 days following the slurry injection using the same electrode configuration as Figure 6.1. Units are mV/A

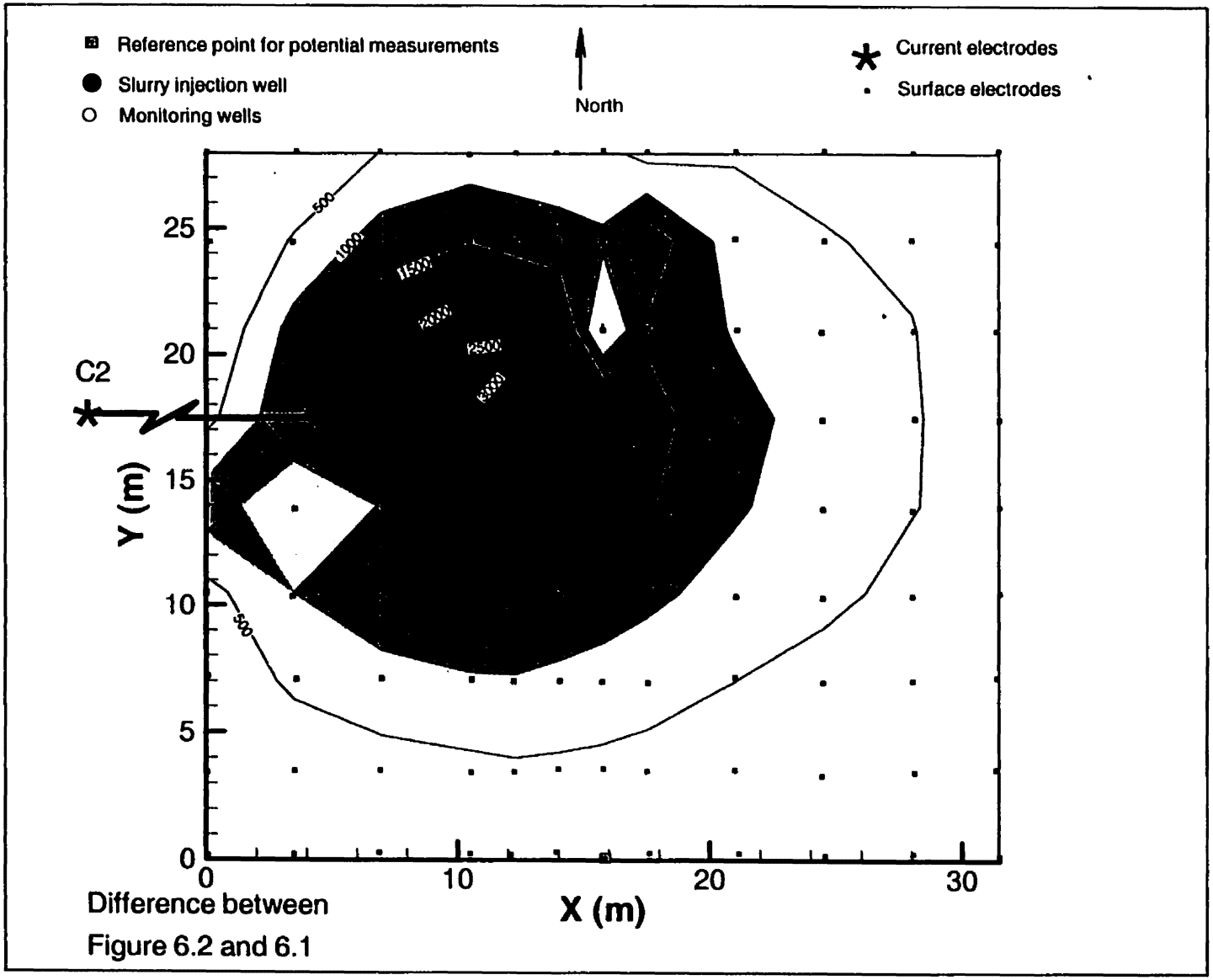


Figure 6.4 The potential differences between background and one day following injection. Units are mV/A

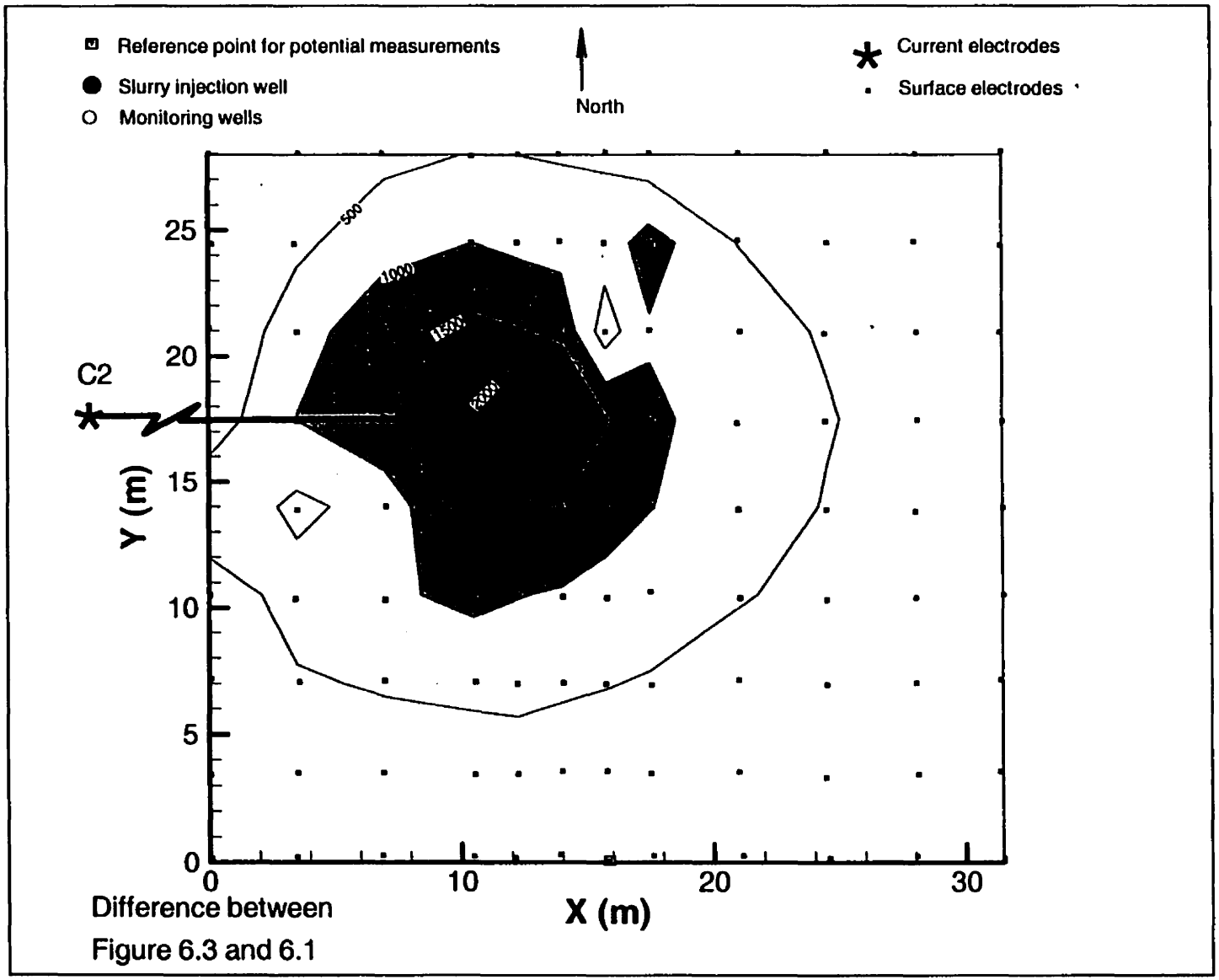


Figure 6.5 The potential differences between background and 6 days following injection. Units are mV/A

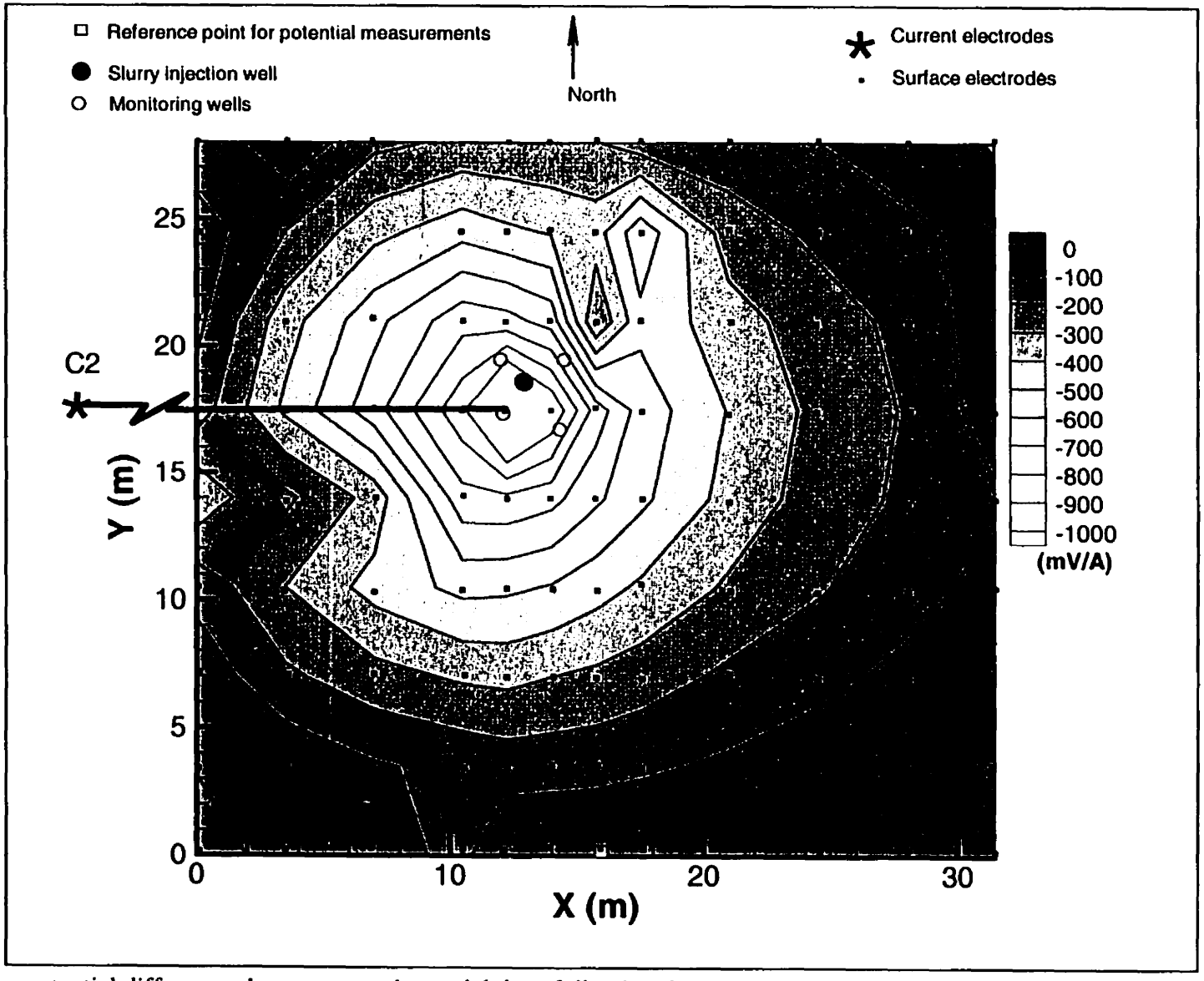


Figure 6.6 The potential differences between one day and 6 days following the injection. Units are mV/A

6.2 Simulation of groundwater regime following the injection

Figures 6.1 to 6.6 have described the measured potential field data. The objective of the next two sections is to simulate these measured data by: (i) modeling the groundwater regime's response to the injection and the resulting distribution, with time, of salinity; (ii) transforming salinity to electrical conductivity; and (iii) modeling the electrical potential field in the derived conductivity distribution for comparison with the field data.

The Cambridge injection site is a complex one because it involves both saturated and unsaturated flow. A simpler experiment (injection entirely within a saturated zone) would have been far more preferable, but a decision was made to stick with the results and try to simulate the measured data. To understand the observed behavior, both the FRAC3DVS and the SALTFLOW models have been used to simulate the Cambridge scenario. Since the slurry was injected in the unsaturated zone, the injection itself was simulated by FRAC3DVS (*Therrien et al.*, 1998), a saturated-unsaturated transport 3-D groundwater model. Because a saline fluid was injected, the fully saturated 3-D density-dependent flow and mass transport model, SALTFLOW, has been used to simulate the transport of the slurry following injection. The ERT model is mathematically equivalent to steady-state groundwater flow. The codes are designed to conditionally solve the problem, based on the input. If it is a transient scenario, they will take the route with the time-dependent variable; otherwise, the steady-state route is automatically selected, in which there is no time-dependency of the parameters.

The boundary conditions for flow and ERT are:

Flow boundary condition:

- Transient flow condition
- No flow at the side boundaries parallel to X direction;
- Constant flow rate (2 meters head in 60 meters horizontal distance) at the side boundaries parallel to Y direction;
- No recharge from the surface; and,
- No flow from the bottom surface.

ERT boundary condition:

- Steady-state condition;
- Constant (zero potential) at the side boundaries;
- No flow boundary at the bottom;
- No recharge from the surface; and,
- Free water table.

The details of the model inputs including boundary conditions are presented in Appendix H for the Cambridge scenario.

The simulation was for 8000 litres of fresh water followed by 6000 litres of saline water, injected at (2000, 2000, 987), 2 metres above the water table, at 500 litres per minute. The transport process was simulated for 6 days, based on a hydraulic conductivity of 10×10^{-4} m/s for the sand layer (*Reed*, 1996) and on the following additional assumptions: a hydraulic conductivity for the top soil (clay) of 5×10^{-6} m/s, a groundwater flow of 2.6×10^{-1} m/s in the x direction; all other unsaturated zone hydraulic properties as given by El-Kadi (1985); no recharge for the top surface (for simplicity since the top layer is a clay), and a salinity concentration of 0.1 for the first pumping step and one for the second pumping step of injection period (so that it can be used as a coefficient to the electrical resistivity of the layers). The sections and plan views of these simulations are presented in Figures 6.7 to 6.10.

Figures 6.7a to 6.7d show the evolution of pressure heads (representing water table variations) from initial steady-state conditions to 6 days after the slurry injection. The original water table is presented in Figure 6.7a. Figure 6.7b shows that the slurry injection has caused an increase of about 5 meters in the water table around the injection well. Figures 6.7c and 6.7d shows that the water table has returned to its original level after one day and it shows a steady level thereafter. There is a high-pressure head region above the water table in Figure 6.7c that represents the extra gravitational water content because of the slurry injection. This extra water content is the main driving force for the slurry in the unsaturated zone, moving it towards the water table.

Figures 6.8a to 6.8d show the simulated total pressure variations from the initial steady-state condition to 6 days after the slurry injection. Figure 6.8a shows a uniform pressure distribution at the steady-state condition. Figure 6.8b shows a high-pressure region around the injection range caused by the slurry injection. This high-pressure region starts to dissipate after the injection has stopped. Figures 6.8c and 6.8d show this process.

Figures 6.9a to 6.9d show the simulated saturation variations from steady-state condition to 6 days after the slurry injection. These figures are consistent with the pressure head results (Figures 6.9a to 6.9d). Figures 6.9b and 6.9c show the extra water content caused by the slurry injection, the main driving force in moving the plume from the unsaturated zone toward the saturated zone.

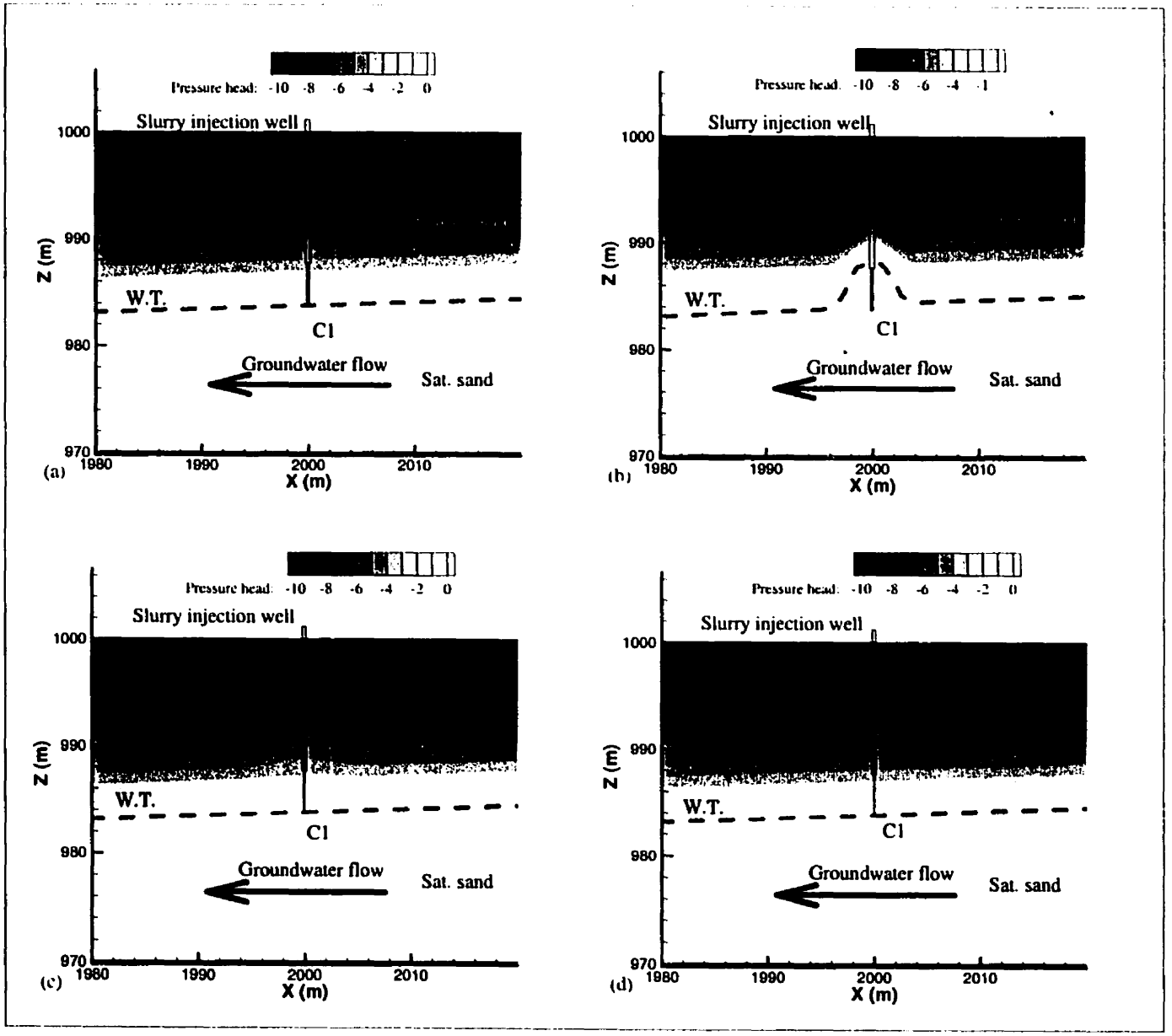


Figure 6.7 Simulated pressure head variations in the X-Z plane at Cambridge site: (a) background, (b) following slurry injection, (c) one day following the slurry injection, (d) 6 days following the slurry injection

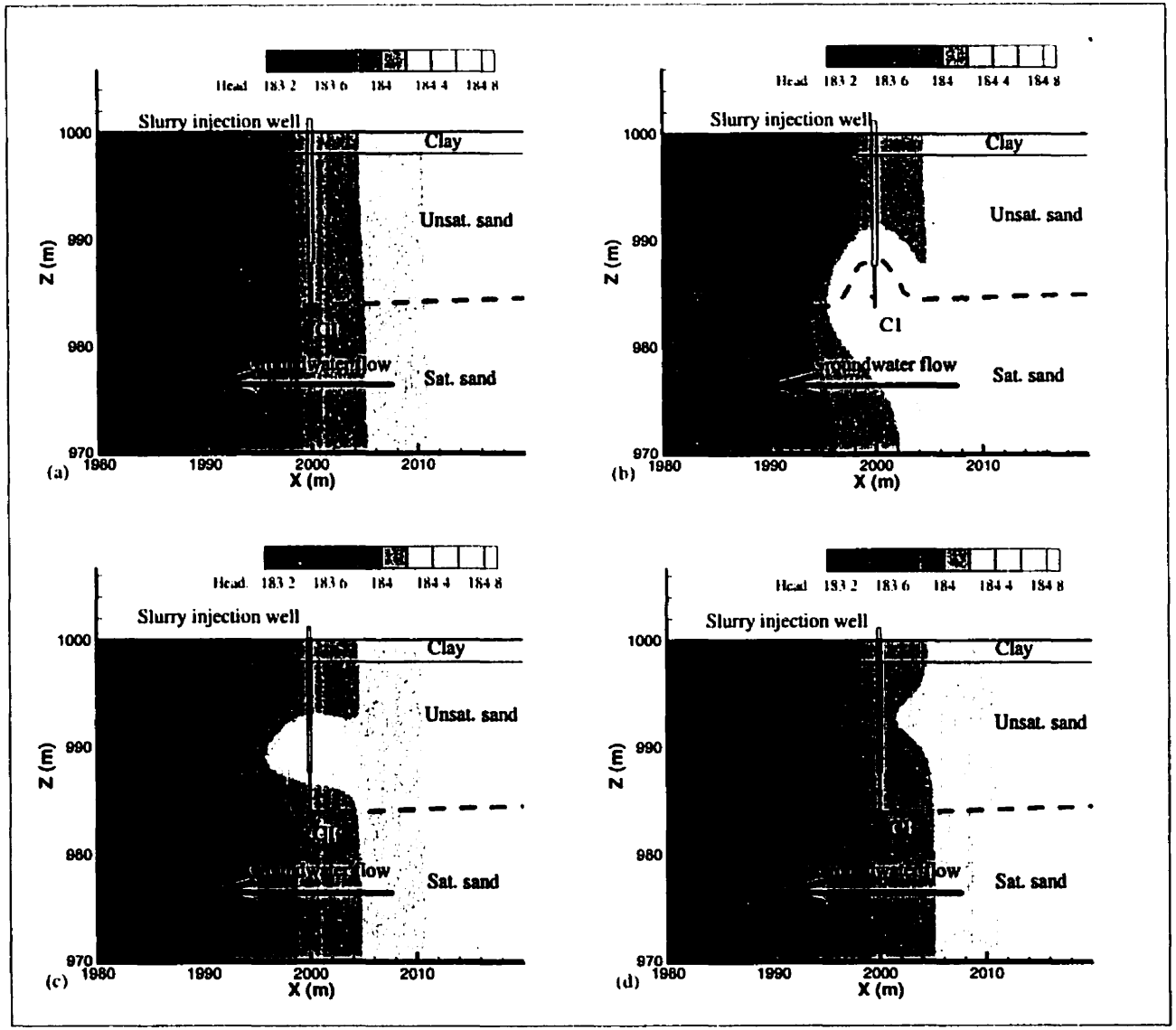


Figure 6.8 Simulated total head (pressure head plus elevation head) variations in the X-Z plane at Cambridge site: (a) background, (b) following slurry injection, (c) one day following the slurry injection, (d) 6 days following the slurry injection. Units are m

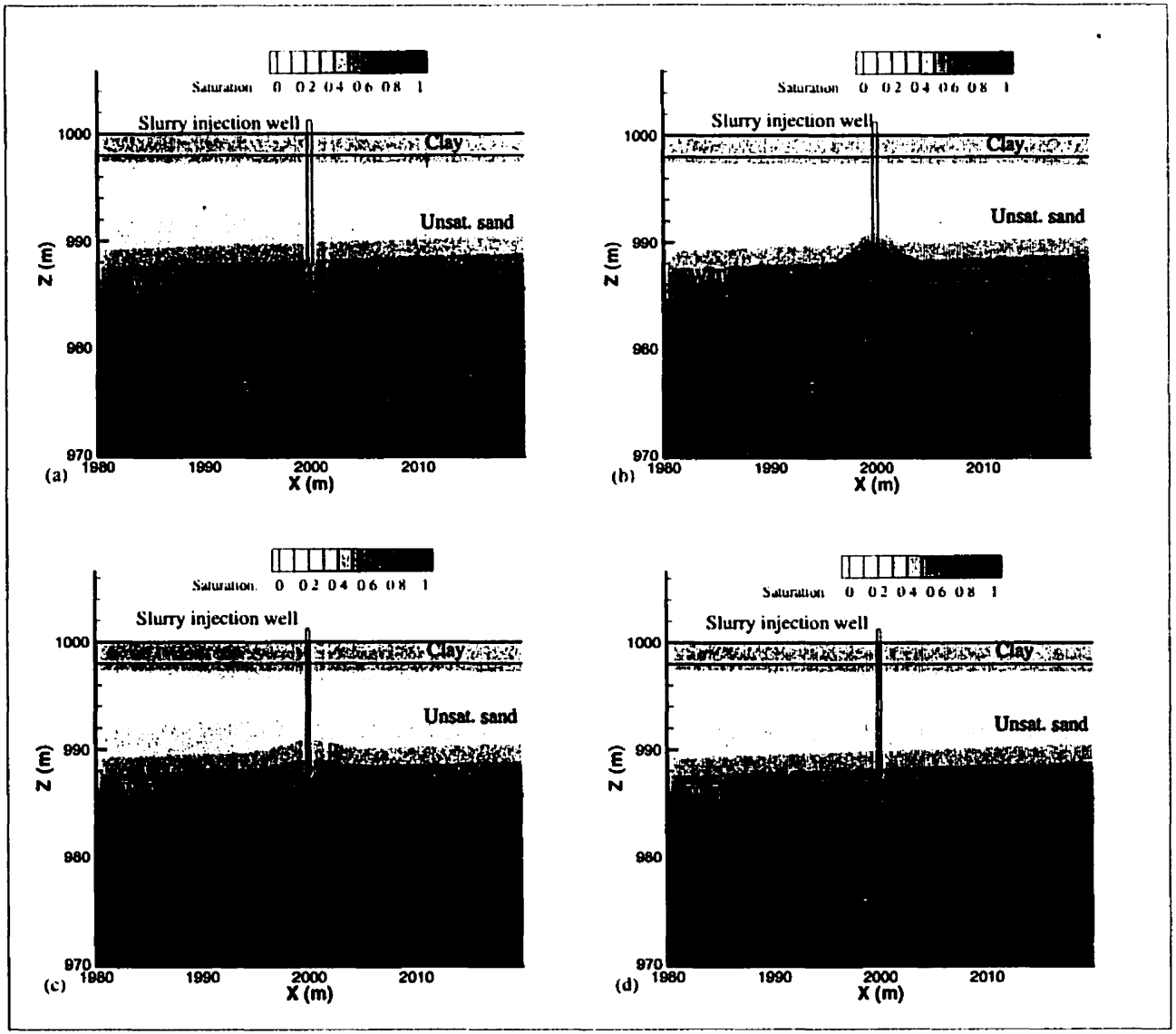


Figure 6.9 Simulated saturation variations in the X-Z plane at Cambridge site: (a) background, (b) following slurry injection, (c) one day following the slurry injection, (d) 6 days following the slurry injection. The change in the pattern saturation of clay layer compare to sand layer is because of difference in soil-water characteristic curves of these two materials

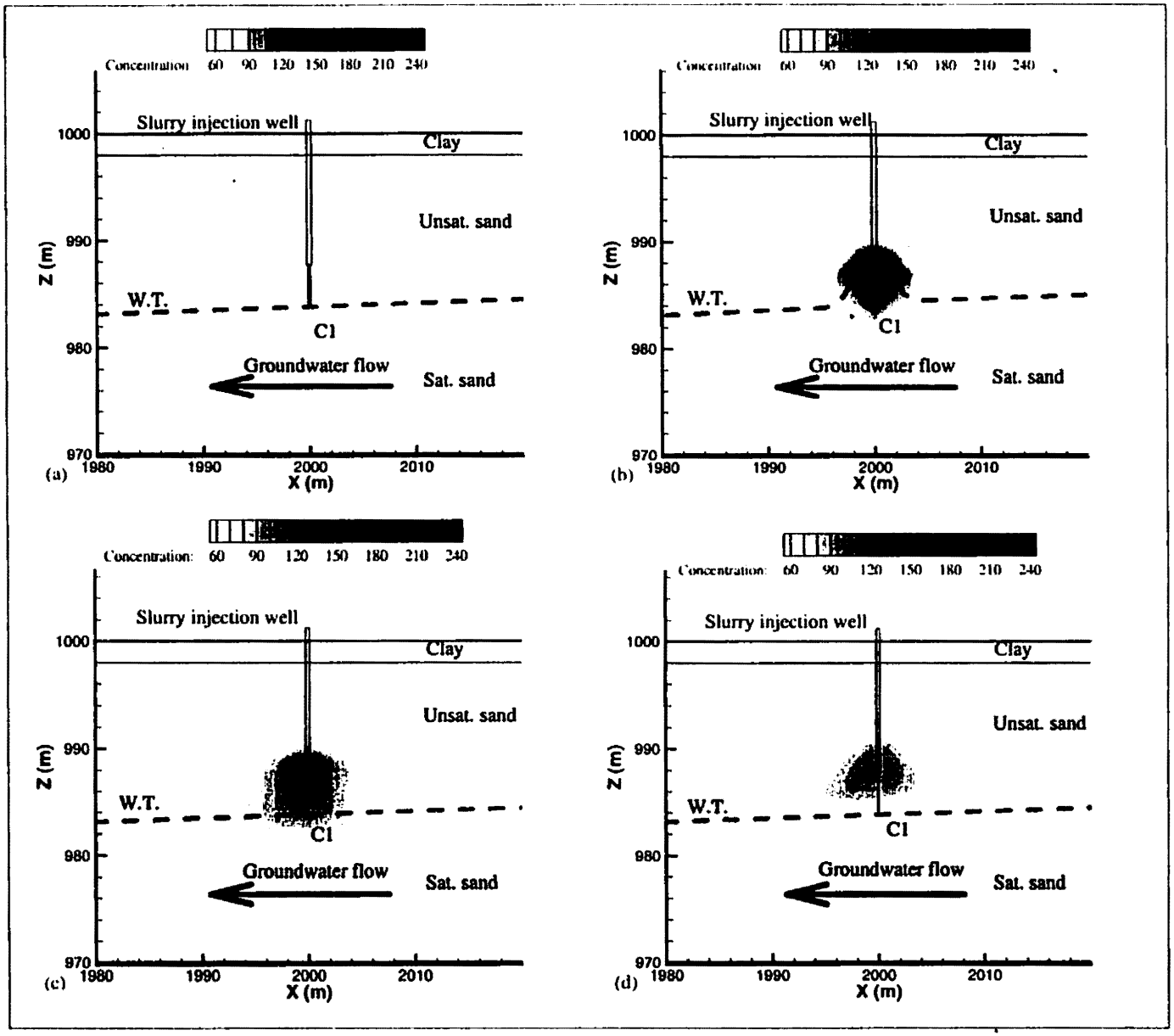


Figure 6.10 Simulated salt concentration in the X-Z plane at Cambridge site: (a) background, (b) following slurry injection, (c) one day following the slurry injection, (d) 6 days following the slurry injection

Figures 6.9a to 6.9d show the simulated saturation variations from steady-state condition to 6 days after the slurry injection. These figures are consistent with the pressure head results (Figures 6.9a to 6.9d). Figures 6.9b and 6.9c show the extra water content caused by the slurry injection, the main driving force in moving the plume from the unsaturated zone toward the saturated zone.

Figure 6.10 shows simulated salt concentrations at the steady-state condition (a), following the injection (b), and at one day (c) and 6 days (d) after the slurry injection. The maximum water table elevation following injection was 11 meters below ground surface, but the salt concentration was distributed up to 6 meters below the surface. The injection point has a higher hydraulic head than the region above the (dynamic) water table and that causes an unsaturated flow of the slurry to a higher level. Since most of initial hydraulic parameters were either assumed or extracted from the literature, the simulated results would not expected to be exactly the same as real measurements.

Figure 6.10 shows the concentration distribution. Since there is no recharge from the top surface, after the change of pore water concentration from the injection, the pore water concentration in the unsaturated zone will change only based on diffusion processes. If one wants to see the downward movements of the injection plume, one should look at the mass distribution rather than concentration distributions.

6.3 Simulation of the ERT response to the injection

The purpose of this section is to show the possibility of combining a groundwater transport-flow model and an electric field forward model to study the behaviour of the electric field over a conductive plume. This procedure may be used for the ERT inversion as an initial guess of resistivity distribution for a conductive or a resistive plume.

The simulation has tried to mimic the Cambridge ERT scenario (Figures 2.4 and 5.4); however, a single model can not be expected to fit the measurements perfectly. The aim is primarily to give an example of how modelling of a more complete data set might be initiated. Current was injected in the equivalent of the SW monitoring well, roughly 2 m away from the injection well, which also contains 5 potential electrodes and is 0.75 metres below the water table. The salt concentration distribution of the injected slurry at each step (Figures 6.10, a-d) was used as input to SALTFLOW to compute the ERT response of each step (the input files of FRAC3DVS and SALTFLOW for these simulations are presented in Appendix G). SALTFLOW has been modified to convert the pore water electrical

conductivity to formation electrical conductivity. The following equation (based on Archie's law Equation 2-6) is used to calculate the electrical resistivity distribution of the simulated electric potentials in the Cambridge scenarios:

$$\sigma_t(t) = a\,\sigma_w(t)\,\Phi^n S_w^n(t) \qquad (6\text{-}1)$$

where $\sigma_t(t)$ is the new formation electrical conductivity at time t following injection, $\sigma_w(t)$ is the pore water conductivity at time t following injection. Background conductivities were assigned to those elements, which were not affected by the slurry injection. The coefficients of the Archie's Equation were varied by trial and error so that the simulated potential field approached the measured value. The background electrical conductivities for the site were extracted from conductivity well logs of the monitoring wells (*Gilson*, 1996).

A mesh of 95 by 77 by 27 (X=4000m, Y=4000m, Z=1000m, respectively) was used for a three-layer case (2m clay at top, 14m unsaturated sand between the clay layer and saturated sand layer beneath) with a conductive anomaly (based on the slurry plume obtained from the flow-transport simulation) at the center. Around the current electrodes, finer meshes were used and these get coarser gradually towards the boundaries. A zero potential was assigned to the lateral boundaries of the model.

The casing used for the slurry injection well was a 2-inch Steel casing, which was electrically highly conductive. Based on the following formulations, the casing was implemented in the simulations:

$C_v = A \times \sigma_{steel}$ = element x-section $\times\ \sigma_{element}$

$\sigma_{steel}\ (\text{pi}(r_2^2 - r_1^2) \times l)$ = element x-section $\times\ \sigma_{element}$

$\sigma_{element} = \sigma_{steel}\ (\text{pi}(r_2^2 - r_1^2) \times l)$ / element x-section

$\sigma_{steel} = 5.1e^{+8}$ (from page 290 of *Telford et al.*, 1993)

$r_1 = 1.75" = 0.04445m$

$r_2 = 2" \quad = 0.0508m$

$\sigma_{element} = 5.0e^{+8}\ (3.14(2.58064e^{-03} - 1.9758025e^{-03}) \times 1\ m/(1m \times 1m^2)$

$\sigma_{element} = 95004 \sim 100000\ /m^2$ of elemental x-section in the model

The simulated potential fields for background, 1 day following injection and 6 days following injection are presented in Figures 6.11 and 6.12 for the X-Z and X-Y planes respectively. The results were obtained based on a value of 2.3 for the coefficient a and a value of 2 for m and a value of 2 for n in Equation 6-1. These numbers resulted in model voltages similar to those observed in the measurements.

A comparison between measured data from the Cambridge site (Figures 6.1 to 6.3) and the simulated potential fields show reasonable consistency of the potential field behaviour. Background potentials are low at the surface. The slurry plume causes an increase of the potential field by about 1500 mV/A (Figure 6.12b). This high potential decreases as the slurry injection stops and time passes (Figure 6.11c and 6.11d), again consistent with the trend of the measured results.

For the downhole electrodes, the comparison of model and measured results is best shown in tabular form. Table 6.1 compares the measured and simulated potentials for the downhole electrodes at the three different time steps. Again emphasizing that a perfect match is not expected with a single simulation, the Table should be examined only for similar trends.

Table 6.1 Simulated and measured potential values for the downhole electrodes at the Cambridge site

Row	Step	Background		1 day after slurry injection		7 days after slurry injection	
		Measurement	Simulation	Measurement	Simulation	Measurement	Simulation
1	SW monitoring well	C1	C1	C1	C1	C1	C1
2	SE monitoring well	6.4263	6.4211	5.5278	3.5912	6.0806	6.0093
3	NW monitoring well	5.1538	5.2654	4.5753	3.5039	5.0438	5.1263
4	NE monitoring well	4.6140	4.3231	4.1606	3.1150	4.5677	4.6631
5	0.5 below slurry injection point	4.7266	4.7331	4.0210	3.4153	4.4231	4.4016
6	1.5 below slurry injection point	5.3983	5.0412	4.3924	3.4483	4.8661	4.8345
7	2.0 below slurry injection point	5.7408	5.6459	4.8665	3.4894	5.3232	5.3369
8	2.5 below slurry injection point	6.4592	6.5536	5.3635	3.5429	5.8898	5.8974
9	3.0 below slurry injection point	6.7101	6.7726	5.9257	3.6572	6.5083	6.5114

Units are V/Amps

The simulation results show, in general, a decrease of electric potential at the downhole electrodes level as the voltage requirements for a one ampere current drop with the increasingly conductive ground path. The one exception to this, at the potential electrode one metre below the current injection point, may be a result of trying to simulate a measurement so close to the current electrode.

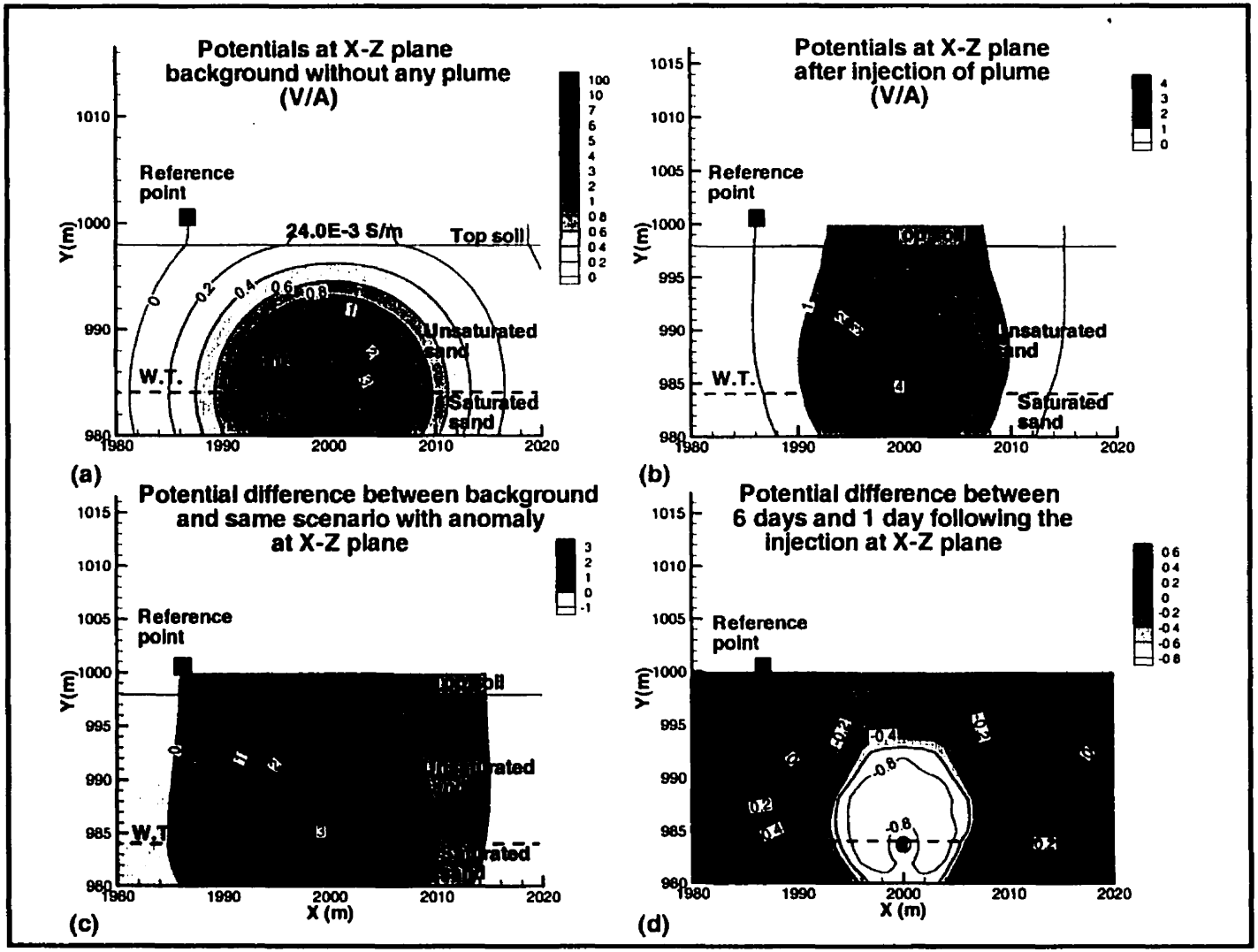


Figure 6.11 Simulated potentials with respect to a reference point the X-Z plane for Cambridge scenario: (a) background, (b) one day after slurry injection, (c) 6 days after slurry injection, (d) the potential difference between one day and 6 days after slurry injection. Units are V/A

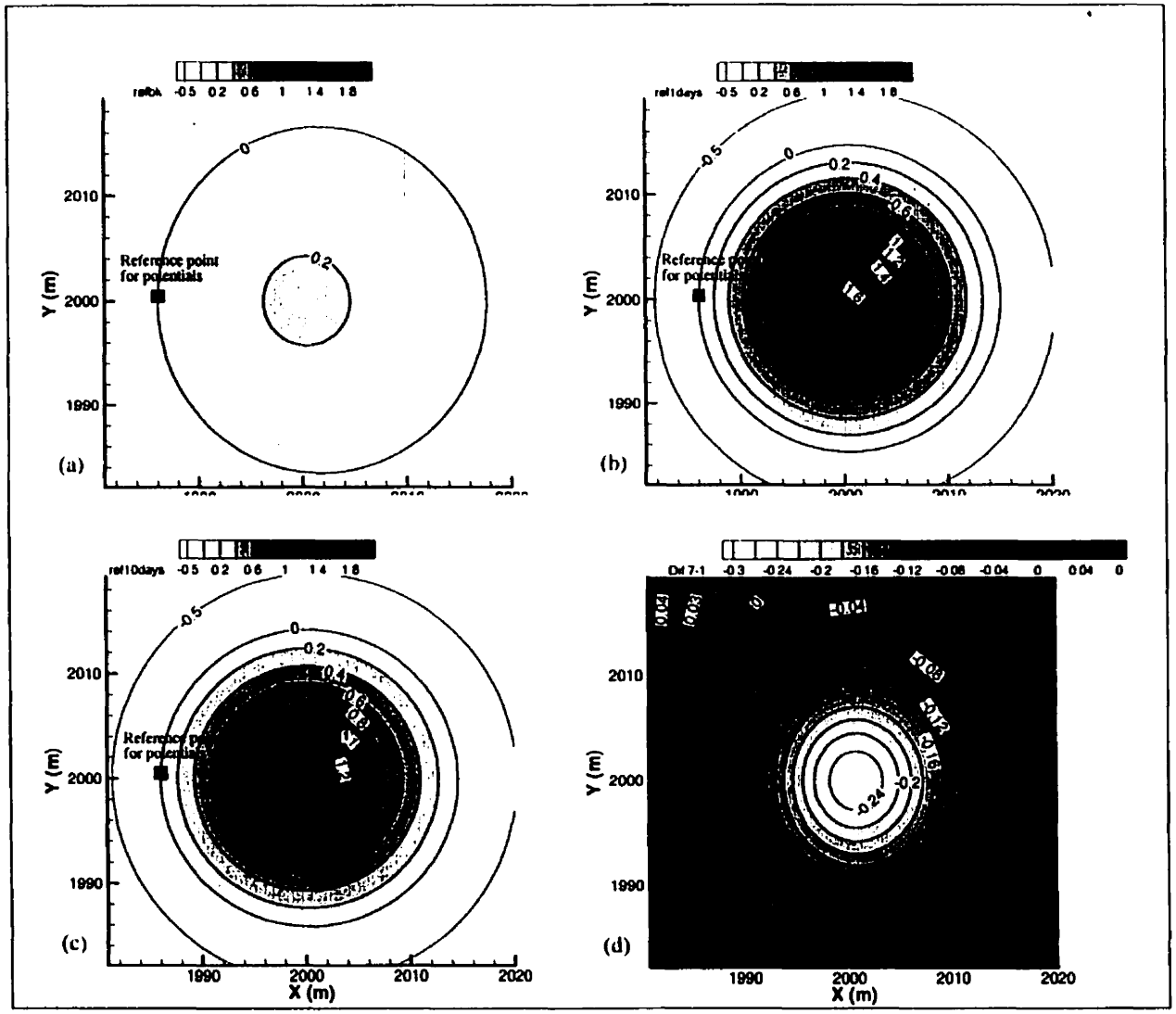


Figure 6.12 Simulated potentials with respect to a reference point in the X-Y plane for the Cambridge scenario: (a) background, (b) one day following the slurry injection, (c) 6 days following the slurry injection, (d) the potential difference between one day and 6 days following the slurry injection. Units are V/A

Because of high changes in the conductivity of a zone above the current electrode, the energy required for the current to reach to the surface is less than background (shielding effect); therefore the voltage on the surface has increased. The downhole electrodes show a drop of voltage with respect to the background because the current has found a preferred path condition and is reoriented so that less energy is concentrated through the direct downhole passes. The model and field data have been statistically checked, using Equations J-1 to J-4 in Appendix J. The results show an acceptable fit for these two approaches (Table 6.2)

Table 6.2 Statistical evaluations of simulated and measured potential values for the Cambridge site

Time	Surface electrodes				Downhole electrodes			
	RMSE	CD	EF	CRM	RMSE	CD	EF	CRM
Background	1.2428	1.0020	0.0020	-0.0196	0.0162	0.7273	0.2727	-0.0180
One day after injection	13.0829	1.0108	0.0107	0.0011	0.0400	0.5108	-0.9577	-0.0399
One week after injection	57.0058	0.6748	-0.4820	-0.1831	0.0243	0.9978	0.0022	0.0059

The scatter and residual plots of measured and predicted data were plotted in Figure 6.13 to 6.15. The simulated and measured data fit within an acceptable range. The reasons for a not complete fit may be counted as a short time monitoring for a long-term process, improper assumptions for required parameter in the simulations and the equipment difficulties presented in Appendix C. A better fit would be accessible through an inverse approach.

Another objective was to check the ability of ERT to monitor the movement of subsurface resistivity anomalies. The measurements at one and 6 days following injection were subtracted to produce the contour map of change in Figure 6.6. This map is reproduced in Figure 6.16b) and compared with the simulated change in potential (from 6.12d) reproduced in 6.16 a. The change in the simulated and measured data over the 6 day period is similar in its trend, although the absolute magnitudes are not well matched (Figure 6.16). It should be noted also that the ERT response to this change in the plume's configuration is substantial, 2 to 3 orders of magnitude above a typical instrumental resolution of 1millivolt in the mapped area shown in Figure 6.6 or 6.16a.

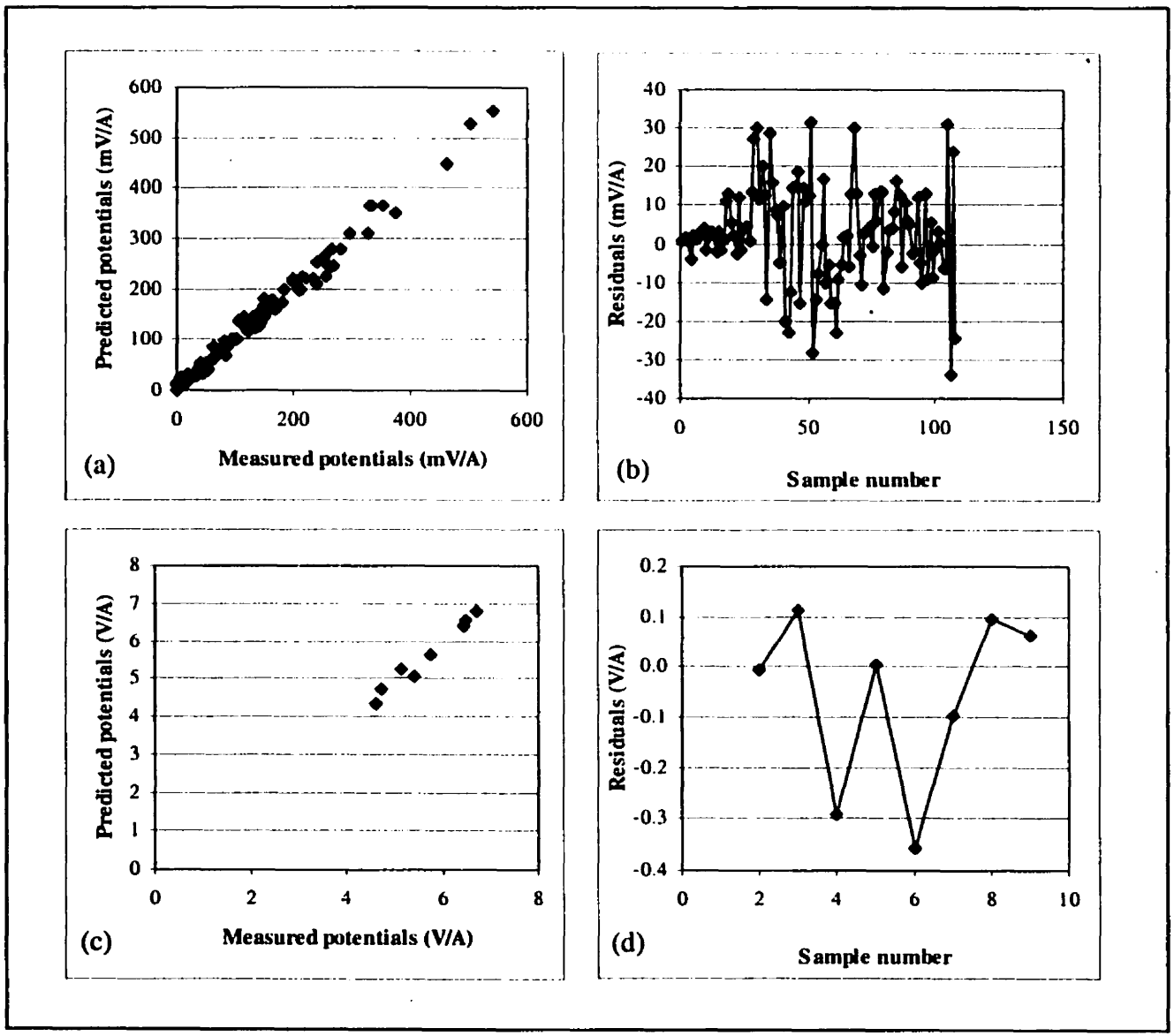


Figure 6.13 Scatter and residual plots of background measured and predicted potentials at Cambridge site: (a) scatter plot of potential at surface, (b) residual plot of potential at surface, (c) scatter plot of potential at downhole electrodes, (d) residual plot of potential downhole electrodes

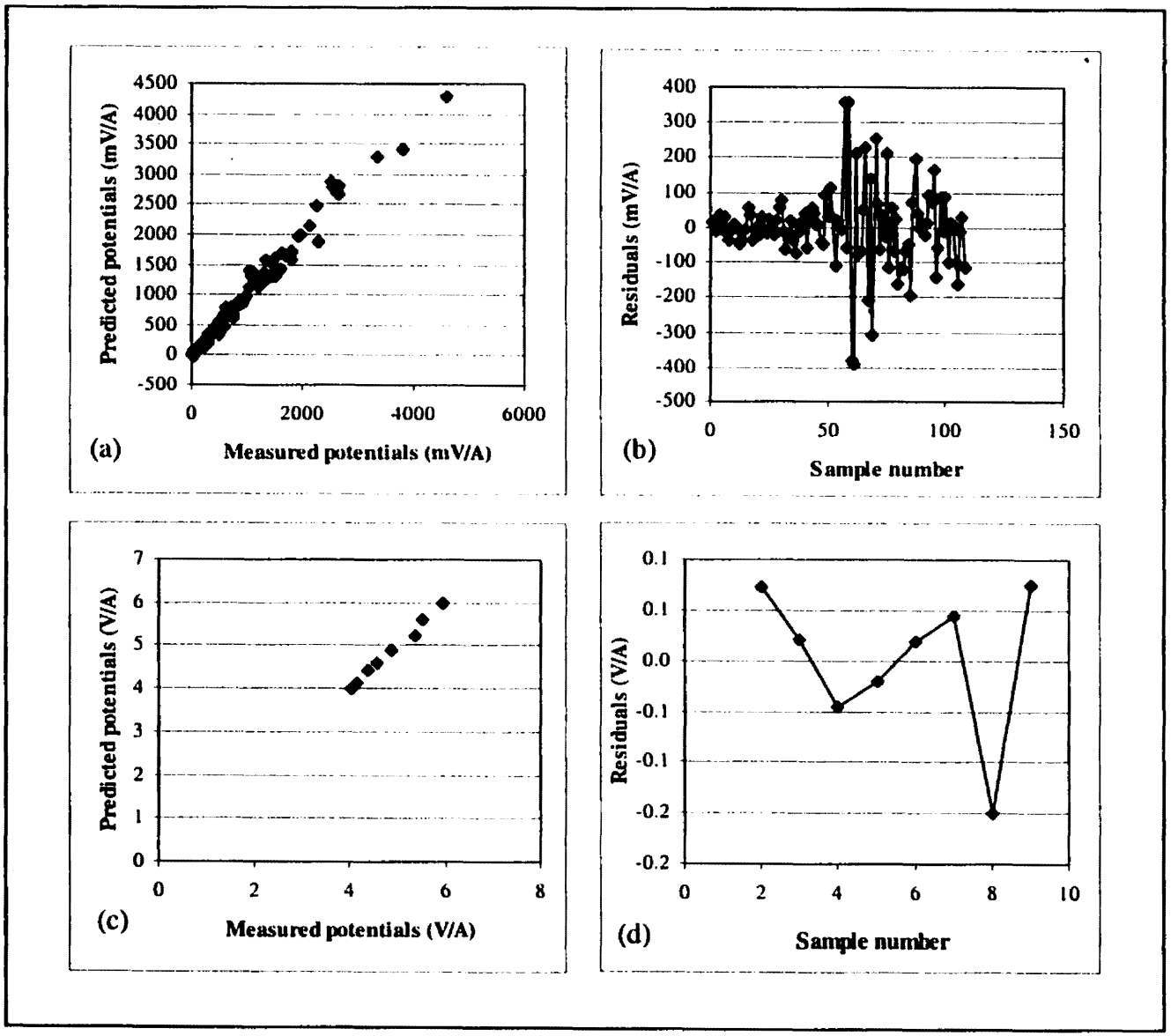


Figure 6.14 Scatter and residual plots of measured and predicted potentials one day following the injection at Cambridge site: (a) scatter plot of potential at surface, (b) residual plot of potential at surface, (c) scatter plot of potential at downhole electrodes, (d) residual plot of potential downhole electrodes

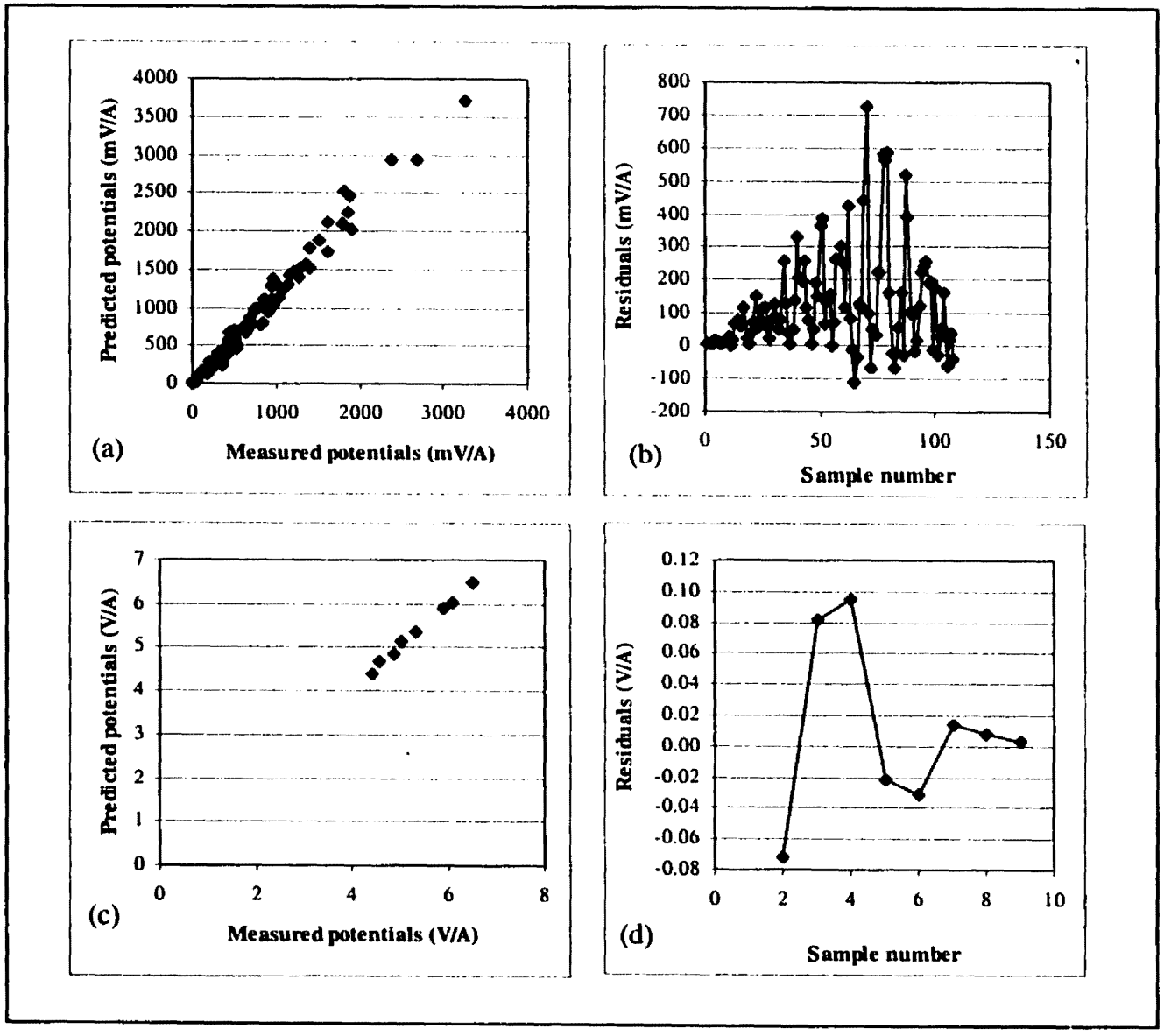
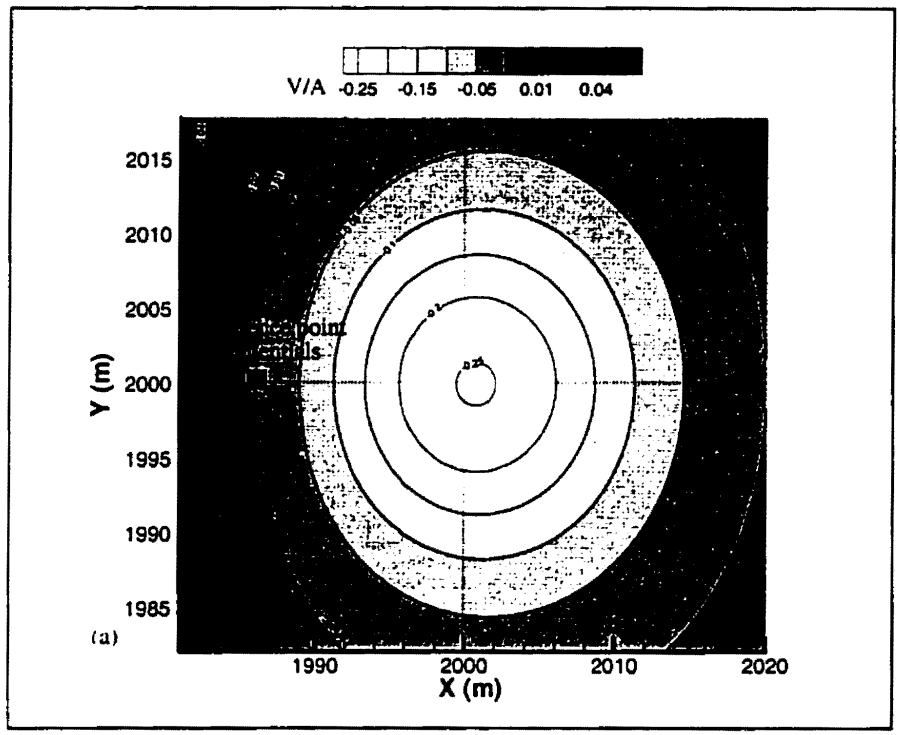


Figure 6.15 Scatter and residual plots of measured and predicted potentials one week following the injection at Cambridge site: (a) scatter plot of potential at surface, (b) residual plot of potential at surface, (c) scatter plot of potential at downhole electrodes, (d) residual plot of potential downhole electrodes



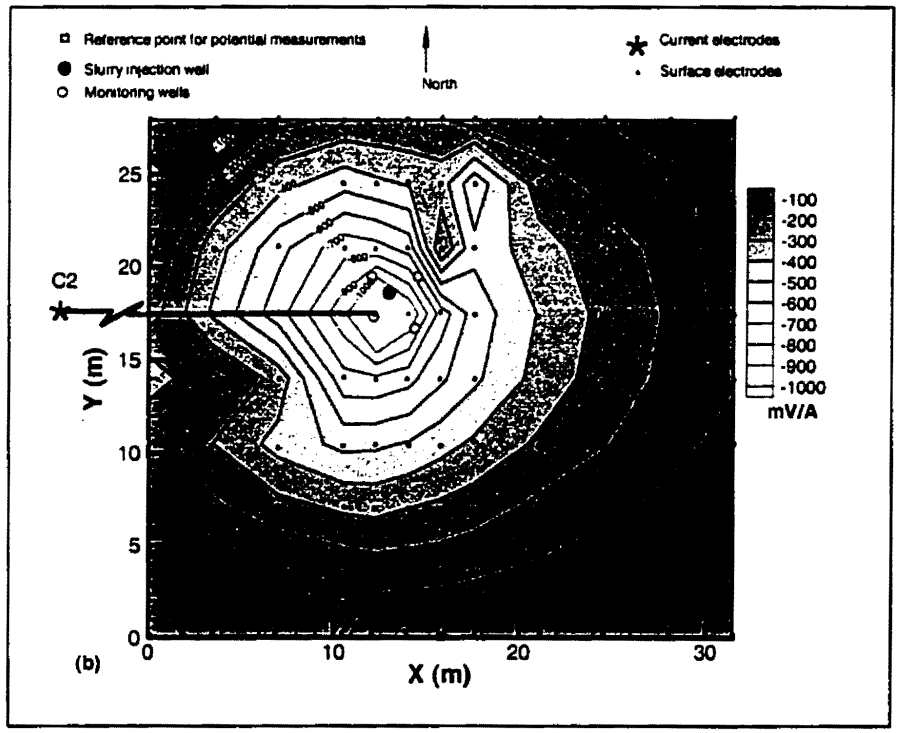


Figure 6.16 Simulated and measured changes in potential (V/A) between 1 day and 6 days following the injection in the Cambridge site at X-Y plan: (a) simulation, (b) measured

In summary, the data collected from the Cambridge site have been reasonably simulated by this preliminary model of a complex scenario. Further more, it is clear that ERT is capable of detecting both the injection itself and the changes in subsurface resistivity caused by its movement.

6.4 Adjoint Sensitivity analysis

Detecting the ERT anomaly is an important step, but there are other practical issues. One is how to place a small number of electrodes in the most efficient arrangement to monitor a particular situation. The other is the use of models such as SALTFLOW or FRAC3DVS to interpret a data set. Direct modeling by trial and error in three dimensions is extremely time-consuming and costly. Eventually some sort of automated model fitting or inversion process should be considered.

For both these issues, it will be important to understand the sensitivity of the ERT responses throughout the measurement region to perturbations in the source parameters (i.e., its conductivity distribution, dimensions, depth, etc). Sensitivity analysis offers a shortcut to this goal by computing the partial derivatives, as discussed in sections 2.4.3.

The simulation at the Cambridge site for one day following the slurry injection (Figure 6.11c) was used as an example of the application of adjoint sensitivity analysis to evaluate the sensitivity of the potential field distribution to changes in source parameters.

The program FRACT3DVS was used to simulate this scenario, for two different electrode arrangements. The first arrangement was with one of the current electrodes placed at the water table (2000,2000,984) at the center of grid and the other one placed at the ground surface 10 meters away from the grid center (1990,2000,1000). The second arrangement was with both current electrodes placed at the ground surface 30 meters away from each other at the center of the grids {(1985,2000,1000) and (2015,2000,1000)}. Figures 6.17 to 6.20 present the results for these two electrode configurations. The potential field of (a) the background, (b) immediately after the injection, (c) the difference between the background and the post-injection, and (d) the state sensitivity of the scenario for changes in the conductivity of the source zone for X-Y and X-Z planes are presented in one page (for each plan) for a better comparison.

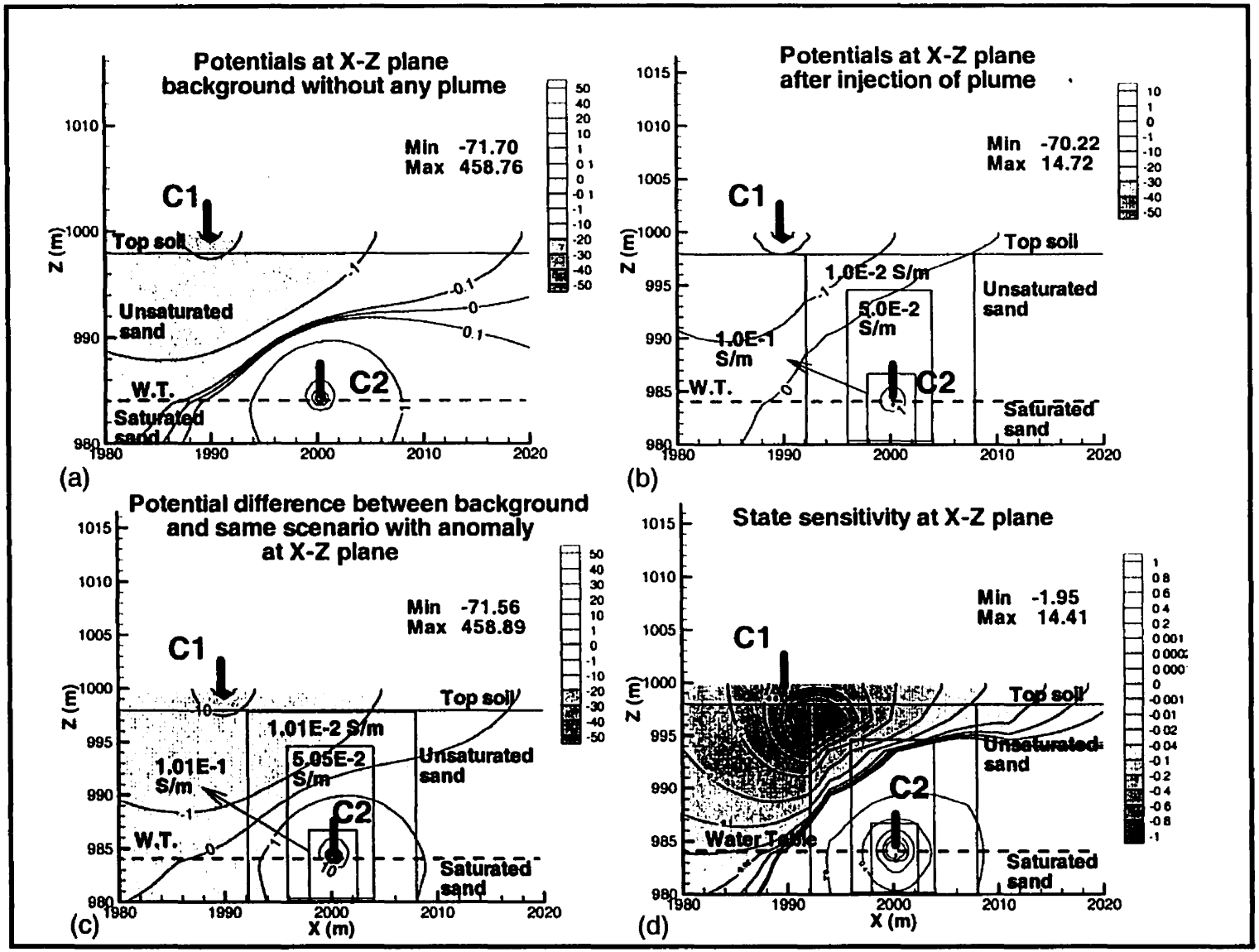


Figure 6.17 Potential (V/A) and state sensitivity distribution in the X-Z plane for a dipole set at surface (1990,2000,1000) and downhole (2000,2000,984): (a) background, (b) including conductive anomaly in the scenario, (c) the potential differences between background and after the existence of conductive anomaly, (d) state sensitivity distribution. Current electrodes as shown

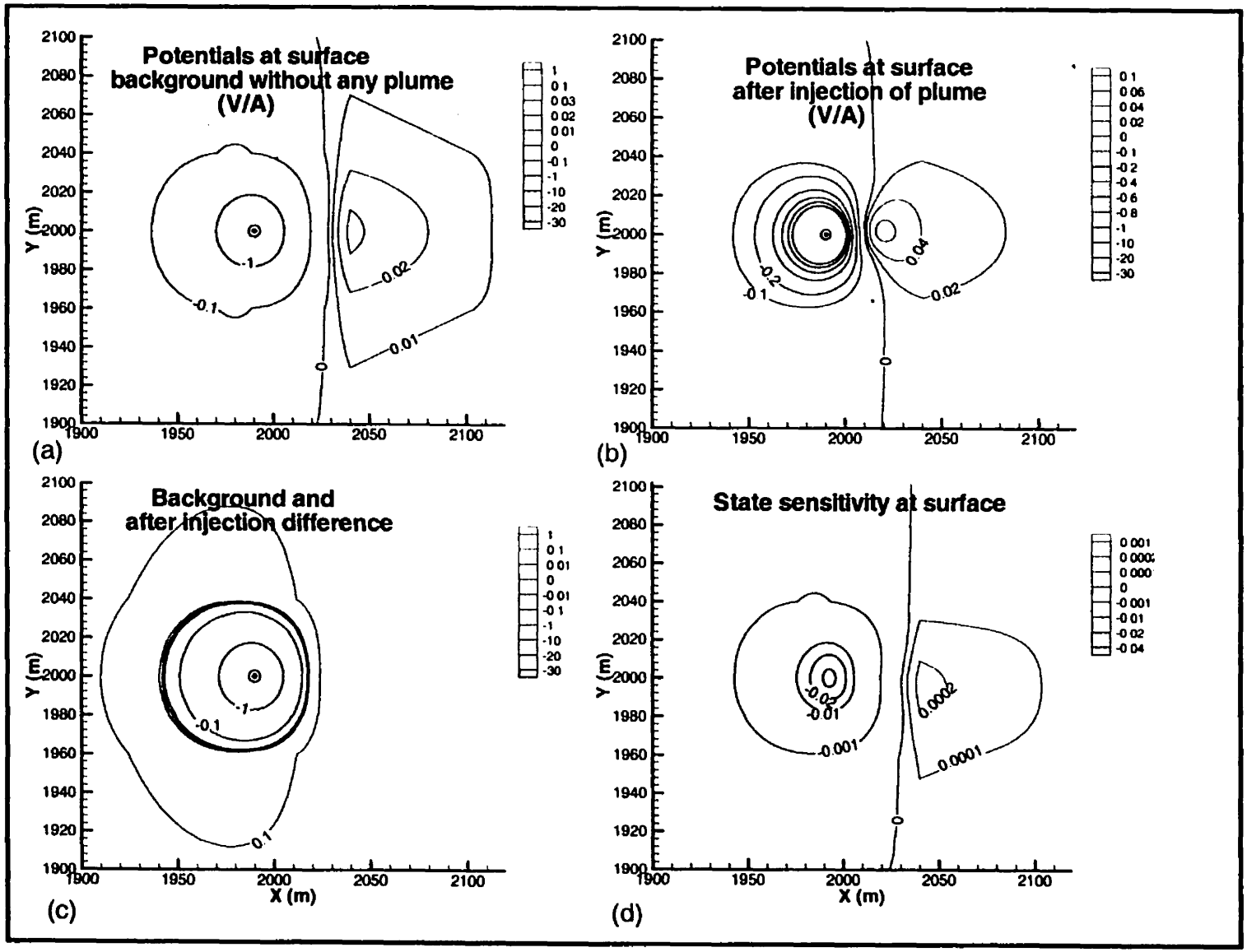


Figure 6.18 Potential (V/A) and state sensitivity distribution in the X-Y plane for a dipole set at surface and downhole: (a) background, (b) including anomaly in the scenario, (c) the potential differences between background and after the existence of conductive anomaly, (d) state sensitivity distribution

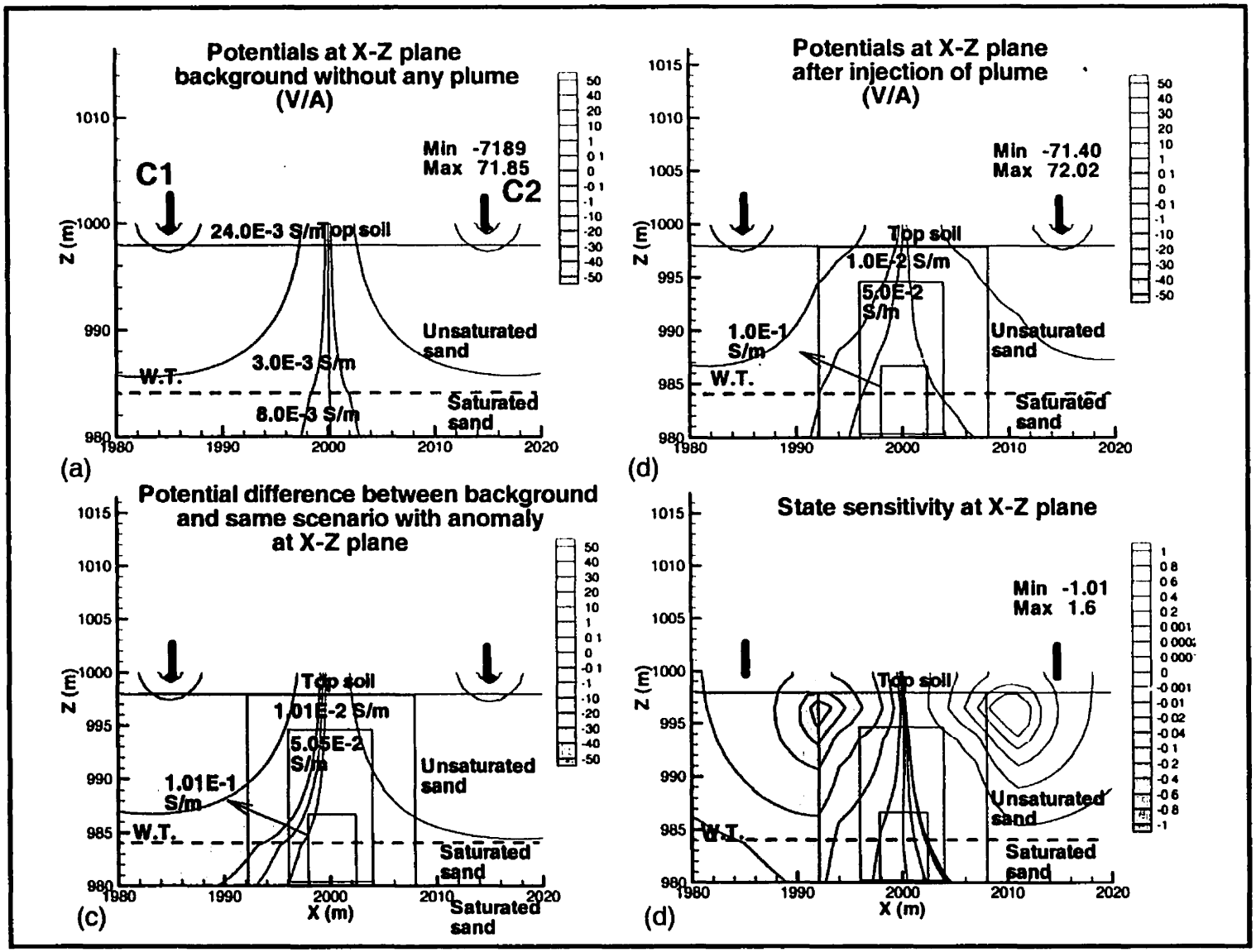


Figure 6.19 Potential and state sensitivity distribution in the X-Z plane for a dipole set at surface (1985,2000,1000) and (2015,2000,1000): (a) background, (b) including anomaly in the scenario, (c) the potential differences between background and after the existence of conductive anomaly, (d) state sensitivity distribution. Current electrodes as shown

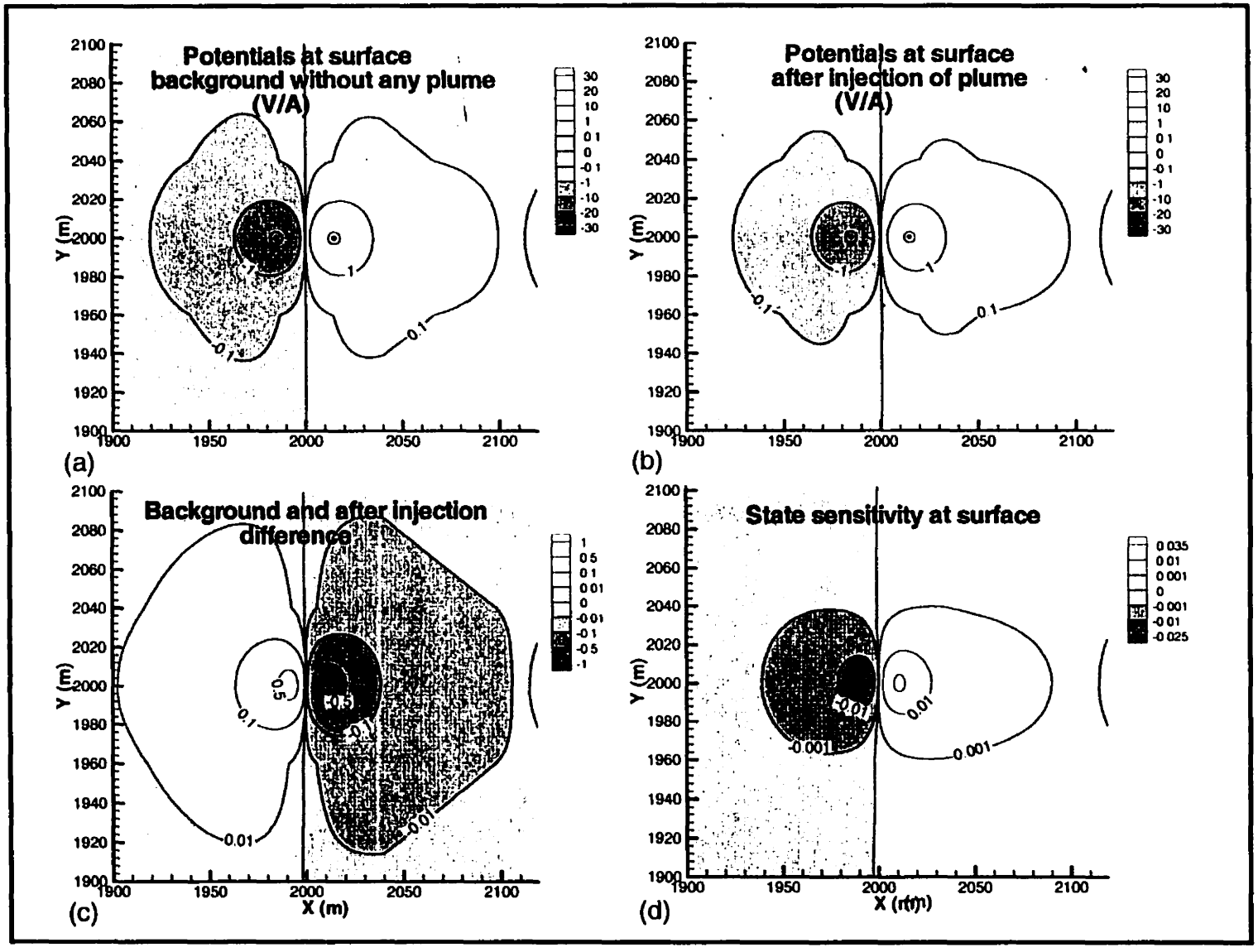


Figure 6.20 Potential and state sensitivity distribution in the X-Y plane for a dipole set at surface (AB/2 = 15 m): (a) background, (b) including anomaly in the scenario, (c) the potential differences between background and after the existence of conductive anomaly, (d) state sensitivity distribution

The state sensitivity maps (part d in Figures 6.17-6.20) show the percentage change in ERT response that would be produced by a 1% change in the conductivity of the source region, for the particular current electrode arrangement at this particular time (1 day post injection) in the history of the simulated saline plume. Note, for example, that there are regions of zero sensitivity, where no response would be expected. Electrodes placed in these zones would not be particularly effective for monitoring at this particular time. The state sensitivity plots show that the response increases in some areas, decreases in others. We note that the sensitivity does depend on the current electrode configuration. Finally we note that, compared to computing two complete models 1% apart in conductivity, the adjoint sensitivity requires the time equivalent of roughly 1.3 individual model computations.

6.5 Evaluation new ERT measuring system

The evaluation of commercial resistivity measuring systems (Appendix B) has shown that they are not well designed for fast high quality ERT data collection. One part of this thesis has been the design and implementing of a more appropriate measuring system for ERT measurement so that the data collection can be increased in speed, accuracy, and repeatability. This system has yet to be field tested, so that the evaluation given here is based on bench measurements.

6.5.1 Precision

The measuring system performance is presented in this section. The data summarized here in graphs are given in Appendix F. There are two sources of gain in the new system: the first is the voltage divider gain on the switching board, and the other one is on the A/D converter board. Both gains are programmable and are controlled by the written program in LabVIEW software. The most efficient combinations of these gains were used to calculate the precision of the system over 8 ranges of measurement, based on the A/D converter resolution (which is 16 bits, 1 in 65,536). Figure 6.21 shows these voltage ranges and their calculated precision expressed both in volts and as a percentage of the range minimum (Table F.1).

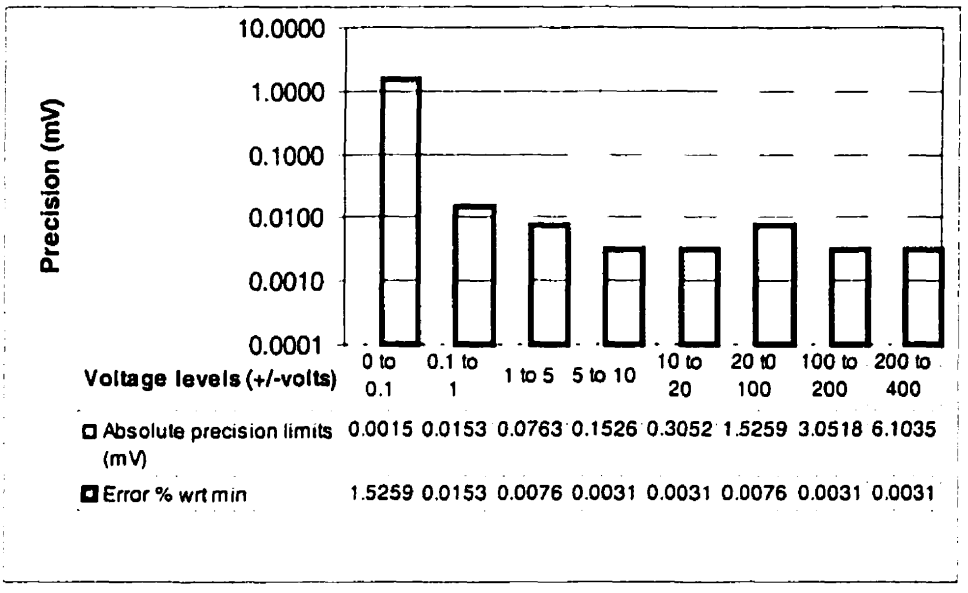


Figure 6.21 Precision achieved at each input voltage range of the ERT measurement system. The percentage error is given with respect to the minimum in each range, except for the lowest range where it is with respect to the maximum.

6.5.2 System Noise

The system performance has also been checked in a series of laboratory tests. Figure 6.22 shows the laboratory setup. These tests have been conducted for both sources of gain in the new system. The first set of tests was to check the noise level of the system itself, which was carried out by shorting all the input channels on the A/D converter board to produce a voltage input of zero. Figure 6.23 displays the internal noise level on one of the system's 64 channels , which is representative of the rest (Table F.2).

The results show that there is 4 to 9 mV DC offset on each channel and about ±0.05 mV variation of the signal input. Since the prototype switching board is build as a "wire-rap" and not as its final printed circuit board form, and since the wire used for connections was not shielded, this variation of the input signal might be due to the cross-talk between those wires. We can be reasonably certain that these noise levels will be reduced significantly by using a well-designed printed circuit board. In addition, a proper stacking procedure would help to reduce the noise level. The default configuration for stacking in the new ERT measuring system is:

- Only the last one-third of each half pulse is used to remove the IP effects;
- At least 10 samples in each half pulse are stacked (two procedures are explained on pages 56-57). This is intend to cancel out random noise and enhance the signal amplitude with respect to the background; and,
- Data are collected for 1 minute.

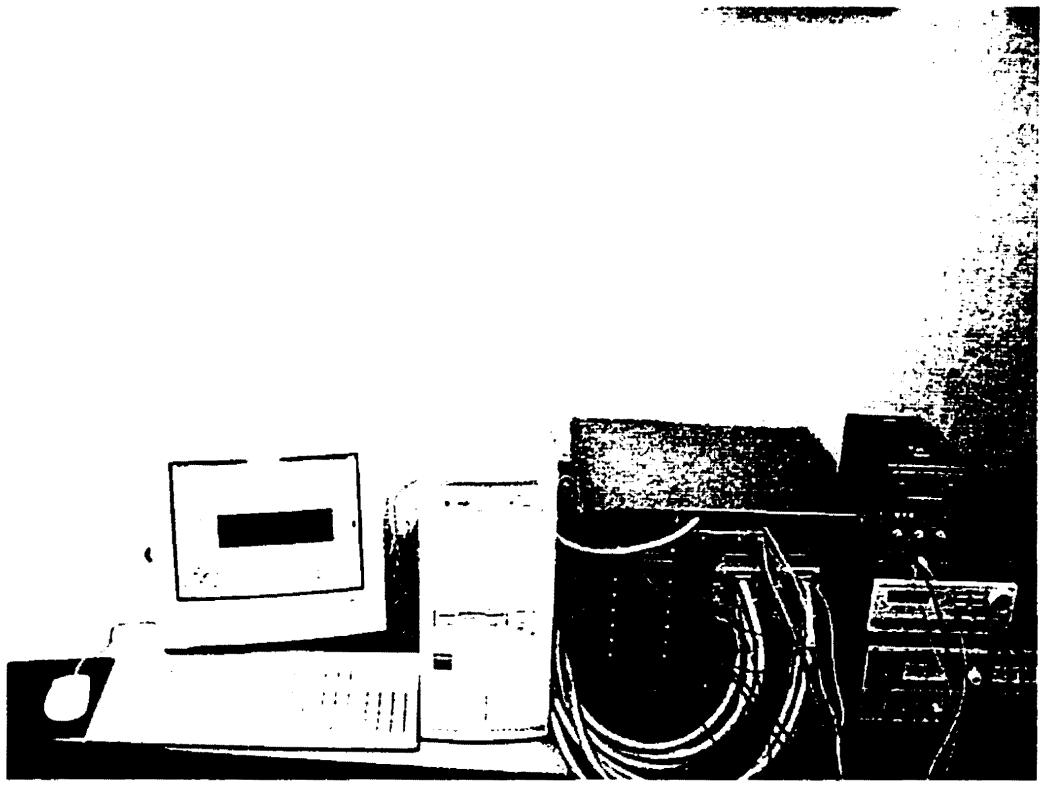


Figure 6.22 The new ERT measuring system laboratory setup

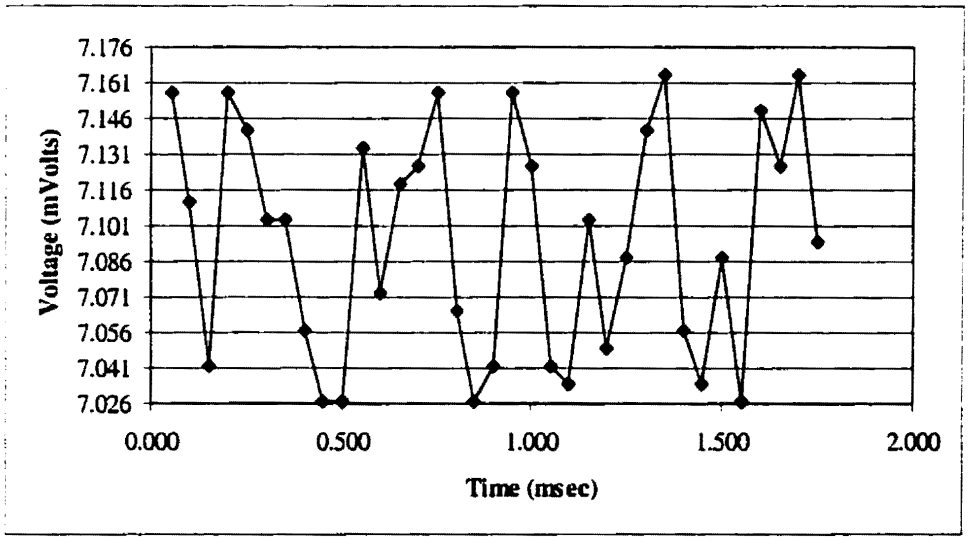


Figure 6.23 Noise level of one (shorted) channel of the ERT measuring system, measured on the first range of Figure 6.18 (0 to 0.1 mV)

6.5.3 Accuracy

The second set of laboratory tests was to check the readings of the new system for different voltage levels. This was accomplished by connecting a high precision DC source directly to the input channels of the system. Figure 6.24 shows the standard deviation of the measured values for direct voltage inputs ranging from 7 to 110,000 millivolts for one of the 64 channels. The measured data are presented in Table F.3 in Appendix F. The accuracy between 1 and 400 volts is comparable to the theoretical precision of the system. On the most sensitive range, the accuracy is estimated as only 0.05 millivolts. Since some of the error may originate in the DC source, the accuracy of the system might be better than these results suggest.

The results obtained show that the new system is capable of performing ERT measurement with an adequate speed and resolution. This system is more sensitive to noises in the low voltage range. The noise level should drop by using a well-designed printed circuit board and stacking the data.

6.5.4 Environmental influences

The above estimates of noise and accuracy do not take into account possible environmental parameters, such as temperature and humidity. The system has not been tested for sensitivity to these factors, so the influences can only be estimated from the ratings of the individual components.

The operating ranges of the different components used in new ERT measuring system are presented in Table 6.3. Overall this system can operate between 0 to 55 °C within the range of 5 to 85% relative humidity. Since the new system has different levels of voltage inputs, uncertainty analysis is evaluated based on these levels.

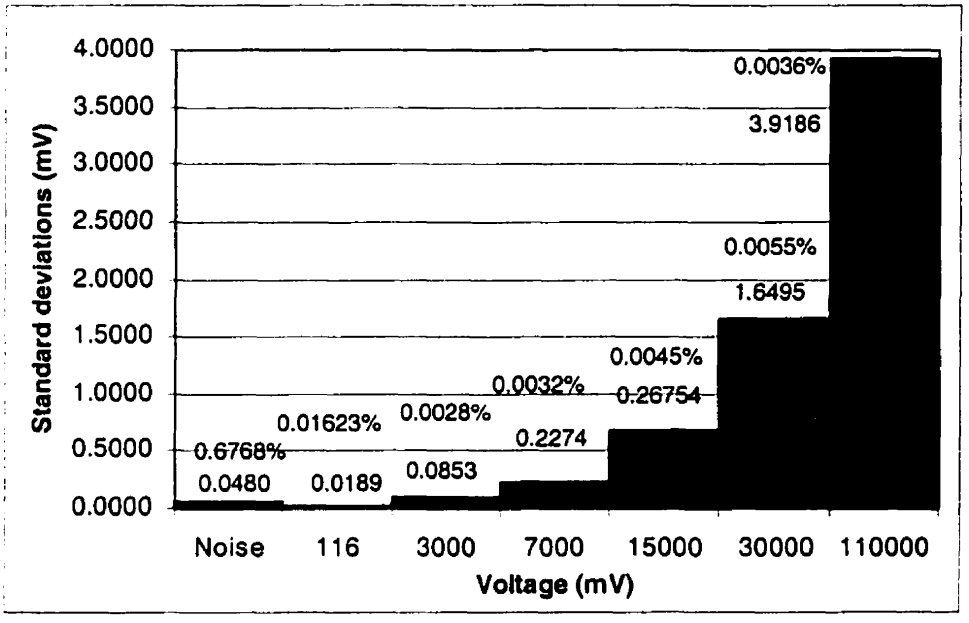


Figure 6.24 Standard deviations of data collected at different voltage levels

Table 6.3 Environmental operating ranges of different components used in the new ERT measuring system

Condition for operation	A/D	AMUX	DI	DO	Reed relay 4 poles	Reed relay 2 poles	Diodes	Darlington array
Temperature (° C)	0 to 55	0 to 70	0 to 50	0 to 50	-40 to 70	-40 to 71	-65 to 200	-20 to 85
Relative humidity (%)	5 to 90	5 to 90	0 to 90	0 to 90	5 to 85	5 to 85	N/A	N/A

N/A: *Not Available*

Since most of required data for evaluating the uncertainty of the measuring system are not available, the uncertainty of the measurement of new ERT measuring system has been estimated with an error margin of 0.01%, and based on the information of Figure 6.21 and the data in Appendix D. The estimated uncertainty of measurements is presented in Table 6.4. Based on the estimated measurement uncertainty, the new system has a better performance in the lower voltage ranges (up to 10 V).

Table 6.4 Estimated measurement uncertainty of new ERT system

	Voltage levels							
Level (V)	0 - 0.1	0.1 - 1	1 - 5	5 - 10	10 - 20	20 - 100	100 - 200	200 - 400
Gain	100	10	2	1	10	2	1	1
Absolute precision limits (±mV)	0.00153	0.0153	0.0763	0.1526	0.3052	1.5259	3.0518	6.1035
Uncertainty WRT Min. of each level (±mV)	0.00153	0.0168	0.0928	0.2441	0.5467	2.0674	5.6933	12.345
Uncertainty WRT Max. of each level (±mV)	0.0030	0.0318	0.1678	0.3941	0.8467	3.5674	8.6933	18.3450

The better uncertainty analysis would be obtained after extracting the behavior type curve of the new system with respect to environmental parameters (such as: temperature, humidity, noise level, etc).

Chapter 7

SUMMARY

Tomographic monitoring of time-dependent processes is the topic of much recent research in environmental and exploration problems. Electrical resistivity tomography (ERT) is considered one of the best and least expensive monitoring methods. The ERT technique is still in the process of development as a monitoring tool, requiring both improvements in its technology and a wider variety of applications to reach its eventual potential.

This research has concentrated on a very specific potential application of ERT, namely, monitoring waste injection of a slurry under high pressure. The waste is usually more conductive than its host and yields a resistivity contrast, with respect to its background; this may be used to monitor the evolution of the injection process. Using a permanent electrode arrangement for long term monitoring can remove many of the effects the host's heterogeneity and anisotropy when the process is analyzed in time.

The first objective of this thesis was to make ERT measurements of a slurry injection test using downhole and surface electrodes, to get first hand experience of the problem. Fortunately, we were able to piggyback on an injection experiment that took place in

nearby Cambridge, Ontario, and obtained a reasonably representative dataset extending from before to 10 days following the injection.

ERT data of a field trial of waste slurry injection were obtained.

This initial evaluation of the ERT technique as a monitoring tool for waste injection studies showed that for it to be effective, there were several issues to be considered. First, the injection process is very fast and large subsurface changes occur during short periods of time (minutes to hours). The commercially available resistivity systems available for our experiment could not make measurements fast enough to handle data collection and processing of what might be hundreds of electrodes in the required time frame. The first objective, then, was to design and construct a more suitable ERT measuring system. This system has been designed, and the potential measuring part constructed (Chapter 4) and evaluated in a series of lab tests (Section 6.4). As constructed, it can measure the voltage response at 64 electrodes in less than one minute, and can readily be expanded to 256 electrodes which could be sampled in the same time. Thus a process, such as slurry injection, can be monitored and the results displayed visually in real time.

The current electrode power supply (for injecting currents of one or more amperes into the ground) has been designed and contracted out for construction, but due to circumstances largely beyond the author's control, has not yet been delivered.

An ERT measuring system that would overcome the shortcomings encountered during the initial measurements has been designed and partially constructed. In its current configuration it can simultaneously (within minutes) measure voltages from 64 electrodes and can readily be expanded to 256 electrodes.

The second objective involved modeling. The injection at Cambridge was a truly 4-dimensional process, occurring in 3-space as well as time. The author did not have access to robust, well documented 3-dimensional ERT modeling software for undertaking a direct or inverse interpretation of the Cambridge data. The solution was to adapt the SALTFLOW model – a thoroughly documented and tested three dimensional groundwater flow and transport model with an excellent "front end" - as a platform for both the groundwater and resistivity modeling of the saline transport resulting from the waste injection. SALTFLOW was modified to solve the saline transport model, translate

salinity in space and time to electrical resistivity, and (based on equivalences described in equation 6.1) to solve the ERT model. In addition, replacement of the original sparse matrix solver with the WATSOLV subroutine (VanderKwaak et al., 1998) for sparse matrix solution, which has been the modified by author, improved the performance of SALTFLOW for our purposes. Section 3.3 presented results which showed that a preconditioned CG method combined with nested dissection ordering give faster convergence. The incomplete Cholesky-Conjugate Gradient (ICCG) method is the most efficient of the models for both level-based and drop-tolerance based preconditioning. The most efficient results were obtained by ILL^t(1,0.0) and ILL^t(∞,0.01) using the ICCG algorithm with nested dissection ordering. In addition, implementing a line element in place of grid points to represent the current injection makes the solution faster and reduces the model oscillation in the vicinity of the current electrodes, which results in lower grid densities in these areas.

A well documented, robust and "user friendly" 3-dimensional groundwater flow model has been adapted for the ERT direct model, which can serve to model both the hydraulics and the electrical response of the injected waste. The model was used to simulate- in an approximate manner - the field results from the Cambridge experiment. While a detailed match of data and model was not attempted, the general nature of the field results was clearly simulated by the model.

The third objective was to develop a sensitivity analysis as a means of predicting where the most appropriate locations for electrodes are for a given monitoring problem. Positioning several hundred electrodes for maximum effect in a given monitoring situation is not always intuitive. It is well known that the sensitivity of ERT monitoring drops as sensors are removed from the vicinity of the anomaly. Also, the number of downhole sensors that can be used is restricted by many factors. If the most probable subsurface developments can be guessed at, and their ERT responses modeled, more rational positioning choices can be made. However, brute force modeling of all possible subsurface scenarios is very time consuming. The author instead has set out to develop sensitivity analysis of a given model that would allow a less cumbersome evaluation of the influences of subsurface change on the ERT response.

There is a second and potentially more important application of sensitivity analysis in inversion of the data. Although this thesis has not attempted to formulate the inverse

problem, the provision of a sensitivity analysis along with a good forward model is clearly a step along this path.

Adjoint sensitivity analysis is a useful and a fast method with which to try to deal with these problems. Adjoint sensitivity is capable of generating a clear picture of the sensitivity distribution of different points with respect to the anomaly. Its main advantage is that it requires less iteration (consequently less costs) of the forward model compared to general state sensitivity, which needs to run a large number of forward models. An adjoint sensitivity analysis for the SALTFLOW model has been developed and discussed.

Adjoint sensitivity analysis has been developed for the SALTFLOW model that allows the experimenter to evaluate how best to position electrodes in the field for a hypothesized monitoring scenario. The analysis is also an important step along the path to any fully or partially automated inversion of the measured data.

Chapter 8

RECOMMENDATIONS FOR FUTURE WORK

This section makes several recommendations for work that should be undertaken to follow up or build on the work described in this thesis.

8.1 Modeling

The slurry injection at the Cambridge site took place just above the water table. As a result, the flow-transport model for simulating the injection plume had to deal with unsaturated as well as saturated, density-driven flow. This required the use of both SALTFLOW and FRAC3DVS for the groundwater simulation. If further slurry injection trials are to take place above the water table, either SALTFLOW should be modified to cover this concept or FRAC3DVS should be modified to cover the density driven flow condition.

8.1.1 Forward

The forward model can be improved by converting the code to FORTRAN version 90. This version allows a wider range of precision in the dimensioning of variables. This advantage would allow the user to employ the available computer memory more efficiently.

8.1.2 Inversion

The adjoint sensitivity method may be used to perform the inverse part of the ERT problem. Groundwater models of the process to be monitored process would serve as a good initial estimate to obtain the inverse model. The main advantage of adjoint sensitivity is the availability of quantitative values of sensitivity of each element with respect to a selected region (i.e., the conductive plume). Using this property along with a numerical approach such as one of the least squares methods should facilitate convergence of the model towards the measured data.

Eventually, joint inversion of both ERT and hydrogeological data measured at a site should be possible, which would result in a better estimation of the injection process.

8.2 Equipment

8.2.1 Data acquisition

The control part of the ERT system should be implemented in a digital printed circuit board or a micro component form. This will reduce the required wiring, and therefore noise levels.

The new ERT measurement system was not field tested as part of this thesis work. Since the electronic components used in this system are somewhat temperature and humidity dependent, a series of environmental tests should be conducted on these boards/components. If the collected data are very dependent on temperature, a thermocouple should be installed in the system and used to correct the measurements, based on test calibrations.

8.2.2 Power supply

A programmable power supply with a wide dynamic output range would allow the power output to be increased automatically during data acquisition to a level such that more of the collected data can have an acceptable precision.

References:

Alfano, L. (1962). *Geoelectrical prospecting with underground electrodes.* Geophysical Prospecting, 10, 290-303.

Anderson, D.K., R.C. Tozer, and I.L. Freeston (1995). *Analytic Solution of the Forward Problem for Induced Current Electrical-Impedance Tomography Systems.* IEE Proceedings-Science Measurement and Technology, 142 (6), 425-432.

Andrews, R.J., R. Barker, and L.M. Heng (1995). *The application of electrical tomography in the study of the unsaturated zone in chalk at three sites in Cambridgeshire, United Kingdom.* Hydrogeology Journal, 3 (4), 17-31.

Artola, J. and J. Dell (1994). *Broyden quasi-Newton method applied to electrical impedance tomography.* Electronics Letters, 30 (1), 27-28.

Asch, T. and H.F. Morrison (1989). *Mapping and monitoring electrical resistivity with surface and sub-surface electrode arrays.* Geophysics, 54, 235-244.

Asch, T. and H.F. Morrison (1986). *Interpretation of borehole-to-surface DC resistivity measurements at a contaminant site: A case study.* Proceedings of the surface and borehole geophysical methods and ground water instrumentation, NWWA, Denver, 127-147.

Axelsson, O. (1994). *Iterative solution methods.* Cambridge University Press, Cambridge.

Barker, R.D. (1995). *Apparatus and methods for simple resistivity experiments.* Teaching Earth Sciences, 20(3), 88-96.

Barker, R.D. (1992). *A simple algorithm for electrical imaging of the subsurface.* First Break 10, 53-62.

Barker, R.D. (1989). *Depth of investigation of collinear symmetrical four-electrode arrays.* Geophysics, 54 (8), 1031-1037.

Barrett, R., M. Berry, T. F. Chan, J. Demmel, J. Donato, J. Dongarra, V. Eijkhout, R. Pozo, C. Romine, and H. Van der Vorst (1994). *Templates for solution of linear systems:building block for iterative methods.* SAIM, 2nd edition, Philadelphia, PA.

Beasely, C.W. and H.S. Ward (1986). *Three dimensional mise-a-la-masse modeling applied to mapping fracture zones.* Geophysics, 51, 98-113.

Benedict, R.P, R.B. Abernethy, and G. Osolsobe (1986). *Measurement uncertainty: instruments and apparatus.* ANSI/ASME PTC 19.1-1985, New York, 68.

Bevc, D. and H.F. Morrison (1991). *Borehole-to-surface electrical resistivity monitoring of salt water injection experiment.* Geophysics, 56, 769-777.

Bing, Z. and S.A. Greenhalgh (1997). *A synthetic study on crosshole resistivity imaging using different electrode arrays.* Exploration Geophysics. 28 (1-2), 1-5.

Binley, A., W. Daily, and A. Ramirez (1997). *Detecting leaks from environmental barriers using electrical current imaging.* J. Env. and Eng. Geophysics, 2 (1), 11-19.

Binley, A, P. Pinheiro and F. Dickin (1996). *Finite element based three-dimensional forward and inverse solvers for electrical impedance tomography.* Proceedings of Colloquium on Advances in Electrical Tomography, Computing and Control Division, IEE, June 1996, Manchester, Digest No. 96(143), 6/1-6/3.

Binley, A., S. Henry-Plouter, and B. Shaw (1996). *Examination of solute transport in an undisturbed soil column using electrical resistance tomography.* Water Resources Research, 32(4), 763-769.

Binley, A., B. Shaw, and S. Henry-Pulter (1996). *Flow pathways in porous media electrical resistance tomography and dye staining image verification.* Measurement Science & Technology, 7 (3), 384-390.

Bois, P., M. La Porte, M. Lavergne, and G. Thomas (1972). *Well-to-well seismic measurements.* Geophysics, Vol. 37, 471-480.

Booth, M.J., and I. Basarabhorwath (1996). *Comparing electrode configurations for electrical impedance tomography.* Electronics Letters, 32 (7), 648-649.

Carr, J.J. (1991). *Microcomputer interfacing: A practical guide for technicians, engineers, and scientists.* Englewood Cliffs, New Jersey, Prentice-Hall, Inc., P.

Chapman, L.J. and D.F. Putnam (1984). *The physiography of southern Ontario, & accompanied map P.2715 (1:600,000).* Ontario Geological Survey, Special Volume 2, Page 270.

Chavent, G., M. Dupuy, and P. Lemonnier (1975). *History matching by use of optimal control theory.* Soc. Petrol. Eng. J., 15, 74-86.

ComputerBoards Inc. 1995. *Data acquisition and control: Digital I/O; Volume 10.* Mansfield, Masachuset.

Cripps, M. (1989). *Computer interfacing connection to the real world.* London: Edward Arnold: a division of Hodder & Stoughton.

Daily, W. and E. Owen (1991). *Cross-borehole resistivity tomography.* Geophysics, 56, 228-1235.

Daily, W.D., E. Owen, and D.J. LaBrecque (1990). *Cross-borehole electrical resistivity tomography.* SEG Abstracts, 60, 573-574.

Daily, W. and A. Ramirez (1998). *Electrical impedance tomography of a Perchloroethelyne release.* J. Env. & Eng. Geophysics, 1, 189-201.

Daily, W. and A. Ramirez (1995). *Electrical resistance tomography during in-situ trichloroethylene remediation at the Savannah River Site.* Journal of Applied Geophysics, 33 (4), 239-249.

Daily, W., A. Ramirez, D.J. LaBrecque, and W. Barber (1995). *Electrical resistance tomography experiments at the Oregon Graduate Institute.* Journal of Applied Geophysics, 33 (4), 227-237.

Daily, W., A. Ramirez, D.J. LaBrecque, and J. Nitao (1992). *Electrical resistivity tomography of vadose water movement.* Water Resources Research, 28 (5), 1429-1442.

Daniels, J.J. (1983). *Hole-to-surface resistivity measurements.* Geophysics, 48, 1006-1019.

Daniels, J.J. (1977). *Three-dimensional resistivity and induced polarization modeling using buried electrodes.* Geophysics, 35, 98-109.

Das, U.C. and A.T. de Hoop (1995). *Efficient computation of apparent resistivity curves for depth profiling of a layered earth.* Geophysics, 60 (6), 1691-1697.

De Lima, O.A.L., H.K. Hedison, K. Sato, and M.J. Porsani (1995). *Imaging industrial contaminant plumes with resistivity techniques.* J. Applied Geophysics, 34, 93-108.

Dey A. and H.F. Morrison (1979). *Resistivity modeling for arbitrary shaped three-dimensional structures.* Geophysics, 44, 753-780.

Dey, A. (1976). *Resistivity modeling for arbitrary shaped two-dimensional structures, part II: User's guide to the FORTRAN algorithm RESIS2D.* LBL Rep. LBL-5283, Lawrence Berkeley Laboratory, Univ. Of California, Berkeley.

Dickin, F.J., R.A. Williams, and M.S. Beck (1993). *Determination of composition and motion of multicomponent mixtures in process vessels using electrical impedance tomography .1. Principles and process engineering applications.* Chemical Engineering Science, 48 (10), 1883-1897.

Dickin, F. and M. Wang (1996). *Electrical resistance tomography for process applications.* Measurement Science & Technology, 7 (3), 247-260.

Director, S. W. and R.A. Rohrer (1969). *The generalized adjoint network and network sensitivities.* IEEE Trans. Circuit Theory, CT-16, 313-323.

Djamdji, F., A.C. Gorvin, I.L. Freeston, R.C. Tozer, I.C. Mayes, and S.R. Blight (1996). *Electrical impedance tomography applied to semiconductor wafer characterization.* Measurement Science & Technology, 7 (3), 391-395.

Dogru, A. H. and J.H. Seinfield (1981). Comparison of sensitivity coefficient calculation methods in automatic history matching. Soc. Petrol. Eng. J., 21, 551-557.

Duba, A., J. Roberts, B. Bonner (1997). *Electrical properties of geothermal reservoir rocks as indicators of porosity distribution.* Proceedings: 22nd Workshop on Geothermal Reservoir Engineering Stanford, CA January 27-29, 1997, SGP-TR-155.

Duff, I.S., A.M. Erisman, and J.K. Reid (1986). *Direct methods for sparse matrices.* Clarendon Press, Oxford.

Eaton, J.K. and L. Eaton (1995) *LabTutor. A friendly guide to computer interfacing and LabVIEW programming.* New York: Oxford University Press.

El-Kadi, A. I. (1985). *On estimating the hydraulic properties of soil, Part 1.: Comparison between forms to estimate the soil-water characteristic function.* Advanced Water Resources, 8, 136-147.

El-Wahiedi, M.M, F. Merlanti, and M. Pavan (1992). *Geoelectrical resistivity survey of the central part of Azraq basin (Jordan) for identifying saltwater / freshwater interface.* J. Applied Geophysics, 29, 125-133.

Enfield, C.G., T.E. Short, C.L. Miller, and E.A. Sudicky (1993). *Use of impedance tomography to monitor non-aqueous phase liquid movement; the forward problem.* Agronomy Abstracts, 85, 204.

Forsyth, P. (1994). *Iterative methods for sparse matrices, (CS770d Course notes).* Department of Mathematics and computer Sciences, University of Waterloo.

Fox, R.C., G.W. Hohmann, T.J. Killpack, and L. Rijo (1980). *Topographic effects in resistivity and induced-polarization surveys.* Geophysics, 45 (1), 75-93.

Frasheri, A. (1993). *Interpretation problems of electric sounding and profiling in regions of complicated geology and rugged terrain.* Geophysical transactions, 38 (1), 55-66.

Frind, E.O. and J.W. Molson (1993). *SALTFLOW: Version 2.0, Density-dependent flow and mass transport model in three dimensions, User guide.* Waterloo Centre for Groundwater Research, University of Waterloo, 68.

Frohlich, R.K, J.J. Fisher, and E. Summerly (1996). *Electric-hydraulic conductivity correlation in fractured crystalline bedrock:Central Landfill, Rhode Island, USA.* J. Applied Geophysics, 35, 249-259.

Frohlich, R.K, D.W. Urish, J. Fuller, and M. O'Reilly (1994). *Use of geoelectrical methods in groundwater pollution surveys in a coastal environment.* J. Applied Geophysics, 32, 139-154.

Garrett, P.H. (1994). *Advanced instrumentation and computer I/O design: Real-time system computer interface engineering.* New York: IEEE Press.

Gasulla, M., J. Jordana, R. Pallas-Areny, and J.M. Torrents (1996-?7). *Subsurface resistivity measurements using square waveforms.* IEEE Instrumentation & Measurement Technology Conference, May 19-21, Ottawa, Canada, 4, 1252-1255.

George, A.J., J. Liu, and E. Ng (In press). *Computer solution of sparse linear systems.*

George, A.J. (1970). *Computer implementation of the finite element method.* Ph.D. Thesis, Dept. of Computer Sciences, Stanford University.

Gilson, E.W. (1996). *Application of borehole ground penetrating radar in near surface environments.* M.Sc. Thesis, Dept. Earth Sciences, Univ. Waterloo, Canada, 71-81.

Greenberg, H.J. (1996). *Mathematical Programming Glossary.* University of waterloo.

Greenhouse, J.P. and M.M. Williams (1985). *Geophysical monitoring of ground water contamination around waste disposal sites.* GWMR, Fall, 63-69.

Greenhouse, J.P. and R.D. Harris (1983). *Migration of contaminants in ground water at a land field: A case study. 7. DC VLF, and inductive resistivity surveys.* J. Hydrology, 63, 177-197.

Greenhouse J.P., D.D. Slaine, and P. Gudjurgis (1998). *Applications of Geophysics in Environmental Investigations (CD-ROM).* Matrix Multimedia, Canada

Griffiths, D.H. and R.D. Barker (1994). *Electrical imaging in archaeology.* Journal of Archaeological Science, 21, 153-158.

Gustafson, E.P. and R.B. McEuen (1987). *Minimizing interpretation ambiguities through joint inversion of surface electrical data.* GWMR, 7 (4), 101-113.

Holladay, J.S. and G.F. West (1984). *Effect of well casings on surface electrical surveys.* Geophysics, 49 (2), 177-188.

Hounsfield, G.N. (1972). *A method of and apparatus for examination of a body by radiation such as X-Ray or gamma-radiation.* British patent No. 1283915, London.

Ichikawa K. and H. Ishibashi (1990). *An investigation method of groundwater flow in a rock mass using resistivity tomography.* Eos Transactions, American Geophysical Union, 71 (28), 878.

Jaafari, A. and G. Joos (1995). *Compact high voltage low frequency power supply.* Proceedings of the 1995 IEEE 10th Annual Power Electronics Conference. Part 2 (of 2), Conference Proceedings - IEEE Applied Power Electronics Conference and Exposition - APEC v 2, 1995, IEEE, Piscataway, NJ, USA, 821-825.

Jackson, P.D., M.A. Lovell, C. Pitcher, C.A. Green, C.J. Evans, R. Flint, A. Forster, and P.K. Harvey (1991). *High-resolution electrical resistivity imaging of core samples.* Abstracts of the 13th European formation evaluation symposium. Br. Geol. Surv., Keyworth, United Kingdom, The Log Analyst, 32 (1), 36.

Jackson, P.D. and M.A. Lovell (1991). *The correspondence of electrical current and fluid flow in rocks: the impact of electrical-resistivity core imaging.* 14th European formation evaluation symposium, abstracts, The Log Analyst, 32 (5), 624.

Jackson, P.D. and D. M. McCann (1994). *Non-destructive geophysical site investigation--an aid to the redevelopment of sites in urban areas with groundwater problems.* British Geological Survey, UK; Inst. of Civil Eng. Groundwater Problems in Urban Areas Conf. Proc., London, UK (Thomas Telford), Jun 2-3, 93, 134-148.

Jackson, P.D. and R.D. Ogilvy (1990). *Electrical resistivity imaging for the assessment of geological structures in site investigation.* Proceedings; Sixth International Congress, International Association of Engineering Geology, Amsterdam, Netherlands. August 6-10. 1990, 6, 969-978.

Jones, O.C., J.T. Lin, and L. Ovacik (1992). *Investigation of Electrical-Impedance Imaging Relative to 2-Phase, Gas-Liquid Flows.* Chemical Engineering Communications, 118, 299-325.

Johnson, G.W. (1994). *LabVIEW graphical programming: practical applications in instrumentation and control.* New York, McGraw-Hill, Inc., 522.

Kamm, L.J. (1996). *Understanding electro-mechanical engineering: an introduction to mechatronics.* New Jersey, IEEE Press, 382.

Kalinski, R.J., W.E. Kelly, I. Bogardi, and G. Pesti (1993). *Electrical resistivity measurements to estimate travel times through unsaturated ground water protective layers.* J. Applied Geophysics, 30, 161-173.

Kelly, W.E. (1976). *Geoelectric sounding for delineating ground water contamination.* Groundwater, 14. 6-10.

Kim, Ok-Kee , W.A. Nokes, H.M. Buettner, W.D. Daily, and A.L. Ramirez (1994). *Electrical resistance tomography imaging of spatial moisture distribution in pavement sections.* Transportation Research Record 143 (5), 69-76.

Kingman, J.E.E. (1995). Personal communication.

Klefstad, G., L.V.A. Sendlein, and R.C. Palmquist (1975). *Limitations of the electrical resistivity method in landfill investigations.* Groundwater, 13 (5), 418-427.

Kline, S.J., (1985_a). *The purpose of uncertainty analysis.* Journal of Fluid Engineering,107, 153-160.

Kline, S.J. (1985_b), *1985 Symposium on Uncertainty Analysis Closure.* Journal of Fluid Engineering, 107, 153-160.

Kotre, C.J. (1996). *Subsurface electrical impedance imaging using orthogonal linear electrode arrays.* IEE Proc.-Sci. Meas. Technol., 143 (1), 41-46.

Kotre, C.J. (1995). *Sub-surface electrical impedance imaging using orthogonal linear electrode arrays.* IEE Colloquium (Digest) n 099, 1995. IEE, Stevenage, London, UK, 12/1-12/4.

Kumar, R. and M.V.R. Chowdary (1977). *Effect of vertical contact on Wenner resistivity soundings.* Geophysical Prospecting, 25, 471-480.

Kumata, M., A. Chiba, and R. Kubota (1993). *Model tank experiments for basic study on resistivity tomography.* SEG Annual Meeting Expanded Technical Program Abstracts with Biographies, 63, 1309-1311.

LaBrecque, D.J. (1990). *Comparison of maximum entropy and smoothest inversion for resistivity tomography.* SEG Abstracts, 60, 546-549.

LaBrecque, D.J., M. Milleto, W. Daily, A. Ramirez, and E.Owen (1996). *The effect of noise on OCCAM's inversion of resistivity tomography data.* Geophysics, 61(2), 538-548.

LaBrecque, D.J., G. Morelli, W. Daily, A. Ramirez, and P. Lundegard (1995). *OCCAM's inversion of 3D ERT data.* Proc. of the International Symposium on Three Dimensional Electromagnetics, Richfield, Connecticut, 471-482.

LaBrecque, D.J., E. Owen, W. Dailey, and A.L. Ramirez (1992). *Noise and Occam's inversion of resistivity tomography data.* SEG Annual Meeting Expanded Technical Program Abstracts with Biographies, 62, 397-400.

LaBrecque, D.J., A.L. Ramirez, W.D. Daily, A.M. Binley, and S.A. Schima (1996). *ERT monitoring of environmental remediation processes.* Measurement Science and Technology, 7(3), 375-383.

Laine, D.L., G.T. Darilek and A.M. Binley (1997). *Locating geomembrane liner leaks under waste in a landfill.* Proceedings of the International Geosynthetics '97 Conference, Long Beach, CA, USA, Industrial Fabrics Association International, Saint Paul, Minnesotam, 1, 407-411.

Laine, D.L., A.M. Binley, and G.T. Darilek (1997). *How to locate liner leaks under waste.* Geotechnical Fabrics Report, 15(6), 34-36.

Lancaster, D. (1975). *Active-filter cookbook.* Indiana: Howard W. Sams & Co., Inc., P. 240

Lemonnier, H. and J.F. Peytraud (1996). *Diphase flow tomographic techniques.* Original Title: Techniques tomographiques en ecoulement diphasique. Houille Blanche, 1-2, 86-97.

Leismann, H.M. and E.O. Frind (1989). *A symmetric-matrix time integration scheme for the efficient solution of advection-dispersion problems.* Water Resources Research, 25, 1133-1139.

Lewins, J. (1964). *Importance: the adjoint function.* Pergamon Press, New York.

Li, J., K.H. Lee, I. Javandel, and G. Xie (1995). *Nonlinear three-dimensional resistivity inverse imaging for direct current data.* SEG Annual Meeting Expanded Technical Program Abstracts with Biographies, 65.

Li, Y. (1992). *Inversion of three-dimensional direct current resistivity data.* Ph.D. Thesis, University of British Columbia. Vancouver, BC, Canada, 165.

Lionheart, W. (1997). *Conformal uniqueness results in anisotropic electrical impedance tomography.* Inverse Problems, 13 (1), 125-134.

Llera, F.J., M. Sato, K. Nakatsuka, and H. Yokoyama (1990). *Temperature dependence of the electrical resistivity of water-saturated rocks.* Geophysics, 55(5), 576-585.

Loh, W.W. and F.J. Dickin (1996). *Improved modified Newton-Raphson algorithm for electrical-impedance tomography.* Electronics Letters, 32 (3), 206-207.

Loke, M.H. and R.D. Barker (1996). *Rapid least-squares inversion of apparent resistivity pseudosections by a quasi-Newton method.* Geophysical Prospecting. 44 (1), 131-152.

Loke, M.H. and R.D. Barker (1996). *Practical techniques for 3-D resistivity surveys and data inversion.* Geophysical Prospecting, 44, 499-523.

Loke, M.H. and R.D. Barker $(1995)_a$. *Improvements to the Zohdy method for the inversion of resistivity sounding and pseudosection data.* Computers & Geosciences, 21, 321-332.

Loke, M.H. and R.D. Barker $(1995)_b$. *Least-squares deconvolution of apparent resistivity pseudosections.* Geophysics, 60, 1682-1690.

Louis, A.K. and F. Natterer (1983). *Mathematical problems of computerized tomography.* Proc. IEEE, Rev. Sci. Instrum., 54, 379-389.

Lovell, M.A., P.D. Jackson, and P.K. Harvey (1992). *Reservoir characterization and quantification; the application of high-resolution electrical resistivity core-imaging.* AAPG Bulletin, 76 (7), 1115.

Lui, J.W-H. and A.H. Sherman (1976). *Comparative analysis of Cuthill-McKee and reverse Cuthill-McKee ordering algorithm for sparse matrices.* SIAM J. Numer. Anal., 13, 198-213.

Lundegard, P.D. and D.J. LaBrecque (1995). *Air sparging in a sandy aquifer (Florence, Oregon, U.S.A.): actual and apparent radius of influence.* Journal of Contaminant Hydrology, 19 (1), 1-27.

Ma, Y., H. Wang, L.A. Xu, and C. Jiang, 1997. *Simulation study of the electrode array used in an ERT system.* Chemical Engineering Science, 52 (13), 2197-2203.

Mann, R., F.J. Dickin, M. Wang, T. Dyakowski, R.A. Williams, R.B. Edwards, A.E. Forrest, and P.J. Holden (1997). *Application of Electrical-Resistance Tomography to Interrogate Mixing Processes at Plant-Scale.* Chemical Engineering Science, 52 (13), 2087-2097.

Matias, M.S., M.M. da Silva, P. Ferreira, and E. Ramalho (1996). *A geoelectrical and hydrogeological study of aquifers contamination by a landfill.* J. Applied Geophysics, 32, 155-162.

Mazac, O., W.E. Kelly, and I. Landa (1987). *Surface geoelectrics for groundwater pollution and protection studies.* J. Hydrol., 93, 277-294.

Mazac, O., L. Benes, I. Landa, and A. Maskova (1990_a). *Determination of the extent of oil contamination in groundwater by geoelectrical methods.* In S.H. Ward (ed.), Geotechnical and Environmental Geophysics, 2, SEG, Tulsa, Oklahoma, 2, 107-112.

Mazac, O., M. Cislerova, W.E. Kelly, I. Landa, and D. Venhodova (1990_b). *Determination of hydraulic conductivity by surface geoelectrical methods.* In S.H. Ward (ed.), Geotechnical and Environmental Geophysics, SEG, Tulsa, Oklahoma, 2, 107-112.

McElwee, C.D. (1982). *Sensitivity analysis and groundwater inverse problem.* Groundwater, 20(6), 723-735.

McElwee, C.D. and M.A. Yukler (1978). *Sensitivity of groundwater models with respect to variations of transmissivity and storage.* Water Resources research, 14 (3), 451-457.

Meiksin, Z.H. (1990). *Complete guide to active filter design, OP AMPS, & passive components.* New Jersey: Prentice-Hall, P. 228.

Merkel, R.H. (1971). *Resistivity analysis for plane-layer halfspace models with buried current sources.* Geophysics, 19, 626-639.

Merkel, R.H. and S.S. Alexander (1971). *Resistivity analysis for models of a sphere in a halfspace with buried current sources.* Geophysical Prospecting, 19, 640-651.

Morelli, G. and D.J. LaBrecque (1996). *Advances in ERT inverse modeling.* J. of Env. and Eng. Geophysics, 1, 171-186.

Narayan, S. and M.B. Dusseault (1995). *Electrical resistance tomography for monitoring shallow enhanced recovery processes.* Proceedings of the International Heavy Oil Symposium, Calgary, Alberta, Canada, Society of Petroleum Engineers (SPE), Richardson, TX, USA. 183-194.

Narayan, S. (1994). *Subsurface-to-surface resistivity method for monitoring in-situ processes using a combination of surface and subsurface electrodes.* Ph.D. Thesis, Dept. Earth Sciences, Univ. Waterloo, Canada, 287.

National Instruments (1997). *Instrumentation reference and catalogue.* Austin,TX.

National Instruments (1996). *LabVIEW graphic programming for instrumentation: Cross-reference.* Austin,TX.

Neuman, S.P. (1980_a). *Adjoint-state finite element equations for parameter estimation.* Proceedings of Third International Congress on Finite Elements in Water Resources, University of Mississippi.

Neuman, S.P. (1980_b). *A statistical approach to the inverse problem of aquifer hydrology, 3 improved solution method and added perspective.* Water Resources Research, 16(2), 331-346.

Nishigaki, M., T. Sudinda, Y. Sasaki, M. Inoue, and T. Moriwaki (1996). *Laboratory determination of transverse and longitudinal dispersion coefficients in porous media.* Journal of Groundwater Hydrology. 38 (1), 13-27.

Noel, M. and B. Xu (1992). *Cave detection using electrical resistivity tomography.* Cave Science, 19 (3), 91-94.

Noel, M. and B. Xu (1991). *Archaeological investigation by electrical resistivity tomography: a preliminary study.* Geophysical Journal International, 107 (1), 95-102.

Noguchi, K., S. Goto, T. Yuda, K. Furuya, M. Shibamoto, and H. Nishino (1991). *In-situ experimental study on resistivity tomography in tunnels.* Proceedings of the Congress of the International Society for Rock Mechanics, 7, 577-580.

Oblow, E.M. (1978). *Sensitivity theory for reactor thermal-hydraulics problem.* Nucl. Sci. Eng., 68, 322-337.

Osiensky, J.L. and P.R. Donaldson (1995). *Electrical flow through an aquifer for contaminant source leak detection and delination of plume evaluation.* J. of Hydrology, 169, 243-263.

Ostrowski, K.L., S.P. Luke, and R.A. Williams (1996). *Application of conjugate harmonics to electrical process tomography.* Measurement Sci. Technol., 7, 316-324.

Ott, H.W. (1988). *Noise reduction technique in electronic systems.* US, John Wiley &sons, Inc., P. 426.

Owen, E.W. and W.D. Daily (1988). *The calibration of a low frequency impedance tomographic apparatus for rock sample measurements.* Eos, Transactions, American Geophysical Union, 69 (44), 1185.

Pallas-Areny, R. and J.A. Brescoli (1995). *Electrical impedance measurements by synchronous sampling applied to square waveforms.* IEE Colloquium (Digest) n 099, 1995, IEE, Stevenage, London, UK, 7/1-7/4.

Parra, J.O. (1988). *Electrical response of a leak in geomembrane liner.* Geophysics, 53, 1445-1453.

Petrick, W.R., J. W.R. Sill, and S.H. Ward (1981). *Three-dimensional resistivity inversion using alpha centers.* Geophysics, 46, 1148-1162.

Pfannkuch, H.O. and B.A. Labno (1977). *Design and optimization of ground water monitoring network for pollution studies.* Ground water, 14, 455-462.

Pfannkuch, H.O. (1982). *Problems of monitoring network design to detect unanticipated contamination.* GWMR/ Winter, 67-76.

Pinheiro, P.A.T., W.W. Loh, and F.J. Dickin (1998). *Three-dimensional reconstruction algorithm for Electrical Resistance Tomography.* IEE Proc.-Sci. Meas. Tech., 145 (3), 85-93.

Pinheiro, P.A.T., W.W. Loh, and F.J. Dickin (1997). *Smoothness-constrained inversion for two-dimensional electrical resistance tomography.* Measurement Science and Technology, 8, 293-302.

Pous, J., P. Queralt, and R. Chavez (1996). *Lateral and topographic effects in geoelectric soundings.* J. of Appl. Geophysics, 35, 237-248.

Pruess, K., M. Wilt, G.S. Bodvarsson, and N.E. Goldstein (1983). *Simulation and resistivity modeling of a geothermal reservoir with waters of different salinity.* Geothermics, 12 (4), 291-306.

Radon, J. (1917). *On the determination of functions from their integrals along certain manifolds.* Berichte Sach-sische Akademic der Wissen-schaften, 69, 262-277.

Ramirez, A., W. Daily, A. Binley, D. LaBrecque, and D. Roelant (1996). *Detection of leaks in underground storage tanks using electrical resistance methods.* J. Env. and Eng. Geophysics, 1 (3), 189-203.

Ramirez, A., W. Daily, A. Binley, D. LaBrecque, and D. Roelant (1996_a). *2-D electrical-resistance tomography.* Measurement Science & Technology, 8 (3), 293-302.

Ramirez, A., W. Daily, A. Binley, and D. LaBrecque (1996_b). *Tank leak detection using electrical resistance methods.* Proceedings of Symposium on the Application of Geophysics to Engineering and Environmental Problems, Environmental and Engineering Geophysical Society, Keystone, Colorado, April 28- May 1, 1996, 763-772.

Ramirez, A., W. Daily, A. Binley, D. LaBrecque, and D. Roelant (1995). *Detection of leaks from underground storage tanks using electrical resistance tomography.* Lawrence Livermore Nat. Laboratory, UCRL-JC-122180, Livermore, CA.

Ramirez, A., W. Daily, D. LaBrecque, E. Owen, and D. Chesnut (1993). *Monitoring an underground steam injection process using electrical resistance tomography.* Water Resources Research, 29 (1), 73-87.

Ramirez, A.L., W. Daily, D.J. LaBrecque, E.W. Owen, and D.A. Chesnut (1992). *Electrical resistance tomography used to monitor subsurface steam injection.* SEG Annual Meeting Expanded Technical Program Abstracts with Biographies, 62, 492-494.

Ramirez, A.L.; W.D. Daily, and R.L. Newmark (1995). *Electrical resistance tomography for steam injection monitoring and process control.* Journal of Environmental & Engineering Geophysics, 1, 39-51.

Ranieri, G., G. Barrocu, and R. Tocco (1989). *Salt-water intrusion monitoring by resistivity and IP-tomographic methods.* Proceedings of 10th Salt-Water Intrusion Meeting. Geologisch Instituut R.U.G. (S 8), Ghent, 1988. 345-348.

Ranieri, G., G. Barrocu, and R. Tocco (1988). *Salt-water intrusion monitoring by resistivity and IP-tomographic methods.* Natuurwetenschappelijk Tijdschrift, 70 (1-4), 345-348.

Reed, A.C. (1996). *Hydraulic fracturing in non-cohesive soils.* M.A.S. Thesis, Dept. Civil, Univ. Waterloo, Canada, 145-178.

Renon, V., J.L. Lucius, and E.M. Oblow (1980). *A statistical sensitivity analysis of a simple nuclear waste repository model.* Rep. ORNC/TM-7310, Oak Ridge Nat. Lab., Oak Ridge, Tenn.

Renon, Y. (1988). *Uncertainty analysis.* CRC Press, Florida, 282.

Reynolds, J.M. (1998). *An introduction to applied and environmental geophysics.* John Wiley & Sons, New York, USA.

Roberts, J.J. and W. Lin (1992). *Electrical resistivity of Topopah Springs Tuff as a function of water saturation.* Eos, Transactions, American Geophysical Union, 73 (43), Suppl., 224.

Roca-Ramisa, L., J. Mendoza, M.A. Sanchez-Galindo, and M. Angel (1994). *Evaluation of fracture distribution and continuity in carbonate reservoirs using wellbore imaging tools.* Proceedings of the SPE International Petroleum Conference and Exhibition of Mexico. 81-96.

Roy, A. (1972). *Depth of investigation in Wenner, three-electrode, and Dipole-Dipole DC resistivity methods.* Geophysical Prospecting, 20 (3), 329-340.

Roy, A. (1971). *Depth of investigation in direct current methods.* Geophysics, 36 (5), 943-959.

Roy, A. and A. Apparao (1977). *Limiting depth of detection in line electrodes systems.* Geophysical Prospecting, 25, 758-767.

Saad, Y. (1996). *Iterative methods for sparse linear systems.* PWS Publishing Company, Boston.

Saito, H., H. Shima, T. Toshioka, S. Kaino, and H. Ohtomo (1990). *A case study of geotomography applied to a detailed investigation of a highway bridge foundation.* American Society for Testing and Materials Special Technical Publication, 1101, 17-34.

Santos, F.D.M., A.R.A. Afonso, and L.A.M. Victor (1997). *Study of the Chaves geothermal field using 3-D resistivity modeling.* J. Applied Geophysics, 37, 85-102.

Santos, F.D.M., A. Dupis, A.R.A. Afonso, and L.A.M. Victor (1997). *1-D joint inversion of AMT and resistivity data acquired over a graben.* J. Applied Geophysics, 38, 115-129.

Sasaki, Y. (1994). *Anisotropic resistivity tomography; a model study for characterization of fractured rocks.* SEG Annual Meeting Expanded Technical Program Abstracts with Biographies, 64, 252-255.

Sasaki, Y. (1992). *Resolution of resistivity tomography inferred from numerical simulation.* Geophysical Prospecting, 40 (4), 453-463.

Sasaki, Y. (1990). *Two-dimensional joint inversion of magnetotelluric and dipole-dipole resistivity data.* Geophysics, 54 (2), 254-262.

Sasaki, Y. and K. Matsuo (1990). *Surface-to-tunnel resistivity at a copper mine.* SEG Abstracts, 60, 550-553.

Sasaki, Y. and K. Matsuo (1993). *Surface-to-tunnel resistivity tomography at the Kamaishi Mine.* Geophysical Exploration, 46 (2), 128-133.

Schenkel C.J. (1994). *DC resistivity imaging using a steel cased well.* SEG Annual Meeting Expanded Technical Program Abstracts with Biographies. 64, 403-406.

Schima, S., D.J. LaBrecque, and P.D. Lundegard (1996). *Monitoring air sparging using resistivity tomography.* Ground Water Monit. Remediation, 16 (2), 131-138.

Schmid, G. and D. Braoss (1988). *Comparison of fast equation solvers for groundwater flow problems.* Groundwater flow and quality modeling, (Custodio et al. Ed.), NATO ASI Series C, 224, 173-188.

Schwarz, A. (1996). *Multi-Tomographic Flame Analysis with a Schlieren Apparatus.* Measurement Sci. Technol., 7, 406-413.

Sen, P.N. and P.A. Goode (1992). *Influence of temperature on electrical conductivity on shaly sands.* Geophysics, 57 (1), 89-96.

Shima, H. (1995). *Inversion in electrical and electromagnetic exploration.* Journal of Geography, 104 (7), 952-971.

Shima, H. (1989). *Resistivity tomography; basic concepts and its applications.* Geophysical Exploration, 42 (6), 442-457.

Shima, H., (1989). *Effects on reconstructed images of surrounding resistivity structures in resistivity tomography.* SEG Abstracts, 59 (1), 385-389.

Shima, H. and H. Saito (1989). *Automatic 3D resistivity inversion of cross-hole data.* Technical Programme and Abstracts of Papers - European Association of Exploration Geophysicists, 51, 159-160.

Shima, H. and T. Sakayama (1987). *Resistivity tomography: An approach to 2-D resistivity inverse problems.* Society of exploration geophysics, Fifty-seventh Annual International Meeting and Exposition, October 11-15, 1987, 59-61.

Scriba, H. (1981). *Computation of the electric potential in three-dimensional structures.* Geophysical Prospecting, 29, 790-802.

Slater, L., A. Binley, and D. Brown (1997). *Electrical imaging of fractures using ground-water salinity change.* Ground Water, 35(3), 436-442.

Slater, L. D.Brown, and A. Binley (1996). *Determination of hydraulically conductive pathways in fractured limestone using cross-borehole electrical resistivity tomography.* European Journal of Environmental and Engineering Geophysics, 1(1), 35-52.

Slater, L., A. Binley, W. Daily, R. Johnson, and M. Perrot (1996). *Mapping a density driven inorganic contaminant plume in a controlled field experiment using ERT.* Proceedings of 2nd Meeting of the Environmental and Engineering Geophysics Society, Nantes, 2-5 September 1996, 200-203.

Spies, B.R. (1996). *Electrical and electromagnetic borehole measurements; a review.* Surveys in Geophysics, 17 (4), 517-556.

Spies, B.R. and R.G. Ellis (1995). *Cross-borehole resistivity tomography of a pilot-scale, in-situ vitrification test.* Geophysics, 60 (3), 886-898.

Spies, B.R. and R.G. Ellis (1993). *Borehole resistivity tomography of a pilot-scale in-situ vitrification test.* SEG Annual Meeting Expanded Technical Program Abstracts with Biographies, 63, 472-475.

Spitzer K. (1995). *A 3-D finite difference algorithm for DC resistivity modeling using conjugate gradient methods.* Geophysical J. International, 123, 903-914.

Sprunt, E.S. (1992). *CT imaging of electrical resistivity measurements: non-uniform water saturation can be a problem.* Fault mechanics and transport properties of rocks: a festschrift in honor of W. F. Brace, Evans Brian (editor) and Wong Teng fong (editor), Academic Press San Diego, CA, USA, 371-387.

Sprunt, E.S., K.P. Desai, M.E. Coles, R.M. Davis, and E.L. Muegge (1991). *CT-scan-monitored electrical-resistivity measurements show problems achieving homogeneous saturation.* SPE Formation Evaluation, 6 (2), 134-140.

Straub, A (1995_a). *General formulation of the electric stratified problem with a boundary integral equation.* Geophysics, 60 (6), 1656-1670.

Straub, A (1995_b). *Properties of the kernel function in electric stratified problems.* Geophysics, 60 (6), 1671-1681.

Stewart, D.I., L.J. West, S.R. Johnston, and A.M. Binley (1997). *Electrokinetic transport in natural soil cores.* In Eds. Goumans, J.J.J.M., Senden, G.J. and van der Sloot, H.A.: Waste Materials in Construction. Studies in Environmental Science 71, 689-698.

Strobel, G.S. (1995). *Moisture distribution computed from electrical-impedance tomographic data of a bentonite clay/sand material.* Pinawa, MB: Whiteshell Laboratories, Geotechnical Science & Engineering Branch, 1995. 14.

Sugimoto, Y., S. Asakawa, S. Senna, and K. Nishida (1995). *2-D resistivity inversion software E-Tomo and some examples of the field survey.* Geophysical Exploration, 48 (4), 270-271.

Sugano, T. (1991). *Evaluation of reliability in computerized geotomographic image model selection by electrical methods.* Memoirs of the Faculty of Engineering, Kyoto University, 53, Part 2, 72-92.

Sugimoto, Y. (1995). *Monitoring of electrolyte tracer in ground water using resistivity tomograph: numerical experiment.* Geophysical Exploration, 48 (4), 251.

Sweeney, J.J. (1983). *Detection and characterization of a perched aquifer with an electrical resistivity survey.* Natl. Symp. Aquifer Restor. Groundwater Monit., Columbus, OH (USA), 25 May 1983, NTIS, Springfield, VA (USA), 26.

Sykes, J.F., J.L. Wilson, and R.W. Andrews (1985). *Sensitivity analysis for steady-state flow using adjoint operators.* Water Resources Research, 21(3), 359-371.

Synder, D.D. and R.M. Merkel (1973). *Analytic models for the interpretation of electrical surveys using buried current electrodes.* Geophysics, 38, 513-529.

Takahashi, T., H. Saito, and H. Shima (1991). *Field study on geophysical imaging techniques at the Buckhorn test facility in Illinois.* Expanded abstracts with biographies, 1991 technical program, 61st annual international SEG meeting, SEG Abstracts, 61, 460-463.

Tamburi, A., R. Allard, and U. Roeper (1985). *Tomographic imaging of ground water pollution plumes.* In: Proceedings; Second Canadian/ American conference on hydrogeology; Hazardous Wastes in Ground Water: A Soluble Dilemma. National Water Well Association, Dublin OH, 162-167.

Tamburi, A., U. Roeper, and A. Wexler (1988). *Application of impedance-computed tomography to subsurface imaging of pollution plumes.* Ground-Water Contamination: Field Methods. ASTM STP 963, A.G. Collins and A.I. Johnson, Eds., American Society for Testing and Materials, Philadelphia PA, 1988, 86-100.

Telford, W.M., L.P. Geldart, and, R.E. Sheriff (1993). *Applied geophysics.* Cambridge University Press, Cambridge, USA.

Texas Instruments (1993). *High-voltage high-current Darlington transistor arrays.* Technical paper, Texas Instruments, Dalas, Texas.

Therrien, R., E.A. Sudicky, and R.G. McLaren (1998). *FRAC3DVS: An efficient simulator for three-dimensional, saturated-unsaturated groundwater flow and chain-*

decay solute transport in porous or discretely-fractured porous formations. Groundwater Simulation Group, Earth Sciences department, University of Waterloo.

Thomas, R.E. (1982). *Uncertainty Analysis.* Rep. ONWI-380, Off. Nucl. Waste Isol., Battelle Mem. Inst. Columbus, Ohio.

Tinney, W.F. and J.W. Walker (1967). *Direct solution of sparse network equations by optimally ordered triangle factorization.* Proc. IEEE, 55, 1801-1809.

Urish, D.W. (1983). *The practical application of surface electrical resistivity to detection of groundwater pollution.* Ground water, 21, 144-152.

Van, G.P., S.K. Park, K. Stephen, and P. Hamilton (1991). *Monitoring leaks from storage ponds using resistivity methods.* Geophysics, 56 (8), 1267-1270.

VanderKwaak, J.E., P.A. Forsyth, K.T.B. MacQuarrie, and E.A. Sudicky (1998). *WATSOLV, sparse matrix iterative solver.* Department of Earth Sciences, University of Waterloo.

Vauhkonen, M., J.P. Kaipio, E. Somersalo, and P.A. Karjalainen (1997). *Electrical-Impedance Tomography with Basis Constraints.* Inverse Problems, 13 (2), 523-530.

Vemuri, V. and W.J. Karplus (1969). *Identification of non-linear parameters of groundwater basins by hybrid computations.* Water Resources Research, 5 (1), 172-185.

Wait, J.R. (1982). *Geo-electromagneticsm.* Academic Press, New York, 268.

Wang, M., F.J. Dickin, and R.A. Williams (1995). *Modeling and analysis of electrically conductive vessels and pipelines in electrical-resistance process tomography.* IEE Proceedings-Science Measurement and Technology, 142 (4), 313-322.

Wang, T., J.A. Stodt, D.J. Stierman, and L.C. Murdoch (1991). *Mapping hydraulic fractures using a borehole-to-surface electrical resistivity method.* Geoexploration, 28, 349-369.

Wang, X. and X. Li (1996). *The image reconstruction of electric resistivity by Zohdy inversion and its application effects.* Geophysical & Geochemical Exploration, 20 (3), 228-233.

West, L.J., D.I. Stewart, A.M. Binley, and B. Shaw (1997). *Resistivity imaging of electrokinetic transport in soil.* Geoenvironmental Engineering, Proceedings of the International Conference on Geoenvironmental Engineering, held in Cardiff, September 1997, Thomas Telford, 565-574.

Wexler, A.L. and C.J. Mandel (1985). *An impedance computed tomography algorithm and system for ground water and hazardous waste imaging.* Proceedings; Second Canadian/ American conference on hydrogeology; hazardous wastes in ground water; a soluble dilemma, 156-161.

Wurmstich, B. and K. Spitzer (1995). *Comparison of two finite difference approaches and five algorithm for 3-D resistivity modeling.* SEG 64th Annual Meeting Expanded Technical Program Abstracts with Biographies. 64, 381-383.

Wurmstich, B. and F.D. Morgan (1994). *Modeling of steaming potential responses causes by oil well pumping.* Geophysics, 59, 46-56.

Xie, M. (1991). *Software reliability modeling.* Singapore: World Scientific Publishing Co. Pte. Ltd., P. 212.

Yabuuchi, S. and K. Hasegawa (1995). *An analysis method for investigation of resistivity distribution along the drift using resistivity tomography; Part 1.* Geophysical Exploration, 48 (4), 251.

Yadav, G.S. and H. Abolfazli (1998). *Geoelectrical sounding and their relationship to hydraulic parameters in semiarid regions of Jalore, northwestern India.* J. of Appl. Geophysics, 38, 35-51.

Yang, F.W. and S.H. Ward (1985). *Single and cross-borehole resistivity anomalies of thin ellipsoids and spheroids.* Geophysics, 50, 637-655.

Yorkey, T.J. (1990). *Electrical-Impedance Tomography with Piecewise Polynomial Conductivities.* Journal of Computational Physics, 91 (2), 344-360.

Yorkey, T.J. (1986). *Comparison reconstruction methods for electrical impedance tomography.* Ph.D. Thesis, Dept. Elect. Comput. Eng., Univ. Wisconsin, Madison, WI 53706.

Zhang, J., R.L. Mackie, and T.R. Madden (1995). *3-D resistivity forward modeling and inversion using conjugate gradients.* SEG Annual Meeting Expanded Technical Program Abstracts with Biographies. 64, 377-380.

Zohdy, A.A.R. (1968). *The effect of current leakage and electrode spacing errors on resistivity measurements.* Geophysical Survey Research, U.S. Geol. Survey Prof. Paper 600-D, D258-D264.

Appendix A: Literature review

The resistivity of rock varies significantly with the porosity and resistivity of the contained pore fluids. Other factors affecting rock resistivity include pore structure, the degree of saturation, temperature, and the conducting mineral content. As a result resistivity tomography has several possible geological and hydrogeological applications, including monitoring of ground-water pollution, enhanced oil recovery monitoring, describing geothermal systems, and in mineral exploration. It has considerable potential for engineering applications, such as the detection of fracture zones, core sample studies, site investigation and location of buried metal. Measuring changes in sub-surface resistivities over time should be useful for monitoring processes such as contaminant migration, stream flooding in enhanced oil recovery, geothermal fluids production, and for determining the integrity of a mined geologic repository for waste disposal. All of these processes involve substantial changes in the resistivity structure in a reasonably well-defined region, and in principle ERT methods should allow tracking changes over time.

Since Narayan has presented a good literature review on resistivity methods in 1994 in his Ph.D. thesis, the focus of this section will be on more recent publications and completion of his work. Recent works can be classified into following divisions:

i. Engineering and industrial applications and core and soil sample analysis;
ii. Groundwater process monitoring, steam injection monitoring, and monitoring leakage from storage ponds and liners under waste disposal sites;
iii. Inverse algorithm, three-dimensional resistivity and ERT evaluations, and ERT case studies;
iv. Instrumentation and waveform analysis for ERT, and
v. Study of physical properties by resistivity methods.

The non-invasive property of ERT methods is one of the main characteristics that draw the investigators' attention to this technique. ERT has been successfully employed in a wide range of problems including engineering applications (chemical process engineering, site investigation, core and soil sample analysis), biomedical, and environmental applications. Tables A-1 and A-2 present a few of the published results of ERT applications in engineering studies.

The study of rock cores and soil samples is fundamental to soil and rock mechanics, petroleum engineering, and soil sciences. Recently, attention has turned toward the application ERT in rock core and soil sample analysis (Table A-2) and successful results have been obtained.

Among other parameter, the success of electrical technique in locating subsurface contaminated plume depends on the resistivity contrast between anomaly and its surroundings, the shape and size of the plume, and the location of plume with respect to the electrode grids among other parameters. Electrical techniques have been used to detection and monitoring of contamination by invading fluids from oil and ore production and processing, to map leakage from landfills and waste disposal sites, and to evaluate pollution from industrial sources (Table A-3 to A-7).

Leakage from a landfill or a polluted site moves in a preferred pathway controlled by the most conductive pathway in the formation (Table A-5), combined with the pressure and flow boundary conditions. Early detection of plumes can minimize the cost of groundwater remediation at these sites. Surface electrical methods are the least expensive non-invasive geophysical methods, which, in proper conditions, can give successful results in detecting and monitoring of such processes (*Osiensky and Donaldson* 1995).

Table A.1 Engineering and industrial applications of ERT

References	Significance or major conclusions
Ma et al. (1997)	*The greater the number of electrodes and the longer the size of electrodes, the better the resolution of the ERT images of conductive regions within the chemical refinery vessels.*
Mann et al (1997)	*Air-core vertex detection, miscible fluid mixing, and gas-liquid mixing process were illustrated using ERT method in a tank model.*
Daniels et al. (1996)	*3-D resistivity discontinuities were modeled using a (HSPICE) discrete component model for process flow applications.*
Dickin and Wang (1996)	*Design and operation of ERT instrumentation for process applications were presented.*
Djamdji et al. (1996)	*EIT was used to map the resistivity distribution of silicon wafers or conducting films.*
Ostrowski et al. (1996)	*2-D analytical solution based on conjugate harmonics was presented for EIT/ECT industrial system design.*
Wang et al. (1995)	*ERT was successfully used to image inside a conducting process vessel from its conductive boundary, using analytical and FEM model. The sensitivity distribution was evaluated based on the derived relations based on the sensitivity density coefficient reconstruction algorithm to demonstrate the effects of different electrode geometries.*
Dickin et al. (1993)	*EIT was introduced to evaluate the composition and motion of aqueous based process reactors and pipeline flow.*
Jones et al. (1992)	*Potential use of EIT was introduced for two-phase flow study. Improvement of computation time for EIT problem solution is required.*

Table A-2 Core and soil sample analysis

References	Significance or major conclusions
West et al. (1997)	*ERT was shown to be capable of monitoring the soil resistivity changes during electrokinetic soil treatment; resistivity changes correlated with chemical changes of soil during the process. The author concluded that ERT may be used in monitoring electrokinetic remediation in the field.*
Binley et al. (1996)	*ERT was applied to study of flow pathways in porous media along with dye staining image verification.*
Jackson and Lovell (1991)	*Electrical resistivity imaging was used successfully to monitor fluid flow though a core sample and to assess the impact of heterogeneity on the petrophysical analysis.*
Jackson et al. (1991)	*A new technique was introduced to image anisotropic resistivity structure by partitioned electrical current either horizontally or vertically in core samples.*
Sprunt et al. (1991)	*Simultaneous application of X-ray computerized tomography and ERT for core sample moisture distribution analyses were presented.*
Owen and Daily (1988)	*Quantitative evaluation of the water distribution of rock samples was conducted using EIT techniques based on the calibration of results with the true values.*

The literature on 3-D resistivity numerical modeling may be classified in three main divisions: finite difference, finite element, and boundary element based models (Table A-7). A true solution of ERT needs a fast reliable forward model to compare the results of the inversion part and to finalize the resistivity distribution in the interested region.

Table A-3 Steam injection monitoring

References	Significance or major conclusions
Ramirez et al. (1996)	*The authors demonstrated the capability of ERT in monitoring and control in a subsurface thermal remediation when this technique is combined with other data sets such as temperature.*
Ramirez et al. (1993)	*ERT was used to detect steam invasion through soil resistivity changes in time and space.*

Table A-4 Monitoring groundwater processes

References	Significance or major conclusions
Daily and Ramirez (1998)	*EIT was evaluated for Perchloroethelyne (PCE) release detection. The result shows EIT is capable of PCE detection because of the resistivity contrasts.*
Binley et al. (1997)	*Successful leakage detection using ERT was presented for a number of field experiments.*
Binley et al. (1996)	*A successful experiment was conducted on the examination of solute transport in an undisturbed soil column using a biomedical-type ERT system. More electrodes increase the image resolution.*
LaBrecque et al. (1996)	*The effectiveness of ERT was evaluated for monitoring of several environmental remediation processes in two field experiments.*
Ramirez et al. (1996)$_a$ & $_b$	*The performance of ERT has been evaluated as a leak detection method for buried storage tanks in two field case studies.*
Schima et al. (1996)	*The air flow pattern of an air sparging process was monitored by cross-borehole ERT. ERT is more accurate in defining the radius of influence than conventional techniques.*
Slater et al. (1996)	*Mapping the spatial distribution of fractured hydrologically complex limestone was conducted before, during and after a saline fluid injection, using cross-hole ERT. The results were consistent with borehole television logging.*
Slater et al. (1996)	*Reconstruction of cross-hole ERT data revealed the location of preferential flow pathways in fractured rock. ERT results were consistent with closed-circuit television logging and double-packer testing data.*
Daily and Ramirez (1995)	*ERT was used in monitoring of an in-situ trichloroethylene remediation experiment. The flow of injected air and water was controlled by local variations in formation permeability and is almost non-modified through the injection.*
Daily et al. (1995)	*Two field experiments demonstrated the capability of ERT for the detection of hydrocarbon distribution in saturated and unsaturated zones, and the detection and delineation of the extent of sparged zones were illustrated. The simulation of the detection of oil leakage from a tank by ERT was presented.*
Osiensky and Donaldson (1995)	*A modified mise-a-la-mass method was successfully applied to monitor the evaluation of a conductive plume in time. This method was very sensitive to resistivity changes of groundwater. Sensitivity of this method reduces with depth of investigation.*

Table A-4 Continued

References	Significance or major conclusions
Lundegard and LaBrecque (1995)	*An air sparging remediation experiment was monitored with conventional methods (such as water table mounding, soil gas pressure and composition, and tracer gas response) and cross-borehole ERT. In comparison, ERT was more sensitive to the pattern of air flow in the saturated zone.*
Spies and Ellis (1995)	*Application of ERT in monitoring of different stages of in-situ vitrification process was presented.*
Daily et al. (1992)	*ERT images were consistent with known geology and numerical flow simulation with respect to soil type. ERT is a useful method to monitor the moisture front movement in heterogeneous soil.*
Ichikawa and Ishibashi (1990)	*The distribution of the fracture zone at a dam site was imaged using ERT method. The data were collected before and after a saline injection to the fracture zone.*
Tamburi et al. (1988)	*A 3-d ERT algorithm and system has been described. Laboratory and field experiments show that ERT is a promising method for groundwater studies.*
Tamburi et al. (1987)	*An EIT algorithm and system were introduced as Electro-scan system for imaging of pollution plumes.*
Greenhouse and Williams (1985)	*In geophysical monitoring of contamination of waste disposal, it was suggested to consider future changes, minimal permanent installations, high priority of simplicity and reliability, clear definition of measurement limitation, and well-defined unrelated noise level.*
Tamburi et al. (1985)	*ERT was applied to groundwater pollution plume in lab and field*

Table A-5 Monitoring leaks from storage ponds and liners under waste

References	Significance or major conclusions
Laine et al. (1997)	*A surface electrode grid was used to locate the leak from a liner under waste. A non-linear least-square technique was used to invert the data.*
Van et al. (1991)	*A set of permanent electrodes was installed on grids beneath and around the investigation site. Successful results were obtained from the resistivity method in detecting leakage from the pond.*
Parra (1988)	*This study proposed mapping the electrical response due to a short circuit across an insulating liner, which results from conductive fluid in a hole.*
Greenhouse and Harris (1983)	*The resistivity method was used to map conductive zones of contaminated groundwater.*

Table A-6 ERT Case studies

References	Significance or major conclusions
Andrews et al. (1995)	*A set of successful conducted field experiments was presented on the imaging of shallow depth soil profiles using the ERT method.*
Narayan and Dusseault (1995)	*A simulation analysis applied ERT to Enhanced Oil Recovery (EOR); general requirements were presented.*
Kim et al. (1994)	*ERT was used successfully to image the moisture distribution and movement in pavement.*
Roca-Ramisa et al. (1994)	*Micro- and micro-resistivity tools were introduced for well logging. Differentiation between natural and drilling induced fractures was achieved by analyzing the results of both micro- and micro-resistivity tools at the same time.*
Schenkel (1994)	*Reduction of sensitivity in radial and vertical extent was detected. Dipole-dipole array showed the best results in a cased well. Single well survey has limited resolution while cross-hole configuration was able to reconstruct the layers.*
Kumata et al. (1993)	*Results of a tank model were successfully compared with a 2.5-Dimensioanl FEM and theoretical potential field.*
Noel and Xu (1992)	*It was determined that the ERT method gives clearer results in detecting underground cavities than is achieved by pseudosection method.*
Noguchi et al. (1991)	*A successful application of ERT on rock mass analysis for tunneling was presented.*
Daily et al. (1990)	*ERT was applied to cross borehole study.*
Sasaki and Matsuo (1990)	*Copper mineral deposits were detected by ERT application of surface to tunnel.*
Ranieri et al. (1989)	*The possibilities of tomographic technique application to geo-electrical methods were analyzed. Laboratory tests showed that ERT can identify different salt-concentration zones in salt-water intrusion monitoring.*
Shima (1989)	*It was suggested that in case of surrounding resistivity structure, good images could be reconstructed from a combination of in-line data and cross-line data, analyzing an area outside the exploration area, and extension of one side of the exploration line (about 40%).*

Table A-7 Three-dimensional resistivity and ERT evaluations

References	Significance or major conclusions
Pinheiro et al. (1998)	*The possibility of using Pentium PC's for 3-D ERT data processing was demonstrated.*
Duraiswami et al. (1997)	*The boundary element method was applied to solve 2- and 3-D EIT problem, assuming constant-conductivity interior regions to simplify the region shape parameterization for efficiency.*
Santos et al. (1997)	*3-D resistivity data were collected, analyzed, and successfully compared with the previously collected 1- and 2-D resistivity data from geothermal field. The achieved model was consistent with the previous model and geological information.*
Boothe and Basaarab-Horwath (1996)	*Uniformly distributed electrode configuration results in better images than peripheral arrangements. A greater number of independent measurements lead to image improvement.*
Binley et al. (1996)	*A general description of forward and inverse solutions of 3-D ERT was presented. 3-D ERT has been suggested to offer the true images of the phenomena.*
Kotre (1996)	*In pure surface ERT, the author concluded that better resolution would be obtained if the electrode grids were treated as two orthogonal sets of parallel linear arrays.*
Anderson et al. (1995)	*An analytical solution for a single target in a 2-D electrical impedance tomography (EIT) circular environment was developed which takes into account both conductivity and permitivity values.*
Kotre (1995)	*A sensitivity coefficient weighted filter backprojection image reconstruction algorithm was applied to sub-surface image reconstruction. This algorithm along with two orthogonal sets of parallel linear electrodes was shown to a useful imaging performance. The robustness of the algorithm when it is used with incomplete data sets was demonstrated.*
Spitzer (1995)	*A 3-D finite difference forward model was presented. The preconditioned conjugate gradient method was shown to be the most efficient matrix solver among five methods.*
Sasaki (1994)	*Anisotropic resistivity tomography was used to numerically evaluate the characterization of fractured rock using a 2-D inversion model.*
Sasaki (1992)	*The resolution of ERT was numerically evaluated. The dipole-dipole method was suggested for high-resolution data and the pole-dipole was a good compromise between the dipole-dipole and pole-pole method.*
Takahashi et al. (1991)	*Seismic and cross-hole resistivity tomography showed the best results in the reconstruction of oil-bearing formations among various imaging techniques tested.*

The inverse algorithm is one of the most important mathematical challenges in ERT studies. The published results show that there is still work to be done in this field to reach to a true 3-D inverse algorithm for ERT applications (Table A-8).

Table A-8 Inversion

References	Significance or major conclusions
Pinheiro et al. (1997)	*A 12-bit data acquisition system for real time imaging was introduced. Smoothness-constrained inversion was shown to be superior to the Marquardt-Levenberg regularization in the presence of Gaussian noise.*
Vauhkonen et al. (1997)	*A new method of implementing prior information of conductivity in the optimization algorithm was introduced that is based on the approximation of the prior covariance matrix by simulated samples of feasible conductivities.*
LaBrecque et al. (1996)	*Occam's Inversion algorithm was discussed for borehole ERT. Misleading effects of noise were explained. A smart way of using this method was suggested.*
Loh and Dickin (1996)	*Modification of Newton-Raphson was presented by operating on the non-zero values of sparse matrix, and applying preconditioning.*
Loke and Barker $(1996)_a$	*The required number of pole-pole potential measurements were reduced to one-third by making measurements along vertical, horizontal, and 45° diagonals passing through the current electrodes without degrading the image resolution.*
Loke and Barker $(1996)_b$	*An inversion technique based on smoothness-constrained least-squares method was introduced for calculation of resistivity pseudosections. Initial values were based on homogenous earth; next iteration guess values were calculated using a quasi-Newton method to estimate the partial derivatives. These approaches reduce the computer running time. Tests showed that this technique is insensitive to random noise.*
Morelli and LaBrecque (1996)	*A 2-D ERT inversion algorithm was introduced based on Occam's-style, weighted-least-square method. This approach reduced the effect of systematic noise in data.*
Li et al. (1995)	*A full 3-D inversion of ERT data was developed. Application of quasi-convexity property of non-linear regularizing inverse problem and selection of optimum regularizing parameters lead to high-resolution, accurate and stable inversion.*
Loke and Barker $(1995)_a$	*Multiplication of a scaling factor calculated from the last two iterations increased the convergence speed. Using a weighted average of resistivity differences for layer resistivity improved the stability of Zohdy's inversion*
Loke and Barker $(1995)_b$	*A 2-D ERT algorithm was introduced based on smoothness-constrained and least-squares.*

Table A-8 Continued

References	Significance or major conclusions
Zhang et al. (1995)	*Conjugate gradient relaxation technique along with an incomplete Cholesky decomposition preconditioning were applied for a 3-D resistivity forward and inverse algorithm. An experimental result was presented for a leakage monitoring.*
Artola and Dell (1994)	*A quasi-Newton based 2-D EIT was presented, which to solve the forward problem at each iteration and updating the inverse at the same time. Both steps take O (n^2) operations (each takes 0.11 s on a 25 MHz 68040 based NeXT station).*
Li (1992)	*Two 2-D inversion algorithms were developed to construct conductivity images directly, or by combining the charge density images obtained by inverting multiple sets of common current potentials using the Born approximation. 3-D inversion was developed based on few assumptions and solution of a sequence of 1-D inversion algorithms, which was called approximate inverse mapping (AIM) formulization. A forward model and AIM were used to analyse the observed data.*
LaBrecque (1990)	*In a numerical study, the smoothest inversion produced much better results for 2-D cross-hole ERT than maximum entropy inversion.*
Yorkey (1990)	*A Gauss-Newton solution was presented to solve non-linear problem of ERT based on piecewise polynomial function.*
Sasaki (1989)	*The application of joint inversion to magnetotelluric and dipole-dipole resistivity was described. The combination of smoothness-constrained least-squares and modified Gram-Schmidt methods was used. Numerical and field results showed that the joint inversion method improves the resolution of 2-D resistivity data.*
Gustafson and McEuen (1987)	*Joint inversion of multiple resistivity data sets was found to improve the quality of interpretation. Joint inversion is not sensitive to random noise but may not converge for the data with systematic noise.*
Shima and Sakayama (1987)	*The authors introduced the alpha center method for forward algorithm and a hybrid non-linear least square method as an inversion algorithm for 2-dimensional ERT (numerical study).*

Few publications are available on resistivity and ERT instrumentation. Table A-9 presents some of the recent publications on this issue.

Table A-9 Resistivity instrumentation, power supply and waveform analysis for ERT

References	Significance or major conclusions
Gasulla et al. (1997)	*Synchronous sampling at flat part of square waves was found to reduce the interference compared with sinusoidal waves.*
Barker 1995	*A brief description of resistivity systems was introduced.*
Jaafari and Joos 1995	*The use of a combination of electronic and electromechanical switching components results in implementation of a compact, efficient, affordable and low weight power supply for field operation.*
Pallas-Areny and Brescoli (1995)	*A new circuit for synchronous sampling was presented. It was suggested that square waves are easier to generate and can be applied to EIT using a demodulator for synchronous sampling and band-pass filter to isolate the noise at low frequency.*

The interpretation of resistivity data directly depends on our understanding of the effects of different parameters on the electrical field. The effects of different parameters on the collected resistivity data have been studied and reported in many publications (such as: *Zohdy* 1968, *Roy and Apparao* 1971, *Roy* 1972, *Klefstad et al.* 1975, *Kumar and Chowdary* 1977, *Roy and Rao* 1977, *Fax et al.* 1980, *Holladay and West* 1984, *Barker* 1989, *Sen and Goode* 1992, *Frasheri* 1993) and still can be seen in the recent publications (*Pous et al.* 1996, *Yadav and Abolfazli* 1998). Table A-10 presents the most recent publications on the study of physical properties by resistivity methods.

Table A-10 Study of physical properties by resistivity methods

References	Significance or major conclusions
Bing and Greenhalgh (1997)	*A synthetic study showed that the dipole-dipole and pole-dipole arrays are better for cross-hole resistivity imaging than are pole-pole arrays. Scanning observations and electrode separations were the most effective parameters in the resistivity image resolution in these two arrays.*
Nishigaki et al. (1996)	*Using a 2-dimensional inversion and pole-pole electrode configuration, ERT was used to evaluate and to determine the longitudinal and transverse dispersion parameters of a laboratory sample. Results of FEM analysis and conventional methods were consistent.*
Llera et al. (1990)	*Temperature dependence of resistivity in several water-saturated rocks was investigated (above 200°C). An increase in temperature reduces the resistivity of rocks.*

Appendix B. An example of a solved forward problem

In electrical impedance imaging, a low frequency AC (or DC) electric current is injected onto a regional surface and the peripheral potential is measured. The image of the distribution of electrical conductivity within the region is reconstructed by inverse calculation. Therefore, there are two aspects in electrical impedance tomography:

i. The forward solution; and,
ii. The inverse solution.

The forward problem here is the calculation of the potential field generated by a DC or a low frequency AC current, and the governing equation is a Laplace's equation (Equation 2-10).

A forward problem is presented here as an example. The problem has a high degree of symmetry, and is amenable to development of an analytical solution.

As an example of solving Laplace's equation in 3-D using analytical methods, consider a cylindrical cell of radius R and length 2a which is filled with a standard solution of known conductivity. The electrodes are placed on the periphery at the middle of the cylinder (Z = 0 plane) as a set of point electrode sources (Figure B-1).

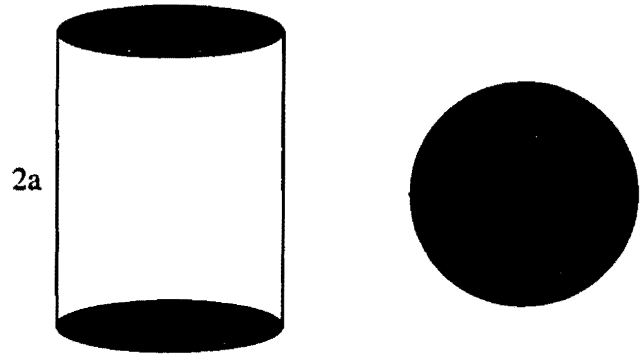


Figure B-1 Schematic projection of a cylindrical object

Steady current flows through two electrodes which are located at $(r, \phi_1, 0)$ and $(r, \phi_2, 0)$. Therefore we have:

$$\nabla^2 V(r,\theta,z) = 0 \tag{B-1}$$

and in terms of the cylindrical coordinates, Laplace's equation in three dimensions is:

$$\frac{1}{r}\frac{\partial}{\partial r}\left(r\frac{\partial V}{\partial r}\right) + \frac{1}{r^2}\frac{\partial^2 V}{\partial \theta^2} + \frac{\partial^2 V}{\partial z^2} = 0 \tag{B-2}$$

To solve the Laplace equation we separate the variables, and substitute:

$$V(r,\theta,z) = R(r) \cdot \Phi(\theta) \cdot Z(z) \tag{B-3}$$

This leads to;

$$\Phi Z\frac{d^2 R}{dr^2} + \frac{1}{r}\Phi Z\frac{dR}{dr} + \frac{1}{r^2} R Z\frac{d^2\Phi}{d\theta^2} + R\Phi\frac{d^2 Z}{dz^2} = 0 \tag{B-4}$$

Upon division of both sides by $R\Phi Z$; then:

$$\frac{1}{R}\frac{d^2 R}{dr^2} + \frac{1}{rR}\frac{dR}{dr} + \frac{1}{r^2\Phi}\frac{d^2\Phi}{d\theta^2} + \frac{1}{Z}\frac{d^2 Z}{dz^2} = 0 \tag{B-5}$$

Since the three terms are separate functions of (r,θ) and z, respectively, they each must be constant:

$$\frac{1}{R}\frac{d^2 R}{dr^2} + \frac{1}{rR}\frac{dR}{dr} + \frac{1}{r^2\Phi}\frac{d^2\Phi}{d\theta^2} = -\frac{1}{Z}\frac{d^2 Z}{dz^2} = \lambda^2 \tag{B-6}$$

The parameter λ is an arbitrary real positive parameter. The last differential equation can be solved as:

$$\frac{d^2 Z}{dz^2} + \lambda^2 Z = 0 \tag{B-7}$$

The solution is;

$$Z(z) = A_1 \cos(\lambda z) + A_2 \sin(\lambda z) \tag{B-8}$$

Because the potential is an even function, V (z) = V (-z), then A_2 must be zero, therefore:

$$Z(z) = A_1 \cos(\lambda z) \tag{B-9}$$

After rearranging the left-hand side of equation (B-6) we get:

$$\frac{r^2}{R}\frac{d^2R}{dr^2} + \frac{r}{R}\frac{dR}{dr} - \lambda^2 r^2 = -\frac{1}{\Phi}\frac{d^2\Phi}{d\theta^2} = m^2 \tag{B-10}$$

Again we have two separate parts which are functions of r and θ, respectively:

$$\frac{d^2\Phi}{d\theta^2} + m^2 \Phi(\theta) = 0 \tag{B-11}$$

With the result of this differential equation being:

$$\Phi(\theta) = B_1 \cos(m\theta) + B_2 \sin(m\theta) \tag{B-12}$$

The radial component can be put into standard form as a modified Bessel's equation:

$$\frac{d^2R}{dr^2} + \frac{1}{r}\frac{dR}{dr} - \left(\lambda^2 + \frac{m^2}{r^2}R\right) = 0 \tag{B-13}$$

And the solution can be expressed as:

$$R(r) = C_1 I_m(\lambda r) + C_2 K_m(\lambda r) \tag{B-14}$$

Where I_m and K_m represent the modified Bessel's functions of order m. The subscript m can not be zero because $I_0(\lambda r) = \infty$.

For r = 0 the potential must be finite [$K_m(0)$ = infinity] then $C_2 = 0$ and the result will be:

$$R(r) = C_1 I_m(\lambda r) \tag{B-15}$$

Finally, the general form of the solution is arrived by combining equations B-8, B-12, and A-15:

$$V(r,\theta,z) = \sum A_m I_m(\lambda r)\cos(\lambda z)\cos(m\theta) + B_m I_m(\lambda r)\cos(\lambda z)\sin(m\theta) \quad \text{(B-16)}$$

The problem is now reduced to finding the unknown parameters by using the boundary conditions.

Because the conductivity in air (outside the cylinder) is equal to zero, then the variation of the potential over the planes z = -a and z = +a, in the z direction, must also be zero, i.e.,

$$\left.\frac{d\,V(r,\theta,z)}{dz}\right|_{z=\pm a} = 0 \quad \text{(B-17)}$$

then:

$$\left.\frac{V(r,\theta,z)}{z}\right|_{z=\pm a} = \sum \pm\lambda \sin(\lambda a)\,[A_m I_m(\lambda r)\cos(m\theta) + B_m I_m(\lambda r)\sin(m\theta)] = 0 \quad \text{(B-18)}$$

and sin (λa) will be zero for $\lambda a = n\pi$,therefore $\lambda = n\pi/a$ for $n \geq 0$.

However, for n = 0 (λ = 0), $I_m(0) = 0$, and hence the potential all terms will be zero , then $\lambda \neq 0$ and $n \neq 0$, and the solution will be:

$$V(r,\theta,z) = \sum\sum A_{mn} I_{mn}(\lambda r)\cos(\lambda z)\cos(m\theta) + B_{mn} I_{mn}(\lambda r)\cos(\lambda z)\sin(m\theta) \quad \text{(A-19)}$$

Another boundary condition according to the position of two current electrodes is:

$$\left.\frac{\partial V}{\partial r}\right|_{r=R} = -\frac{I_0}{R\sigma}\,\delta(z)\,[\,\delta(\theta-\phi_1) - \delta(\theta-\phi_2)\,] \quad \text{(B-20)}$$

By differentiation of V we have:

$$\sum_{m=0}^{\infty}\sum_{n=0}^{\infty} \left(A_{mn} I_{mn} (\lambda R) \cos (m\theta) \cos (\lambda z) + B_{mn} I_{mn} (\lambda R) \sin (m\theta) \cos (\lambda z) \right) = -\frac{I_0}{Rs} \delta(z) \left[\delta(\theta - \Phi_1) - \delta(\theta - \Phi_2) \right] \quad \text{(B-21)}$$

Where I'_{mn} is the derivative of I_{mn}.

The two unknown parameters A_{mn} and B_{mn} must be solved. For this we can use the orthogonality and the Dirac delta function properties. Multiply both sides of the equation (B-21), by cos ($\lambda' z$) and cos ($m'\theta$) and integrate over z (from -a to a) and θ (from 0 to 2π) respectively.
For simplicity we solve each side part by part, then in the left hand side for z component we:

$$\int_{-a}^{a} \cos (\lambda z) \cos (\lambda z)\, dz = \frac{a}{\pi} \int_{0}^{2\pi} \cos(\lambda \frac{a}{\pi} z) \cos (\lambda \frac{a}{\pi} z)\, dz = \frac{a}{\pi} \begin{cases} \pi \delta_{\lambda\lambda'} & \lambda \neq 0 \\ 2\pi & \lambda = \lambda' = 0 \end{cases} \quad \text{(B-22)}$$

We know that $\lambda \neq 0$, then the solution of this part will be ($a\, \delta_{\lambda\lambda'}$). For the θ-dependent part in the left-hand side, we have:

$$\int_0^{2\pi} \sin(m\theta) \cos(m\theta')\, d\theta = 0 \quad \text{(B-23)}$$

Then the second term in the left-hand side of Equation (B-21) will be omitted and we have for the first term:

$$\int_0^{2\pi} \cos(m\theta) \cos(m'\theta)\, d\theta = \begin{cases} \pi \delta_{mm'} & m \neq 0 \\ 2\pi & m = m' = 0 \end{cases} \quad \text{(B-24)}$$

Because m cannot be zero, the solution becomes $\pi\delta_{mm'}$.

Finally the left-hand side will be:

$$\sum_{m=1}^{\infty}\sum_{n=1}^{\infty}(a\delta_{m'})(\pi\delta_{nn'})A_{mn}\,\mathrm{I}'_m(\lambda R) \tag{B-25}$$

On the right-hand side of equation (A-21), we have:

$$-\frac{I_0}{R\sigma}\int_{-a}^{a}\cos(\lambda' z)\,\delta(z)\,dz\int_0^{2\pi}\cos(m'\theta)\,[\delta(\theta-\Phi_1)-\delta(\theta-\Phi_2)]\,d\theta \tag{B-26}$$

and then:

$$\int_{-a}^{a}\cos(\lambda' z)\,\delta(z)\,dz=\cos(0)=1 \tag{B-27}$$

$$\int_0^{2\pi}\cos(m'\theta)\delta(\theta-\Phi_1)d\theta-\int_0^{2\pi}\cos(m'\theta)\delta(\theta-\Phi_2)\,d\theta=-\frac{I_0}{R\sigma}[\cos(m'\Phi_1)-\cos(m'\Phi_2)] \tag{B-28}$$

Therefore equation (B-21) will become;

$$\sum_{m=1}^{\infty}\sum_{n=1}^{\infty}(a\delta_{m'})(\pi\delta_{nn'})A_{mn}\,\mathrm{I}'_m(\lambda R)=-\frac{I_0}{R\sigma}[\cos(m'\Phi_1)-\cos(m'\Phi_2)] \tag{B-29}$$

According to the Dirac delta function definition;

$$\delta_{nn'}=\begin{cases}1 & if\quad n=n'\\ 0 & if\quad n\neq n'\end{cases} \tag{B-30}$$

The solution only for m = m′ and λ = λ′ has been solved, therefore:

$$\sum_{m=1}^{\infty}\sum_{n=1}^{\infty}\pi a\,A_{mn}\,\mathrm{I}'_m(\lambda R)=-\frac{I_0}{R\sigma}[\cos(m\Phi_1)-\cos(m\Phi_2)] \tag{B-31}$$

and finally the solution for parameter A_{mn} will be:

$$A_{mn}=\frac{I_0}{Ra\pi\sigma\,\mathrm{I}'_m(\lambda R)}[\cos(m\Phi_2)-\cos(m\Phi_1)] \tag{B-32}$$

For finding the parameter Bmn we follow the same procedure as before. The z-dependent component remains the same and the solution takes the form (a $\delta_{\lambda\lambda'}$) for left-hand hand side and (1) for the right hand side. For the θ dependent component we multiply both sides of Equation (B-22) by sin (pθ) and integrate from 0 to 2π.
Consider the left-hand side, for the first term we have:

$$\int_0^{2\pi} \cos(m\theta)\sin(p\theta)\,d\theta = 0 \tag{B-33}$$

Then the first term will be omitted, and for the second term we have:

$$(a\delta_{\lambda\lambda'})B_{mn}\,I'_m(\lambda R)\int_0^{2\pi} \sin(m\theta)\sin(p\theta)\,d\theta = a\,B_{mn}\,I'_m(\lambda\,R)\begin{cases}\pi\,\delta_{mp} & m\neq 0\\ 0 & m=p=0\end{cases} \tag{B-34}$$

We know that m ≠ 0, then the solution will be $\pi\,\delta_{mp}$. For the right-hand side we have:

$$-\frac{I_0}{R\sigma}\left[\int_0^{2\pi} \sin(p\theta)\,\delta(\theta-\Phi_1)\,d\theta - \int_0^{2\pi} \sin(p\theta)\,\delta(\theta-\Phi_2)\right] = -\frac{I_0}{R\sigma}\left[\sin(p\Phi_1)-\sin(p\Phi_2)\right] \tag{B-35}$$

And finally we have:

$$(a\,\delta_{\lambda\lambda'})(\pi\,\delta_{mp})\,B_{mn}I'_m(\lambda\,R) = \frac{I_0}{R\sigma}\left[\sin(p\Phi_2)-\sin(p\Phi_1)\right] \tag{B-36}$$

According to the definition of the Dirac delta function for m = p and λ = λ′ the solution will be:

$$\pi a\,B_{mn}I'_m(\lambda\,R) = \frac{I_0}{R\sigma}\left[\sin(m\Phi_2)-\sin(m\,\Phi_2)\right] \tag{B-37}$$

Then the B_{mn} parameter is:

$$B_{mn} = \frac{I_0}{Ra\pi\sigma I'_m(\lambda R)}\left[\sin(m\Phi_2)-\sin(m\Phi_1)\right] \tag{B-38}$$

And finally the general solution of the potential field is equal to:

$$V(r,\theta,z)=\sum_{m=1}^{\infty}\sum_{n=1}^{\infty} A_{mn}\left[\mathrm{I}_m(\frac{n\pi}{a}r)\cos(\frac{n\pi}{a}z)\cos(m\theta)\right]+B_{mn}\left[\mathrm{I}_m(\frac{n\pi}{a}r)\cos(\frac{n\pi}{a}z)\sin(m\theta)\right] \tag{B-39}$$

where:

$$A_{mn}=\frac{I_0}{Ra\pi\sigma \mathrm{I}'_m(\lambda R)}\left[\cos(m\Phi_2)-\cos(m\Phi_1)\right] \tag{A-40}$$

and;

$$B_{mn}=\frac{I_0}{Ra\pi\sigma \mathrm{I}'_m(\lambda R)}\left[\sin(m\Phi_2)-\sin(m\Phi_1)\right] \tag{B-41}$$

The potential difference between two electrodes, V_1 $(R,0,\theta_1)$ and V_2 $(R,0,\theta_2)$, can now be written as:

$$\Delta V=\frac{I_0}{Ra\pi\sigma}\frac{\mathrm{I}_m\left(\frac{n\pi}{a}R\right)}{\mathrm{I}'_m\left(\frac{n\pi}{a}R\right)}\left\{\begin{array}{l}\left[\left(\cos(m\theta_1)-\cos(m\theta_2)\right)\left(\cos(m\Phi_2)-\cos(m\Phi_1)\right)\right]\\+\left[\left(\sin(m\theta_1)-\sin(m\theta_2)\right)\left(\sin(m\Phi_2)-\sin(m\Phi_1)\right)\right]\end{array}\right\} \tag{B-42}$$

B.1 Application

A 3-dimensional algorithm is developed for electrical resistivity tomography (ERT) of a finite cylinder. To use the solution practically, electrodes for data collection should be placed around the sample in a cross-sectional plane at the mid-height of the cylinder, and axial variations of the potential field should be considered. Electrical current will be induced in the sample from two of the electrodes, and potential differences will be measured through a series of paired electrodes in the cross-sectional plane. This algorithm is suitable for studying of any uniform cylindrical objects (i.e., permeameter, core sample, etc.) for geological and engineering problems.

A permeameter can be used to collect data in cylindrical specimens, and issues such as changes of salinity of fluid, saturation, and phase saturation (oil/water/gas) are of interest. With a properly monitored specimen, the algorithm can be used to analyze some of these

effects, or more generally, to explore the relationship between hydraulic conductivity and electrical resistivity of the sample.

Appendix C. Equipment evaluation

One of the objectives of the primary experiment in the Cambridge sand pit site was to evaluate and select the most appropriate equipment available for collecting ERT data. Different resistivity meters were studied (Table C-1) and the Syscal Junior System (manufactured by IRIS Instruments, in France) was finally selected from all of those studied. Since there were some doubtful field readings by the Syscal Junior System, a set of different repeated measurements was conducted in the field and laboratory. These tests can be divided into two groups, field tests, and lab tests.

C.1 Field tests

The field tests of the system are shown in figures C-1 and C-2. Figure C-1 is a plot of 30 times measurements of 5 cycles with a fixed electrode arrangement for different resistivity meter gage positions. There is a ± 2-3 % shift for different gage positions with respect to each other. In addition, a linear drift (increasing trend) can be seen in the readings of different gage positions. Also, some jumps have been detected in the collected data.

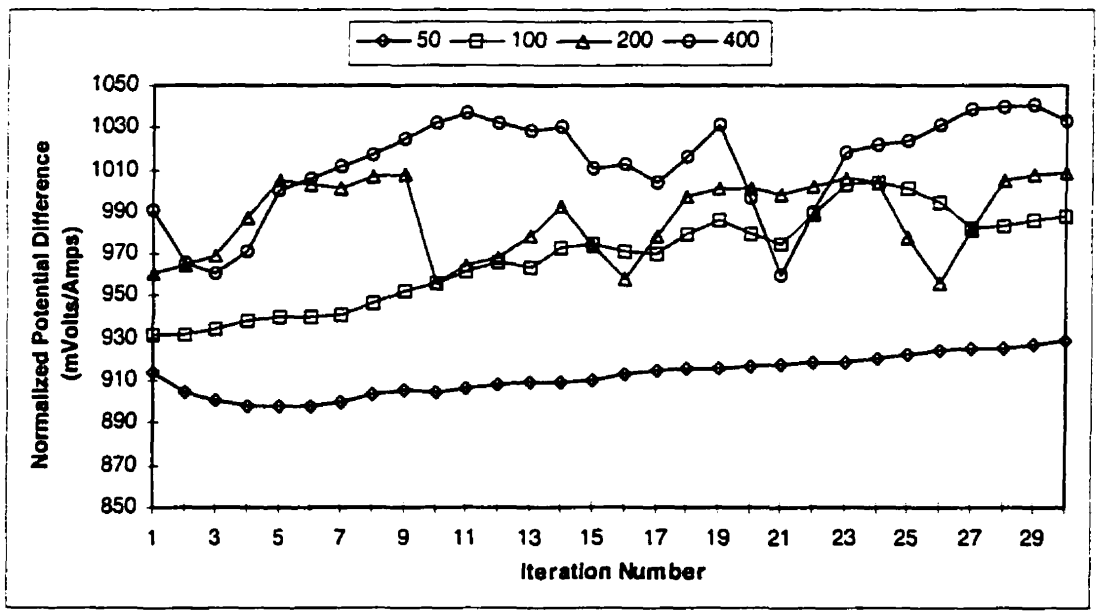


Figure C-1 Resistivity meter response in repeated measurements in the field for different gage positions

Table C-1 Commercial resistivity meters specifications

Row	Company	Model	Measurement system	Current Range		Output power (Watts)	Claim Accuracy and reliability	Memory capacity	Input Voltage (Volts)	Operating Temp. Range: (°C)	# of channels (Receiver)
				mA	V						
1	IRIS Inst.	Syscal Junior	Four electrodes	800	400	50	better than 0.5%	818 points	±5	-20 to +70	1
2	Syntrex	Geopluse	Four electrodes	100	180	18	0.001 ohm	NA	NA	0 to 50	1
3	OYO	Mc-Ohm-2115	Four electrodes	200	200	40	0.001 ohm	NA	NA	NA	3
4	Campus	MRT System	Four electrodes	1000	700	NA	0.001 ohm	NA	NA	NA	1
5	Interpex	RESIX-IP2D	Four electrodes	NA	NA	NA	NA	NA	NA	NA	1
6	ABEM	Terrameter SAS 4000	Four electrodes	500	1000	NA	0.25%	2MB	NA	NA	4
7	AGI Advanced Geosiences, Inc.	Sting/Swift (R1)	Four electrodes	500	500	NA	better than 1.0%	>3000 points	500	NA	1
8	Bison		Four electrodes	NA	NA	NA	NA	NA	NA	NA	1
9	Androtec	IP & TDR-6	Four electrodes	NA	NA	NA	0.25%	NA	NA	NA	6

*NA: Not available

For one current dipole electrode arrangement, the electric potentials of all surface electrodes have been measured with respect to a fixed point. The same procedure has been repeated and the results of these two measurements are presented in Figure C-2. There is a larger fluctuation in collected data for the small electric potential differences than for the larger ones.

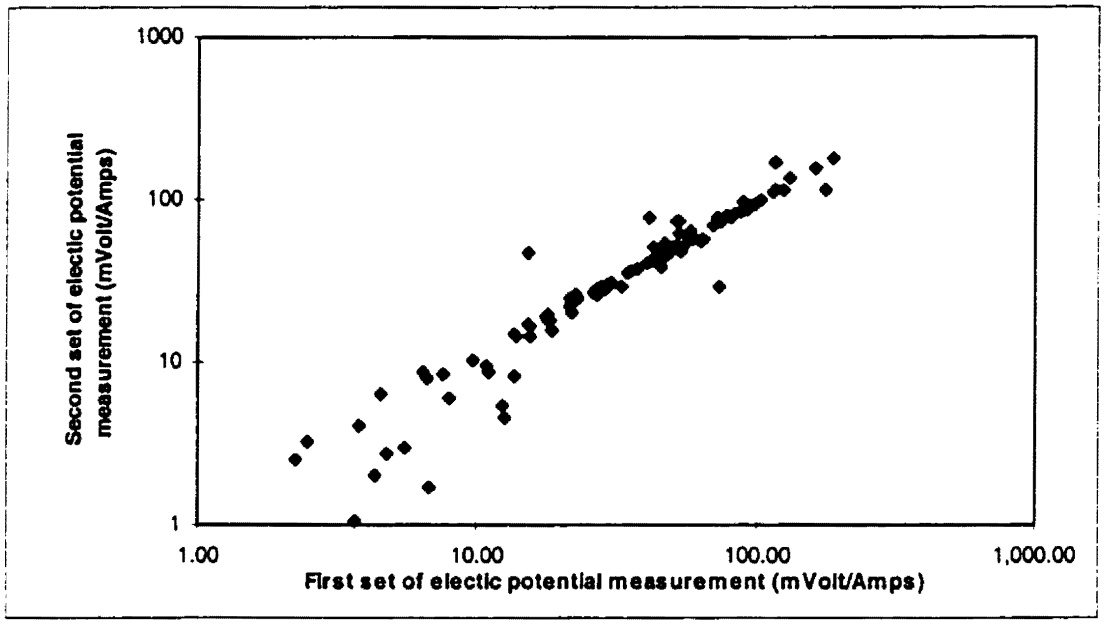


Figure C-2 Plot of two set of repeated measurements in the field for the same electrode arrangements

C.2 Laboratory tests

The results of laboratory tests are presented in Figures C-4 to C-8. The first set of measurements is the data collection of the resistivity meter for different resistors at four gage positions (50, 100, 200, and 400 volts). The error has been calculated with respect to the true resistance of each resistor. The error is bigger for the low resistivity resistors.

The laboratory setup is schematically presented in Figure C.3. The resistor R is the one that has been changed in different tests.

In addition, two sets of resistor networks have been prepared (Figure C-9). The Syscal Junior resistivity meter has been checked to read for 32 times of 5 cycles for different resistivity meter gage positions and the results have been presented in Figures C-10 and C-11.

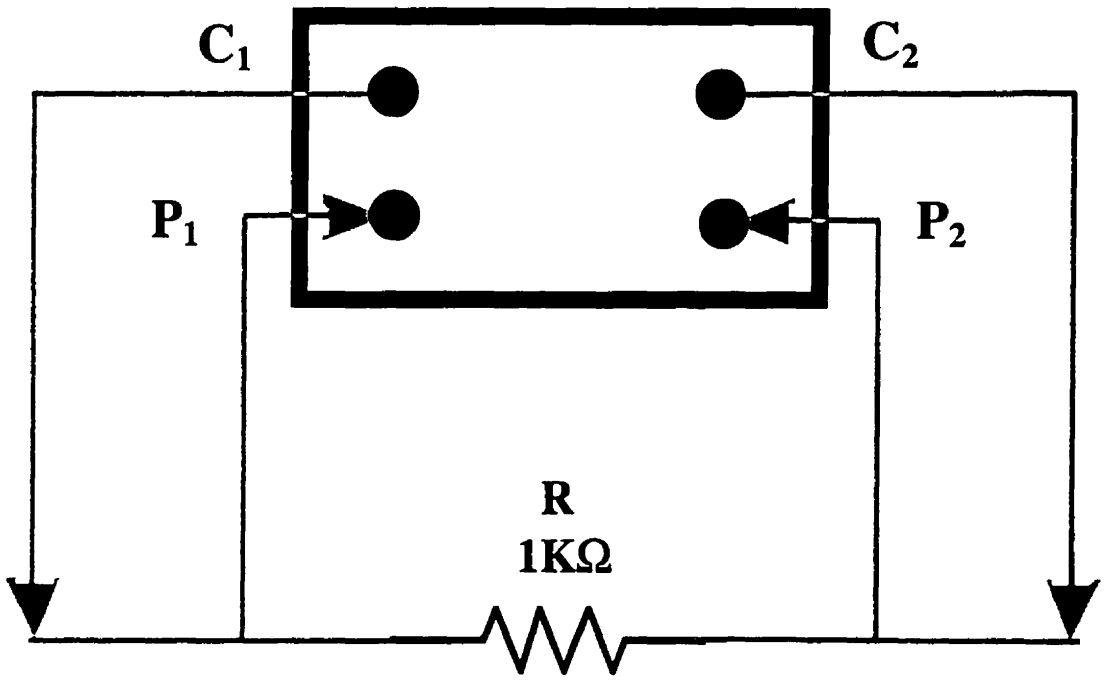


Figure C.3 Schematic diagram of laboratory setup

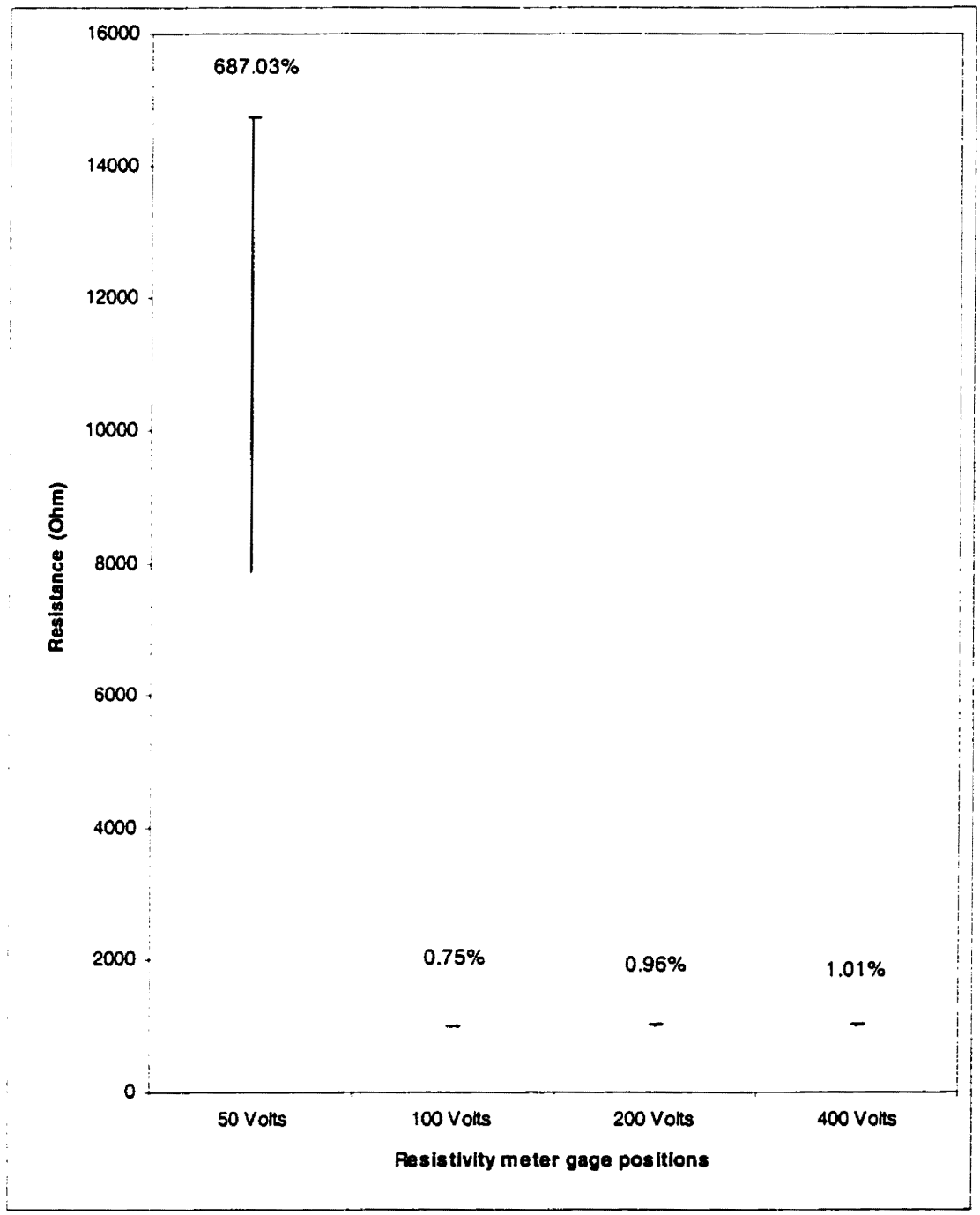


Figure C-4 Syscal Junior resistivity meter readings for 1.0 kΩ resistor at different gage positions

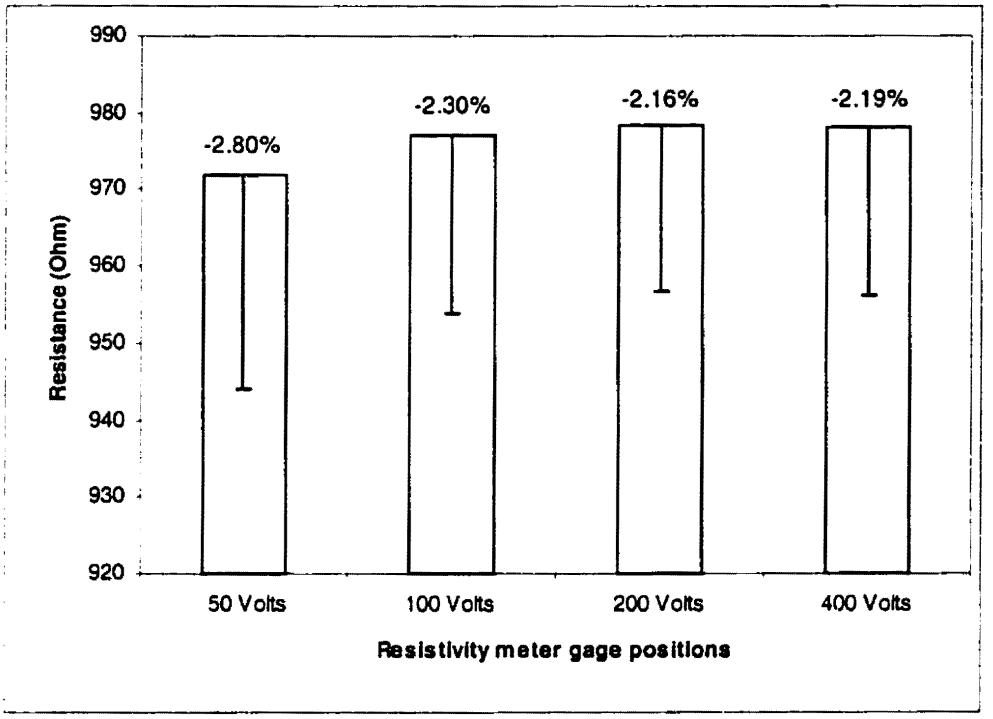


Figure C-5 Syscal Junior resistivity meter readings for 1.0 kΩ resistor at different gage positions

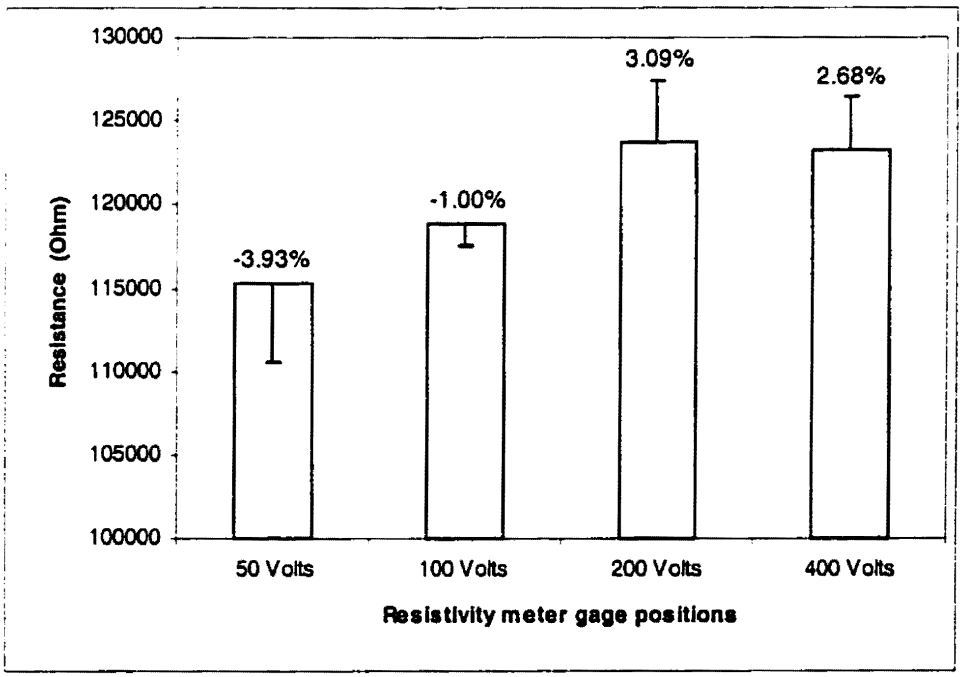


Figure C-6 Syscal Junior resistivity meter readings for 120 kΩ resistor at different gage positions

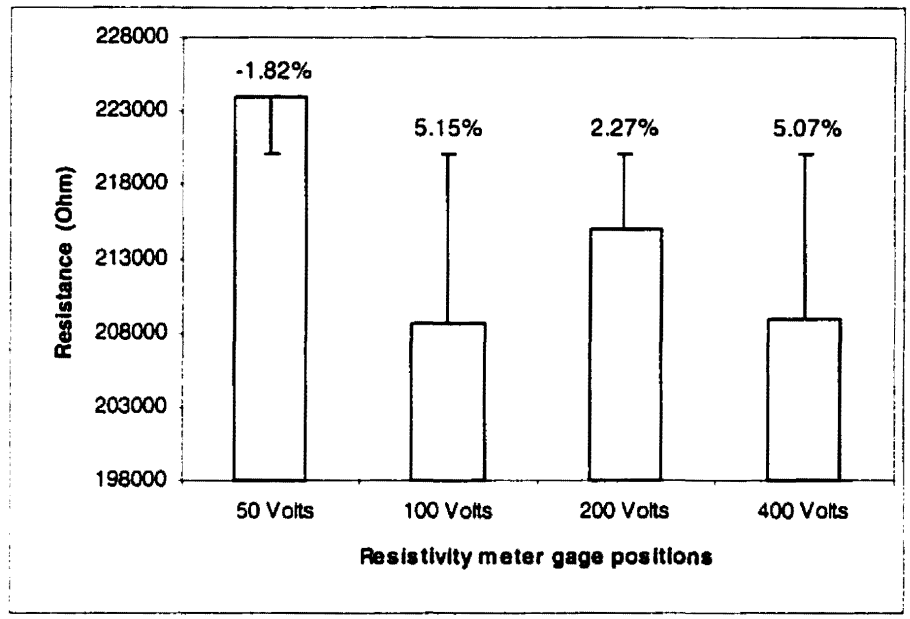


Figure C-7 Syscal Junior resistivity meter readings for 220 kΩ resistor at different gage positions

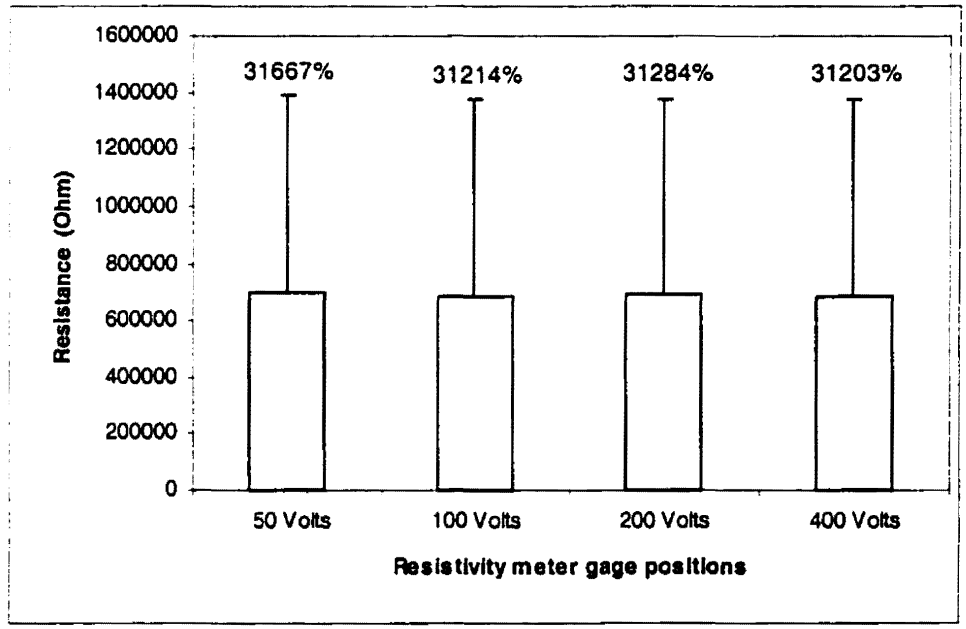
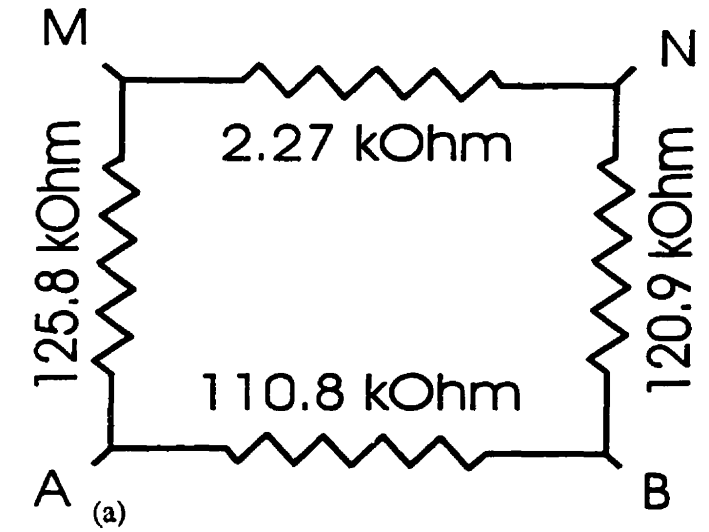


Figure C-8 Syscal Junior resistivity meter readings for 2.2 kΩ resistor at different gage positions



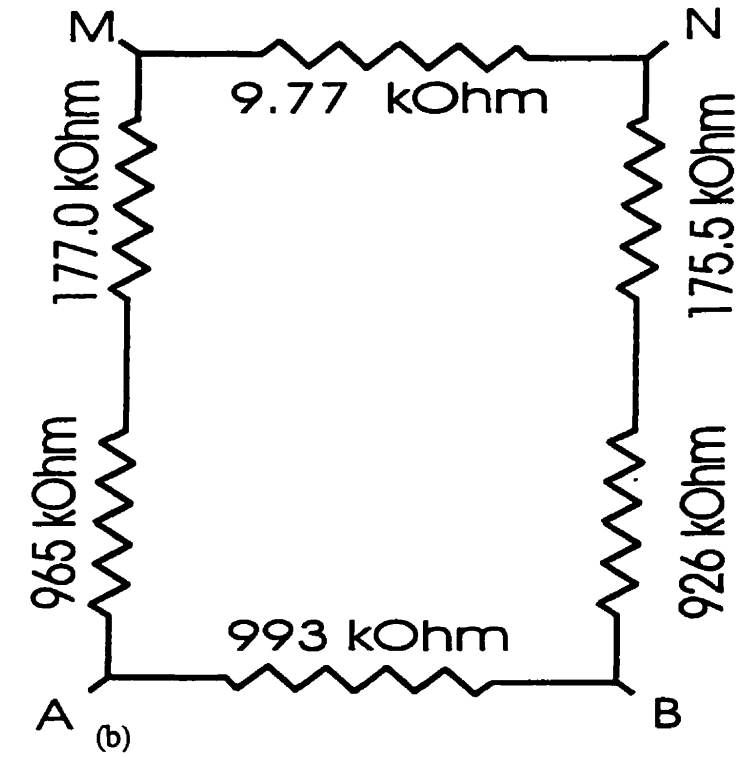


Figure C-9 Schematic diagram of two resistance networks: (a) first resistor network, (b) second resistor network

In Figure C-10 there is almost ± 3 % error detected for different gage positions. The results from the second resistor network (Figure C-11) shows that the resistance of this network is most probably out of the accuracy range of this system.

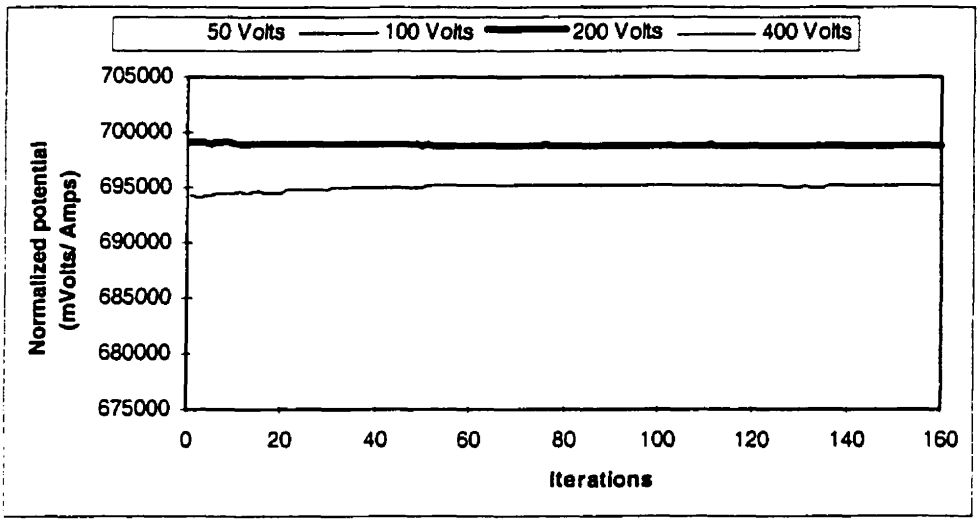


Figure C-10 Repeated lab measurements of the first resistor network for different gage positions

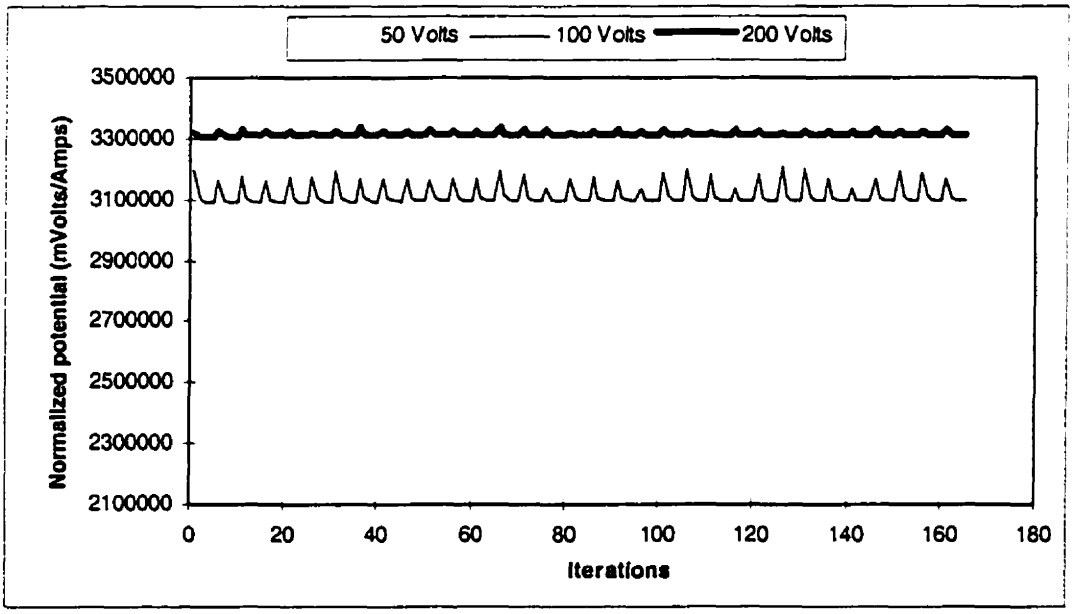


Figure C-11 Repeated lab measurements of the second resistor network for different gage positions

C.3 Equipment evaluation results

From the results presented in the previous sections, it can be concluded that:

i. There is a typical reading uncertainty of about ± 2%;
ii. This error can be more or less random with time or as an almost linear slope;
iii. There are also occasions where very large differences occur between repeated measurements on the same electrodes, when one reading becomes very close to zero;
iv. The error behavior is somewhat different between field and lab measurements.

The maximum voltage input limit of the Syscal Junior (± 5 volts) was the main problem in the data collection. The downhole potential electrode readings were greater than 5 volts whenever the current was passing through one of the downhole electrodes. These readings were very important for checking the effects of injected saline to the electrical field. Comparing with the simulated results, the collected data are fairly reliable for evaluating the objectives of Cambridge experiment.

Appendix D. The specifications of the devices, components and softwares used in the ERT system:

There are two main parts in this system:

1. Switch network and computer interfacing; and
2. Power supply.

Since the power supply is not finished yet, and the delivery time is not clear, the explanation of that unit will be omitted. It is more desirable to explain each device and component separately. Devices and components that have been used in the switching network and computer interfacing include the following.

D.1 Switch network and computer interfacing

The following is a brief introduction to the devices and components used for the ERT automated system:

D.1.1 Devices:

D.1.1.1 A/D converter board specifications:

AT-MIO-16XE-50 from National Instruments (National Instruments 1997)

Typical for 25° C unless otherwise noted.

Analog Input

Input characteristics	
Number of channels	16 single-ended, 16 non-reference single-ended or 8 differential (software selectable per channel)
Type of ADC	Successive approximation
Resolution	16 bits, 1 in 65,536
Maximum sampling rate	20 kS/s guaranteed
Input signal ranges	
Input coupling	DC
Maximum working voltage (signal + common mode)	The common-mode signal (the average of the two signals in a differential pair) should remain within ±8 V of ground and each input should remain within ±11 V of ground.
Overvoltage protection	±25 V powered on, ±15 V powered off
Inputs protected	ACH<0..15>, AISENSE
FIFO buffer size	512 samples
Data transfers	DMA

DMA modes	Single transfer, demand transfer
Configuration memory size	512 words
Transfer characteristics	
Relative accuracy in LSB	±0.5 typical, ±1.0 max

Gain (Software selectable)	Range (Software selectable)	
	bipolar	uni-polar
1	±10 V	0 to 10 V
2	±5 V	0 to 5 V
10	±1 V	0 to 1 V
100	±0.1 V	0 to 0.1 V

DNL	±0.5 typical, ±1.0 max
No missing codes	16 bits, guaranteed
Amplifier characteristics	
Input impedance	
Normal, powered on	7 G½ in parallel with 100 pF
Powered off	820 ½ min
Overload	820 ½ min
Input bias current	±10 nA
Input offset current	±20 nA

CMRR, DC to 60 Hz

Gain	CMRR
1	80 DB
2	86 DB
10	100 DB
100	120 DB

Dynamic characteristics
Bandwidth (-3 dB)

Gain	Bandwidth
1, 2	63 kHz
10	57 kHz
100	33 kHz

Settling time to ±1 LSB
for full-scale step 50 µs max, all gains and ranges

System noise in LSBrms (including quantization noise)
Gain = 1, 2, 10 0.5

Gain = 100	0.8 bipolar, 1.4 unipolar
Crosstalk	-85 dB max, DC to 20 kHz
Stability	
Recommended warm-up time	15 minutes
Onboard calibration reference	
DC Level	5.000 V (±2.0 mV)
(actual value stored in EEPROM)	
Temperature coefficient	±2 ppm/°C max
Long-term stability	±15 ppm/ Ã1,000 h
Analog output for AT-MIO-16XE-50	
Output characteristics	
Number of channels	2
Resolution	12 bits, 1 in 4,096
Maximum update rate	20 kS/s
Type of DAC	Double-buffered
FIFO buffer size	None
Data transfers	DMA, interrupts, programmed I/O
DMA modes	Single transfer, demand transfer
Transfer characteristics	
Relative accuracy (INL)	±0.5 LSB max
DNL	±1 LSB max
Monotonicity	12 bits, guaranteed
Offset error	
After calibration	±0.5 mV max
Before calibration	±85 mV max
Gain error (relative to calibration reference)	
After calibration	±0.01% of output max
Before calibration	±1% of output max
Voltage output	
Range	±10 V
Output coupling	DC
Output impedance	0.1 ½ max
Current drive	±5 mA
Protection	Short-circuit to ground
Power-on state	0 V (± 85 mV)
Dynamic characteristics	
Settling time to ±0.5 LSB (±0.01%)	
for full-scale step	50 µs
Slew rate	2 V/µs
Noise	40 µVrms, DC to 1 MHz
Glitch energy (at midscale transition)	
Magnitude	±30 mV
Duration	10 µs
Stability	
Offset temperature coefficient	±25 µV/°C

Gain temperature coefficient	±15 ppm/°C
Onboard calibration reference	
Level	5.000 V (±2 mV) (actual value stored in EEPROM)
Temperature coefficient	±2 ppm/°C max
Long-term stability	±15 ppm/ Ã1,000 h

Digital I/O

Number of channels	8 input/output	
Compatibility	TTL/CMOS	
Digital logic levels		
Level	Minimum	Maximum
Input low voltage	0 V	0.8 V
Input high voltage	2 V	5 V
Input low current (V in = 0 V)	–	-320 µA
Input high current (V in = 5 V)	–	10 µA
Output low voltage (I out = 24 mA)	–	0.4 V
Output high voltage (I out = 13 mA)	4.35 V	–
Power-on state	Input (High-Z)	
Data transfers	Programmed I/O	

Timing I/O

Number of channels	2 up/down counter/timers, 1 frequency scaler
Resolution	
Counter/timers	24 bits
Frequency scaler	4 bits
Compatibility	TTL/CMOS
Base clocks available	
Counter/timers	20 MHz, 100 kHz
Frequency scaler	10 MHz, 100 kHz
Base clock accuracy	±0.01%
Maximum source frequency	20 MHz
Minimum source pulse duration	10 ns, edge-detect mode
Minimum gate pulse duration	10 ns, edge-detect mode
Data transfers	DMA
DMA modes	Single transfer, demand transfer

Triggers

Digital trigger	
Compatibility	TTL
Response	Rising or falling edge
Pulsewidth	10 ns min

RTSI

Trigger Lines	7
Bus Interface	Master (PCI only), slave
Power requirements	+5 VDC (±5%), 0.75 A
Power available at I/O connector	+4.65 to +5.25 VDC, 1 A

Physical

Dimensions (not including connectors)	33.8 by 9.9 cm (13.3 by 3.9 in.)
I/O connector	68-pin male SCSI-II type

Operating environment

Ambient temperature	0° to 55° C
Relative humidity	10% to 90%, noncondensing
Storage environment	
Ambient temperature	-20° to 70° C
Relative humidity	5% to 95%, noncondensing

D.1.1.2 Multiplexer board specifications

Amux-64T from National Instruments (National Instruments 1997)

Typical for 25° C unless otherwise noted.

Analog input

Input characteristics

Number of channels	
Single AMUX-64T board	64 single-ended or 32 differential
Two boards	128 single-ended or 64 differential
Four boards	256 single-ended or 128 differential
Input signal ranges	Same as MIO board
Input impedance	
Powered on	Å500 ½ in series with MIO input impedance
Powered off	Å500 ½ for |V IN | >0.7 V
Input coupling	DC
Overvoltage protection	±35 V powered on, ±20 V powered off
Inputs protected	CH<0..63>

Dynamic characteristics

Settling time to 10 V step

	MIO ±0.012% (±0.5 LSB) Accuracy	
Gain	with One AMUX-64T	with Four AMUX-64Ts
0.5 to 5	5 µs	9 µs
10	6 µs	9 µs
20	6 µs	11 µs
50	7 µs	11 µs
100	9 µs	14 µs

Stability

Recommended warm-up time	15 minutes
Cold-junction reference	
Output	10 mV/°C
Accuracy	±1.0° C from 0° to 110° C
Power requirement	+5 VDC, 78 mA

Physical

Dimensions	26.9 by 12.4 cm (10.6 by 4.9 in.)
Signal connections	64 screw terminals
I/O connectors	Two 50-pin male ribbon connectors
	One 68-pin male connector

Environment

Operating temperature	0° to 70°C
Storage temperature	-20° to 70°C
Relative humidity	5% to 90% noncondensing

D.1.1.3 Digital input board specifications

The CIO-DI192 board senses 192 contact closures from a single card in a PC. The CIO-DI192 provides 192 lines of TTL digital input capable of reading signals from other TTL devices as well as solid state relays and any 0 to 5V source.

In input mode, no setup programming is required. As a result the state of the ports is not subject to glitching or reset as are programmable digital I/O chips.

The CIO-DI192 uses a 50-pin connector. The CIO-DI192 has four connectors. Each 50-pin connector carries 48 inputs and power.

Power consumption

+5 V Supply 280 mA typical / 380 mA max

Digital input

Input high	2.0V min, 7.0V max
Input low	0.8V max, -0.5V min
Undefined	0.8V to 2.0V

Chip will be damaged if input is < -0.5V or > 7.0V

Environmental

Operating temperature	0-50 ° C
Storage temperature	-20-70 ° C
Humidity	0 to 90% non-condensing
Weight	5 oz (ComputerBoards Inc. 1995)

D.1.1.4 Digital output board specifications:

The CIO-DO192H board has 192 high drive digital output lines (or 192 bit digital output high drive). Cabling to the CIO- 192H is via standard 50 pin, 0.10 inch spacing IDC type ribbon cable connectors. Each cable carries 48 digital output lines, +5 volts and ground. The DO192H has four connectors.

The 82C55 can source or sink 2.5mA per I/O line. High drive boards can source 15 mA and sink 64 mA. The CIO-DO boards are fixed in an output state at all times there is no programming required to initialize the output registers. The output registers hold the state of the 8 bits most recently written to that port.

Power consumption

+5 V supply	450 mA typical / 660 mA max

Digital output

Output high	2.0V min, 7.0V max
Output low	0.8V max, -0.5V min

Environmental

Operating temperature	0-50 ° C
Storage temperature	-20-70 ° C
Humidity	0 to 90% non-condensing
Weight	5 oz(ComputerBoards Inc. 1995)

D.2 Components

D.2.1 Electromechanical relays

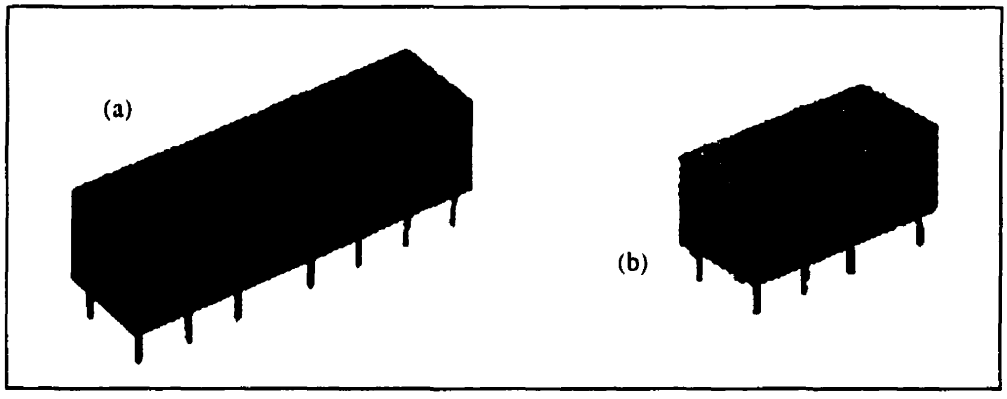


Figure D-1 Electromachanical Reed Relays: (a)DS4E-M-12V from Aromat Canada, Inc. (for elements K1 and K2 of Figure 4.11), (b) DS2E-M-12V from Aromat Canada, Inc. (for element K3 of Figure 4.11)

D.2.2 High-voltage high-current Darlington transistor arrays

Relay drivers ULN20003AN Texas Instruments for element UA of Figure 4.11 (Texas Instrument 1993)

The ULN2003A is a monolithic high-voltage, high-current Darlington transistor array. It consists of seven npn Darlington pairs that feature high-voltage output with common cathode clamp diodes for switching inductive loads. The collector-current rating of a single Darlington pair is 500 mA. The Darlington pairs may be paralleled for higher current capacity.

Specifications

- 500-mA rated collector current (single output)
- High-voltage outputs 50 V
- Output clamp diodes
- Inputs compatible with various types of logic
- Relay driver applications

- absolute maximum ratings at 25°C free-air temperature (unless otherwise noted)
- Collector-emitter voltage 50 V
- Input voltage, V_I 30 V
- Peak collector current (see Figures 14 and 15) 500 mA
- Output clamp current, I_{OK} 500 mA
- Total emitter-terminal current –2.5 A
- Continuous total power dissipation

Package	T_A = 25°C A Power Rating (mW)	TA = 25°C Derating factor Above (mW/°C)	T_A = 85°C Power Rating (mW)
D	950	7.6	494
N	1150	9.2	598

- Operating free-air temperature range, T_A –20 to 85°C
- Storage temperature range, T_{stg} –65 to 150°C
- Lead temperature 1,6 mm (1/16 inch) from case for 10 seconds 260°C

Parameters	Conditions		ULN2003A			unit
			min	type	max	
V_I(on) On-state input voltage	V_{CE} = 2 V	I_C = 200 mA			2.4	V
		I_C = 250 mA			2.7	
		I_C = 300 mA			3	
V_{CE} (sat) Collector-emitter saturation voltage	I_I = 250 µA, I_C = 100 mA			0.9	1.1	V
	I_I = 350 µA, I_C = 200 mA			1	1.3	
	I_I = 500 µA, I_C = 350 mA			1.2	1.6	
I_{CEX} Collector cutoff current	V_{CE} = 50 V, I_I = 0				50	µA
	V_{CE} = 50 V, TA = 70°C, II = 0				100	
V_F Clamp forward voltage	I_F = 350 mA			1.7	2	V
$I_{I(off)}$ Off-state input current	V_{CE} = 50 V, I_C = 500 µA ,T_A = 70°C		50	65		µA
I_I Input current	V_I = 3.85 V			0.93	1.35	mA
I_R Clamp reverse current	V_R = 50 V				50	µA
	V_R = 50 V, T_A = 70°C				100	
C_I Input capacitance	V_I = 0, f=1MHz			15	25	pF

D.2.3 Octal buffers and line drivers with 3-state outputs

SN74LS244 octal buffers and line drivers with 3-sate outputs are used for modification of digital I/O boards. These octal buffers and line drivers are designed specifically to improve both the performance and density of three-state memory drivers, clock drivers, and bus-oriented receivers and transmitters. The operation temperature range is from 0 to 70 °C.

D.2.4 Filter components:

Capacitor, a Siemens MKT polyester film capacitor 463-B32529-C105-J, (for element C1 of Figure 4.11).

Specifications

Climatic category in accordance with I_{EC}	68-155/100/56
Lower category temperature T_{min}	- 55 °C
Upper category temperature T_{max}	+ 100 °C (+ 125 °C for 1000 h and $V_C = 0.5V_R$)
Damp heat test	56 days/40 °C/93 % relative humidity
Limit values after damp	Capacitance change $\|\Delta C/ C\| \leq 5$ %

Heat test	Dissipation factor change Δ tan δ ≤ 5 × 10 -3 (at 1 kHz) Insulation resistance R is ³ 50 % of minimum or time constant t = C R × R is as-delivered values
Reliability: Reference conditions0,5 × V R ;40 °C	
Failure rate	1 ×10 -9 /h = 1 fit
Service life	200000 h
Failure criteria:	
Total failure	Short circuit or open circuit
Failure due to variation of parameters	Capacitance change |Δ C/ C| > 10 % Dissipation factor tan d > 2 × upper limit value. Insulation resistance R is < 150 MW (C R £ 0,33 mF) or time constant t = C R × R is < 50 s (C R > 0,33 mF)
DC test voltage	1,4 × V R , 2 s
Category voltage V_C Operation with dc voltage or ac voltage V_{rms} up to 60 Hz	T≤ 85 °C: $V_C = 1.0 \times V_R$ or $1.0 \times V_{rms}$
	T =100 °C: $V_C = 0.8 \times V_R$ or $0.8 \times V_{rms}$
Category voltage for short operating periods	T≤ 100 °C: $1.25 \times V_C$ for max 2000 h
	T =125 °C: $V_C = 0.5 \times V_R$ or $0.5 \times V_{rms}$ for max 1000 h

Resistor, a Phillips metal film resistor 0.6 W 1% 353-MRS25F 13K (for element R3 of Figure 4.11).

Specifications

DESCRIPTION	VALUE
Resistance range	1 Ω to 10 MΩ
Resistance tolerance and series	±1%; E24/E96 series
Maximum dissipation at Tamb =70 °C	0.6 W
Thermal resistance (Rth)	150 K/W
Temperature coefficient	£ ±50 ´ 10 -6 /K
Maximum permissible voltage (DC or RMS)	350 V
Basic specifications	IEC 115-1 and 115-2
Climatic category (IEC 68)	55/155/56

Stability after:

Load:

ΔR/R max.: ±0.5% +0.05 Ω
ΔR/R max.: ±0.5% +0.05 Ω

Climatic tests:

Δ R/R max.: ±0.5% +0.05 Ω
Δ R/R max.: ±0.5% +0.05 Ω

Soldering:

Δ R/R max.: ±0.1% +0.05 Ω
Δ R/R max.: ±0.1% +0.05 Ω

Short time overload Δ R/R max.: ±0.25% +0.05 Ω

D.2.5 Protection unit components:

Voltage divider components:

Resistor, an IRC thick film metal glaze resistor 3 W 5% 211-GS3-100M (for element R1 of Figure 4.11)

Power rating	3W @ 25°C
	2W @ 70°C
Resistance range	1 ohm to 3M ohm
Tolerance	±1%, 2%, and 5%
Leads	Tin-lead electroplated copper
TCR	±50(T2) ppm/°C - (available on values greater than 10 ohms)
	±100(T0) ppm/°C
	±200 ppm/°C
Voltage rating	1000V max.
Dielectric strength	1000V min.
Identification	Printed style

	Test	Maximum ΔR Limits
Load life	%ΔR	2.0
TCR ppm	%ΔR	100/50
STOL	%ΔR	0.20
Moisture	%ΔR	0.40
Temp. cycle	%ΔR	0.20
Solder effect	%ΔR	0.20
Term. strength	%ΔR	0.10
Shock	%ΔR	0.10
Vibration	%ΔR	0.10

Resistor, a Phillips metal film resistor 0.6 W 1% 353-MRS25F 4M75 (for element R2 of Figure 4.11)

Specifications

DESCRIPTION	VALUE
Resistance range	1 Ω to 10 MΩ
Resistance tolerance and series	±1%; E24/E96 series
Maximum dissipation at Tamb =70 °C	0.6 W
Thermal resistance (Rth)	150 K/W
Temperature coefficient	£ ±50 ´ 10 -6 /K
Maximum permissible voltage (DC or RMS)	350 V
Basic specifications	IEC 115-1 and 115-2
Climatic category (IEC 68)	55/155/56

Stability after

Load:

ΔR/R max.: ±0.5% +0.05 Ω

ΔR/R max.: ±0.5% +0.05 Ω

Climatic tests

Δ R/R max.: ±0.5% +0.05 Ω

Δ R/R max.: ±0.5% +0.05 Ω

Soldering

Δ R/R max.: ±0.1% +0.05 Ω

Δ R/R max.: ±0.1% +0.05 Ω

Short time overload Δ R/R max.: ±0.25% +0.05 Ω

Low voltage protection unit components:

Zener diodes, two Motorola zener 10V 1W 5% DO41 3001N47540A (for elements D1 and D2 of Figure 4.11)

Specification

Surge Rating of 98 Watts @ 1 ms

Maximum Limits Guaranteed On Up To Six Electrical Parameters

Weight	0.4 gram (approx)

Rating:

DC Power Dissipation @ T A = 50°C	1W
Derate above 50°C	6.67 mW/°C
Operating and Storage Junction Temperature Range	– 65 to +200 °C

Terminals, connectors, IC sockets, wires and cables are the other required miscellaneous for this system.

D.3 Software

The following is the list of software programs used for computer interfacing:

i. LabVIEW version 5.0 (National Instruments);
ii. InstCal version 3.4 (ComputerBoards, Inc.); and,
iii. Universal Library and its extension to LabVIEW version 4.2 (ComputerBoards, Inc.).

Appendix E. Cambridge preliminary experiment results

Table E.1 The data sets of Figure 6.1 to 6.3 for Cambridge preliminary experiment electric potential measurements (in TECPLOT format). Units are mV/A

TITLE="Potential measurements in cambridge sand pit, current electrodes at 80m west of injection well and SW monitoring well VARIABLES="X (m)","Y (m)","Z (m)","Background, Jan 19","After Inj., Jan 20","One week after, Jan 26 " ZONE J=12 I=9 K=1					
31.50	0.00	0.00	52.7626	324.5182	230.4079
31.50	3.50	0.00	15.8219	111.0787	78.8659
31.50	7.00	0.00	18.3712	73.4770	52.1687
31.50	10.50	0.00	43.5507	225.2524	159.9292
31.50	14.00	0.00	62.0735	384.8533	273.2458
31.50	17.50	0.00	65.3791	160.5788	114.0109
31.50	21.00	0.00	27.4857	89.9785	63.8847
31.50	24.50	0.00	77.1819	216.2876	153.5642
31.50	28.00	0.00	137.1995	370.5475	263.0887
28.00	0.00	0.00	31.2026	241.4066	171.3987
28.00	3.50	0.00	12.8866	13.1467	9.3342
28.00	7.00	0.00	51.0640	256.3742	182.0257
28.00	10.50	0.00	83.3192	472.4002	335.4041
28.00	14.00	0.00	102.4120	620.3897	440.4767
28.00	17.50	0.00	99.2469	659.3266	468.1219
28.00	21.00	0.00	80.3171	606.4330	430.5674
28.00	24.50	0.00	43.9521	426.0767	302.5145
28.00	28.00	0.00	1.3939	174.3148	123.7635
24.50	0.00	0.00	12.3040	47.1285	33.4612
24.50	3.50	0.00	38.9699	168.7052	119.7807
24.50	7.00	0.00	86.0612	436.4119	309.8524
24.50	10.50	0.00	127.9108	723.9374	513.9956
24.50	14.00	0.00	143.8166	878.0906	623.4443
24.50	17.50	0.00	145.0303	940.7945	667.9641
24.50	21.00	0.00	119.5053	837.0114	594.2781
24.50	24.50	0.00	75.0396	620.1289	440.2915
24.50	28.00	0.00	21.5369	342.9148	243.4695
21.00	0.00	0.00	0.7468	46.8600	33.2706
21.00	3.50	0.00	61.1564	286.0818	203.1181
21.00	7.00	0.00	115.9281	615.1817	436.7790
21.00	10.50	0.00	167.1754	982.1236	697.3078
21.00	14.00	0.00	201.1150	1260.7690	895.1460

Table E.1 Continued

21.00	17.50	0.00	199.2184	1360.5290	965.9756
21.00	21.00	0.00	233.8901	1190.4380	845.2110
21.00	24.50	0.00	106.9987	851.4750	604.5473
21.00	28.00	0.00	39.3644	492.2888	349.5250
17.50	0.00	0.00	7.0660	8.5456	6.0674
17.50	3.50	0.00	77.1270	399.9989	283.9992
17.50	7.00	0.00	149.4911	860.9683	611.2875
17.50	10.50	0.00	214.8266	1322.9020	939.2604
17.50	14.00	0.00	261.4034	1798.8350	1277.1729
17.50	17.50	0.00	268.1952	1922.8900	1365.2519
17.50	21.00	0.00	211.6612	1629.6150	1157.0267
17.50	24.50	0.00	183.0161	1967.1890	1396.7042
17.50	28.00	0.00	151.5616	479.4949	340.4414
15.75	0.00	0.00	6.3423	2.3986	1.7030
15.75	3.50	0.00	83.5513	458.1281	325.2710
15.75	7.00	0.00	163.2997	958.8794	680.8044
15.75	10.50	0.00	240.1836	1505.5850	1068.9654
15.75	14.00	0.00	296.9621	2132.1510	1513.8272
15.75	17.50	0.00	332.5198	2607.5890	1851.3882
15.75	21.00	0.00	239.5171	698.7543	496.1156
15.75	24.50	0.00	139.6598	1221.4910	867.2586
15.75	28.00	0.00	52.2718	690.4140	490.1939
14.00	0.00	0.00	0.0000	0.0000	0.0000
14.00	3.50	0.00	82.4150	486.4323	345.3669
14.00	7.00	0.00	170.2030	1033.6820	733.9142
14.00	10.50	0.00	254.8952	1692.7060	1201.8213
14.00	14.00	0.00	327.8135	2526.2220	1793.6176
14.00	17.50	0.00	462.6045	3791.4010	2691.8947
14.00	21.00	0.00	268.4780	2280.4370	1619.1103
14.00	24.50	0.00	142.9445	1350.2350	958.6669
14.00	28.00	0.00	43.9150	707.4660	502.3009
12.25	0.00	0.00	10.7965	45.7998	32.5179
12.25	3.50	0.00	76.9400	500.4843	355.3439
12.25	7.00	0.00	170.4923	1126.8800	800.0848
12.25	10.50	0.00	252.1034	1787.0110	1268.7778
12.25	14.00	0.00	334.3074	2669.5840	1895.4046
12.25	17.50	0.00	539.9446	4593.3470	3261.2764
12.25	21.00	0.00	281.4452	2543.5930	1805.9510
12.25	24.50	0.00	140.0665	1449.2910	1028.9966
12.25	28.00	0.00	30.8435	738.6929	524.4720
10.50	0.00	0.00	50.2034	411.8536	292.4161
10.50	3.50	0.00	62.3755	437.5308	310.6469
10.50	7.00	0.00	156.4228	1085.7290	770.8676

Table E.1 Continued

10.50	10.50	0.00	165.5135	1819.2030	1291.6341
10.50	14.00	0.00	148.2351	2636.4560	1871.8838
10.50	17.50	0.00	352.8746	3355.5700	2382.4547
10.50	21.00	0.00	264.6255	2640.5670	1874.8026
10.50	24.50	0.00	135.8724	1601.6460	1137.1687
10.50	28.00	0.00	13.6071	744.6762	528.7201
7.00	0.00	0.00	18.8389	243.7451	173.0590
7.00	3.50	0.00	10.3777	310.4619	220.4279
7.00	7.00	0.00	93.9654	908.0844	644.7399
7.00	10.50	0.00	154.6454	1504.7280	1068.3569
7.00	14.00	0.00	131.8186	1157.2210	821.6269
7.00	17.50	0.00	180.4877	2273.1040	1613.9038
7.00	21.00	0.00	130.4466	1960.2810	1391.7995
7.00	24.50	0.00	38.4991	1263.4240	897.0310
7.00	28.00	0.00	61.3829	590.7804	419.4541
3.50	0.00	0.00	22.6799	49.1216	34.8763
3.50	3.50	0.00	64.0415	86.1980	61.2006
3.50	7.00	0.00	0.0858	627.8334	445.7617
3.50	10.50	0.00	35.1762	1036.7740	736.1095
3.50	14.00	0.00	51.7018	618.1574	438.8918
3.50	17.50	0.00	19.2113	1446.7310	1027.1790
3.50	21.00	0.00	43.2789	1219.5170	865.8571
3.50	24.50	0.00	117.4884	689.6771	489.6707
3.50	28.00	0.00	207.8898	64.3897	45.7167
0.00	0.00	0.00	223.2250	713.0987	506.3001
0.00	3.50	0.00	168.2795	302.5550	214.8141
0.00	7.00	0.00	135.0784	126.2811	89.6596
0.00	10.50	0.00	121.9153	460.1563	326.7110
0.00	14.00	0.00	35.4898	1323.9050	939.9726
0.00	17.50	0.00	151.3728	496.1866	352.2925
0.00	21.00	0.00	257.6692	249.5711	177.1955
0.00	24.50	0.00	502.4487	167.0113	118.5780
0.00	28.00	0.00	375.6134	588.4851	417.8244
ZONE J=2 I=2 K=1					
14.92	19.64	-16.76	C2	C2	C2
14.92	19.64	-16.76	6426.2900	5527.7900	6080.5700
12.36	16.89	-16.76	5153.7500	4575.2800	5043.8100
12.01	19.71	-16.76	4614.0000	4160.6000	4567.6600
ZONE J=1 I=5 K=1					
13.88	18.34	-13	4726.5900	4021.0400	4423.1400
13.88	18.34	-13.5	5398.2900	4392.4200	4866.1300
13.88	18.34	-14	5740.8200	4866.5000	5323.1500
13.88	18.34	-14.5	6459.2200	5363.4700	5889.8200
13.88	18.34	-15.5	6710.1300	5925.7000	6508.2700

Appendix F: New ERT system evaluation and calibration results

Table F.1 Calculated precision data of the new ERT measuring system (graphically presented in Figure 6.18)

Level (V)	Gain	Absolute precision limits (mV)	Error % wrt min	Error % wrt max
0 to 0.0001	100	0.0015	1.5259	0.0015 0.0000
0.0001 to 0.1	10	0.0153	0.0153	0.00153 0.00000
1 to 5	2	0.0763	0.0076	0.00153 0.00000
5 to 10	1	0.1526	0.0031	0.00153 0.00000
10 to 20	0.5	0.3052	0.0031	0.00153 0.00000
20 t0 100	0.1	1.5259	0.0076	0.00153 0.00000
100 to 200	0.2	3.0518	0.0031	0.00153 0.00000
200 to 400	0.05 or 0.025	6.1035	0.0031	0.00153 0.00000

Table F.2 Laboratory evaluation of the new ERT measuring system results for different voltage ranges (graphically presented in Figure 6.19 and 6.20)

Sample No.	Time (msec)	Input voltage to the new ERT system (mV)						
		7.1	116.6	3070	7068	15005	30010	110041
1	0.05	7.157	116.568	3070.223	7068.684	15004.190	30008.698	110040.991
2	0.10	7.111	116.589	3070.329	7068.501	15004.794	30009.873	110045.759
3	0.15	7.042	116.596	3070.223	7068.319	15005.397	30012.224	110045.759
4	0.20	7.157	116.610	3070.170	7068.136	15006.001	30009.873	110036.224
5	0.25	7.141	116.568	3070.276	7068.319	15004.794	30008.698	110040.991
6	0.30	7.103	116.554	3070.276	7068.866	15004.190	30008.698	110036.224
7	0.35	7.103	116.589	3070.117	7068.684	15005.397	30009.873	110040.991
8	0.40	7.057	116.561	3070.065	7068.319	15006.001	30012.224	110045.759
9	0.45	7.027	116.575	3070.117	7068.136	15004.190	30011.049	110036.224
10	0.50	7.027	116.603	3070.170	7068.866	15005.397	30008.698	110036.224
11	0.55	7.134	116.610	3070.065	7068.866	15004.794	30009.873	110040.991
12	0.60	7.073	116.596	3070.117	7068.319	15005.397	30009.873	110045.759
13	0.65	7.118	116.575	3070.223	7068.684	15004.190	30007.523	110045.759
14	0.70	7.126	116.568	3070.170	7068.136	15005.397	30008.698	110036.224
15	0.75	7.157	116.561	3070.223	7068.501	15006.001	30009.873	110040.991
16	0.80	7.065	116.596	3070.329	7068.319	15005.397	30013.399	110040.991
17	0.85	7.027	116.575	3070.329	7068.501	15006.001	30009.873	110045.759
18	0.90	7.042	116.554	3070.117	7068.684	15004.190	30008.698	110036.224
19	0.95	7.157	116.568	3070.223	7068.684	15004.794	30007.523	110045.759
20	1.00	7.126	116.603	3070.117	7068.501	15006.001	30013.399	110040.991
21	1.05	7.042	116.610	3070.329	7068.684	15004.190	30012.224	110045.759
22	1.10	7.034	116.582	3070.223	7068.136	15006.001	30011.049	110040.991
23	1.15	7.103	116.554	3070.117	7068.319	15004.794	30008.698	110040.991
24	1.20	7.050	116.582	3070.065	7068.501	15005.397	30009.873	110040.991
25	1.25	7.088	116.568	3070.065	7068.136	15005.397	30012.224	110036.224
26	1.30	7.141	116.596	3070.170	7068.319	15004.190	30012.224	110036.224
27	1.35	7.164	116.589	3070.276	7068.319	15004.794	30009.873	110045.759
28	1.40	7.057	116.554	3070.276	7068.501	15006.001	30007.523	110040.991
29	1.45	7.034	116.568	3070.170	7068.684	15005.397	30008.698	110045.759
30	1.50	7.088	116.554	3070.223	7068.866	15004.190	30008.698	110036.224
31	1.55	7.027	116.596	3070.223	7068.501	15006.001	30011.049	110036.224
32	1.60	7.149	116.603	3070.329	7068.501	15004.794	30009.873	110036.224
33	1.65	7.126	116.610	3070.223	7068.319	15004.794	30012.224	110045.759
34	1.70	7.164	116.561	3070.065	7068.501	15006.001	30011.049	110040.991
35	1.75	7.095	116.575	3070.170	7068.684	15005.397	30008.698	110045.759
Mean		7.095	116.5807	3070.1944	7068.4856	15005.1385	30010.0750	110041.1276
Standard		**0.048**	**0.0189**	**0.0853**	**0.2274**	**0.6754**	**1.6495**	**3.9186**
Maximum		7.164	116.6101	3070.3287	7068.8665	15006.0008	30013.3994	110045.7587
Minimum		7.027	116.5540	3070.0647	7068.1360	15004.1901	30007.5229	110036.2240

Table F.3 Laboratory evaluation of the new ERT measuring system results for different voltage ranges (graphically presented in Figure 6.20)

Input voltage to the system (mV)	Standard deviations	% of standard deviations with respect to input voltage
7	0.0480	0.6768
116	0.0189	0.0162
3000	0.0853	0.0028
7000	0.2274	0.0032
15000	0.6754	0.0045
30000	1.6495	0.0055
110000	3.9186	0.0036

Appendix G: Input Data file listings to FRAC3DVS and SALTFLOW models to simulate Cambridge experiment:

G.1 FRAC3DVS inputs

Material properties in mprops file

The material properties have been given to FRAC3DVS by a file named as mprops. This file is the same through all the steps.

```
Sand
1.0                         ! kxx
1.0                         ! kyy
1.0                         ! kzz
0.0                         ! storage coefficient
0.35                        ! porosity
.false.                     ! true if tabular data
0.06  .5  1.9 .4736 0. 0.
10.0                        ! longitudinal dispersivity
0.1                         ! transverse dispersivity
0.1                         ! transverse vertical dispersivity
0.1                         ! tortuosity
2.65                        ! bulk density
0.00                        ! immobile zone porosity
0.00                        ! mass transfer coefficient
Unsat Sand
1.0                         ! kxx
1.0                         ! kyy
1.0                         ! kzz
0.0                         ! storage coefficient
0.35                        ! porosity
.false.                     ! true if tabular data
0.06  .5  1.9 .4736 0. 0.
10.0                        ! longitudinal dispersivity
0.1                         ! transverse dispersivity
0.1                         ! transverse vertical dispersivity
0.1                         ! tortuosity
2.65                        ! bulk density
0.00                        ! immobile zone porosity
0.00                        ! mass transfer coefficient
Clay
7.8e-6                      ! kxx
7.8e-6                      ! kyy
7.8e-6                      ! kzz
0.0                         ! storage coefficient
0.35                        ! porosity
.false.                     ! true if tabular data
0.2 .25  1.8 .4445 0. 0.    ! ,beta,
10.0                        ! longitudinal dispersivity
0.1                         ! transverse dispersivity
0.1                         ! transverse vertical dispersivity
0.1                         ! tortuosity
2.65                        ! bulk density
0.00                        ! immobile zone porosity
0.00                        ! mass transfer coefficient
```

Rest of the data input

The other specifications have transferred to FRAC3DVS though a file with "*.np" extension. This file was modified in each major step (like steady-state, pumping, and Transport).

salt.np file for steady-state

```
ERT Forward modeling trails  "Injection in unsatuatrion part" (Parsa)

generate variable blocks
 79
 79
 34

! xi(1)....xi(79)
1970.0 1972.0  1974.0 1976.0  1978.0 1980.0  1981.0 1982.0  1983.0
1984.0  1985.0 1986.0 1987.0 1988.0
1989.0 1990.0  1990.5 1991.0  1991.5 1992.0  1992.5 1993.0  1993.5
1994.0  1994.5 1995.0 1995.5 1996.0
1996.5 1997.0  1997.5 1998.0  1998.5 1998.75 1999.0 1999.25 1999.5
1999.75 1999.9 2000.0 2000.1 2000.25
2000.5 2000.75 2001.0 2001.25 2001.5 2002.0  2002.5 2003.0  2003.5
2004.0  2004.5 2005.0 2005.5 2006.0
2006.5 2007.0  2007.5 2008.0  2008.5 2009.0  2009.5 2010.0  2011.0
2012.0  2013.0 2014.0 2015.0 2016.0
2017.0 2018.0  2019.0 2020.0  2022.0 2024.0  2026.0 2028.0  2030.0

! yi(1)....yi(79)
1970.0 1972.0  1974.0 1976.0  1978.0 1980.0  1981.0 1982.0  1983.0
1984.0  1985.0 1986.0 1987.0 1988.0
1989.0 1990.0  1990.5 1991.0  1991.5 1992.0  1992.5 1993.0  1993.5
1994.0  1994.5 1995.0 1995.5 1996.0
1996.5 1997.0  1997.5 1998.0  1998.5 1998.75 1999.0 1999.25 1999.5
1999.75 1999.9 2000.0 2000.1 2000.25
2000.5 2000.75 2001.0 2001.25 2001.5 2002.0  2002.5 2003.0  2003.5
2004.0  2004.5 2005.0 2005.5 2006.0
2006.5 2007.0  2007.5 2008.0  2008.5 2009.0  2009.5 2010.0  2011.0
2012.0  2013.0 2014.0 2015.0 2016.0
2017.0 2018.0  2019.0 2020.0  2022.0 2024.0  2026.0 2028.0  2030.0

! zi(1)....zi(34)
970.0 973.0 976.0 978.0 979.0  980.0  981.0  982.0 982.5 983.0  983.5
984.0 984.5
985.0 985.5 986.0 986.5 986.75 987.0  987.25 987.5 988.0 988.5
989.0 990.0 991.0 992.0 994.0 996.0  998.0  998.5  999.0 999.5 1000.

done grid definition

steady state
finite difference mode

unsaturated
set kwrith
1
```

```
choose nodes all
initial head
984.0

clear chosen elements
choose elements block
0.   2030.
0.   2030.
980.    998.
zone chosen elements
2
clear chosen zones
choose zone number
2
read material properties
Unsat Sand

clear chosen elements
choose elements block
0.   2030.
0.   2030.
998.   1000.
zone chosen elements
3
clear chosen zones
choose zone number
3
read material properties
Clay

clear chosen nodes
choose nodes x plane
1970.0
1.e-5
specified head
1
0.0, 983.0              ! time on, head

clear chosen nodes
choose nodes x plane
2030.0
1.e-5

specified head
1
0.0, 985.00              ! time on, head

clear chosen nodes
choose nodes block
1980.   2010.
1980.   2010.
980.    990.
write chosen nodes
gbnew.nd

newton absolute convergence criteria
```

```
1.e-4
newton residual convergence criteria
1.e20
```

salt.np file for Pumping step

```
ERT Forward modeling trails  "Injection in unsatuatrion part" (Parsa)

generate variable blocks
 79
 79
 34

! xi(1)....xi(76)
1970.0 1972.0  1974.0 1976.0  1978.0 1980.0  1981.0 1982.0  1983.0
1984.0  1985.0 1986.0 1987.0 1988.0
1989.0 1990.0  1990.5 1991.0  1991.5 1992.0  1992.5 1993.0  1993.5
1994.0  1994.5 1995.0 1995.5 1996.0
1996.5 1997.0  1997.5 1998.0  1998.5 1998.75 1999.0 1999.25 1999.5
1999.75 1999.9 2000.0 2000.1 2000.25
2000.5 2000.75 2001.0 2001.25 2001.5 2002.0  2002.5 2003.0  2003.5
2004.0  2004.5 2005.0 2005.5 2006.0
2006.5 2007.0  2007.5 2008.0  2008.5 2009.0  2009.5 2010.0  2011.0
2012.0  2013.0 2014.0 2015.0 2016.0
2017.0 2018.0  2019.0 2020.0  2022.0 2024.0  2026.0 2028.0  2030.0

! yi(1)....yi(76)
1970.0 1972.0  1974.0 1976.0  1978.0 1980.0  1981.0 1982.0  1983.0
1984.0  1985.0 1986.0 1987.0 1988.0
1989.0 1990.0  1990.5 1991.0  1991.5 1992.0  1992.5 1993.0  1993.5
1994.0  1994.5 1995.0 1995.5 1996.0
1996.5 1997.0  1997.5 1998.0  1998.5 1998.75 1999.0 1999.25 1999.5
1999.75 1999.9 2000.0 2000.1 2000.25
2000.5 2000.75 2001.0 2001.25 2001.5 2002.0  2002.5 2003.0  2003.5
2004.0  2004.5 2005.0 2005.5 2006.0
2006.5 2007.0  2007.5 2008.0  2008.5 2009.0  2009.5 2010.0  2011.0
2012.0  2013.0 2014.0 2015.0 2016.0
2017.0 2018.0  2019.0 2020.0  2022.0 2024.0  2026.0 2028.0  2030.0

! zi(1)....zi(31)
970.0 973.0 976.0 978.0 979.0  980.0  981.0  982.0 982.5 983.0  983.5
984.0 984.5
985.0 985.5 986.0 986.5 986.75 987.0  987.25 987.5 988.0 988.5
989.0 990.0 991.0 992.0 994.0 996.0  998.0  998.5  999.0 999.5 1000.

done grid definition

! used for injection and transport of saline

transient flow
adaptive timesteps
output times
 2

! First pumping step with tab water
 0.02
```

```
! Second pumping step with saline mixture
 0.036
initial timestep
1.e-5


finite difference mode

unsaturated
set kwrith
1

set kwrithc
1

restart file for heads


clear chosen elements
choose elements block
1970.  2030.
1970.  2030.
980.   998.
zone chosen elements
2
clear chosen zones
choose zone number
2
read material properties
Unsat Sand

clear chosen elements
choose elements block
1970.  2030.
1970.  2030.
998.  1000.
zone chosen elements
3
clear chosen zones
choose zone number
3
read material properties
Clay


clear chosen nodes
choose nodes x plane
1970.0
1.e-5
specified head
1
0.0, 983.0              ! time on, head

clear chosen nodes
choose nodes x plane
2030.0
1.e-5
```

```
specified head
1
0.0, 985.00                ! time on, head

skip on
! The unit of recharge input is based on the other inputs unit
clear chosen faces
choose faces top
uniform rainfall
0.002        ! Recharge from the surface(m/days)

skip off

clear chosen nodes
choose nodes block
1980.   2010.
1980.   2010.
980.    990.
write chosen nodes
gbnew.nd

newton absolute convergence criteria
1.e-4
newton residual convergence criteria
1.e20


! not needed if you would like to use a Steady-state flow with no well
clear chosen nodes
make well node
2000.   2000.   987.
500.
.08
.08

do transport

solute parameters
salt
4.32e-5
0.0
0
0.0
0.0
0.0

clear chosen nodes
choose nodes block
2000.0   2000.0
2000.0   2000.0
987.0    987.00

specified concentration
2
0.0    0.02      0.1
0.02   1.e20     1.0
```

salt.np file for Transport step

```
ERT Forward modeling trails  "Injection in unsatuatrion part" (Parsa)

generate variable blocks
 79
 79
 34

! xi(1)....xi(76)
1970.0 1972.0  1974.0 1976.0  1978.0 1980.0  1981.0 1982.0  1983.0
1984.0  1985.0 1986.0 1987.0 1988.0
1989.0 1990.0  1990.5 1991.0  1991.5 1992.0  1992.5 1993.0  1993.5
1994.0  1994.5 1995.0 1995.5 1996.0
1996.5 1997.0  1997.5 1998.0  1998.5 1998.75 1999.0 1999.25 1999.5
1999.75 1999.9 2000.0 2000.1 2000.25
2000.5 2000.75 2001.0 2001.25 2001.5 2002.0  2002.5 2003.0  2003.5
2004.0  2004.5 2005.0 2005.5 2006.0
2006.5 2007.0  2007.5 2008.0  2008.5 2009.0  2009.5 2010.0  2011.0
2012.0  2013.0 2014.0 2015.0 2016.0
2017.0 2018.0  2019.0 2020.0  2022.0 2024.0  2026.0 2028.0  2030.0

! yi(1)....yi(76)
1970.0 1972.0  1974.0 1976.0  1978.0 1980.0  1981.0 1982.0  1983.0
1984.0  1985.0 1986.0 1987.0 1988.0
1989.0 1990.0  1990.5 1991.0  1991.5 1992.0  1992.5 1993.0  1993.5
1994.0  1994.5 1995.0 1995.5 1996.0
1996.5 1997.0  1997.5 1998.0  1998.5 1998.75 1999.0 1999.25 1999.5
1999.75 1999.9 2000.0 2000.1 2000.25
2000.5 2000.75 2001.0 2001.25 2001.5 2002.0  2002.5 2003.0  2003.5
2004.0  2004.5 2005.0 2005.5 2006.0
2006.5 2007.0  2007.5 2008.0  2008.5 2009.0  2009.5 2010.0  2011.0
2012.0  2013.0 2014.0 2015.0 2016.0
2017.0 2018.0  2019.0 2020.0  2022.0 2024.0  2026.0 2028.0  2030.0

! zi(1)....zi(31)
970.0 973.0 976.0 978.0 979.0  980.0  981.0  982.0 982.5 983.0  983.5
984.0 984.5
985.0 985.5 986.0 986.5 986.75 987.0  987.25 987.5 988.0 988.5
989.0 990.0 991.0 992.0 994.0 996.0  998.0  998.5  999.0 999.5 1000.

done grid definition

! used for transport of saline after injection
transient flow
adaptive timesteps
initial time
0.036
output times
15
0.1
0.2
0.4
0.6
```

```
0.8
1.0
2.0
3.0
4.0
5.0
6.0
7.0
8.0
9.0
10.0

finite difference mode

unsaturated
set kwrith
1

set kwrithc
1

restart file for heads

restart file for concentrations

clear chosen elements
choose elements block
1970.  2030.
1970.  2030.
980.   998.
zone chosen elements
2
clear chosen zones
choose zone number
2
read material properties
Unsat Sand

clear chosen elements
choose elements block
1970.  2030.
1970.  2030.
998.  1000.
zone chosen elements
3
clear chosen zones
choose zone number
3
read material properties
Clay

clear chosen nodes
choose nodes x plane
1970.0
1.e-5
specified head
1
```

```
0.0, 983.0              ! time on, head

clear chosen nodes
choose nodes x plane
2030.0
1.e-5

specified head
1
0.0, 985.00               ! time on, head

clear chosen nodes
choose nodes block
1980.  2010.
1980.  2010.
980.   990.
write chosen nodes
gbnew.nd

newton absolute convergence criteria
1.e-4
newton residual convergence criteria
1.e20

! not needed if you would like to use a Steady-state flow with no well
clear chosen nodes
make well node
2000.  2000.  987.
!500.
0.0
.08
.08

do transport

solute parameters
salt
4.32e-5
0.0
0
0.0
0.0
0.0

clear chosen nodes
choose nodes block
2000.0  2000.0
2000.0  2000.0
987.0   987.00

specified concentration
2
0.0   0.02     0.0
0.02  1.e20    0.0
```

G.2 SALTFLOW inputs

The SALTFLOW reads all of the required input data from a single file (salt.data), only the salt concentrations of slurry injection were read in from another sets of files. In case of background potential simulations, there was no concentration file and input was inputted from salt.data file only.

salt.data file for background

```
SALTFLOW MODEL - Potential filed at Cambridge Shallow Slurry Fracture
Injection Simulation
95 x 77 x 27 Potential distribution nodes
March 11, 1999 - Background without any anomaly (prior to inection)
 0  1  0  1  1  0  0                ;KPRT,KCNTRL,KWT,KINT,KINTV,KGO,kchk
   15   15   10                     ;ngx,ngy,ngz
1000. 1800. 1910. 1930. 1960. 1980. 1998. 1999.5 2000.5 2002. 2020.
2040. 2200.0 3000. 4000.    ;xlim
1000. 1800. 1920. 1960. 1980. 1998. 1999.5 2000.5 2002. 2020. 2040.
2080. 2200.0 3000. 4000.    ;ylim
900. 970. 982. 983. 985. 986. 987. 990.998. 1000.      ;zlim
1  2  5  10   5  10  18  3  4   3  18  10  2  2  1    ;nlx
1  2  1   1   10  18   3   4  3 18  10  1  1  2  1    ;nly
1  2  4   1   4   1   2  3  4   4                     ;nlz
10   0.  0.0000                    ;nwtl,datum,gamma
0  0  0  0   -1                    ;ix,iy,iz1,iz2 breakthrough
1  1  1  1  0  0                   ;B.C.'S (FLOW)(Type) -
x0,x1,y0,y1,z0,z1
1   77    1    26     0.0                -1
1   77    1    26     0.0                -1
1   95    1    26     0.0                -1
1   95    1    26     0.0                -1
     1   71440  8.00e-03  8.00e-03  8.00e-03  +1 ; 1-10  NEL,KX,KY,KZ
(m/s)  Bottom Sand layer
 71441  157168  3.00e-03  3.00e-03  3.00e-03  +1 ;11-22  NEL,KX,KY,KZ
(m/s)  Unsat Sand layer (Injection layer)
157169  185744 24.00e-03 24.00e-03 24.00e-03  -1 ;23-26  NEL,KX,KY,KZ
(m/s)  Clay layer
0 0  0 0  0 0   0.e+0  0.e+0  0.e+00  -1  ;INDEXED K
.00000     .35                          ;SS,POROSITY
0    0.0                                ;INIT,H0 (READ FLOW I.C.)
0    0    0    0    0    0              ;B.C.'S (TRANSPORT)
0      0.      0.       0.              ;IVEL,VX,VY,VZ (m/s)
0.1  0.010 0.0500   5.00e-11  0.0e-0  1.0 ;AL,ATH,ATV,DD,decay,ret
1  95   1 77  1  26    0.0  0.0   -1     ;initial condition
.00001    .001       .00001   11   11    ;CCP,CCc,CCW,MAXIT1,MAXIT2
1.0    1.00                               ;OVER-RELAX HEADS,TEMP
57    0   0    0    0                    ;KNOX(1-5)TRANSV. SECTION
39    0   0    0    0                    ;KNOY(1-5)LONG.  SECTION
    0.     0.    0.        0.       0.    ;five 3d print times (days)
    0.     1.0      0.5     2   -1        ;t0,t1,dt,kplot(days)
 0.         1.      1.0                   ;hinc,rinc,sfact
 54   39   10  11   +0.5    0.    +1      ;source/sink (m^3/s/node)
 13   39   26  27   -0.5    0.    -1      ;source/sink (m^3/s/node)
```

salt.data file for after slurry injection

The only difference between this input file and the background one is a flag parameter (kchk =2) to read the concentration file the rest or data are the same.

Appendix H: Glossary of term used

Note:

More information about each of the following words or phrases can be found in Axelsson 1994[1], Barrett et al. 1994[2], Duff et al 1986[3], Greenberg 1997[4], Greenhouse et al. 1997[5], National Instruments 1996[6] and Saad 1996[7].

A

A	Ampers
AC	Alternative current
ACH<0..7>	Analog (input) channel 0 through 7 signals[8]
ACK*	Acknowledge Input signal[9]
A/D	Analog-to-Digital
Adaptive methods	Iterative methods that collect information about the coefficient matrix during the iteration process, and use this to speed up convergence.
ADC	A/D converter
Adjacency matrix	The n by n binary matrix, say A, to represent node adjacency in a simple graph: A(i,j)=1 if node i is adjacent to node j. In the undirected case, A is symmetric. In the directed case, the adjacency means there is an arc from i to j. In the case of a multigraph, A(i, j) = number of edges whose endpoints are nodes i and j.[4]
Adjacent basis	Two bases are adjacent if they differ by exactly one column (so one is reachable from the other by a pivot).[4]
Adjoint	The classical adjoint of a matrix A is its transpose matrix of cofactors: $Adj(A)_ij = (-1)^{(i+j)} \det(A^{*(j,i)})$, where $A^{*(j,i)}$ is the transpose of A with j-th column of A and i-th row of A deleted. The Hermitian adjoint, A*, is the transpose of the conjugate. The latter is generally what is meant by the adjoint in most contexts, and we simply have A*=A' when A is real-valued.[4]
Admissible	Generically, this means something satisfies conditions. One example is the admissibility of a direction of change of some parameter, such as a right-hand side of a linear program (LP) from b to b+th, where t is some scalar and h is the direction of change. For a positive value of t, this might cause the LP to become infeasible, no matter how small t is chosen. In that case it is common to call the direction vector inadmissible. For a perturbation to be admissible in this context, it is required that the mathematical program has a solution in some neighborhood of that direction. For the example, h is admissible if the (primal) LP is feasible for all t in [0, t*) for some t* > 0.[4]
Affine function	Let $f:X \to R^n$. Then, f is affine if X is a convex set and f(ax + (1-a)y) = af(x) + (1-a)f(y) for all x, y in X and a in [0, 1]. Equivalently, f is affine if it is both convex and concave. Moreover, if $X=R^n$, f is the translation of a linear function: ax+b.[4]

AGND	Analog Ground signal
AIGATE	Analog input gate signal
AIGND	Analog input Ground signal
AISENSE	Analog input sense signal
AISENSE/AIGND	Analog input sense/analog input ground signal
AISENSE2	Analog input sense 2 signal
Algorithm	An iterative method that generates a sequence of the form $x^{(k+1)} = S_k(A_k(x^k))$, where x^0 is given (called the initial point); A_k is an algorithm map that yields a set of policies, given the current point, x^k; and S_k is a selection function (in case A_k has more than one policy in it). Note that the algorithm map and selection function can depend on the iteration number (k). A concrete example is of the form $x^{(k+1)} = x^k + s_k d^k$, where s_k is a scalar parameter, called the step size and d^k is a vector, called the direction of change. The step size may require a selection from a line search solution (if there are many optimal solutions); one is to select the least value (perhaps above some threshold).
ANSI	American National Standards Institute
AOGND	Analog output ground signal
Apparent resistivity/conductivity	The resistivity of homogeneous isotropic ground that would give the same voltage/current or secondary/primary field ratios as observed in the field with resistivity or EM methods. The apparent conductivity is the reciprocal of the apparent resistivity.
Aquifer	Rocks or unconsolidated sediments that are capable of yielding a significant amount of water to a well or a spring.
Aquitard	Geological formations of low hydraulic conductivity, typically saturated, but yielding a limited amount of water to wells. Also referred to as a confining unit.
Artificial variable	A variable, say v, added to an equation, $h(x) = 0$. The resulting system, $h(x) + v = 0$, is feasible upon letting $v = -h(x)$ for a chosen x. Then, the objective function is modified to penalize nonzero values of v. Often, $v \geq 0$ is required, multiplying h by -1, if necessary, to get started. This grew from linear programming, where a Phase I objective is used to find a solution with v=0 (or ascertain that the original system has no feasible solution) by minimizing $\text{Sum}_i\{v_i\}$ (ignoring the original objective, cx).
ASCII	American Standard code for Information Interchange
ASIC	Application-specific integrated circuit
ATE	Automatic test equipment

Automatic differentiation

A process for evaluating derivatives of a function that depends only on an algorithmic specification of the function, such as a computer program. (The term "automatic" stems from having the derivatives produced when executing the program to evaluate the function.)
There are two modes:

1. *forward* - direct parse and evaluation, introducing intermediate variables in the usual way, as rules of differentiation are applied.
2. *reverse* - evaluates entries in the code list first, and lastly differentiates the intermediate and independent variables in reverse order.

While the forward mode is more straightforward and easier to implement, the reverse mode is computationally superior for scalar functions, as its complexity is independent of the number of intermediate variables. More generally, if $F:R^n \rightarrow R^m$, the forward mode has complexity of O(n), and the backward mode has complexity of O(m). [1]

B

Backward error

The size of perturbations δA of the coefficient matrix and δb of the right hand side of a linear system $Ax = b$, such that the computed iterate $x^{(i)}$ is the solution of $(A + \delta b)\, x^{(i)} = b + \delta b$.

Backward substitution

The recursion to solve a nonsingular upper triangular system, Ux=b. It starts with x(n) = b(n)/U(n,n), then
x(j) = [b(j) - sum_i{U(i, j)x(i): i > j}] / U(j, j) for j=n-1,...,1. [1]

Backward triangularization

An algorithm to rearrange a matrix by recursively assigning a singleton column to the rear (with its only row, as its pivot). The recursion applies to the submatrix defined by omitting the assigned column and row (and reducing other column counts accordingly). This results in a lower triangular rearrangement if, and only if, such a rearrangement exists. [1]

Band matrix

A matrix A for which there are nonnegative constants p, q, such that $a_{i,j} = 0$ if $j < i-p$ or $j > i+p$. The two constants p, q are called the left and right halfbandwidth respectively.

Basic

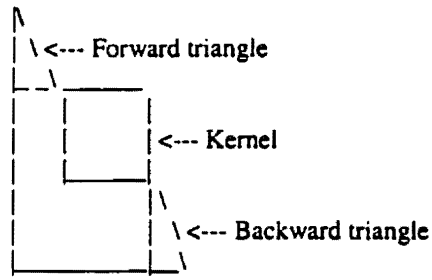
Associated with a submatrix of A, say B, whose columns comprise a basis for R^m (i.e., B consists of m linearly independent columns of A, which is a basis for R^m). [1]

Related terms and concepts

Adjacent basis	One that differs in exactly one column from a given basis.
Basic column	A column of the basis matrix.
Basic variable	The variable, say x_j, associated with the j-th column of the basis matrix.
Basic level	The value of a basic variable.
Basic solution	The solution (x) obtained by setting nonbasic values to some bound value (like 0), resulting in a unique solution for the basic variables. That is, Ax=b is equivalent to Bu + Nv = b, where A=[B N] and x=[u v]. Upon fixing the value of v, the nonsingularity of B gives the basic solution with $u = [B^{-1}][b - Nv]$. (In a standard LP, v=0, so $u=[B^{-1}]b$.)
Basic feasible solution	A basic solution that is feasible -- i.e., the basic values satisfy their bounds. (In a standard LP, this means $[B^{-1}]b \geq 0$.)

Basis kernel

After performing forward triangularization, if the basis does not triangularize completely, backward triangularization is applied. The result is a (rearranged) blocking of the basis into three segments:



Each row and column in the kernel has at least 2 nonzeroes. [4]

Bedrock

A general term referring to rock that underlies unconsolidated materials. [6]

Bi-conjugate gradient (BiCG)

The Bi-conjugate gradient method generates two CG-like sequences of vectors, one based on a system with the original coefficient matrix $\mathbf{A}$, and one on $\mathbf{A}^T$. Instead of orthogonalizing each sequence, they are made mutually orthogonal, or "bi-orthogonal". This method, like CG, uses limited storage. It is useful when the matrix is nonsymmetric and nonsingular; however, convergence may be irregular, and there is a possibility that the method will break down. BiCG requires a multiplication with the coefficient matrix and with its transpose at each iteration.

Bi-conjugate gradient stabilized (Bi-CGSTAB)

The Bi-conjugate gradient stabilized method is a variant of BiCG, like CGS, but using different updates for the $\mathbf{A}^T$-sequence in order to obtain smoother convergence than CGS.

BIOS

Basic input/output system or built-in operation system

Black box

A piece of software that can be used without knowledge of its inner workings; the user supplies the input, and the output is assumed to be correct.

Bland's rule

This is for pivot selection in the simplex method to avoid cycling:

- If more than one (nonbasic) column has the same reduced cost, choose the one with lowest index.
- If more than one (basic) column has the same determining value to leave the basis, select the one with the lowest index. [5]

BLAS	Basic Linear Algebra Subprograms; a set of commonly occurring vector and matrix operations for dense linear algebra. Optimized (usually assembly coded) implementations of the BLAS exist for various computers; these will give a higher performance than implementation in high level programming languages.
Block factorization	See: Block matrix operations.
Block matrix operations	Matrix operations expressed in terms of submatrices.
BNF	Backus-naur form. A common representation for language grammers in computer science
Breakdown	The occurrence of a zero divisor in an iterative method.

C

C	Celsius
CalDAC	Calibration DAC
Cholesky decomposition	Expressing a symmetric matrix A as a product of a lower triangular matrix L and its transpose L^T, that is, $A = LL^T$.
Cholesky factorization	Given an mxm symmetric matrix A, a lower triangular matrix, L, is obtained, called the Cholesky factor, such that $A = LL'$. This is particularly useful for solving linear systems, $Ax=b$, by using forward substitution, $Ly=b$, then backward substitution, $L'x=y$. The original algorithm assumes A is positive definite, but it can apply more generally. [4]
CIN	Code interface node
CLKB1,CLKB2	Counter B1, B2 Clock signals
cm	Centimeters
CMOS	Complementary metallic oxide semiconductor
CMRR	Common-mode rejection ratio
CNTINT	Counter Interrupt signal
Compatibility theory	The idea that a solution's character does not change for a particular perturbation. In linear programming the character could be an optimal basis, and the theory is concerned with whether a particular basis remains optimal when the data is changed in a prescribed direction. A Fundamental Theorem of Basis Compatibility is the following: h is an admissible direction for perturbing (b, c) if, and only if, it is compatible with some equilibrium basis. The range of compatiblity of a basis, B, for a direction, h, is the greatest step for which B remains optimal: sup{t: B is optimal for the LP defined by r + th}. The basis spectrum is the greatest range: sup{range(B; h): B is optimal for the LP defined by r}.[4]

Condition number — See: Spectral condition number.

Conductance — The product of conductivity and thickness [Siemens].

Conduction current — Electrical current resulting from the movement of free charges (constant with displacement current).

Conductivity (electrical) — The ability of a material to conduct electrical current. In isotropic material, it is the reciprocal of resistivity. Units are Siemens/m.

Conjugate gradient (CG) — The conjugate gradient method derives its name from the fact that it generates a sequence of conjugate (or orthogonal) vectors. These vectors are the residuals of the iterates. They are also the gradients of a quadratic functional, the minimization of which is equivalent to solving the linear system. CG is an extremely effective method when the coefficient matrix is symmetric positive definite, since storage for only a limited number of vectors is required.

Conjugate gradient method — An ascent method for unconstrained optimization such that successive directions are conjugate with respect to the hessian for a quadratic objective function.

Conjugate Gradient squared (CGS) — The conjugate gradient squared method is a variant of BiCG that applies the updating operations for the $\mathbf{A}$-sequence and the $\mathbf{A}^T$-sequences both to the same vectors. Ideally, this would double the convergence rate, but in practice convergence may be much more irregular than for BiCG, which may sometimes lead to unreliable results. A practical advantage is that the method does not need the multiplication with the transpose of the coefficient matrix.

Conjugate vectors — With respect to a symmetric matrix, A, u and v are conjugate if u'Av = 0. (In particular, if A=I, u and v are conjugate if they are orthogonal.)

Constraint qualification — Conditions on the constraint functions (g and h) that are sufficient to make the Lagrange Multiplier Rule valid. Here is an example to illustrate what can go wrong: Max x: $x^2 \leq 0$. Since x=0 is the only feasible solution, it is optimal. The Lagrange Multiplier Rule requires that there exist u for which f' - ug' = 0, but f' = 1 and g' = 0, so no such u can exist. Slater used this example in illustrating his interiority condition. The classical qualification, given by Lagrange's multiplier theorem without inequality constraints, is that grad_h(x) have full row rank, which stems from the Implicit Function Theorem. Another constraint qualification is that all constraint functions be affine (even with redundant constraints). Each constraint qualification gives a sufficient condition for the LMR to be valid. A constraint qualification is necessary if it must hold in order to guarantee that the LMR is valid for all f in C^1 having optimal value at x.

Convergence — The fact whether or not, or the rate at which, an iterative method approaches the solution of a linear system. Convergence can be

- Linear — Some measure of the distance to the solution decreases by a constant factor in each iteration.
- Superlinear — The measure of the error decreases by a growing factor.

Smooth	The measure of the error decreases in all or most iterations, though not necessarily by the same factor.
Irregular	The measure of the error decreases in some iterations and increases in others. This observation unfortunately does not imply anything about the ultimate convergence of the method.
Stalled	The measure of the error stays more or less constant during a number of iterations. As above, this does not imply anything about the ultimate convergence of the method.

Convergence (of an algorithm)

The algorithm is represented as the point-to-set map, x' in A(x), where there is some selection function to choose x' when A(x) has more than one member. Convergence means that the sequence, {xk}, has a limit point, say x, such that x satisfies certain conditions. Ideally, the conditions are that x is an optimal solution, at least locally, but this is often not the definition used in a convergence theorem. (For example, in unconstrained optimization, most algorithms converge to a stationary point, which need not be even a local optimum.)

Let $\{s^k\} \to 0$, where s^k is a scalar series pertaining to the series $\{x^k\}$. Typically, $s^k = \|x^k - x\|$, which is sometimes called policy convergence (to a solution, x). We could also have $s^k = f(x^k) - f^*$, where f is the objective function, in which case the concern is with value convergence to an optimal value, f^*.

Related terms and concepts

Dual convergence	Dual values, notably Lagrange multipliers, converge to a dual solution.
Geometric convergence	Same as linear convergence, but usually used when the sequence is exactly a geometric progression: $s^k = r^k(s^0)$.
Global convergence	Usually means the same as globally convergent, but some mean that the algorithm convergences to a global solution.
Globally convergent	Convergence to a solution from any starting point.
Linear convergence	Order = 1 and rate < 1.
Local convergence	Some mean locally convergent, but some mean that the limit point is a local optimum (or just satisfies necessary conditions -- see Myth NLP-5 to avoid misconception).
Locally convergent	There exists an open neighborhood of 0 such that $\{s^k\} \to 0$ from any s^0 in the neighborhood.
Order of convergence	Sup{p: lim $\|s^{(k+1)}\|/\|s^k\|^p$ < inf}. Order=1 is linear and order=2 is quadratic convergence. Most (non-finite) algorithms to solve mathematical programs are between linear and quadratic. Let $v^k = \|s^k\|$ and suppose $v^0 = 1$ (for notational convenience). The term order derives from the approximate equation, $v^{(k+1)} := r(v^k)^p$, where r is the rate. If this equation were exact, we would have $v^k = r^k$ if p=1, and $v^k = r^{[(p^k-1)/(p-1)]}$ if p > 1, for all k. If r=.1 and p=1, we gain one decimal place each time: $v^1 = .1$, $v^2 = .01$, $v^3 = .001$, etc. If p=2, the number of accurate decimal places approximately doubles each iteration: $v^1 = .1$, $v^2 = .0001$, $v^3 = .0000001$, etc. Unfortunately, the underlying equation is not exact -- see NLP Myth-2 to avoid misconception. Some authors call this q-order convergence to distinguish it from variations on the definition of order. Each definition is designed to capture the notion of how many digits of accuracy are added as the sequence approaches its limit.
Rate of convergence	This is the successive ratios, $\|s^{(k+1)}\|/\|s^k\|$, but it is generally used to mean the limiting ratio: lim $\|s^{(k+1)}\|/\|s^k\|^p$, given the order is p.
Sublinear convergence	Order = 1 and rate = 1 (slower than all linear convergence) -- e.g., $s^k = 1/k$.
Superlinear convergence	Order = 1 and rate = 0 (faster than all linear convergence) -- e.g., $s^k = (1/k)^k$.

Stochastic convergence	This applies when the successor point is a random variable, as in simulated annealing. Here are the most common types of convergence for a sequence of random variables, $\{X_n\} \rightarrow X$. with probability 1 or almost everywhere (abbr., a.e.). $P\{\lim X_n = X\} = 1$.
in probability	$P\{\|X_n - X\| > e\} \rightarrow 0$ for all $e > 0$.
in distribution	The sequence of cumulative distribution functions (cdf), converges point-wise: $F_n(x) \rightarrow F(x)$ for all x at which F is continuous, where F_n is the cdf of X_n and F is the cdf of X.
in p-th mean	$E\{\|X_n - X\|^p\} \rightarrow 0$. For p=2, this is called convergence in quadratic mean or in mean square.
CONVERT	Convert signal
CPU	Central processing unit
Cross-hole	Geophysical methods carried out between borehole (see also tomography).
Current density	A measure of current flow through a given (oriented) area [Ampers/m^2].
Cycling (in linear programming)	Revisiting a basis, mainly referring to a simplex method, so that the algorithm would cycle through the same sequence of bases, not converging to an optimal one.

D

°	Degree
D/A	Digital-to-analog
D*/A	Data/Address signal
DAC	D/A converter
DAC0OUT	Analog channel 0 output signal
DAC1OUT	Analog channel 1 output signal
DAC0OUT, DAC1OUT	Digital-to-analog converter 0, 1 output signal
DAC OUTPUT UPDATE	DAC output update signal
DACWRT	DAC Write signal
DAQ	Data Acquisition
DAQD*/A	Data Acquisition Board Data/Address line signal
DATA	Data lines at the specified port signal
dB	Decibels
DC	Direct current
Decomposition principle	The idea of decomposing a mathematical program into two or more sets of variables and associated constraints. The purpose is to separate some

	portion with special structure from the rest of the mathematical program.
Dense matrix	Matrix for which the number of zero elements is too small to warrant specialized algorithms to exploit these zeros.
DGND	Digital ground signal
Diagonally dominant matrix	See: Matrix properties.
DIFF	Differential mode
DIN	Deutsche Industrie Norme
DIO	Digital input/output
DIP	Doule-inline package
Dipole	A pair of equal charges or poles of opposite signs.
Direct method	An algorithm that produces the solution to a system of linear equations in a number of operations that is determined a priori by the size of the system. In exact arithmetic, a direct method yields the true solution to the system. See: Iterative method.
Distributed memory	See: Parallel computer.
Divergence	An iterative method is said to diverge if it does not converge in a reasonable number of iterations, or if some measure of the error grows unacceptably. However, growth of the error as such is no sign of divergence: a method with irregular convergence behavior may ultimately converge, even though the error grows during some iterations.
DMA	Direct memory acess
DNL	Differential nonlinearity
Domain decomposition method	Solution method for linear systems based on a partitioning of the physical domain of the differential equation. Domain decomposition methods typically involve (repeated) independent system solution on the subdomains, and some way of combining data from the subdomains on the separator part of the domain.
Dual	Another mathematical program with the property that its objective is always a bound on the original mathematical program, called the primal. Suppose the dual is Min{F(y): y in Y}. Then, $F(y) \leq f(x)$ for all feasible x in the primal and all y in Y. This immediately implies that if the primal is feasible, the dual cannot be unbounded, and vice versa: if the dual is feasible, the primal cannot be unbounded. It also implies that if the dual is unbounded, the primal must be infeasible (and vice versa). A dual provides a sufficiency test for optimality, for if feasible x and y can be found such that $f(x)=F(y)$, it follows that x is optimal in the primal and y is optimal in the dual. Weak duality is when this is all that can be guaranteed. Strong duality is when an optimal solution to one problem ensures the existence of an optimal solution to the other and

	that their optimal objective values are equal. There are particular duals of significance.
DUT	Device ubder test

E

EEPROM	Electrically erased programmable read-only memory
EISA	Extended industry standard architecture
EIT	Electrical Impedance Tomography
Electric field	A vector field describing the force on a unit electric charge [Newton's/Coulomb = Volts/meter].
Electrode	A piece of metallic material which acts as an electric conduct with a non-metal. In chemistry, it refers to an instrument designed to measure an electrical response which is proportional to the condition being assessed (i.e. pH, resistivity).
Elementary matrix	One that differs from the identity matrix in one column (or row). It arises in linear programming, particularly for the product form of the basis: $B= E_1 E_2 ... E_m$, where each E_i is an elementary matrix.
EOF	End-of-file
EPP	Enhanced Parallel Port
ERT	Electrical Resistivity Tomography
EXTCONV*	External convert signal
EXTREF	External reference signal
EXTRIG	External Trigger signal
EXTSTROBE	External strobe signal
EXTUPDATE*	External update signal

F

Feasible	A point is feasible if it satisfies all constraints. The feasible region (or feasibility region) is the set of all feasible points. A mathematical program is feasible if its feasible region is not empty.
FFT	Fast fourier transform
Field of values	Given a matrix A, the field of values is the set $\{x^T Ax : x^T x = 1\}$. For symmetric matrices this is the range $[\lambda_{min}(A), \lambda_{Max}(A)]$.
FIFO	First-in-first-out

Fill

A position that is zero in the original matrix A but not in an exact factorization of A. In an incomplete factorization, some fill elements are discarded.

Forward error

The difference between a computed iterate and the true solution of a linear system, measured in some vector norm.

Forward transformation (abbr. FTRAN)

This applies to the factored system, $[E_1\ E_2\ \ldots\ E_n]x = b$, where each E_i is an elementary matrix. The recursion is:

$$E_1 x_1 = b$$
$$E_2 x_2 = x_1$$
$$\ldots$$
$$E_n x_n = x_{(n-1)}$$

In the end, $x = x_n$ is the solution. Each elementary system is solved as follows. For notational convenience, suppose the system is $Ex = y$, and v is the distinguished p-th column of E. Then,

$$x(p) = y(p)/v(p), \text{ and } x(i) = y(i) - v(i)x(p) \text{ for } i \text{ not= } p.$$

This is what is done in the (revised) simplex method, and each elementary solution is a pivot operation.[4]

Forward triangularization

An algorithm to rearrange a matrix by recursively assigning a singleton row to the front (with its only column, as its pivot). The recursion applies to the submatrix defined by omitting the assigned row and column (and reducing other row counts accordingly). This results in a lower triangular rearrangement if, and only if, such a rearrangement exists.[4]

FREQ_OUT

Frequency output signal

ft

Feet

G

G

LabVIEW graphic programming language

Galvanic

Tdescribes geophysical techniques that require direct contact with the ground in order to pass current. The alternative is to induce currents in the earth.

GATB <0..2>

Coumter B0, B1, B2 Gate signals

Gaussian elimination

A method to solve Ax=b that performs elementary row operations on A to annihilate successive elements of A in order to reduce A to an upper triangular matrix, U. On paper, the same operations are applied to b, then the solution is obtained by solving the resulting upper triangular system. In a computer, the product of the matrices effecting the elementary row operations is a lower triangular matrix, L, with unit diagonal. Once this phase is completed, the system Ax=b becomes LUx=b. This is then solved in two steps: forward substitution solves

	Ly=b; then backward substitution solves Ux=y. (Of course, computer implementations vary.). [4]
Gauss-Jordan elimination	A method to solve Ax=b that performs elementary row and column operations on A to annihilate successive elements of A in order to reduce A to an identity matrix. On paper, the same operations are applied to b, then the solution is obtained by solving the resulting identity system. In a computer, the matrices effecting the elementary operations are saved as elementary matrices, say $\{E_i\}$. Then, the system is equivalent to $[E_1*E_2*...*E_n]x=b$, and forward transformation is applied to solve for x. This is what is done in the (revised) simplex method, and each iteration is a pivot operation. [4]
Generalized minimal residual or (GMRES)	The generalized minimal residual method computes a sequence of orthogonal vectors (like MINRES), and combines these through a least-squares solve and update approach. However, unlike MINRES (and CG), it requires storing the whole sequence, so that a large amount of storage is needed. For this reason, restarted versions of this method are used. In restarted versions, computation and storage costs are limited by specifying a fixed number of vectors to be generated. This method is useful for general nonsymmetric matrices.
Geophysical monitoring	Observing the change in a geophysical measurement with time.
GPCTR0_GATE	General purpose counter 0 gate signal
GPCTR1_GATE	General purpose counter 1 gate signal
GPCTR0_OUT	General purpose counter 0 output signal
GPCTR1_OUT	General purpose counter 1 output signal
GPCTR0_SOURCE	General purpose counter 0 clock source signal
GPCTR1_SOURCE	General purpose counter 0 clock source signal
Ground penetrating radar (GPR)	A geophysical method in which bursts of electromagnetic energy are transmitted downwards from the surface, to be reflected and refracted by velocity contrasts within the subsurface. Also known as "Ground Probing Radar".

H

h	Hour
Halfbandwidth	See: Band matrix.
Hessian	The matrix of second partial derivatives of a function (assumed to be twice differentiable). This is often denoted $H_f(x)$, where f is the function and x is a point in its domain. [4]
hex	Headecimal
Hz	Hertz

I

I/O	Input/output
I_{OH}	Current, output high
I_{OL}	Current, output low
IBF	Input buffer full signal
IEEE	Institute for Electrical and Electronic Engineers
Ill-conditioned system	A linear system for which the coefficient matrix has a large condition number. Since in many applications the condition number is proportional to (some power of) the number of unknowns, this should be understood as the constant of proportionality being large.
IML++	A mathematical template library in C++ of iterative method for solving linear systems.
Implicit Function Theorem	Suppose $h:R^n \dashrightarrow R^m$, where $n > m$, and h is in C^1. Further, suppose we can partition the variables, $x = (y, z)$, such that y is m-dimensional with grad_y[h(x)] nonsingular at $x = (y^*, z^*)$. Then, there exists $e > 0$ for which there is an implicit function, f, on the neighborhood, $N_e(z^*) = \{z: \|z-z^*\| < e\}$ such that $h(f(z), z)=0$ for all z in $N_e(z^*)$. Further, f is in C^1 with $grad_f(z^*) = -grad_y[h(x)]^{-1} grad_z[h(z)]$.
in	Inches
IN	Input
INaN	Digital display value for a floating-point representation infinity
Interpolation	The idea of estimating some value between two values. In LP, an interpolation estimate of the optimal objective value, say z(ab+(1-a)b'), is az(b) +(1-a)z(b').
Interpretation	Transforming geophysical measurements into subsurface structure. More general term than inversion.
INTR	Interrupt request signal
Incomplete factorization	A factorization obtained by discarding certain elements during the factorization process (`modified' and `relaxed' incomplete factorization compensate in some way for discarded elements). Thus an incomplete LU factorization of a matrix A will in general satisfy $A \neq LU$; however one hopes that the factorization LU will be close enough to A to function as a preconditioner in an iterative method.
Iterate	Approximation to the solution of a linear system in any iteration of an iterative method.
Iterative method	An algorithm that produces a sequence of approximations to the solution of a linear system of equations; the length of the sequence is

not given a priori by the size of the system. Usually, the longer one iterates, the closer one is able to get to the true solution. See: Direct method.

J

Jacobian

For a transformation, y=f(x), such that f is differentiable, the jacobian is the determinant, |grad_f(x)|. Historically, the number of y-variables equals the number of x-variables, say n, so grad_f(x) is n by n. Today, the jacobian is sometimes defined as the matrix, grad_f(x), allowing the number of functions to be less than the number of variables.[3]

K

Kernel of a basis

See Basis.

Krylov sequence

For a given matrix A and vector x, the sequence of vectors $\{Ai\ x\}_{i\geq 0}$, or a finite initial part of this sequence.

Krylov subspace

The subspace spanned by a Krylov sequence.

L

Lagrange Multiplier Rule (LMR)

From the extension to Lagrange's multiplier theorem:
Suppose x* is in argmax{f(x): g(x) ≤ 0, h(x) = 0}, where f, g, h are in C^1. Then, there exist multipliers (u, v) for which the following conditions hold:

1. grad_x_[f(x*) - ug(x*) - vh(x*)] = 0;
2. u ≥ 0;
3. ug(x*)=0.

Since g(x*) ≤ 0, the last condition, given u ≥ 0, is equivalent to complementary slackness. These are considered first-order optimality conditions, though the Lagrange Multiplier Rule is not always valid -- see constraint qualifications.[4]

LASTCHAN

Last channel (bit)

LED

Light-imitting diode

Linear convergence

See Convergence.

Linear program (LP)

Opt{cx: Ax = b, x ≥ 0}. (Other forms of the constraints are possible, such as Ax ≤ b.) The standard form assumes A has full row rank. Computer systems ensure this by having a logical variable (y) augmented, so the form appears as Opt{cx: Ax + y = b, L ≤ (x, y) ≤ U} (also allowing general bounds on the variables). The original variables (x) are called structural. Note that each logical variable can be a slack, surplus, or artificial variable, depending on the form of the original constraint. This computer form also represents a range constraint with simple bounds on the logical variable. Some bounds can be infinite (i.e., absent), and a free variable (logical or structural) is when both of its bounds are infinite.

LAPACK	A mathematical library of linear algebra routine for dense systems solution and eigenvalue calculations.
LSB	Least significant bit
Local convergence	See Convergence.
Lower triangular matrix	Matrix A for which $a_{i,j} = 0$ if $j > i$.
LQ factorization	A way of writing a matrix A as a product of a lower triangular matrix L and a unitary matrix Q, that is, $A = LQ$.
LU decomposition (of matrix A)	Finding a lower triangular matrix (L) and an upper triangular matrix (U) for which $A=LU$. The advantage is to solve the system $Ax=b$, we first apply forward substitution to solve $Ly=b$, then backward substitution to solve $Ux=y$. Similarly, to solve $vA=c$, first solve $uU=c$, then $vL=u$. [4]
LU factorization /LU decomposition	Expressing a matrix A as a product of a lower triangular matrix L and an upper triangular matrix U, that is, $A = LU$.

M

m	Meters
M-Matrix	See: Matrix properties.
Mapping	Locating geological, chemical or geophysical information in space (as opposed to time, which is monitoring). The results are usually summarized as maps.
Monitoring	Observing the change in a geophysical, hydrogeological or geochemical measurement with time.
Matrix norms	See: Norms.
Matrix properties	We call a square matrix A
Symmetric	if $a_{i,j} = a_{j,i}$ for all i, j.
Positive definite	if it satisfies $x^T Ax > 0$ for all nonzero vectors x.
Diagonally dominant	if $a_{i,i} > \Sigma_{j \neq i} \lvert a_{i,j} \rvert$; the excess amount $min_i \{ a_{i,i} - \Sigma_{j \neq i} \lvert a_{i,j} \rvert \}$ is called the diagonal dominance of the matrix.
An M-matrix	if $a_{i,i} \geq 0$ for $i \neq j$, and it is nonsingular with <Picture> for all i, j.
max.	Maximum
Maximum (pl. maxima)	A feasible point at which the supremum is achieved. An e-maximum is within e of being a maximum: f(x) ≥ f* - e, where f* is the supremum and e > 0.

Mb	Megabytes of memory
Message passing	See: Parallel computer.
MIMI	Manager for Interactive Modeling Interfaces - A modeling system that integrates mathematical programming, database management and artificial intelligence. [1]
min. min	Minimum Minutes
Minimum (pl. minima)	A feasible point at which the infimum is achieved. An e-minimum is within e of being a minimum: $f(x) \leq f^* + e$, where f^* is the infimum and $e > 0$. [4]
Minimum residual (MINRES) and Symmetric LQ (SYMMLQ)	These methods are computational alternatives for CG for coefficient matrices that are symmetric but possibly indefinite. SYMMLQ will generate the same solution iterates as CG if the coefficient matrix is symmetric and positive definite.
MIO	Multifunction I/O [1]
MPL	Mathematical Programming Language. [1]
MSB	Most significant bit
Multigrid method	Solution method for linear systems based on restricting and extrapolating solutions between a series of nested grids.
Modified incomplete factorization	See: Incomplete factorization.
Mutually consistent norms	See: Norms.

N

NaN	Digital display value for a floating-point representation of not a number, typically the result of an undefined operation, such as log(-1).
Natural ordering	See: Ordering of unknowns.
Network	A collection of *nodes*, V, sometimes called *vertices*, plus a collection of *arcs*, A, which are directed from one node to another. [4]
Noise	Any unwanted signal; a disturbance that is not part of signal from a specified source. In electrical or induced polarization (IP) surveys, noise may result from interference of power lines, motor-generators, atmospheric electrical discharges, etc. [1]
Nonstationary iterative method	Iterative method that has iteration-dependent coefficients.
Normal equations	For a non-symmetric or indefinite (but nonsingular) system of equations $Ax = b$, either of the related symmetric systems ($A^T Ax =$

$A^T b$) and ($AA^T y = b; x = A^T y$). For complex A, A^T is replaced with A^H in the above expressions.

Norms

A function $f: R^n \rightarrow R$ is called a vector norm if

- $f(x) \geq 0$ for all x, and $f(x) = 0$ only if $x = 0$.
- $f(ax) = |a| f(x)$ for all a, x.
- $f(x + y) \leq f(x) + f(y)$ for all x, y.

The same properties hold for matrix norms. A matrix norm and a vector norm (both denoted $\| \cdot \|$) are called a mutually consistent pair if for all matrices A and vectors x

$$\| Ax \| \leq \| A \| \| x \|.$$

NRSE

Nonrefernced single-ended mode

O

OBF

Ouput buffer full signal

100% Rule

This pertains to sensitivity analysis in linear programming. In its original form, it uses the convexity of the set of admissible changes in the rim data to test whether a particular change is admissible: any combination of changes can occur as long as the total percentage deviation from the coordinate extremes does not exceed 100%. (Note: this applies to right-hand sides (b) and costs (c) separately.).[4]

Optimal

For a mathematical program in standard form, x* in X (the domain) is an optimal solution if it is a maximum (or a minimum):

1. x* is feasible;
2. f(x*) ≥ f(x) for all feasible x (maximum value).

Some authors refer to an optimal solution when they mean a local optimum; others mean a member of the optimality regions (which are global optima). In either case, the optimal value is the objective value, evaluated at an optimal solution.[4]

Optimum (pl. optima)

Minimum or maximum.

Optimal response function

The optimal value of the objective as a function of parameters, typically the right-hand side:

$$f^*(b, c) = \text{Sup}\{f(x): x \text{ in } X, g(x) \leq b, h(x) = c\}.$$[4]

Order of convergence

See **Convergence.**

Ordering of unknowns

For linear systems derived from a partial differential equation, each unknown corresponds to a node in the discretization mesh. Different orderings of the unknowns correspond to permutations of the coefficient matrix. The convergence speed of iterative methods may depend on the ordering used, and often the parallel efficiency of a method on a parallel computer is strongly dependent on the ordering used. Some common orderings for rectangular domains are:

- The natural ordering; this is the consecutive numbering by rows and columns.

•The red/black ordering; this is the numbering where all nodes with coordinates (i, j) for which $i + j$ is odd are numbered before those for which $i + j$ is even.

•The ordering by diagonals; this is the ordering where nodes are grouped in levels for which $i + j$ is constant. All nodes in one level are numbered before the nodes in the next level.

For matrices from problems on less regular domains, some common orderings are:

•The Cuthill-McKee ordering; this starts from one point, then numbers its neighbors, and continues numbering points that are neighbors of already numbered points. The Reverse Cuthill-McKee ordering then reverses the numbering; this may reduce the amount of fill in a factorization of the matrix. •The Minimum Degree ordering; this orders the matrix rows by increasing numbers of nonzeros.

Orthogonal complement — of a subspace, S. {y: yx = 0 for all x in S}. In particular, if S = {x: x = Av for some v in R^n}, where A is an m by n matrix, its orthogonal complement is {y: yA = 0}.[4]

Orthogonal matrix — A matrix, A, such that AA'=I.

OUT — Output

OUTB0, OUTB1 — Counter B0, B1 output signals

Overburden — All geologic material which lies above bedrock.

P

PA, PB, PC<0..7> — Port A, B, or C 0 through 7 signals

Parallel computer — Computer with multiple independent processing units. If the processors have immediate access to the same memory, the memory is said to be shared; if processors have private memory that is not immediately visible to other processors, the memory is said to be distributed. In that case, processors communicate by message-passing.

Parameter — A constant in a mathematical program, not subject to choice in the decision problem, but one that could vary outside the control of the decisions. Examples are supplies, demands, loss factors, exponents and coefficients in polynomial functions (of the decision variables). Not all coefficients are parameters, as many are zero by the logic of the model. For example, the only data for a standard transportation problem are the costs, supplies and demands. These can depend upon parameters, but the LP matrix does not -- it is the incidence matrix of the network. In general, parameters are data-dependent constants, rather than logically fixed for all instances of the model. Some parameters are simply units of measurement, such as the amount of energy (Btu) in a ton of coal, whereas some parameters are uncertain, like demand for a product.[4]

Partial conjugate gradient method — The conjugate gradient method is performed for some number of iterations, say k (< n), then it is restarted (If k=0, this is the special case of Cauchy's steepest descent.). [3]

PC — Personal computer

Perturbation — An imprecise term that means changing some parameter value (or function) and seeing what effect this has on the solution. This embodies continuity and differentiability properties of the optimal responses: objective value, policy set and perhaps dual values too. This is what is sometimes called marginal analysis of solutions, and changes are limited to some neighborhood of the initial values. Some use perturbation function to mean the optimal objective value, even for large changes in the parameters, as in parametric programming. [4]

PFI — Programmable function input

PGIA — Programmable gain instrumentation amplifier

Phase I & Phase II — Phase I of a mathematical program is finding a feasible solution, and Phase II is entered with a feasible solution to find an optimal solution. The standard Phase I is:

$$\text{Max } \text{Sum}_i\{u_i\} + \text{Sum}_i\{v_i + w_i\}: u, v, w \geq 0,$$
$$g(x) - u \leq 0, h(x) - v + w = 0.$$

Then, for any x, one could set $u = g(x)^+$, $v = h(x)^+$ and $w = -h(x)^-$ to have a feasible solution to the Phase I mathematical program. The optimal objective value is 0 if, and only if, u=0 and v=w=0, in which case x is feasible in the original mathematical program (to commence Phase II). The Phase I problem is sometimes called an elastic program (thinking of the artificial variables (u,v,w) as providing "elastic" behavior in the levels of constraint violation).

In linear programming, the standard Phase I & II are:

I. Min ev: x, v >=0, Ax + v = b, and
II. Max cx: x ≥ 0, Ax = b, where b ≤ 0 (multiply by -1 for i: $b_i < 0$). [5]

Pipelining — See: Vector computer.

Pivot — This is the algebra associated with an iteration of Gauss-Jordan elimination, using the forward transformation. The tableaux for a pivot on element a(p,q) (not=0), which means nonbasic variable x_q enters the basis in exchange for basic variable x_p, are as follows:

Before pivot:

Basic Var.	Level	Nonbasic x_j	x_q
x_I	b_I	a(i,j)	a(i,q)
x_p	b_p	a(p,j)	a(p,q)*

obj	-z	d_j	d_q

After pivot:

Var.	Basic Level	Nonbasic x_j	x_p
x_i	$b_i - b_p\, a(i,q)/a(p,q)$	$a(i,j) - a(i,q)a(p,j)/a(p,q)$	$-a(i,q)/a(p,q)$
x_q	$b_p/a(p,q)$	$a(p,j)/a(p,q)$	$1/a(p,q)$
obj	$-z - b_p\, d_q/a(p,q)$	$d_j - a(p,j)d_q/a(p,q)$	$-d_q/a(p,q)$

A pivot is primal degenerate if the associated basic solution (x) does not change (i.e., the nonbasic variable enters the basis, but its level remains at the same bound value, in which case no basic variable changes level). Similarly, the pivot is dual degenerate if the associated dual solution (i.e., pricing vector and reduced costs) does not change. For dealing with degenerate pivots, see Bland's rule and the TNP rule.

Positive definite matrix (A). $x'Ax > 0$ for all nonzero x. Also See: Matrix properties.

POSTTRIG Posttrigger mode

ppm Parts per million

Precision The reproducibility of a measurement; the closeness of each of a set of similar measurements to the arithmetic mean of that set.

Preconditioner An auxiliary matrix in an iterative method that approximates in some sense the coefficient matrix or its inverse. The preconditioner, or preconditioning matrix, is applied in every step of the iterative method.

PRETRIG Pretrigger mode

Pricing This is a tactic in the simplex method, by which each variable is evaluated for its potential to improve the value of the objective function. Let $p = c_B[B^{-1}]$, where B is a basis, and c_B is a vector of costs associated with the basic variables. The vector p is sometimes called a dual solution, though it is not feasible in the dual before termination. p is also called a simplex multiplier or pricing vector. The price of the j_{th} variable is $c_j - pA_j$. The first term is its direct cost (c_j) and the second term is an indirect cost, using the pricing vector to determine the cost of inputs and outputs in the activity's column (A_j). The net result is called the reduced cost, and its value determines whether this activity could improve the objective value.

Processing Geophysically, to change data so as to emphasize certain aspects or correct for known influences, thereby facilitating interpretation.

Q

No specific terms begin with Q.

R

Radar	A system whereby short electromagnetic waves are transmitted and any energy which is scattered back by reflecting objects is detected. Acronym for "radio detection and ranging".
RC	Resistance-capacitance
RD*	Read signal
R_{EXT}	External resistance
Receiver	The part of an acquisition system which senses the information signal.
Red/black ordering	See: Ordering of unknowns.
Reduced system	Linear system obtained by eliminating certain variables from another linear system. Although the number of variables is smaller than for the original system, the matrix of a reduced system generally has more nonzero entries. If the original matrix was symmetric and positive definite, then the reduced system has a smaller condition number.
Relaxed incomplete factorization	See: Incomplete factorization.
Residual	If an iterative method is employed to solve for x in a linear system $Ax = b$, then the residual corresponding to a vector y is $yA - b$.
Resistivity (electrical)	Electrical resistance to the passage of a current, expressed in ohm-meters; the reciprocal of conductivity.
Resolution	Refers to the smallest unit of measurement that can be distinguished using a particular instrument or method; based on the ability to separate two measurements which are very close together..
Right-hand side (RHS)	When considering constraints of the form $g(x) \leq b$ and $h(x)=c$, the (b,c) is called the right-hand side.
rms	Root mean square
RSE	Referenced single-ended mode
RTD	Resistive temperature
RTSI	Real time system integration

S

s	Seconds
S	Samples
SCANCLK	Scan clock signal

SCXI	Signal conditioning extentions for instrument
SDK	Software developer's kit
SE	Single-ended inputd
Search direction	Vector that is used to update an iterate.
Self potential (SP)	A geophysical method measuring the natural, static voltage existing between sets of point on the ground surface..
SERCLK	Serial clock signal
SERDATIN	Serial data in signal
SERDATOUT	Serial data out signal
Shared memory	See: Parallel computer.
Sensitivity analysis	The concern with how the solution changes if some changes are made in either the data or in some of the solution values (by fixing their value). Marginal analysis is concerned with the effects of small perturbations, maybe measurable by derivatives. Parametric analysis is concerned with larger changes in parameter values that affect the data in the mathematical program, such as a cost coefficient or resource limit. Under suitable assumptions, the multipliers in the Lagrange Multiplier Rule provide derivatives of the optimal response function -- i.e., under certain conditions, (u, v) = grad_f*(b, c). For special approaches in LP, see compatibility theory, the 100% Rule, and the tolerance approach.
Simplex method	An algorithm invented to solve a linear program by progressing from one extreme point of the feasible polyhedron to an adjacent one. The method is an algorithm strategy, where some of the tactics include pricing and pivot selection.
Simultaneous displacements	Method of Jacobi method.
SI	System Integrator
SISOURCE	SI counter clock signal
Slack variable	In an inequality constraint of the form $g(x) \leq b$, the slack is b-g(x), which is designated by the slack variable, s. Then, the original constraint is equivalent to the defining equation, $g(x) + s = b$, plus $s \geq 0$.
SLOT0SEL	Slot 0 select signal
Sparse matrix	Matrix for which the number of zero elements is large enough that algorithms avoiding operations on zero elements pay off. Matrices derived from partial differential equations typically have a number of nonzero elements that is proportional to the matrix size, while the total number of matrix elements is the square of the matrix size.

Specific conductance — Strictly speaking identical to electrical conductivity the term is used in hydrogeology to refer to the conductivity of surface and ground water and expressed in micro Siemens per centimeter. It is a direct function of the total dissolved solids in the water.

Spectral condition number — The product

$$\| Ax \|_2 \ \| A^{-1} \| = \frac{\lambda_{max}^{1/2}(A^T A)}{\lambda_{min}^{1/2}(A^T A)}$$

where λ_{max} and λ_{min} denote the largest and smallest eigenvalues, respectively. For linear systems derived from partial differential equations in 2D, the condition number is proportional to the number of unknowns.

Spectral radius — The spectral radius of a matrix A is $\max \{|\lambda(A)|\}$.

Spectrum — The set of all eigenvalues of a matrix.

SPICLK — Serial peripheral interface clock signal

SS — Slot-select signal

STARTSCAN — Start scan signal

Stationary iterative method — Iterative method that performs in each iteration the same operations on the current iteration vectors.

STB — Strobe input signal

Stopping criterion — Since an iterative method computes successive approximations to the solution of a linear system, a practical test is needed to determine when to stop the iteration. Ideally this test would measure the distance of the last iterate to the true solution, but this is not possible. Instead, various other metrics are used, typically involving the residual.

Storage scheme — The way elements of a matrix are stored in the memory of a computer. For dense matrices, this can be the decision to store rows or columns consecutively. For sparse matrices, common storage schemes avoid storing zero elements; as a result they involve indices, stored as integer data, that indicate where the stored elements fit into the global matrix.

Successive displacements — Method of Gauss-Seidel method.

Symmetric matrix — See: Matrix properties.

T

Target — The object at which an investgative survey is aimed.

TC — Terminal count

Template — Description of an algorithm, abstracting away from implementational details.

THD	Total harmonic distortion
Time domain	In geophysics, refers to measurements analysis according to their behavior in time. The usual alternative is frequency domain measurements.
Tomography	A method for determining the distribution of physical properties within the earth by inverting the results of a large number of measurements made in three dimensions (e.g. Seismic, radar, resistivity, EM) between different source and receiver locations.
TRIG	Trigger signal
TTL	Transistor-transistor logic
Tune	Adapt software for a specific application and computing environment in order to obtain better performance in that case only itemize.
typ	Typical

U

UI	Update interval
UISOURCE	Update interval counter clock signal
Unbounded mathematical program	The objective is not bounded on the feasible region (from above, if maximizing; from below, if minimizing). Equivalently, there exists a sequence of feasible points, say $\{x^k\}$ for which $\{f(x^k)\}$ diverges to infinity (minus infinity if minimizing).
UP/BP*	Unipolar/bipolar bit
Upper triangular matrix	Matrix A for which $a_{i,j} = 0$ if $j < i$.
UPDATE	Update signal
UUT	Unit under test

V

V	Volts
$V\pm_{in}$	Positive/negative input voltage
V_{cm}	Common-mode noise
V_{diff}	Differential input voltage
VDC	Volts direct current
V_{EXT}	External voltage
VI	Virtual instrument

V_{IH}	Volts, input high
V_{IL}	Volts, input low
V_{in}	Volts in
V_m	Measured voltage
V_{rms}	Volts. root-mean-square
V_{OH}	Volts, output high
V_{OL}	Volts, output low
V_{ref}	Reference voltage
V_s	signal source

Vector computer	Computer that is able to process consecutive identical operations (typically additions or multiplications) several times faster than intermixed operations of different types. Processing identical operations this way is called "pipelining" the operations.
Vector norms	See: Norms.

W

W	Watts
Well log	A record describing geologic formations and well testing or development techniques used during well construction. Often refers to a geophysical well log in which the physical properties of the formations are measured by geophysical tools, E-logs, neutron logs, etc...
WFTRIG	Waveform generation trigger signal
WRT	Write signal

X

No specific terms begin with X.

Y

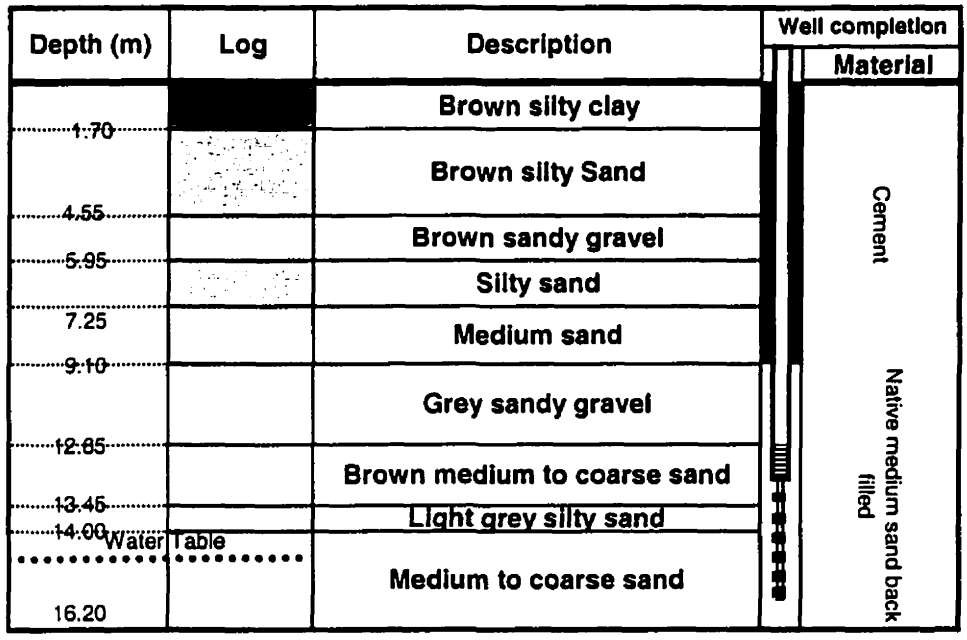
No specific terms begin with Y.

Z

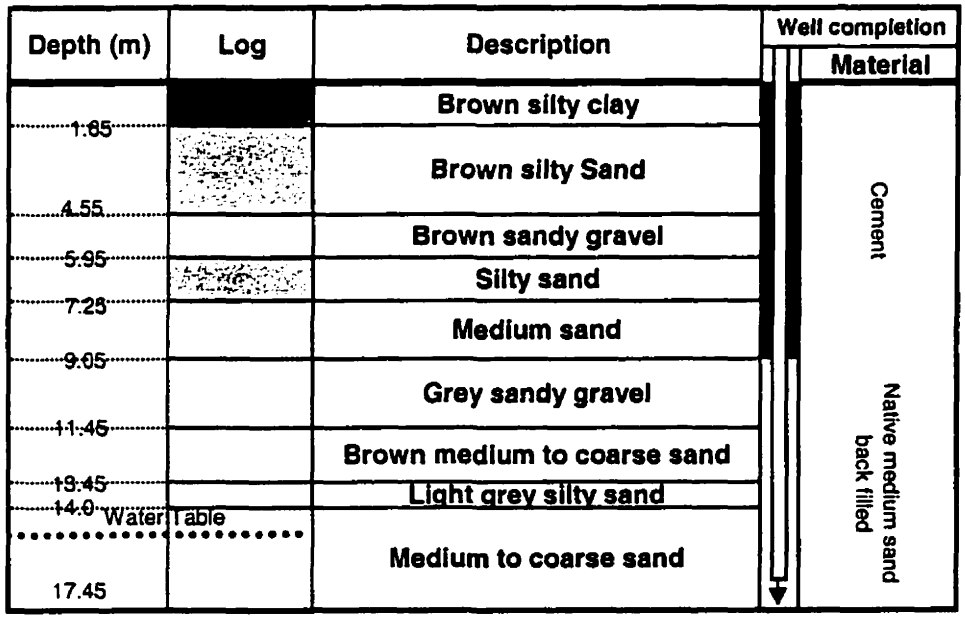
No specific terms begin with Z.

Appendix I. Logs of wells at Cambridge site

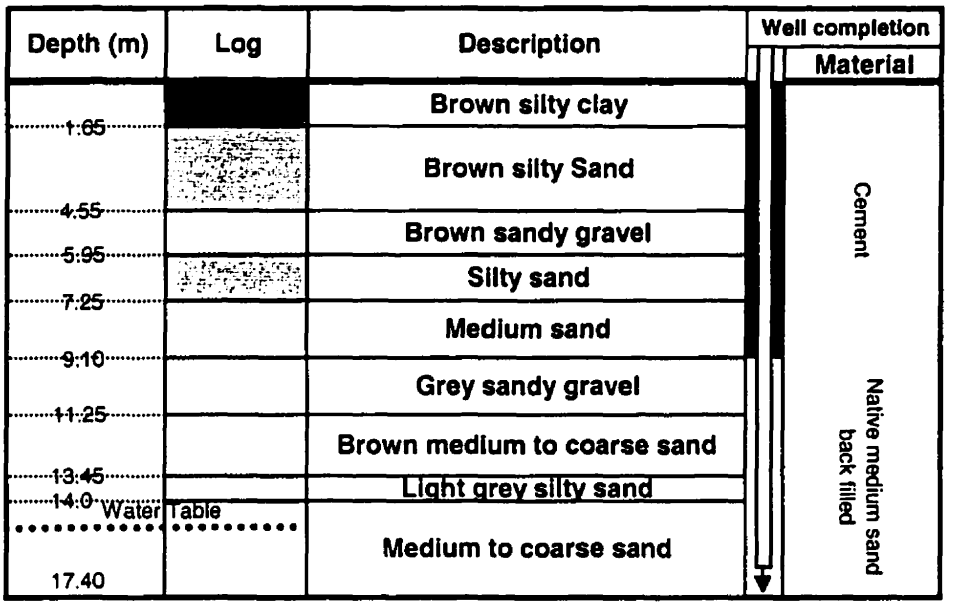
Soil samples were collected from five wells during the drilling of wells at Cambridge site for stratigraphic determination. The results are presented in Figure I-1 to I -5. An average stratigraphic distribution observed in these wells is presented in Figure 2.5



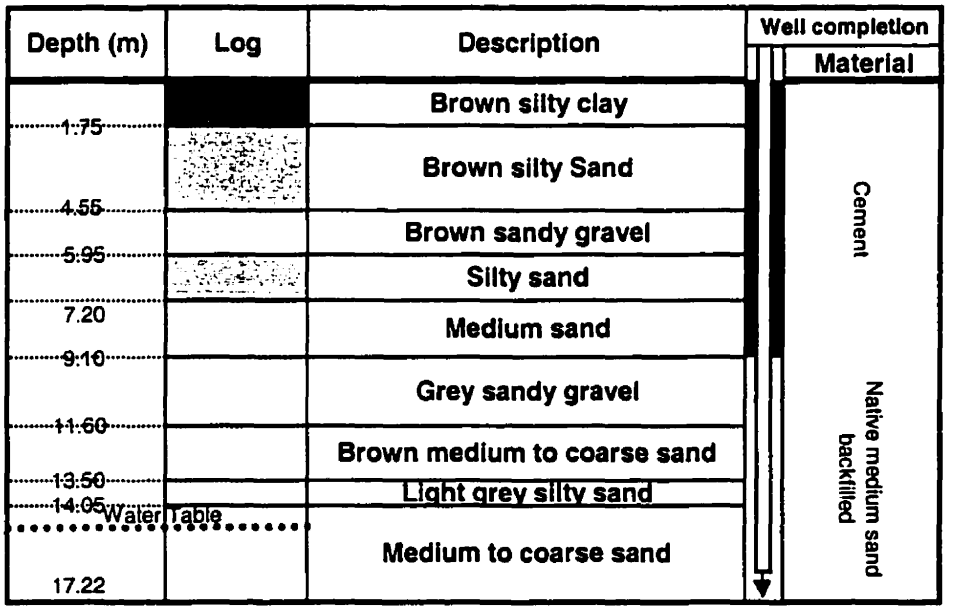
I.1 Stratigraphic units in Injection well of Cambridge site



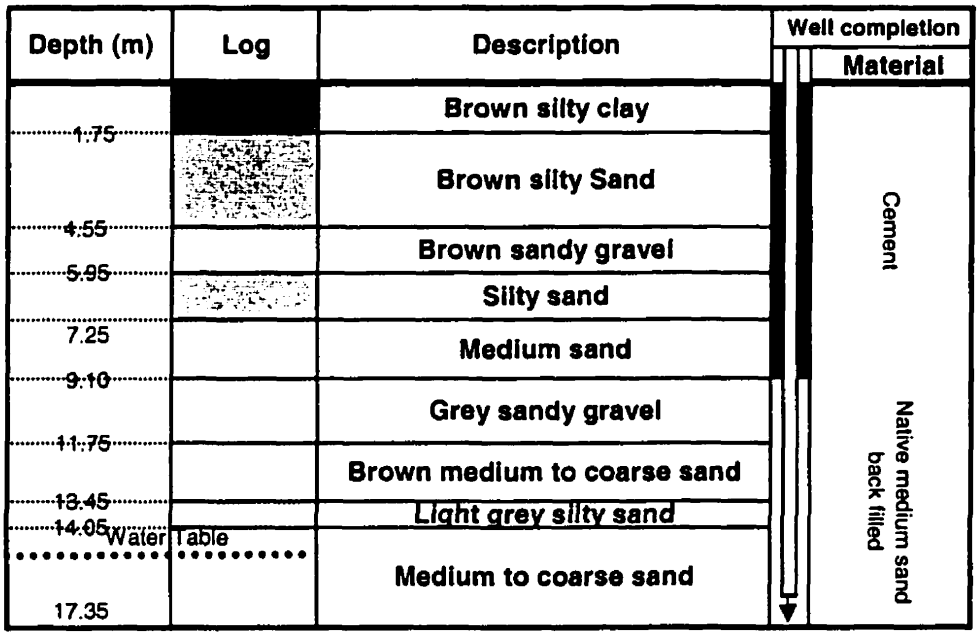
I.2 Stratigraphic units in NE-monitoring well of Cambridge site



I.3 Stratigraphic units in NW-monitoring well of Cambridge site



I.4 Stratigraphic units in SE-monitoring well of Cambridge site



I.5 Stratigraphic units in SW-monitoring well of Cambridge site

Appendix J. ERT Model Calibration

A one-layer case (Figure J.1) was defined for SALTFLOW and also solved analytically (Telford et al., 1996). The results are compared in a scatter plot (Figure J.2).

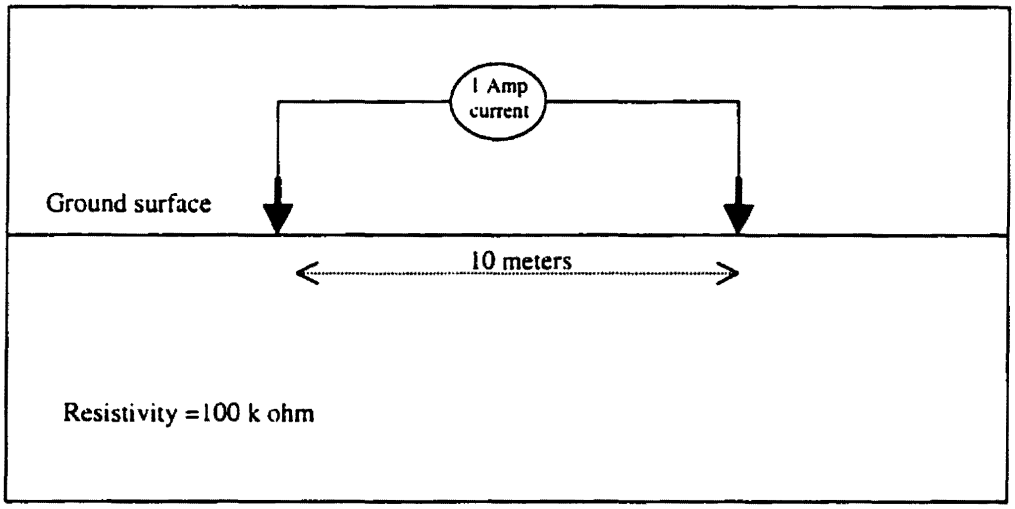


Figure J.1 Schematic diagram of one layer model

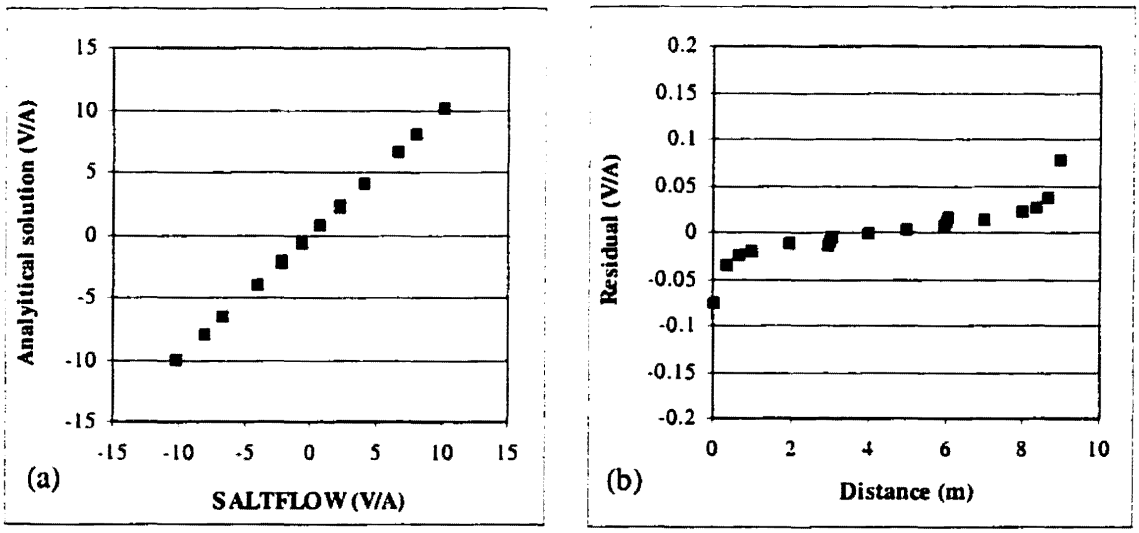


Figure J.2 Scatter and residual plots of a one-layer case solved analytically and by SALTFLOW: a) scatter plot, and b) residual plot

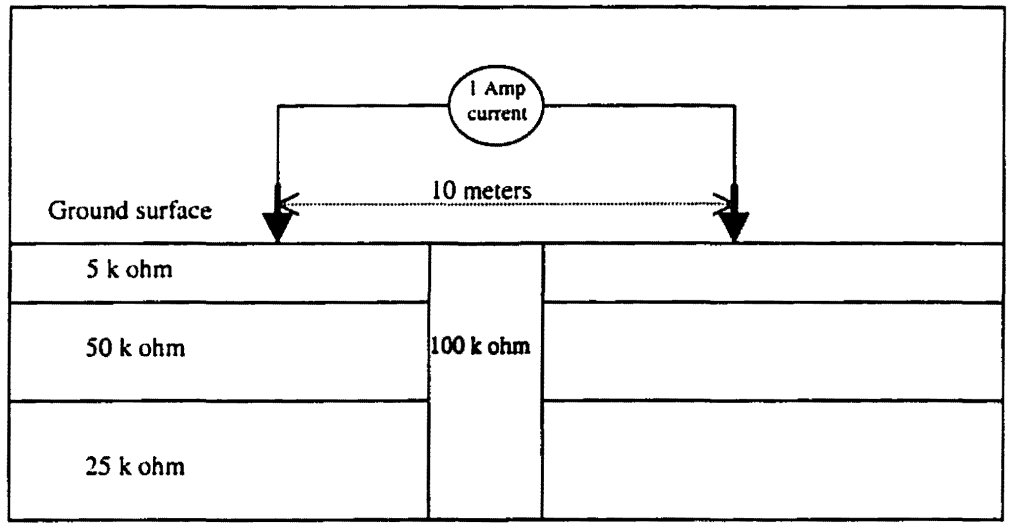


Figure J.3 Schematic diagram of three-layer model with a high resistive vertical column in the middle

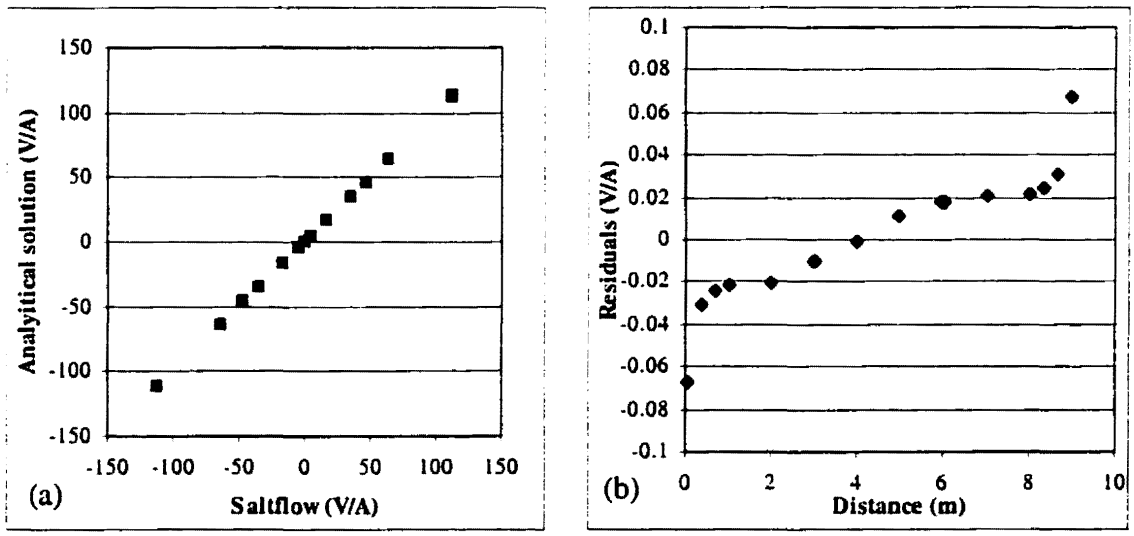


Figure J.4 Scatter and residual plots of a three-layer case three-layer model with a high resistive vertical column in the middle solved analytically and by SALTFLOW: a) scatter plot, and b) residual plot

The statistical comparison was performed on the results based on the following procedures:

Root mean square error (RMSE):

$$RMSE = \frac{\left[\sum_{i=1}^{n}(V_{c_i} - V_{a_i})^2 / n\right]^{0.5}}{\bar{V}} \qquad \text{(J-1)}$$

Coefficient of determination (CD):

$$CD = \frac{\sum_{i=1}^{n}(V_{O_i} - \bar{V}_O)^2}{\sum_{i=1}^{n}(V_{c_i} - \bar{V}_O)^2} \qquad \text{(J-2)}$$

Modelling efficiency (EF):

$$EF = \frac{\sum_{i=1}^{n}(V_{O_i} - \bar{V}_O)^2 - \sum_{i=1}^{n}(V_{C_i} - \bar{V}_O)^2}{\sum_{i=1}^{n}(V_{O_i} - \bar{V}_O)^2} \qquad \text{(J-3)}$$

Coefficient of residual mass (CRM):

$$CRM = \frac{\sum_{i=1}^{n} V_{O_i} - \sum_{i=1}^{n} V_{C_i}}{\sum_{i=1}^{n} V_{O_i}} \qquad \text{(J-4)}$$

The second scenario was a three-layer case with a vertical resistant wall in the middle of the grids (figure J.3). This scenario was solved analytically and also with SALTFLOW model. The results are plotted against in Figure J.4. The statistical results of both scenarios are presented in Table J.1. The results show the simulated and the analytical results have a good match and the ERT simulations of the combined model are reliable.

Table J.1 Statistical results of two scenarios solved analytically and by the SALTFLOW model

Scenario	Statistics			
	RMSE	CD	EF	CRM
One layer case	0.0107	0.0012	0.9735	0.9924
Three layer case with a vertical wall	0.0154	0.0025	0.9689	0.9904